

**Generalized Prandtl-Ishlinskii Hysteresis Model and its Analytical Inverse for
Compensation of Hysteresis in Smart Actuators**

Mohammed Al Janaideh

A Thesis
in
The Department
of
Mechanical and Industrial Engineering

Presented in Partial Fulfillment of the Requirements
for the Degree of Doctor of Philosophy at
Concordia University
Montreal, Quebec, Canada

June, 2009

© Mohammad Al Janaideh, 2009



Library and Archives
Canada

Published Heritage
Branch

395 Wellington Street
Ottawa ON K1A 0N4
Canada

Bibliothèque et
Archives Canada

Direction du
Patrimoine de l'édition

395, rue Wellington
Ottawa ON K1A 0N4
Canada

Your file *Votre référence*
ISBN: 978-0-494-63346-5
Our file *Notre référence*
ISBN: 978-0-494-63346-5

NOTICE:

The author has granted a non-exclusive license allowing Library and Archives Canada to reproduce, publish, archive, preserve, conserve, communicate to the public by telecommunication or on the Internet, loan, distribute and sell theses worldwide, for commercial or non-commercial purposes, in microform, paper, electronic and/or any other formats.

The author retains copyright ownership and moral rights in this thesis. Neither the thesis nor substantial extracts from it may be printed or otherwise reproduced without the author's permission.

AVIS:

L'auteur a accordé une licence non exclusive permettant à la Bibliothèque et Archives Canada de reproduire, publier, archiver, sauvegarder, conserver, transmettre au public par télécommunication ou par l'Internet, prêter, distribuer et vendre des thèses partout dans le monde, à des fins commerciales ou autres, sur support microforme, papier, électronique et/ou autres formats.

L'auteur conserve la propriété du droit d'auteur et des droits moraux qui protègent cette thèse. Ni la thèse ni des extraits substantiels de celle-ci ne doivent être imprimés ou autrement reproduits sans son autorisation.

In compliance with the Canadian Privacy Act some supporting forms may have been removed from this thesis.

While these forms may be included in the document page count, their removal does not represent any loss of content from the thesis.

Conformément à la loi canadienne sur la protection de la vie privée, quelques formulaires secondaires ont été enlevés de cette thèse.

Bien que ces formulaires aient inclus dans la pagination, il n'y aura aucun contenu manquant.


Canada

ABSTRACT

Generalized Prandtl-Ishlinskii Hysteresis Model and its Analytical Inverse for Compensation of Hysteresis in Smart actuators

Mohammad Al Janaideh

Smart actuators such as piezoceramics, magnetostrictive and shape memory alloy actuators, invariably, exhibit hysteresis, which has been associated with oscillations in the open-loop system's responses, and poor tracking performance and potential instabilities of the close-loop system. A number of phenomenological operator-based hysteresis models such as the Preisach model, Krasnosel'skii-Pokrovskii model and Prandtl-Ishlinskii model, have been formulated to describe the hysteresis nonlinearities and to seek compensation of the hysteresis effects. Among these, the Prandtl-Ishlinskii model offers greater flexibility and unique property that its inverse can be attained analytically. The Prandtl-Ishlinskii model, however, is limited to rate-independent and symmetric hysteresis nonlinearities. In this dissertation research, the unique flexibility of the Prandtl-Ishlinskii model is explored for describing the symmetric as well as nonlinear hysteresis and output saturation properties of smart actuators, and for deriving an analytical inverse for effective compensation.

A generalized play operator with dissimilar envelope functions is proposed to describe asymmetric hysteresis and output saturation nonlinearities of different smart actuators, when applied in conjunction with the classical Prandtl-Ishlinskii model. Dynamic density and dynamic threshold functions of time rate of the input are further proposed and integrated in the classical model to describe rate-dependent symmetric and asymmetric hysteresis properties of smart actuators. A fundamental relationship between

the thresholds of the classical and the resulting generalized models is also formulated to facilitate parameters identification. The validity of the resulting generalized Prandtl-Ishlinskii models is demonstrated using the laboratory-measured data for piezoceramic, magnetostrictive and SMA actuators under different inputs over a broad range of frequencies. The results suggest that the proposed generalized models can effectively characterize the rate-dependent as well as rate-independent hysteresis properties of a broad class of smart actuators with output saturation. The properties of the proposed generalized models are subsequently explored to derive its inverse to seek an effective compensator for the asymmetric as well as rate-dependent hysteresis effects. The resulting inverse is applied as a feedforward compensator and simulation results are obtained to demonstrate its effectiveness in compensating the symmetric as well as asymmetric hysteresis of different smart actuators. The effectiveness of the proposed analytical inverse model-based real-time compensator is further demonstrated through its implementation in the laboratory for a piezoceramic actuator.

Considering that the generalized Prandtl-Ishlinskii model provides an estimate of the hysteresis properties and the analytical inverse is a hysteresis model, the output of the inverse compensation is expected to yield hysteresis, although of a considerably lower magnitude. The expected compensation error, attributed to possible errors in hysteresis characterization, is analytically derived on the basis of the generalized model and its inverse. The design of a robust controller is presented for a system preceded by the hysteresis effects of an actuator using the proposed error model. The primary purpose is to fuse the analytical inverse compensation error model with an adaptive controller to achieve to enhance tracking precision. The global stability of the chosen control law and

the entire closed-loop system is also analytically established. The results demonstrated significantly enhanced tracking performance, when the inverse of the estimated Prandtl-Ishlinskii model is considered in the closed-loop control system.

To my mother, to my father, and to my beloved wife Redab

Acknowledgments

My greatest thanks to my thesis supervisors Professors Subhash Rakheja and Chun-Yi Su; I wish to express my honest appreciation for their suggestions, guidance, support, and their human sense in dealing with me during my PhD study.

So much love and thanks to my wife for her encouragement, inspiration, and support. Love, kisses, and gratitude to my beautiful kids, Omar and Razan for their everlasting smile.

Also I would like to thank Dr Ying Feng for her greatest help. Also, I would like to thank Professors Xiaobo Tan and Robert Gorbet for providing me with the experimental results of the magnetostrictive and SMA actuators.

Allanaideh

Table of Contents

List of Figures	xiii
List of Tables	xx
Nomenclature	xxi
Chapter 1: Introduction and Literature Review	1
1.1 Introduction	1
1.2 Experimental Characterization of Hysteresis	4
1.3 Hysteresis Models	9
1.3.1 Physics-Based Hysteresis Models.....	9
1.3.2 Differential Equation-Based Phenomenological Model	11
1.3.3 Operator-Based Hysteresis Models.....	14
1.3.4 Rate-Dependent Hysteresis Models	22
1.4 Hysteresis Compensation	23
1.4.1 Non-Inverse-Based Control Methods	23
1.4.2 Inverse Model-Based Methods	25
1.5 Scope and Objectives	30
1.5.1 Objectives of the Dissertation Research	32
1.6 Organization of the Dissertation.....	32
Chapter 2: Modeling Hysteresis Nonlinearities	35
2.1 Introduction	35
2.2 Prandtl-Ishlinskii Model.....	37
2.2.1 Play Hysteresis Operator.....	37
2.2.2 Input-Output Relationship of The Prandtl-Ishlinskii Model.....	39
2.3 A Generalized Rate-Independent Prandtl-Ishlinskii Model	43

2.3.1	The Generalized Play Hysteresis Operator	43
2.3.2	Input-Output Relationship of the Generalized Prandtl-Ishlinskii Model	46
2.4	Prandtl-Ishlinskii Model Based Rate-Dependent Play Operator	52
2.4.1	Formulation of Rate-Dependent Play Hysteresis Operator	52
2.4.2	Rate-Dependent Prandtl-Ishlinskii Model	55
2.4.3	Rate-dependent Prandtl-Ishlinskii Model Based Dynamic Density Function	57
2.5	Prandtl-Ishlinskii Model Based Generalized Rate-Dependent Play Operator	58
2.5.1	Generalized rate-dependent play hysteresis operator	58
2.5.2	the generalized rate-dependent prandtl-Ishlinskii model	58
2.6	Summary	60
Chapter 3: Characterization of Hysteresis Properties of Smart Actuators		63
3.1	Introduction	63
3.2	Experimental Characterization of Hysteresis of a Piezoceramic Actuator	65
3.2.1	Major Hysteresis Loop Tests	67
3.2.2	Minor Hysteresis Loops Test	70
3.2.3	Influence of the Input Waveform	74
3.3	Input-Output Characteristics of Magnetostrictive Actuators	77
3.4	Input-Output Characteristics of SMA Actuators	80
3.5	Discussions	82
3.6	Summary	84
Chapter 4: Modeling Rate-Dependent and Asymmetric Hysteresis Nonlinearities of Smart Actuators		86
4.1	Introduction	86

4.2	Classical Prandtl-Ishlinskii model for Characterizing Hysteresis in Smart Actuators	88
4.3	Generalized Rate-Independent Prandtl-Ishlinskii Model for Characterizing Hysteresis in Smart Actuators	92
4.3.1	Formulation of Envelope Functions and Parameter Identification.....	92
4.3.2	Experimental Verifications	95
4.4	Rate-Dependent Prandtl-Ishlinskii Model for Characterizing Rate-Dependent Hysteresis of a Piezoceramic Actuator.....	100
4.4.1	Parameters Identification	102
4.4.2	Major Hysteresis Loop Simulation.....	103
4.4.3	Minor Hysteresis Loop Simulation.....	105
4.4.4	Triangular Waveform Input.....	108
4.5	Generalized Rate-Dependent Prandtl-Ishlinskii Model	110
4.5.1	Parameters Identification	111
4.5.2	Experimental Verifications.....	114
4.6	Summary	124
Chapter 5: Formulations of Inverse Prandtl-Ishlinskii Models for Hysteresis Compensation		127
5.1	Introduction	127
5.2	Analytical inversion of the Prandtl-Ishlinskii model	128
5.2.1	Concept of the Initial Loading Curve (Shape Function)	128
5.2.2	Inverse Prandtl-Ishlinskii Model	133
5.2.3	Formulation of Inverse Generalized Prandtl-Ishlinskii Model.....	139
5.2.4	Parameters Identification	143
5.3	Inverse Rate-Dependent Prandtl-Ishlinskii Models	145
5.3.1	Inverse Rate-Dependent Prandtl-Ishlinskii Model	146

5.3.2	Inverse Generalized Rate-Dependent Prandtl-Ishlinskii Model	147
5.4	Inverse Generalized Prandtl-Ishlinskii Model for Compensation	149
5.4.1	Compensation of Asymmetric Hysteresis Loops	149
5.4.2	Compensation of Saturated Hysteresis Loops	151
5.5	Inverse Rate-Dependent Prandtl-Ishlinskii Models for Compensation.....	153
5.5.1	Compensation of Rate-Dependent Hysteresis	153
5.5.2	Compensation of Asymmetric Rate-Dependent Hysteresis	154
5.6	Experimental Verification of Hysteresis Compensation	157
5.6.1	Parameters Identification and Model Validation	157
5.6.2	Motion Tracking Experiment	160
5.6.3	Discussion.....	163
5.7	Summary	163
Chapter 6: Analytical Error of Inverse Compensation with Prandtl-Ishlinskii Model		
.....		165
6.1	Introduction	165
6.2	Problem Statement	166
6.3	Analytical Expression of the Composition of the Prandtl-Ishlinskii Model	167
6.3.1	Illustrative Example	169
6.4	Inverse of the Estimated Prandtl-Ishlinskii Model.....	173
6.5	Analytical Error of the inverse Compensation of the Prandtl-Ishlinskii Model.	176
6.6	Simulation Results.....	179
6.7	Summary	182
Chapter 7: An Adaptive Controller Design for Inverse Compensation Error		185
7.1	Introduction	185

7.2	Problem Statement	186
7.3	Control Design	188
7.4	Simulation Results.....	194
7.5	Summary	197
Chapter 8: Conclusions and Recommendations for Future Studies.....		200
8.1	Major Contributions	200
8.2	Major conclusions	201
8.2.1	Developments in Generalized Hysteresis Models	201
8.2.2	Developments in Inverse Hysteresis Models.....	202
8.2.3	Compensation of Hysteresis Effects Using Inverse Model	203
8.2.4	Error Analysis	203
8.2.5	Adaptive Control Design for Hysteresis Compensation.....	204
8.3	Recommendation for the Future Studies	204
References.....		208

List of Figures

Figure 1.1: Measured hysteresis properties of ferromagnetic materials [1].	5
Figure 1.2: Relay hysteresis operator [1].	15
Figure 1.3: Krasnosel'skii-Pokrovskii operator [4].	18
Figure 1.4: Play hysteresis operator [2].	19
Figure 1.5: Stop hysteresis operator [2].	20
Figure 1.6: Open-loop inverse control system.	26
Figure 1.7: Illustration of numerical hysteresis inversion.	27
Figure 2.1: The output-input properties of the play hysteresis operator.	38
Figure 2.2: Input-output relations of: (a) play operators corresponding to different threshold values, and (b) the Prandtl-Ishlinskii model under $v(t) = 10\sin(2\pi t)$	41
Figure 2.3: Generalized play operator.	44
Figure 2.4: Input-output properties of the play hysteresis operators under $v(t) = 4.6\sin(\pi t) + 3.1\cos(3.4\pi t)$: (a) Classic play operator, $\gamma_l(v) = \gamma_r(v) = v$; and (b) Generalized play operator, $\gamma_l(v) = 6 \tanh(0.4v)$ and $\gamma_r(v) = 6 \tanh(0.25v)$	49
Figure 2.5: Response characteristics of the Prandtl-Ishlinskii hysteresis models employing: (a) classical play operator; and (b) generalized play operator.	50
Figure 2.6: Input-output relations of: (a) the generalized play operators corresponding to different threshold values; and (b) the generalized Prandtl-Ishlinskii model under $v(t) = 4.6\sin(\pi t) + 3.1\cos(3.4\pi t)$, and $\gamma_l(v) = \gamma_r(v) = 6 \tanh(0.4v)$	51
Figure 2.7: The input-output properties of the Prandtl-Ishlinskii model employing the rate-dependent play operator under inputs at different frequencies.	56
Figure 2.8: Simulation results attained from the Prandtl-Ishlinskii model employing the generalized rate-dependent play operator under a complex harmonic input at different fundamental frequencies.	60
Figure 3.1: A schematic representation of the experimental setup.	66

Figure 3.2: Measured major hysteresis loops relating displacement response of a piezoceramic actuator to the applied voltage at different frequencies.....	68
Figure 3.3: Measured major hysteresis loop.....	69
Figure 3.4: (a)Variation in percent hysteresis of major hysteresis loops and, (b) peak-to-peak displacement response at different excitation frequencies.....	69
Figure 3.5: (a) Influence of excitation magnitude on the minor hysteresis loops at an excitation frequency of 100 Hz, and (b) Variation in percent hysteresis of the minor loops as a function of excitation frequency (Bias =20V; Amplitudes: square -5; star-10; and ; triangle -20).....	71
Figure 3.6: Peak-to-peak displacement response of the actuator corresponding to different excitation frequencies and a constant bias input voltage of 20 V: (a) 20±5; (b) 20±10; and (c) 20±20.....	72
Figure 3.7: Variations in percent hysteresis of the minor loops as a function of frequency and bias voltage (amplitude 10 V; square – 30 ± 10; star – 60 ± 10; and triangle – 90 ± 10).....	73
Figure 3.8: Influence of bias voltage on the peak-to-peak displacement response of the piezoceramic actuator under different excitation frequencies (Amplitude=20V; Bias voltage: square – 30 V; star – 60 V; and triangle – 90 V).....	73
Figure 3.9: Comparisons of major hysteresis loops under sinusoidal and triangular excitations at different frequencies (- - - , sinusoidal; ———, triangular; Amplitude = 40 V; Bias =40 V).....	75
Figure 3.10: Comparisons of the sinusoidal and tringular waveforms and their rates at different excitation frequencies: (a) waveforms (b) rates (——— sinusoidal, - - - triangular).....	76
Figure 3.11: Measured output-input responses of a magnetostrictive actuator.....	78
Figure 3.12: Measured hysteresis loops relating displacement response of a magnetostrictive actuator to its applied current at different excitation frequencies.....	78
Figure 3.13: Percent hysteresis of the magnetostrictive actuator under excitations at different excitation frequencies (based on data obtained from [23]).....	79
Figure 3.14: Variations in displacement amplitude response of a magnetostrictive actuator as a function of excitation frequency (based on data obtained from [33]).	79
Figure 3.15: Measured output-input responses of two smart actuators: (a) a two-wire SMA actuator; and (b) a one-wire SMA actuator wire.....	81

Figure 4.1: Comparisons of displacement responses of the classic Prandtl-Ishlinskii hysteresis model with the measured data of a piezoceramic actuator under complex harmonic input (- - - , measured; ——— , model). 90

Figure 4.2: Comparisons of displacement responses of the classical Prandtl-Ishlinskii model with the measured data of two SMA actuators: (a) one-wire SMA actuator wire; and (b) two-wire SMA actuator. (—○— , measured; —△— , model). 91

Figure 4.3: Comparisons of displacement responses of the classical Prandtl-Ishlinskii model with the measured responses of the magnetostrictive actuator (——— , measured; , model). 91

Figure 4.4: Comparisons of displacement responses of the generalized Prandtl-Ishlinskii model with the measured data of two SMA actuators: (a) one-wire SMA actuator wire; and (b) two-wire SMA actuator. (—△— , model; —○— , measured). 96

Figure 4.5: Comparisons of displacement responses of the generalized Prandtl-Ishlinskii model with the measured responses of the magnetostrictive actuator (- - - , measured; ——— , model). 96

Figure 4.6: (a) Comparisons of time histories of displacement responses of the generalized Prandtl-Ishlinskii model with the measured data of the single-wire SMA actuator (- -△- , measured; —○— , model); and (b) variations in the error. 97

Figure 4.7: (a) Comparisons of time histories of displacement responses of the generalized Prandtl-Ishlinskii model with the measured data of the magnetostrictive actuator (- - - , measured; ——— , model); and (b) variations in the error magnitude. 98

Figure 4.8: Comparisons of displacement responses of the Prandtl-Ishlinskii hysteresis models with the measured data of the piezoceramic actuator under complex harmonic (- - - , measured; ——— , model). 99

Figure 4.9: Comparisons of differences in output displacements of the generalized and classical Prandtl-Ishlinskii models and the measured data under complex harmonic input, (—△— , classical model; —○— , generalized model). 99

Figure 4.10: Comparisons of measured responses with the results derived from rate-dependent model under inputs at different excitation frequencies (——— , measured; ——— , model). 104

Figure 4.11: Input output relationships of the rate-dependent play operator at different frequencies. 105

Figure 4.12: Comparisons of measured responses with the results derived from rate-dependent Prandtl-Ishlinskii model under inputs at different fundamental frequencies (——— , measured; ——— , model). 106

Figure 4.13: (a) Time histories of measured and model displacement responses at different fundamental frequencies (---, measured; —, model). (b) Time histories of error in measured and model displacement responses at different fundamental frequencies. 107

Figure 4.14: Comparisons of measured responses with the results derived from rate-dependent Prandtl-Ishlinskii model under triangular inputs at different frequencies (—, measured; —, model). 109

Figure 4.15: (a) Comparisons of measured displacement responses with those of the rate-dependent model under triangular inputs at different excitation frequencies (....., measured; —, model); and (b) Error between the measured and model displacement responses. 110

Figure 4.16: Comparisons of displacement responses of the generalized rate-dependent Prandtl-Ishlinskii model with the measured responses of a magnetostrictive actuator under different input frequencies: (a) Play operator with linear envelope functions, $s_l = s_r = 1$; and (b) Play operator with nonlinear envelope functions, $s_l = s_r = 3$. (—, measured; —, model). 116

Figure 4.17: Comparisons of time histories of displacement responses of models with the measured data of a magnetostrictive actuator at different input frequencies: (a) Play operator with linear envelope function, $s_l = s_r = 1$; and (b) Play operator with nonlinear envelope function, $s_l = s_r = 3$. (—, measured;, model). 117

Figure 4.18: Time histories of errors between the model and measured displacement responses of the magnetostrictive actuator at different input frequencies: (a) play operator with linear envelope functions, $s_l = s_r = 1$; and (b) play operator with nonlinear envelope functions, $s_l = s_r = 3$ 118

Figure 4.19: Comparisons of displacement responses of the generalized rate-dependent model with the measured data of a piezoceramic actuator under different input frequencies (—, measured; —, model): (a) play operator with linear envelope function, $s_l = s_r = 1$; and (b) play operator with nonlinear envelope function, $s_l = s_r = 3$ 121

Figure 4.20: Time histories of displacement responses of the model and the piezoceramic actuator at different input frequencies (—, measured;, model). (a) Rate-dependent play operator with linear envelope functions, $s_l = s_r = 1$; and (b) Rate-dependent play operator with nonlinear envelope functions, $s_l = s_r = 3$ 122

Figure 4.21: Time histories of errors between the model and measured displacement responses of the piezoceramic actuator at different input frequencies: (a) play operator with linear envelope functions, $s_l = s_r = 1$; and (b) play operator with nonlinear envelope functions, $s_l = s_r = 3$ 123


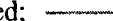
Figure 5.1: the relation between the vertical elevation g and the length of its projection onto the v -axis.....	129
Figure 5.2: Input output relations of Prandtl-Ishlinskii model (5.10).....	131
Figure 5.3: Input output relations of: (a) Initial loading curve (5.11); and (b). Prandtl-Ishlinskii model.....	132
Figure 5.4: Input-output characteristics of: (a) Initial loading curve $\varphi(r)$, and (b) Inverse of initial loading curve $\varphi^{-1}(r)$	134
Figure 5.5: Input-output characteristics of composition initial loading curve $\varphi(r)$ and its inverse $\varphi^{-1}(r)$	135
Figure 5.6: Compensation of symmetric hysteresis using inverse Prandtl-Ishlinskii model.....	139
Figure 5.7: Input-output relations of generalized Prandtl-Ishlinskii model of $\gamma_l(v)=1.3v-0.4$ and $\gamma_r(v)=1.7v-1.9$	151
Figure 5.8: Compensation of asymmetric hysteresis loops with inverse generalized Prandtl-Ishlinskii model of $\gamma_l(v)=v$ and $\gamma_r(v)=1.2v+1.9$	151
Figure 5.9: Input-output relations of generalized Prandtl-Ishlinskii model of $\gamma_l(v) = 8 \tanh(0.22v-0.6)$, $\gamma_r(v)= 7.7 \tanh(0.2v+0.1)+0.1$	152
Figure 5.10: Compensation of saturated hysteresis loops with inverse generalized Prandtl-Ishlinskii model $\gamma_l(v) = 8 \tanh(0.22v-0.6)$, $\gamma_r(v)= 7.7 \tanh(0.2v+0.1)+0.1$	153
Figure 5.11: Compensation of rate-dependent symmetric hysteresis nonlinearities at different excitation frequencies using inverse rate-dependent Prandtl-Ishlinskii model as a feedforward compensator.....	155
Figure 5.12: Compensations of asymmetric rate-dependent hysteresis nonlinearities at different excitation frequencies using inverse generalized rate-dependent Prandtl-Ishlinskii model as a feedforward compensator.....	156
Figure 5.13: Experimental setup for compensation of hysteresis nonlinearities of the piezoceramic actuator using inverse generalized Prandtl-Ishlinskii model as a feedforward compensator.	158
Figure 5.14: Comparisons of output-input responses of the generalized model with the measured responses ( , measured;  , model).....	159

Figure 5.15 Time histories of measured and model displacement responses (- - - - , measured; ————— , model). (b) Time histories of error in measured and model displacement responses.	160
Figure 5.16: Input-output characteristics of the inverse generalized Prandtl-Ishlinskii model.	161
Figure 5.17 (a) Comparison of time-history of error between the output displacement and the input voltage (————— , without inverse feedforward controller; ———— , with inverse feedforward controller). (b) Output-input characteristics of the piezo ceramic stage with Inverse feedforward compensator.	162
Figure 6.1: Hysteretic actuator.	166
Figure 6.2: Open-loop control with inverse compensation.	166
Figure 6.3: Composition of the Prandtl-Ishlinskii model.	168
Figure 6.4: Input-output characteristics of Prandtl-Ishlinskii models: (a) $\Pi_{\psi(r)}[v]$, (b) $\Pi_{\phi(r)}[v]$, and (c) $\Pi_{\eta(r)}[v]$	170
Figure 6.5: Input-ouptut ccharacteristics of initial loading curves (6.17), (6.18), and (6.19).	172
Figure 6.6: Comparison between the outputs of Prandtl-Ishlinskii models (6.16) (.....) and (6.20) (—————).	172
Figure 6.7: Illustration of inverse compensation of the Prandtl-Ishlinskii model.	176
Figure 6.8: Input-output characteristics of: (a) Inverse of Prandtl-Ishlinskii model, (b) Prandtl-Ishlinskii model, and (c) Compensation with the inverse Prandtl-Ishlinskii model.	180
Figure 6.9: (a) The input-output characteristics of the inverse compensation (b) Time histories of the error of the inverse compensation.	181
Figure 6.10: Input-output characteristics of: (a) Inverse of Prandtl-Ishlinskii model, (b) Prandtl-Ishlinskii model, and (c) Compensation with the inverse of the estimated Prandtl-Ishlinskii model.	183
Figure 6.11: (a) The output of the inverse compensation (b) Input-output characteristics of the error of the compensation (c) Time histories of the error.	184
Figure 7.1: Closed-loop control system with inverse compensation.	187

Figure 7.2: (a) Inverse compensation based on the estimated initial loading curve, (b) Control signal with $u_h \neq 0$ and $u_h = 0$, (c) Output of the inverse compensation with $u_h \neq 0$ and $u_h = 0$ (d) Desired trajectory $x_d(t)=12.5\sin(2.3t)$ and the system output $x(t)$, (e) Tracking errors with $u_h \neq 0$ and $u_h = 0$. (———, $u_h \neq 0$; ·······, $u_h = 0$). 198

Figure 7.3: Tracking errors of the output with $u_h \neq 0$ and $u_h = 0$, (a) without considering the inverse, (b) considering the exact inverse. 199

List of Tables

Table 3.1: Hysteresis properties of smart actuators.....	82
Table 3.2: Properties of the Prandtl-Ishlinskii hysteresis models.....	84
Table 4.1: Identified parameters of the classical Prandtl-Ishlinskii model.....	90
Table 4.2: Identified parameters of the classical Prandtl-Ishlinskii model using the reported measured data for two SMA and a magnetostrictive actuators.....	90
Table 4.3: Parameters of the generalized Prandtl-Ishlinskii model identified using the reported measured data for two SMA actuators and a magnetostrictive actuator.....	94
Table 4.4: Identified parameters for the generalized Prandtl-Ishlinskii models using the measured output-input characteristics of the piezoceramic actuator.....	94
Table 4.5: Percent errors between the model and measured displacement responses at different excitation frequencies.....	106
Table 4.6: Weighting constants C_{jf} applied in the minimization function for identification of parameters based upon magnetostrictive and piezoceramic actuator data.....	113
Table 4.7: Identified parameters of the generalized rate-dependent Prandtl-Ishlinskii model using rate-dependent play operator of linear ($s_l = s_r = 1$) and nonlinear ($s_l = s_r = 3$) envelope functions for the magnetostrictive and piezoceramic actuators.....	114
Table 4.8: Displacement and percent peak errors between responses of the models based on linear ($s_l = s_r = 1$) and nonlinear ($s_l = s_r = 3$) envelope functions of rate-dependent play operator and the measured data of the magnetostrictive actuator at different excitation frequencies.....	119
Table 4.9: Peak displacement and percent peak errors between responses of the models based on linear ($s_l = s_r = 1$) and nonlinear ($s_l = s_r = 3$) envelope functions of rate-dependent play operator and the measured data of the piezoceramic actuator at different excitation frequencies.....	124

Nomenclature

\bar{a}	Positive constant of the Krasnosel'skii-Pokrovskii operator.
a_1, a_2, a_3, a_4	Constants.
B	Flux density.
$B_o(t)$	The nonlinear function of the error of the inverse compensation.
b	Control gain.
b_n	Unknown positive parameter.
b_1, b_2, b_3, b_4	Constants.
$C[0, T]$	The space of continuous functions defined on the time interval $[0, T]$.
$C_m[0, T]$	The space of piecewise monotone continuous functions defined on the time interval $[0, T]$.
C_{if}	The weighting constant.
$E_r[.]$	The stop operator.
$E_r[.](t)$	The output of the stop operator.
$E_r[.](0)$	The initial condition of the stop operator.
$e^*(t)$	The error of the inverse compensation due to the numerical inversion.
$e(t)$	The error of the inverse compensation.
\tilde{f}	Material function in Duhem model.

$F_r[.](t)$	The output of the play operator.
$F_r[.](0)$	The initial condition of the play operator.
$F_r^+[.]$	The output of the play operator under increasing input.
$F_r^-[.]$	The output of the play operator under decreasing input.
$F_r[.]$	The play operator.
$g(.)$	Material function in Duhem model
\bar{g}	Dynamic density function.
G	Continuous increasing function.
H	Magnetic field.
\bar{h}	Dynamic function of the rate-dependent Prandtl-Ishlinskii model.
J	The error function.
$K_{\alpha\beta}[.](t)$	The output of the relay operator.
$K_{\alpha\beta}[.](0)$	The initial condition of the relay operator.
$K_{\alpha\beta}$	The relay operator.
L	The Krasnosel'skii-Pokrovskii operator.
$L[.](t)$	The output of the Krasnosel'skii-Pokrovskii operator.
$L[v](0)$	The initial condition of the Krasnosel'skii-Pokrovskii operator.
m_1, m_2	Constants for the dynamic density function \bar{g} .
N	Number of the points.

m_1, m_2	Constants for the dynamic function \bar{h} .
$\tilde{P}^{-1}(t)$	The numerical inverse of the hysteresis model.
$P(t)$	The output of the hysteretic actuator.
p	Density function.
\hat{p}	The density function of the inverse model.
\bar{P}	The dynamic density function of the of the rate-dependent model.
$\hat{\bar{P}}$	The dynamic density function of the inverse of the rate-dependent model.
\hat{p}^*	The estimated density function.
q	Positive constant of the Prandtl-Ishlinskii model based play operator.
Q	Positive integer in Bouc-Wen model.
r	The threshold of the Prandtl-Ishlinskii models.
\bar{r}	The dynamic threshold.
\hat{r}	The threshold of the inverse.
$\hat{\bar{r}}$	The threshold of the inverse the rate- dependent Prandtl-Ishlinskii model.
s_l	The order of the polynomial envelope function $\gamma_l(v)$.
s_r	The order of the polynomial envelope function $\gamma_r(v)$.
S_r	The generalized play operator.
$S_r[v](t)$	The output of the generalized play operator.

$S_r[v](0)$	The initial condition of the generalized play operator.
S_r	The generalized rate-dependent Prandtl-Ishlinskii model.
$S_r(v(t))$	The output of the generalized rate-dependent Prandtl-Ishlinskii model.
sg	Smooth function.
u	The control law.
u_h	The nonlinear term of the control law.
$v(t)$	The system input.
\dot{v}	Time rate of the input.
$v^*(t)$	The output of the inverse compensation.
$\bar{v}(k)$	The time rate of the input under discrete inputs.
$v(t)$	The system input.
$w(t)$	The output of the play operator.
$\bar{w}(t)$	The output of the rate-dependent play operator.
x	The system state space vector.
$y_o(t)$	The output of the Duhem model.
y_m	The measured displacement of the actuator.
Y	Continuous linear or nonlinear functions.
z_r	The order of the dynamic threshold.
$z_o(t)$	The output of the Bouc-Wen model.

$z(t)$	The output of the generalized play operator
$\bar{z}(t)$	The output of the generalized rate-dependent play operator.
z_i	Variables for the back-stepping approach.
α_i	The virtual control at the i th step.
α^*	Constant of Duhem model.
$\bar{\alpha}$	Constant of Bouc-Wen model.
α, β	Thresholds of the relay operator.
$\bar{\beta}$	Constant in Bouc-Wen model.
β_1, β_2	The constants of the higher-order dynamic threshold.
$\bar{\gamma}$	Constant in Bouc-Wen model.
γ_r, γ_l	The envelope functions of the generalized play operator.
$\gamma_l^{-1}, \gamma_r^{-1}$	The inverse of the envelope functions.
$\Gamma[\cdot](t)$	The output of the Presiach model.
$\Gamma[\cdot]$	The Presiach model.
δ_i	Positive design parameters.
ε	Constant for dynamic threshold.
ζ_1, ζ_2	The thresholds of the generalized play operator.
ζ	The initial state of the relay operator.

η	Initial loading curve.
$\Lambda[\cdot](t)$	The output of the Krasnosel'skii-Pokrovskii model.
Λ	The Krasnosel'skii-Pokrovskii model.
λ	Constant for dynamic threshold.
λ_1, λ_2	The constants of the higher-order dynamic threshold.
Π	The Prandtl-Ishlinskii model based play operator.
$\Pi[\cdot](t)$	The output of the Prandtl-Ishlinskii model based play operator.
$\bar{\Pi}$	The rate-dependent Prandtl-Ishlinskii model.
$\bar{\Pi}^{-1}$	The inverse of the rate-dependent Prandtl-Ishlinskii model.
$\bar{\Pi}^{-1}(v(t))$	The output of the inverse rate-dependent Prandtl-Ishlinskii model.
ρ	Constant of the density function.
σ	The ridge function of the Krasnosel'skii-Pokrovskii operator.
τ	Constant of the density function.
φ	Initial loading curve.
$\bar{\Phi}$	The generalized rate-dependent Prandtl-Ishlinskii model.
$\bar{\Phi}(v(t))$	The output of the generalized rate-dependent Prandtl-Ishlinskii model.
$\bar{\Phi}^{-1}$	The inverse of the generalized rate-dependent Prandtl-Ishlinskii model.
$\bar{\Phi}^{-1}(v(t))$	The output of the inverse generalized rate-dependent Prandtl-Ishlinskii model.
$\Phi[v](t)$	The output of the generalized Prandtl-Ishlinskii model.

- $\Phi^+[v](t)$ The output of the generalized Prandtl-Ishlinskii model under increasing input.
- $\Phi[v](t)$ The output of the generalized Prandtl-Ishlinskii model under decreasing input.
- $\Phi^{+1}[v](t)$ The output of the inverse generalized Prandtl-Ishlinskii model under increasing input.
- $\Phi^{-1}[v](t)$ The output of the inverse generalized Prandtl-Ishlinskii model under increasing input.
- ψ Initial loading curve.
- $\Omega[.](t)$ The output of the Prandtl-Ishlinskii model based stop operator.
- Ω The Prandtl-Ishlinskii model based stop operator.

Chapter 1: Introduction and Literature Review

1.1 Introduction

Ferromagnetic materials and smart actuators invariably exhibit hysteresis, which is a path-dependent memory effect where the output relies not only on the current state but also on the past output history. The presence of the hysteresis in smart actuators, such as piezoceramic, magnetostrictive and shape memory alloy actuators (SMA) has been widely associated with various performance limitations. These include the oscillations in the responses of the open-as well as closed-loop systems, and poor tracking performance and potential instabilities in the closed-loop system.

Considerable continuing efforts are thus being made to seek methods for effective compensation of hysteresis effects in order to enhance the tracking performance of smart actuators, particularly for closed-loop micro-positioning systems. The characterization and modeling of the hysteresis properties of smart actuators, however, is vital for designing efficient compensation algorithms. Considering that the hysteresis properties of such actuators are strongly dependent upon the type of materials, magnitude of input and the rate of input in a highly nonlinear manner, the characterizations as well as modeling of the phenomenon pose considerable challenges. For instance, a piezoceramic actuator generally exhibits symmetric minor and major hysteresis loops, while magnetostrictive and SMA actuators yield highly asymmetric hysteresis effects, which further depend upon the rate of input. Smart actuators also exhibit output saturation, which further contributes to the modeling challenge.

A number of hysteresis models have been proposed in the literature for characterizing the hysteresis properties of different materials and smart actuators. These could be broadly classified into phenomenological models [1-5] and physics-based models [6-15]. The most cited phenomenological models include the Preisach, Krasnosel'skii-Pokrovskii and Prandtl-Ishlinskii models. These models have been widely applied to characterize hysteresis properties of smart actuators and ferromagnetic materials. The rate-dependence of hysteresis effects, however, have been considered in only a few studies employing the Preisach model in conjunction with a dynamic density function [73]. The compensation of the hysteresis effects of smart actuators has been the primary focus of many reported studies. Control algorithms based on inverse hysteresis compensators have been suggested to be more effective in compensating the hysteresis effects [23, 30]. Some reported hysteresis models have thus been employed for deriving the inverse hysteresis models to serve as a compensator for the hysteresis effects, particularly these based on the Preisach model. The Preisach model, however, is not analytically invertible; numerical methods are thus employed to obtain approximate inversions of the model. The effectiveness of the approximate inversions in conjunction with different controllers in hysteresis compensation have been demonstrated in a few studies [31, 36].

Unlike the Preisach and Krasnosel'skii-Pokrovskii models, the Prandtl-Ishlinskii model offers an attractive and unique property of being analytically invertible. The Prandtl-Ishlinskii model may thus serve as an effective inverse-based hysteresis compensation method. The Prandtl-Ishlinskii model and its analytical inverse, however, have been limited only to symmetric and rate-independent hysteresis properties. The

inherent flexibility of the model, particularly with respect to the play operators, could permit effective characterization of asymmetric hysteresis effects and output saturation. The rate-dependent hysteresis effects could be also incorporated using this flexible feature. The greatest potential advantage of the Prandtl-Ishlinskii model lies in its analytical invertability, which could be extended for the rate-dependent and asymmetric hysteresis nonlinearities with output saturation. The resulting inverse model would be very attractive for real-time compensation of the hysteresis effects in a wide range of smart actuators with varying hysteresis nonlinearities.

This dissertation research proposes a generalized analytically invertible Prandtl-Ishlinskii model for characterizing rate-dependent symmetric as well as asymmetric hysteresis nonlinearities. A generalized play operator with different envelope functions is proposed for describing asymmetric hysteresis loops with output saturation, while the rate-dependent effects considered by a dynamic density function in the input. The validity of the proposed Prandtl-Ishlinskii formulations is demonstrated using the laboratory-measured hysteresis properties of piezoceramic, magnetostrictive and SMA actuators. The key properties of the proposed generalized model are described and employed in deriving the analytical inverse of the model for its application as a feedforward compensator. An error analysis of the inverse compensator is also presented, and the effectiveness of the compensator is demonstrated.

In this chapter, the relevant reported studies on characterization and modeling of hysteresis properties of smart actuators and materials, and hysteresis compensation methods are discussed. The studies, grouped under relevant subjects, are briefly described

to build essential background, and formulate the scope and objectives of the dissertation research.

1.2 Experimental Characterization of Hysteresis

The extreme challenges in describing the hysteresis in materials and smart actuators have been widely recognized, which are primarily to its strongly nonlinear and memory effects [1, 7]. Consequently, the hysteresis properties of different materials and smart actuators have been widely characterized through experimental means in order to enhance an understanding of the essential properties and to seek modeling methods. Although, the experimentally-measured hysteresis properties of ferromagnetic materials have been extensively reported, the hysteresis properties of smart actuators are reported in a fewer recent studies. This is mostly attributed to recent growth in application of the smart actuators in various sectors, such as micro-positioning sectors. The ferromagnetic materials and smart actuators, generally, exhibit major and minor hysteresis loops in the output-input characteristics and output saturation. As an example, Figure 1.1 illustrates the measured hysteretic relation between the applied magnetic field and the response flux density of a ferromagnetic material. The reported results have shown very similar trends in view of the hysteresis phenomenon [1, 82], which are summarized below:

- The output flux density (B) depends on the past and current values of the input magnetic field (H);
- The output flux density (B) increases as the magnetic field (H) increases and decreases as the magnetic field decreases (H);
- The width of the hysteresis loop, also referred to as the coercivity of the material, corresponding to zero magnetic flux density output (B), increases as the amplitude of the input magnetic field (H) increases;

- The major hysteresis loop can be formed by decreasing and increasing the input of the magnetic fields between the extreme minimum magnetic field (H_{\min}) and maximum (H_{\max}) values;
- The paths for increasing inputs in the (H, B) plane are nonintersecting as are paths for decreasing inputs;
- The output flux density (B) tends to saturate as the input field (H) exceeds certain limit that may depend upon the properties of the material.
- The hysteresis loops are generally considered rate-independent and show insignificant variations under inputs in the low frequency range.

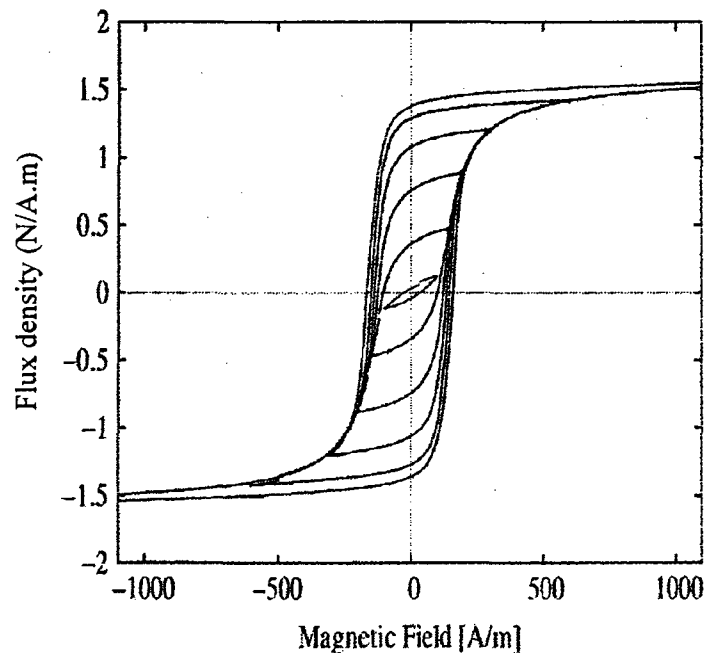


Figure 1.1: Measured hysteresis properties of ferromagnetic materials [1].

The reported experimental studies on smart actuators are systematical reviewed to enhance an understanding of the hysteresis properties of different actuators, particularly the piezoceramic, SMA and magnetostrictive actuators. The piezoceramic actuators have

been the focus of relatively larger number of studies. This may be attributed to their wide applications in micro-positioning applications. These studies consistently show that piezoceramic actuators exhibit strong hysteresis effects between the measured input voltage and output displacement responses. Hysteresis between the command voltage and the actuator position is known to cause inaccuracy and oscillations in the system response, which may lead to instability of the closed-loop system [31]. Ge and Jouaneh [22] performed measurements to characterize the hysteresis properties of a piezoceramic actuator, developed by Physik Instrument Company. The measured data was used to test the validity of the modified Preisach model, proposed by the authors. The actuator used in the study provided a nominal displacement of 20 μ m under an excitation of 1000 V. A capacitive sensor with a resolution of 2.5 nm was used to measure the displacement of the actuator. The measurements were performed under sinusoidal input voltages of constant amplitude (800 V) at two different distinct frequencies (0.1 and 100 Hz). The study concluded that both excitations yield similar hysteresis suggesting negligible effects of the rate of input. The data reported for the 100 Hz excitation, however, revealed slightly higher hysteresis.

Hu and Ben Mrad [64] measured the hysteresis of a piezoceramic actuator, where the nominal displacement was 3000 nm under an input voltage of 100 V. The width of the measured voltage-to-displacement was obtained as 15% of the maximum piezoceramic expansion under a very low frequency. Yu et al. [34] measured the hysteresis of a piezoceramic bimorph actuator, and concluded that the hysteresis is rate-independent only up to 10 Hz. Hughes and Wen [20] measured the hysteresis properties of piezoceramic patches and Nitinal SMA muscles coupled with a cantilever beam. The

measurements were performed to characterize the minor hysteresis loops and wiping-out properties of the beam coupled with the selected actuator, while the beam deflection was measured using strain gauges. The piezoceramic patches showed high degree of congruency in the comparable minor loops and the wiping out property was largely satisfied. The effects of different preloads on the actuators' hysteresis were also investigated by applying high magnitude static force to the tip of the beam. The results showed hysteresis nonlinearities, while the peak displacement response decreased with the preload. All of the reported studies on piezoceramic actuators observed an increase in the width of hysteresis loop with an increase in the excitation magnitude.

The hysteresis properties of shape memory alloys (SMA) and magnetostrictive actuators have also been investigated in a few studies [21, 28, 33]. Such actuators show hysteresis effects together with output saturation which dependent on the type of actuator and nature of input. Magnetostriction is the phenomenon associated with strong coupling between the magnetic and mechanical properties of the materials. Some ferromagnetic materials as Terfenol-D show this phenomenon between the output strain and the applied input current. The output strains are produced due to the applied current and thus the magnetic field, which tends to alter the magnetization of the material. Where the piezoceramic actuators require high voltages (50-100 V) to produce desired strains, magnetostrictive actuators respond to significantly lower voltages. Consequently, these actuators can be excited under low voltage. The SMAs, such as nickel-titanium and copper zinc aluminum alloys, exhibit capability to recover the strain (approximately up to 10%) without permanent deformation [56]. All of the reported studies have considered experimental characterization under sinusoidal inputs, with only few exceptions. Yu et al.

[34] measured the hysteresis properties of a piezoceramic actuator under sinusoidal and triangular input voltage waveforms. The results showed dependence of the hysteresis loop under a sinusoidal input was observed to be larger than that under the triangular input. This could be attributed to the difference in the rates of the two input waveforms. While a triangular waveform yields a constant magnitude of the rate of input, the sinusoidal waveform yields varying rate.

Yu et al. [34] showed that the hysteresis effect in a piezoceramic actuator is rate-independent up to 10 Hz, beyond that the hysteresis of the actuator is rate-dependent and the measured peak displacement amplitude decreases as the frequency of the input voltage is increased. In a similar manner, Ben Mrad and Hu [61] performed measurements to characterize the hysteresis properties of a piezoceramic actuator at different excitation frequencies. The study concluded that the width of the hysteresis loop increases to 38.6% of the measured displacement amplitude at 800 Hz, compared to 15% at a very low frequency. Another study showed that hysteresis of a Terfenol-D magnetostrictive actuator is rate-independent up to 5 Hz [33]. An increase in the frequency of input current resulted in larger width of the hysteresis loop and lower peak-to-peak displacement response. The measured data revealed that the peak-to-peak displacement of the magnetostrictive actuator decreased to approximately 68% of its maximum expansion at a low frequency, when the excitation frequency was increased up to 300 Hz.

1.3 Hysteresis Models

The measured hysteresis properties have been extensively applied to formulate a number of phenomenological and to identify model parameters applicable for specific actuators. A large number of analytical models have been proposed in the literature to characterize the hysteresis properties of smart actuators and ferromagnetic materials. The reported hysteresis models can be classified into physics-based models [6- 15] and phenomenological models [1- 5]. The physics-based models are generally derived on the basis of a physical measure, such as energy, displacement, or stress-strain relationship. Alternatively, the phenomenological models describe the hysteresis properties without attention to the physical properties of the hysteretic system. Many of these models were initially proposed for specific physical systems and were later generalized for applications to other systems.

1.3.1 PHYSICS-BASED HYSTERESIS MODELS

The physics-based models are generally derived on the basis of a physical measure, such as displacement, energy, or stress-strain relationship. Jiles and Atherton [15] developed a hysteresis model on the basis of observed physical properties of ferromagnetic materials. The model comprised analytical expression relating the reversible and irreversible motions of ferromagnetic material particulars. The model was subsequently used by Smith and Ounaies [9] for describing the hysteresis phenomenon of piezoceramic materials. Ikuta et al. [6] proposed a mechanical model to characterize hysteresis in SMA actuators using the stress-strain relationships of the SMA materials. Smith et al. [8] proposed a nonlinear energy-based hysteresis model in conjunction with

the operator-based Preisach model for characterizing hysteresis of magnetostrictive actuators.

The physics-based hysteresis models generally require comprehensive knowledge of the physical phenomenon for the hysteretic system, which may be difficult for particular materials or actuators. Furthermore, the generalization of a physics-based hysteresis model is quite difficult for application to different actuators and materials, since these may encompass different physics properties and structures. Furthermore, inversions of physics-based models have not been explored for applications in hysteresis compensation of smart material actuators. Although the physics-based models can effectively characterize symmetric as well as asymmetric hysteresis effects [6], the rate-dependent hysteresis effects have not been attempted through such models. Considering the complexities associated with physics-based models, the phenomenological models have been emphasized for simulation of the hysteresis effects of different smart actuators and for compensators design. A number of phenomenological models have evolved for characterizing the hysteresis nonlinearities. The primary goal of these models is to accurately predict the hysteresis in order to study the hysteresis effects and to facilitate the design of controllers for compensating the hysteresis effects [20-30, 53, 54]. The most widely cited models based on the input and output behaviors include: the operator based hysteresis models such as Preisach model [1], Krasnosel'skii-Pokrovskii model [4], Prandtl-Ishlinskii model [2]; and differential equation-based hysteresis models such as Duhem model [3] and Bouc-Wen model [17]. These models are briefly described below.

1.3.2 DIFFERENTIAL EQUATION-BASED PHENOMENOLOGICAL MODEL

These models generally constitute a nonlinear differential equation relating the output to the magnitude and direction of the input. The Duhem and the Bouc–Wen models are the most widely used differential equation based models.

Duhem Model

Duhem model is a differential equation-based hysteresis model, where the output $x(t)$ is affected by change in the direction of the input $v(t)$. The output-input relationship is expressed by the following differential equation [3]:

$$\dot{y}_o(t) = \tilde{f}_1(y(t), v(t)) \dot{v}^+(t) - \tilde{f}_2(y(t), v(t)) \dot{v}^-(t) \quad (1.1)$$

where

$$\dot{v}^\pm(t) = \frac{|\dot{v}(t)| \pm \dot{v}(t)}{2} \quad (1.2)$$

where the input $v(t)$ and the output $y_o(t)$ are continuous and differentiable functions over the interval $[0, T]$. An increase in input $v(t)$ causes the output $y_o(t)$ to increase along a particular path. The output, however, tends to decrease along a different path under a decreasing input. This behavior of the output can be expressed as [3]:

$$\frac{dy_o}{dv} = \begin{cases} \tilde{f}_1(v(t), y_o(t)) & \text{for } \dot{v}(t) > 0 \\ \tilde{f}_2(v(t), y_o(t)) & \text{for } \dot{v}(t) < 0 \end{cases} \quad (1.3)$$

Hodgdon and Coleman [18] proposed a differential equation for the input magnetic field (H) and the output flux density (B) to characterize hysteresis in ferromagnetic materials

using Duhem model. This model is analytically presented by the following differential equation:

$$\dot{B}(t) = \alpha^* |\dot{H}(t)| (\tilde{f}(H(t)) - B(t)) + \dot{H}(t)g(H(t)) \quad (1.4)$$

The change in the output B with respect to the input H was expressed by the following differential equations:

$$\frac{dB}{dH} = \begin{cases} \alpha^* [\tilde{f}(H) - B] + g(H) & \dot{H} > 0 \\ -\alpha^* [\tilde{f}(H) - B] + g(H) & \dot{H} < 0 \end{cases} \quad (1.5)$$

where α^* is a constant, and \tilde{f} and g are referred to as material functions. Using (1.4) and (1.5) Hodgdon-Coleman model can also be expressed as [3]:

$$\frac{dB}{dH} = \alpha^* \operatorname{sgn}(\dot{H}) [\tilde{f}(H) - B] + g(H) \quad (1.6)$$

where

$$\operatorname{sgn}(\dot{H}) = \begin{cases} 1 & \text{for } \dot{H} > 0 \\ -1 & \text{for } \dot{H} \leq 0 \end{cases} \quad (1.7)$$

The stability of the Duhem model is ensured by the following properties of the material functions, \tilde{f} and g :

- a) \tilde{f} is a piecewise smooth and monotonically increasing odd function and the derivative $\tilde{f}'(H)$ is non-zero, while $\tilde{f}'(\infty)$ is finite, such that :

$$\tilde{f}(H) = -\tilde{f}(-H) \quad \& \quad \lim_{H \rightarrow \infty} \frac{d\tilde{f}(H)}{dH} < \infty \quad (1.8)$$

- b) g is a piecewise continuous even function of H , and its derivative $g'(\infty)$ is finite, such that:

$$g(H) = g(-H) \ \& \ \lim_{H \rightarrow \infty} \frac{dg(H)}{dH} < \infty \quad (1.9)$$

- c) The materials function must satisfy the following for characterizing hysteresis properties:

$$\lim_{H \rightarrow \infty} [\tilde{f}'(H) - g(H)] = 0 \quad (1.10)$$

- d) The material functions must satisfy the following inequalities for all finite values H , $\tilde{f}'(H)$, and $g(H)$:

$$\tilde{f}'(H) \geq g(H) \geq \alpha e^{\alpha H} \int_H^{\infty} [\tilde{f}'(\xi) - g(\xi)] e^{-\alpha \xi} d\xi \quad (1.11)$$

The above-stated properties of the material functions generally impose severe limitations for the model applications in control system design. The most important property of the Hodgdon-Coleman model, however, is the existence of the minor hysteresis loops in a stable manner [3]. Furthermore, the output of the Duhem model is rate-independent and it yields symmetric hysteresis loops.

Bouc-Wen Model

The Bouc-Wen model [17] is a nonlinear differential equation-based model, which originates from the Bouc model presented in [16]. The model has been extensively used to describe the hysteretic behaviour between the applied displacement and the output force in wide ranges of mechanical systems. This model is presented by the following differential equation:

$$\dot{z}_o = \bar{\alpha} \dot{v} - \bar{\beta} |\dot{v}| (z_o) |z_o|^{Q-1} + \bar{\gamma} \dot{v} |z_o|^Q \quad (1.12)$$

where $z_o(t)$ is output, $v(t)$ is input and Q is a positive integer. The output of the hysteresis model is strongly dependent upon the model constants $\bar{\alpha}$, $\bar{\beta}$, and $\bar{\gamma}$. This differential

equation-based model does not contain material functions that tend to limit the applicability of the Duhem model. The model parameters are generally derived from the measured hysteresis of a particular material or system. Different forms of Bouc-Wen model have been proposed to suit the observed hysteresis properties of different systems, materials, and actuators [78, 79]. Hysteretic systems including hysteretic isolators [18] and magnetorheological fluid dampers [19] are some examples. The major limitations of the Bouc-Wen models are associated with the parameters identifications. The differential equation-based models are not invertible and thus cannot be applied in inverse model-based hysteresis compensation.

1.3.3 OPERATOR-BASED HYSTERESIS MODELS

A number of operator-based phenomenological hysteresis models have been proposed to describe the hysteresis in different smart actuators. Unlike the differential equation-based model, the operator-based models are considered to be better suited for the design of control algorithms for compensating hysteresis effects due to their invertability. These models include: the Preisach model [1, 5]; Krasnosel'skii-Pokrovskii model [4]; and Prandtl-Ishlinskii model [2]. Such models have been widely applied for modeling hysteresis nonlinearities in materials and smart actuators [20-30], and are briefly described below.

Preisach model

The Preisach model has been most widely applied for characterizing the hysteresis properties of ferromagnetic materials and smart actuators [1]. The mathematical formulations of the Preisach model and its application in different fields

have been thoroughly described by Mayergoyz [1]. This classical Preisach model was developed to characterize hysteresis in the ferromagnetic materials [1]. This model comprised a set of relay operators $K_{\alpha\beta}$. For a given input $v(t) \in C_m[0, T]$ and initial state $\xi \in \{-1, 1\}$, the output of the relay operator $K_{\alpha\beta}[v](t)$ is expressed as [1]:

$$K_{\alpha\beta}[v](t) = \begin{cases} +1 & \text{for } v(t) \geq \alpha \\ -1 & \text{for } v(t) \leq \beta \\ K_{\alpha\beta}[v](0) & \text{for } v(t) < \alpha \text{ \& } v(t) > \beta \end{cases} \quad (1.13)$$

where $K_{\alpha\beta}[v](0)$ is given by:

$$K_{\alpha\beta}[v](0) = \begin{cases} +1 & \text{for } v(0) \geq \alpha \\ -1 & \text{for } v(0) \leq \beta \\ \xi & \text{for } v(0) < \alpha \text{ \& } v(0) > \beta \end{cases} \quad (1.14)$$

The above operator forms a rectangular loop relating the input and the output of a hysteretic system, where the output of the operator is either +1 or -1 depending on the value of the current input. The constants α and β define the switching thresholds of the input corresponding to upward and downward shifts in the output, as illustrated in Figure 1.2.

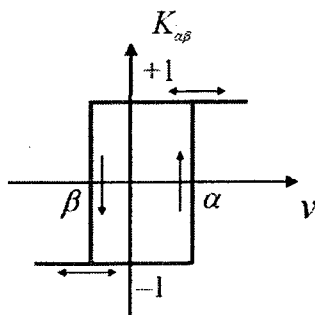


Figure 1.2: Relay hysteresis operator [1, 82].

The output of the relay operator switches from -1 to +1 when the current input is larger than α , and from +1 to -1 when the current input is less than β . It is apparent that the model employs a discontinuous hysteresis operator. For a given input $v(t) \in C_m[0, T]$, the output of the Preisach hysteresis model, which is formulated using the above operator is expressed as [1]:

$$\Gamma[v](t) = \iint_{\alpha \geq \beta} p(\alpha, \beta) K_{\alpha\beta}[v](t) d\alpha d\beta \quad (1.15)$$

where $p(\alpha, \beta)$ is an integrable positive density function, which is identified from the measured data for a particular material or a smart actuator. The argument of the operator is written in square brackets to indicate the functional dependence, since it maps a function to another function.

The Preisach model is completely characterized by two properties [1]: wiping-out and congruent minor-loop properties. The wiping out property means that the output is affected only by the current input and the history of the output, while the effect of all other inputs is wiped out. The congruent minor-loop property requires that all equivalent minor loops be similar. Two minor loops are said to be equivalent if they are generated under monotonically varying inputs of identical amplitudes.

Preisach model (1.15) has undergone many refinements over the past two decades to broaden its applications to a wide range of actuators and materials [1, 20-22, 66]. Different forms of the classical Preisach model have thus evolved to model hysteresis in various materials and smart actuators. Ge and Jouaneh [22] proposed a modified relay operator to characterize the hysteresis in a piezoceramic actuator. The relay operator with threshold values of '-1' and '+1' is replaced by a modified operator with threshold values

of '0' and '+1'. This was based upon the dipole's polarization of piezoceramic materials occurring in only one direction. Hughes and Wen [20] proposed the Preisach model for characterizing hysteresis in piezoceramic and SMA actuators. The study proposed a density function in the form of a second-order polynomial and investigated the fundamental properties of the Preisach model for describing the hysteresis in both the materials. Gorbet et al. [21] applied the first-order-decreasing curves technique to identify the density function (Preisach function) of the Preisach model. In this study different forms of the Preisach functions were explored for characterizing the hysteresis nonlinearities of two-wire and single wire SMA actuators.

Krasnosel'skii-Pokrovskii model

Krasnosel'skii-Pokrovskii operator is a hysteresis operator that is derived from the Preisach relay operator [4]. This operator is constructed based on two functions that are bounded by two piecewise Lipschitz continuous functions. A ridge function is defined in the following manner for formulation of the Krasnosel'skii-Pokrovskii operator:

$$\sigma(x) = \begin{cases} -1 & \text{for } x < 0 \\ -1 + \frac{2x}{\bar{a}} & \text{for } 0 \leq x \leq \bar{a} \\ 1 & \text{for } x > \bar{a} \end{cases} \quad (1.16)$$

where \bar{a} is a constant in the output-input characteristics of the operator that is shown in Figure 1.3. For a given input $v(t) \in C [0, T]$ the output of the Krasnosel'skii-Pokrovskii operator can be expressed as:

$$L(t) = \begin{cases} \max(L(t_-), \sigma(v(t) - \alpha)) & \text{for } v(t) > v(t_-) \\ \min(L(t_-), \sigma(v(t) - \beta)) & \text{for } v(t) < v(t_-) \\ L(t_-) & \text{for } v(t) = v(t_-) \end{cases} \quad (1.17)$$

where the $L(t)$ is the output of the operator and α and β are constants similar to these defined in the relay operator. The Krasnosel'skii-Pokrovskii operator maps $C [0, T]$ to $C [0, T]$ [4]. Considering the finite slope of the operator, it can be concluded that the operator is Lipschitz continuous. The output of the Krasnosel'skii-Pokrovskii model, $\Lambda[v](t)$, is expressed by [4]:

$$\Lambda[v](t) = \iint_{\alpha \geq \beta} p(\alpha, \beta) L[v](t) d\alpha d\beta \quad (1.18)$$

where $p(\alpha, \beta)$ is a integrable positive density function.

The Krasnosel'skii-Pokrovskii model has been used to model the hysteresis properties of different smart actuators. Banks et al. [27] introduced the properties of the Krasnosel'skii-Pokrovskii model to characterize hysteresis nonlinearities in SMA actuators. Galinaities [28] employed the Krasnosel'skii-Pokrovskii operator instead of the relay operator in the Preisach model to characterize and to compensate hysteresis nonlinearities of a piezoceramic actuator.

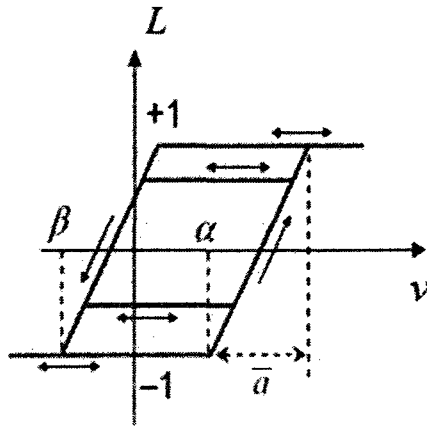


Figure 1.3: Krasnosel'skii-Pokrovskii operator [4, 82].

Prandtl-Ishlinskii model

Similar to the Preisach model, the Prandtl-Ishlinskii model is constructed using the play or stop hysteresis operators. Unlike the discontinuous relay operators in the Preisach model, the play and stop operators are continuous hysteresis operators which are characterized by the input v and the threshold r . A detailed discussion about these operators can be found in [2]. The stop operator has been proposed to characterize the elastic-plastic behavior in continuum mechanics [2]. Figures 1.4 and 1.5 illustrate the input-output characteristics of the play and stop operators, respectively. Figure 1.5 illustrates the linear stress-strain relationship as per Hooke's law, when the stress is below the yield stress r , which is denoted as the threshold. Analytically let $C_m [0, T]$ represents the space of piecewise monotone continuous functions. For any input $v(t) \in C_m [0, T]$, the output of the stop operator, $E_r[v](t)$ is defined by:

$$\begin{aligned}
 E_r[v](0) &= e_r(v(0)) \\
 E_r[v](t) &= e_r(v(t) - v(t_i) + E_r[v](t_i)); \quad t_i \leq t < t_{i+1} \quad \text{and} \quad 0 \leq i \leq N-1 \quad (1.19) \\
 e_r(v) &= \min(r, \max(-r, v))
 \end{aligned}$$

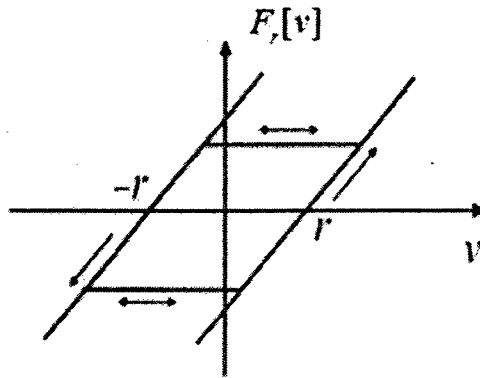


Figure 1.4: Play hysteresis operator [2, 82].

The one dimensional play operator has been described by the motion of a piston within a cylinder of length $2r$. The position of the center of the piston is represented by coordinate v , while the cylinder position is given by w . For any input $v(t) \in C_m[0, t_E]$, the output of the play operator, $F_r[v](t)$ is defined by:

$$\begin{aligned} F_r[v](0) &= f_r(v(0), 0) = w(0), \\ F_r[v](t) &= f_r(v(t), F_r[v](t_i)); t_i \leq t < t_{i+1} \text{ and } 0 \leq i \leq N-1 \\ f_r(v, w) &= \max(v-r, \min(v+r, w)). \end{aligned} \quad (1.20)$$

where $0 = t_0 < t_1 < \dots < t_N = T$ is a partition of $[0, T]$ such that the function v is monotone on each of the sub-intervals $[t_i, t_{i+1}]$.

The maximum value of the stop operator is determined by threshold r in the (v, w) plane. From definitions (1.19) and (1.20), it can be proven that operator $F_r[v]$ is the complement of operator $E_r[v]$ and they are related in the following manner for any piecewise monotone input function $v(t) \in C_m[0, T]$ and threshold $r \geq 0$ [2]:

$$F_r[v](t) + E_r[v](t) = v(t) \quad (1.21)$$

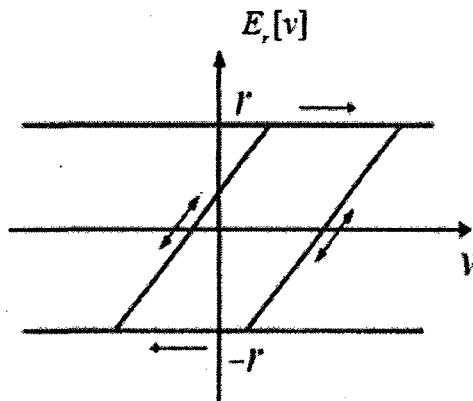


Figure 1.5: Stop hysteresis operator [2, 82].

Due to the nature of the play and stop operators, the above is based on $v(t) \in C_m$ $[0, T]$ of piecewise monotone continuous functions. These, however, can be extended to space C $[0, T]$ of continuous functions. Furthermore, play and stop operators are continuous in time and in space. Continuity in time is significant from a physical perspective, while the continuous parameter dependence is important for development of practical parameter estimation method [30]. Using the stop operator $E_r[v](t)$, the output of the Prandtl-Ishlinskii model, which maps $C[0, T]$ into $C[0, T]$, is defined by [2]:

$$\Omega[v](t) = \int_0^R p(r) E_r[v](t) dr \quad (1.22)$$

where $\Omega[v](t)$ is the output of the Prandtl-Ishlinskii model and $p(r)$ is an integrable density function, satisfying $p(r) \geq 0$, to be identified from the experimental data. The output of the Prandtl-Ishlinskii model is also defined using the play operator $F_r[v](t)$, such that [2]:

$$\Pi[v](t) = qv(t) + \int_0^R p(r) F_r[v](t) dr \quad (1.23)$$

Owing to the unity slope of the play and stop operators, it can be concluded that the outputs of the Prandtl-Ishlinskii models (1.22) and (1.23) are Lipschitz continuous under Lipschitz continuous inputs [2]. Since the density function $p(r)$ vanishes for large values of r , the choice of $R = \infty$ as the upper limit of integration is widely used in the literature as a matter of convenience [2]. Because the play and stop hysteresis operators and density function, defined above, are rate-independent, the Prandtl-Ishlinskii models are applicable for characterizing only rate-independent hysteresis. The Prandtl-Ishlinskii model is a continuous hysteresis model and its inversion has also been derived

analytically [2]. However, the Prandtl-Ishlinskii models, based on the play or the stop operators, are limited to symmetric hysteresis loops due to symmetric properties of the hysteresis operators.

1.3.4 RATE-DEPENDENT HYSTERESIS MODELS

A few operator-based hysteresis models have been proposed to characterize the rate-dependent hysteresis effects [33, 34, 64, 68, 73]. Many of these models were originally proposed for rate-independent hysteresis properties and were later modified to characterize rate-dependent hysteresis. The most common approach to account for rate-dependent effects is to apply a dynamic density function in the classical rate-independent hysteresis model. Mayerqoyz [73] proposed a rate-dependent Preisach model by introducing the time rate of the output in the density function to characterize rate-dependent hysteresis phenomenon. Yu et al. [34] characterized the rate-dependent hysteresis in a piezoceramic actuator using a dynamic density function incorporating the time rate of the input. The study demonstrated the effect of the rate by evaluating the outputs corresponding to input voltages at two distinct frequencies 0.05 and 5 Hz. Ben Mrad and Hu [64] employed the dynamic density function in the Preisach model, where the input was replaced by applying average rate of the input. Model results were evaluated under sinusoidal inputs at six distinct frequencies in the 0.1 to 800 Hz range. The model validity was demonstrated using the measured responses of a piezoceramic actuator, which were presented by only six distinct data points in the major hysteresis loop. Ang et al. [68] proposed a density function in conjunction with the Prandtl-Ishlinskii model and the deadzone operators to characterize the rate-dependent hysteresis

in a piezoceramic actuator. The validity of this model was demonstrated in terms of sinusoidal inputs between 1 and 19 Hz excitation frequencies. The proposed dynamic model reduced the maximum hysteresis error by more than 50%, compared to that attained from the rate-independent hysteresis model.

The above-reported studies were mostly based on the Preisach model coupled with a dynamic density function comprising the rate of either input or the output. This approach, however, may offer limited ability to describe the rate-dependent hysteresis. Alternatively, a dynamical model coupled with the Preisach model was proposed by Tan and Baras [33] in an attempt to characterize the rate-dependent hysteresis effects in a magnetostrictive actuator. The study showed model validity in predicting the major loops under inputs up to 300 Hz.

1.4 Hysteresis Compensation

The hysteresis in smart actuators has been associated with oscillations and poor tracking performance of the closed-loop system. Consequently considerable efforts have been made towards design of controllers for compensation of hysteresis. A vast number of controllers have been proposed to reduce the error due to hysteresis effects. The proposed control algorithms could be classified in two broad categories, namely non-inverse based control methods and inverse based control methods.

1.4.1 NON-INVERSE-BASED CONTROL METHODS

Compensation of hysteresis nonlinearities has been carried out in many studies without considering the inverse of the hysteresis models. Model-based hysteresis

compensation methods employ the phenomenological hysteresis models to construct controllers to compensate for the actuator hysteresis. A number of control methods have been proposed to compensate for smart actuators such as robust adaptive [55], energy-based [56, 60], and sliding model control systems, which employ the hysteresis model of the actuator for constructing the controller. Su et al. [55, 59] proposed an adaptive controller that is employed to control a nonlinear system preceded by unknown Prandtl-Ishlinskii hysteresis nonlinearities. In this study, the proposed controller leads to the desired output and the global stability was presented. Gorbet et al. [56] proposed a control approach based on the energy to control a SMA actuator, which showed hysteresis nonlinearities. The study employed the Preisach model, and verified the energy properties and the state space of the model. The minimum energy states were recommended to formulate the controller synthesis and the passivity was established for the relationship between the input and the time rate of the Preisach model output on the basis of the energy. The results demonstrated the effectiveness of the method in compensating the hysteresis of the SMA actuator. Cruz-Hernandez and Hayward [57] proposed a hysteresis compensation method for piezoceramic and SMA actuators based on shifting of the phase of the periodic signal. The method employed a phaser comprising a parallel combination of a linear filter and a rate-independent Preisach hysteresis model, and concluded that the method could reduce the major and minor hysteresis loops in piezoceramic and SMA actuators. Liaw et al. [81] proposed a sliding model adaptive controller to control a piezoceramic actuator. The piezoceramic actuator is characterized using electromechanical model which is analytically expressed via second-order-

differential equation. In this study, the results show the capability of the proposed sliding mode controller to compensate the hysteresis nonlinearities of the piezoceramic actuator.

The control methods for compensation of hysteresis effects have been also employed for differential equation-based hysteresis models, such as Bouc-Wen and Duhem models. Su et al. [67] used the Duhem model to control a nonlinear system preceded by known hysteresis using adaptive control method. The solution properties of the model were combined with the adaptive control technique. However, the strong nonlinearity together with the lack of exact mathematical properties of the differential models poses complex challenge for the control system design and its real-time control application.

1.4.2 INVERSE MODEL-BASED METHODS

The inverse model-based hysteresis compensation methods generally employ a cascade of a hysteresis model and its inverse together with a controller to compensate for the hysteresis effects. These methods, however, necessitate the formulation of the hysteresis model inverse, which is often a challenging task. The concept of an open-loop inverse control system for compensation of hysteresis effects is shown in Figure 1.6, where v is the input, v^* is the output, and P and P^{-1} are the hysteresis model and its inverse, respectively. This method is pioneered by Tao and Kokotovic [31], and involves the formulation of the inverse operator of the hysteretic system. Their study developed a control algorithm to compensate the hysteresis nonlinearities of a system comprising a linear plant preceded by a hysteresis block representing a hysteretic actuator. An

adaptive hysteresis inverse compensator is cascaded with the hysteretic system to mitigate the effects of hysteresis.

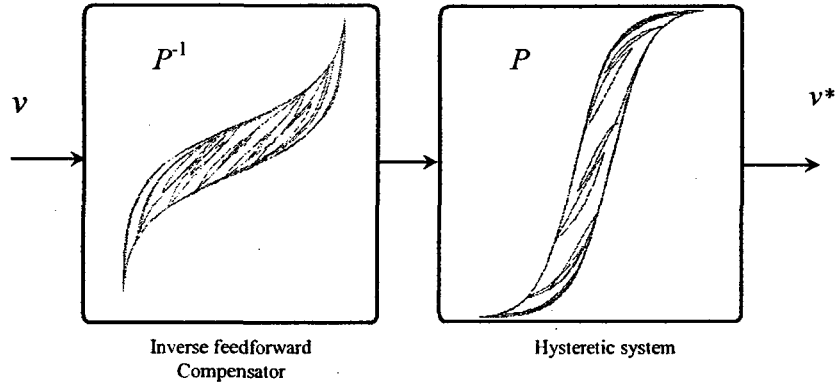


Figure 1.6: Open-loop inverse control system.

Considerable efforts have also been made in deriving the inverse phenomenological operator base hysteresis models in order to seek inverse-based hysteresis compensation. These efforts have resulted in either numerical or analytical inversions of the hysteresis models. The numerical inverse of a model, however, is an approximate right inverse. For a given input $v(t)$, the application of the approximate inverse $\tilde{P}^{-1}[\cdot]$ in the compensator, shown in Figure 1.7, yields an output v^* , such that the output of hysteretic system P is close to v . The evaluation of approximate inverse \tilde{P}^{-1} depends on the initial state of the model $P[v](0)$. The numerical methods employ a preselected range of the input $[v_{\min}, v_{\max}]$. The output of the inverse compensation can be expressed analytically as the composition of P and \tilde{P}^{-1} :

$$v^*(t) = P \circ \tilde{P}^{-1}[v](t) \quad (1.24)$$

Owing to the approximate inverse, the error of the numerical inverse can be defined as:

$$e^*(t) = v(t) - v^*(t) \quad (1.25)$$

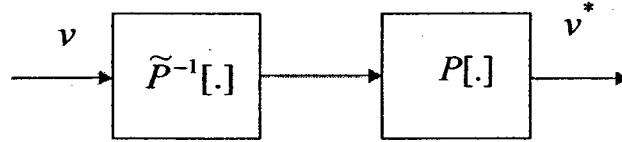


Figure 1.7: Illustration of numerical hysteresis inversion.

Preisach and Krasnosel'skii-Pokrovskii models are not analytically invertible. Different numerical methods have been developed to obtain inversions of these models [23, 26, 41]. Ge and Jouaneh [23] used inverse Preisach model, which was obtained using a numerical algorithm, as a feedforward compensator with PID feedback control system to reduce the hysteresis nonlinearities in a piezoceramic actuator. Inversion of the Krasnosel'skii-Pokrovskii model was applied by Galinaitis [27] in open-loop control system to compensate hysteresis of a piezoceramic actuator. In this study, compensation of hysteresis nonlinearities was demonstrated for sinusoidal inputs of different amplitudes at a low frequency of 0.05 Hz. In a similar manner, Song et al. [41] proposed a modified Preisach model to characterize and to compensate the hysteresis nonlinearities in a piezoceramic actuator with PD-lag and PD-lead controllers with the numerical inverse of the modified model in a closed-loop control system. Reduction in hysteresis nonlinearities was demonstrated experimentally for major and minor hysteresis loops under low excitation frequencies (0.5 Hz). Tan and Baras [25] applied inverse Preisach model, which is obtained numerically, in an adaptive control algorithm to compensate the hysteresis nonlinearities of a magnetostrictive actuator. Janocha and Kuhnen [53] compensated the hysteresis effects of a piezoceramic actuator using inverse Prandtl-

Ishlinskii model, which is constructed numerically, in an open-loop control system. In addition to the above mentioned model-based inverse methods, neural networks and fuzzy system models have also been presented to compensate the hysteresis nonlinearities of the smart actuators by constructing the inverse model [62, 63, 80].

The compensation based numerical inversions of the hysteresis models exhibit several limitations. Firstly, the numerical inverse of model can be considered only as an approximate inverse. This approximation tends to cause errors, when the numerical inverse is used as a feedforward compensator to compensate for hysteresis nonlinearities. Secondly, a numerical inverse of a hysteresis model cannot be considered to be unique. Different numerical algorithms or different limits in the applied input may yield different solutions of the inverse. Furthermore, a numerical inverse is only applicable for the specified input and the initial conditions. The numerical inverse is also computationally intensive, which may limit its real-time control applications. Finally, a numerical inverse of the hysteresis models has not been attempted to include the rate dependence.

The numerically-derived model inversion yields certain degree of error, and thus the tracking error in the output of compensated system responses. The error of the inverse compensation methods based on numerical inversions has not been attempted. While the majority of the studies consider the compensation error to be bounded for the controller design. The stability of the closed-loop control system comprising the controlled plant preceded by the numerical inverse compensation cannot be established due to uncertain inversion error.

Unlike the Preisach and Krasnosel'skii-Pokrovskii models, the Prandtl-Ishlinskii model offers a unique advantage, since its inverse can be obtained analytically. This is

attributed to the initial loading curve concept of the Prandtl-Ishlinskii model which provides an alternative description for the Prandtl-Ishlinskii model and essential basis to derive the analytical inverse. The initial loading curve is a stress-strain curve and is defined when the initial state of the Prandtl-Ishlinskii model is zero and when the input increases monotonically [2]. The analytical inversion of the Prandtl-Ishlinskii model is more attractive to compensate hysteresis nonlinearities in real-time applications. Owing to the analytical exact inverse, the inversion error of the inverse Prandtl-Ishlinskii model is zero. Moreover, this inverse offers significant benefits in real-time control applications. The knowledge of the exact description of the compensation error, in a given application, would facilitate the design of robust controllers and stability analysis, which are lacking with the numerical inverse. However, the advantages of the Prandtl-Ishlinskii model are limited to the class of hysteresis it can describe, namely the symmetric and the rate-independent hysteresis.

The reported studies involving inverse compensation generally exhibit compensation errors, even when the exact Prandtl-Ishlinskii model inverse is employed. This error has been generally attributed to characterization errors. Krejci and Kuhnen [30] applied the analytical inverse of the Prandtl-Ishlinskii model as a feedforward controller to compensate the hysteresis nonlinearities of a piezoceramic actuator. As mentioned before, the advantage of the Prandtl-Ishlinskii model is analytically invertible, and it can be conveniently implemented as a feedforward compensator for mitigating the hysteresis nonlinearities. Characterization of hysteresis properties in smart actuators using phenomenological operator-based hysteresis models generally involves estimation of the density function as well as the thresholds of the hysteresis operator on the basis of

measured data acquired for a particular actuator. The resulting model generally exhibits some degree of error between the model output and the measured characteristics. Ping and Ge [22] showed that the Preisach model derived to characterize the hysteresis nonlinearities in a piezoceramic actuator yields error in the 2 to 3% range. In a similar manner, the Krasnosel'skii-Pokrovskii model that is employed by Galinaitis [27] to characterize the major and minor hysteresis loops of a piezoceramic actuator at 0.05 Hz yields error of 2.8 to 4.3%. Krejci and Kuhnen [30] showed the percentage error of the Prandtl-Ishlinskii model used to characterize hysteresis of a piezoceramic actuator is in the order of 0.82%. The observed errors could be attributed to the characterization error. The estimated hysteresis models have been employed to construct the inverse of the Preisach, Krasnosel'skii-Pokrovskii and Prandtl-Ishlinskii models. The resulting inverse models are also expected to yield compensation errors of comparable order, when applied as a compensator. The systematic model inverse error, however, can be accurately described, when the exact analytical inverse is available.

1.5 Scope and Objectives

A number of hysteresis models have been evolved to characterize the hysteresis properties of various smart actuators. Although these models can provide reasonably good prediction of hysteresis of selected smart actuators, the input rate dependence of the hysteresis is generally not considered. The smart actuators, however, exhibit strong effects of the rate of the applied input on the hysteresis while Preisach model with dynamic density function could adequately describe the rate-dependent and asymmetric hysteresis nonlinearities; its inverse for compensation design is achievable only through

numerical means. The numerically-derived inverse models, invariably, yield compensation errors attributable to the characterization and inverse estimation errors. Furthermore, the errors cannot be accurately predicted and stability of closed-loop system could not be established.

Alternatively, the analytical invertible Prandtl-Ishlinskii hysteresis model could be effectively applied to minimize the errors associated with estimation of the inverse. The exact analytical inverse also facilitates the real-time compensation of the hysteresis effects. The Prandtl-Ishlinskii model, however, is limited to symmetric unbounded and rate-independent hysteresis properties. The Prandtl-Ishlinskii model and its inverse are thus not applicable for hysteresis compensation in class of actuators that exhibit asymmetric major and minor hysteresis loops, output saturation and input rate dependence of the hysteresis effects. These include the piezoceramic, SMA and magnetostrictive actuators.

It is desirable to derive generalized hysteresis models capable of describing symmetric as well as asymmetric hysteresis effects with output saturation over a range of input frequencies. It is also desirable that the models be continuous in order to derive their analytical inverse for their applications in real-time hysteresis compensation. It is hypothesized that the play operator and the density function of the Prandtl-Ishlinskii model can be sufficiently generalized to include the asymmetric hysteresis shapes with output saturation and the rate-dependent hysteresis effects. It is further hypothesized the resulting generalized Prandtl-Ishlinskii can be analytically inverted since it would be a mere extension of the classical Prandtl-Ishlinskii model. The analytical inverse would not only permit the analysis of the error but also the stability of the closed-loop system.

1.5.1 OBJECTIVES OF THE DISSERTATION RESEARCH

The overall goal of the dissertation research is formulated on the basis of the above-mentioned hypotheses. The key goals of the dissertation research involve the formulation of the generalized Prandtl-Ishlinskii model for characterization of asymmetric, saturated and rate-dependent hysteresis properties of different smart actuators, and its inversion.

The specific objectives of the dissertation research are summarized below:

- (a) Develop generalized Prandtl-Ishlinskii models to characterize asymmetric, saturated, and rate-dependent hysteresis properties of smart actuators. Through formulations of a generalized play operator, and dynamic threshold and density functions.
- (b) Characterization of the hysteresis properties of different smart actuators subject to wide ranges of inputs involving variations in type, magnitude and frequency. Analyse the measured characteristics in an attempt to quantify the asymmetric, saturated and rate-dependent hysteresis nonlinearities.
- (c) Formulate analytical inverse of the generalized Prandtl-Ishlinskii models for their application as a feedforward compensator to compensate for the asymmetric, saturated, and rate-dependent hysteresis nonlinearities.
- (d) Derive the error of the inverse compensation of the Prandtl-Ishlinskii model analytically using the initial loading curve.
- (e) Propose a robust controller design for compensation of inverse error through integration of the Prandtl-Ishlinskii model and its inverse in a closed-loop system, and perform stability analysis.

1.6 Organization of the Dissertation

The dissertation research works are systematically organized in six chapters. Chapter 2 describes the analytical formulations of the generalized Prandtl-Ishlinskii

models to describe the rate-dependent symmetric as well as asymmetric hysteresis properties of materials and smart actuators with output saturation. A generalized play hysteresis operator is integrated to the Prandtl-Ishlinskii model for characterizing asymmetric as well as symmetric hysteresis properties with output saturation. A rate-dependent play hysteresis operator is also proposed and applied to the classical Prandtl-Ishlinskii model in conjunction with a dynamic density function to characterize the symmetric rate-dependent hysteresis properties. Furthermore, a generalized rate-dependent play hysteresis operator with dissimilar envelope functions is presented to characterize asymmetric and rate-dependent hysteresis properties.

In Chapter 3, the input-output characteristics of three different smart actuators, including piezoceramic, SMA, and magnetostrictive actuators, are thoroughly analyzed for characterizing their hysteresis properties, particularly the hysteresis loops and their dependence on the rate of the input. For this purpose, a comprehensive experimental study was undertaken to characterize hysteresis properties of a piezoceramic actuator under sinusoidal and triangular waveform excitations in a wide frequency range (1 to 500 Hz). The output-input properties of the SMA and magnetostrictive actuators, acquired from different laboratories, are analyzed to identify the concerned nonlinearities.

The validity and applicability of the generalized Prandtl-Ishlinskii models to characterize symmetric as well as asymmetric rate-independent hysteresis properties of different smart actuators with output saturation are demonstrated in Chapter 4. The validation is demonstrated by comparing the model responses with the measured input-output characteristics of magnetostrictive, SMA, and piezoceramic actuators over a wide range of inputs. Characterization of the rate-dependent hysteresis nonlinearities of

piezoceramic actuators under sinusoidal and triangular input waveforms are carried out over a wide range of excitation frequencies.

Chapter 5 presents the formulations of the analytical inverse of the generalized Prandtl-Ishlinskii models described in Chapter 2. The analytical inversions of the Prandtl-Ishlinskii models are integrated as a feedforward compensator to compensate the asymmetric, saturated and rate-dependent hysteresis effects. The effectiveness of the compensations is illustrated through simulations and laboratory experiments with a piezoceramic actuator.

In Chapter 6, the analytical error of the Prandtl-Ishlinskii model-based inverse compensator is systematically derived analytically. To derive the error of the inverse compensation analytically, the initial loading curve of the Prandtl-Ishlinskii model and composition of the initial loading curve of the Prandtl-Ishlinskii model are presented. Then, the inverse of the estimated Prandtl-Ishlinskii model is derived and presented based on the initial loading curve and its inverse, respectively. Simulation results are attributed to demonstrate for the error of the inverse compensation employing inverse of the estimated Prandtl-Ishlinskii model.

The analytical error model of the inverse compensator is applied to propose a robust controller design in Chapter 7. The stability analysis is further presented for the closed-loop system comprising a plant preceded with the output of the inverse compensation. The major conclusions derived from the study and the major contributions are summarized in Chapter 8 together with thoughts as further desirable studies.

Chapter 2: Modeling Hysteresis Nonlinearities

2.1 Introduction

A number of phenomenological models have been proposed to describe hysteresis in smart actuators. These include the Preisach model [1, 5], the Krasnosel'skii-Pokrovskii model [4], and the Prandtl-Ishlinskii model [2]. The Prandtl-Ishlinskii model offers advantage over the Preisach and the Krasnosel'skii-Pokrovskii models, since its inverse can be computed analytically, which makes it extremely attractive for real-time control applications, particularly for real-time compensation of hysteresis contributions. The classical Prandtl-Ishlinskii model has been applied to characterize symmetric and rate-independent hysteresis properties of materials and smart actuators. The model can yield considerable errors when an asymmetry exists in the hysteresis loops, such as those observed in the output-input properties of the SMA and magnetostrictive actuators [20, 25], or when the output-input relations are dependent on the rate of the applied input.

The hysteresis models have been mostly applied to describe rate-independent hysteresis effects in ferromagnetic and smart actuators, assuming negligible effect of the rate of input. A few studies have experimentally characterized the output-input relationships of different actuators under varying inputs [33, 34, 61, 64]. These clearly showed dependency of the actuator displacement on the rate of input, while the area bounded by the hysteresis loop also increased under increasing input frequency. The data reported for various piezoceramic actuators under different excitation magnitudes and frequencies suggest nearly symmetric major as well as minor hysteresis loops, which are

strongly dependent upon the rate of input. Unlike the piezoceramic actuators, magnetostrictive actuators exhibit highly asymmetric hysteresis property about the input or the output axis. On the basis of laboratory measurements, it has been further shown that hysteresis in magnetostrictive actuators is strongly rate-dependent beyond certain frequencies [33]. Furthermore, the Prandtl-Ishlinskii model cannot describe output saturation of the hysteresis loops, invariably observed in smart actuators. Development of an effective controller for compensating the hysteresis effects necessitates formulations of the models that can provide accurate prediction of the rate-dependent hysteresis properties together with the output saturation.

In an attempt to overcome the limitations of the Prandtl-Ishlinskii model, Kuhnen [29] proposed deadzone operators in addition to the classical play operator of the Prandtl-Ishlinskii model so as to characterize asymmetric hysteresis nonlinearities of the magnetostrictive actuators. Brokate and Sprekels [2] and Visintin [3] have described a nonlinear play operator that may be applied to the Prandtl-Ishlinskii formulation to describe symmetric as well as asymmetric output-input loops coupled with output saturation. A number of dynamic density functions have also been proposed to predict rate-dependent behavior of smart actuators, when integrated to the classical phenomenological models [34, 64, 68]. Alternatively, a dynamical model coupled with the Preisach operator was proposed in an attempt to characterize rate-dependent hysteresis effects [33]. Smith [7] presented a homogenized energy approach using the Preisach model to characterize rate-dependent hysteresis in a magnetostrictive actuator.

In this chapter, generalized Prandtl-Ishlinskii models are systematically formulated to describe the rate-dependent symmetric as well as asymmetric hysteresis properties of

materials and smart actuators with output saturation. A rate-dependent play hysteresis operator is initially proposed and applied to the classical Prandtl-Ishlinskii model in conjunction with a dynamic density function to characterize the symmetric rate-dependent hysteresis properties. A generalized play hysteresis operator is subsequently formulated and integrated to the model for characterizing asymmetric as well as symmetric hysteresis properties with output saturation.

2.2 Prandtl-Ishlinskii Model

The Prandtl-Ishlinskii model utilizes the play operator and the density function to describe the input-output hysteresis relationships. The formulation of the classical Prandtl-Ishlinskii model is introduced below.

2.2.1 PLAY HYSTERESIS OPERATOR

The play hysteresis operator, used in the classical Prandtl-Ishlinskii model, is continuous, rate-independent, and symmetric operator. This hysteresis operator has been thoroughly described in [2]. Figure 2.1 illustrates the output (w) –input (v) characteristics of the play operator, as a function of the threshold r , which is a positive constant. This constant handles the hysteresis nonlinearity of the play operator and the Prandtl-Ishlinskii hysteresis model. The play operator F_r has also been described by the motion of a piston within a cylinder of length $2r$, where the instantaneous position of center of the piston is represented by the coordinate v and that of the cylinder position by w [2].

Analytically, for any input $v(t) \in C_m[0, T]$, where C_m represents the space of piecewise monotone continuous functions, such that the function v is monotone on the

sub-intervals $[t_i, t_{i+1}]$, the output of the play hysteresis operator is analytically expressed for $t_0=0 < t_1 < \dots < t_N = T$ as [2]:

$$\begin{aligned}
 F_r[v](0) &= f_r(v(0), 0) = w(0) \\
 w(t) &= f_r(v(t), F_r[v](t_i)); \text{ for } t_i < t \leq t_{i+1} \text{ and } 0 \leq i \leq N-1; \\
 f_r(v, w) &= \max(v-r, \min(v+r, w))
 \end{aligned}
 \tag{2.1}$$

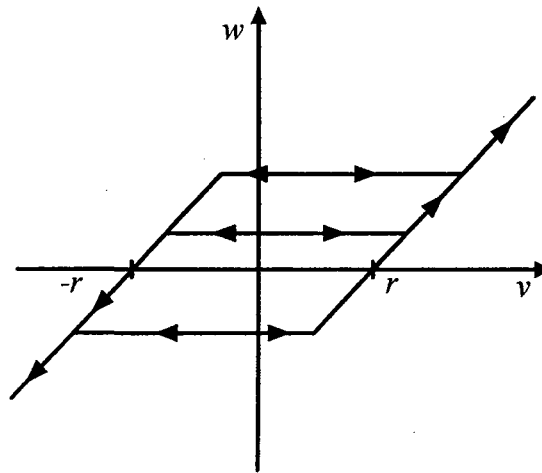


Figure 2.1: The output-input properties of the play hysteresis operator.

The argument of the operator is written in square brackets to indicate the functional dependence, since it maps a function to another function. Some key properties of the play hysteresis operator are briefly described below:

- **Rate-independence:** The play operator $F_r[v]$ is a rate-independent hysteresis operator, such that :

$$F_r[v] \circ G = F_r[v \circ G]
 \tag{2.2}$$

where G is a continuous increasing function, $G: [0, T]$, satisfying $G(0)=0$ and $G(T)=T$. Considering that a number of smart actuators and ferroelectric materials show hysteresis effects dependent on the rate of input, the play hysteresis may yield significant error when used in the Prandtl-Ishlinskii model.

- **Range:** For a given input $v(t) \in C[0, T]$ and threshold $r \geq 0$, the range of the play operator (2.1) is defined as [2]:

$$\begin{aligned} \max_{t \in [0, T]} F_r[v](t) &= f_r(\max_{t \in [0, T]}(v(t)), w(0)) \\ \min_{t \in [0, T]} F_r[v](t) &= f_r(\min_{t \in [0, T]}(v(t)), w(0)) \end{aligned} \quad (2.3)$$

This property shows that the maximum and minimum outputs of the play operator are directly dependent on the input v . Consequently, the play operator is unbounded and cannot describe output saturation output.

- **Lipschitz-continuity:** For a given input $v(t)$ and threshold $r \geq 0$, the output of the play operator (2.1) can be extended to Lipschitz continuous [2]. This property is important to construct the analytical inverse of the Prandtl-Ishlinskii model, for compensation of hysteresis effects in real-time control applications.
- **Memory Effects:** The play operator is a hysteresis operator with nonlocal-memory effect, where the output of the operator depends on the current value of input as well as the past values of output [2].

2.2.2 INPUT-OUTPUT RELATIONSHIP OF THE PRANDTL-ISHLINSKII MODEL

The Prandtl-Ishlinskii model, a phenomenological hysteresis model based operator, is presented as a summation of a number of weighted play hysteresis operator. The Prandtl-Ishlinskii model utilizes play operator F_r , described in (2.1), to describe the following relationship between the output $\Pi[v](t)$ and the input v as [2]:

$$\Pi[v](t) = qv(t) + \int_0^R p(r)F_r[v](t)dr \quad (2.4)$$

where $p(r)$ is termed as a density function, satisfying $p(r) > 0$, and q is a positive constant.

The density function represents a probability distribution in terms of integrals, and serves as a weighting for the play operators. In general, the density function is identified from the experimental data of a particular material or actuator. It can account for the output-input sensitivity of the actuator. The density function of the Prandtl-Ishlinskii model should be always positive to maintain the counter-clockwise direction of the play operator. The Prandtl-Ishlinskii model with the density function maps $C[t_0, \infty)$ into $C[t_0, \infty)$. The density function $p(r)$ generally vanishes for large values of r , while the choice of $R = \infty$ as the upper limit of integration is widely used in the literature for the sake of convenience [2]. This direction of the loop means lagging between the output of Prandtl-Ishlinskii model and the input. It should be mentioned that the hysteresis loops of the smart actuators and ferromagnetic materials are counter-clockwise.

The Prandtl-Ishlinskii model can also be expressed by summation of various play operators together with the density function as:

$$\Pi[v](t) = qv(t) + \sum_{i=1}^n p(r_i)F_{r_i}[v](t) \quad (2.5)$$

where n is the number of the play operators.

Example 2.1: The output-input relations of the play operator and the Prandtl-Ishlinskii model are illustrated by considering the following example. Consider an input of the form $v(t) = 10\sin(2\pi t)$, $t \in [0, 5]$ to the Prandtl-Ishlinskii model that is presented in (2.5). Figure 2.2(a) illustrates the output-input relations of the play operator obtained through solution

of (2.1) upon considering five different values of threshold r . The results clearly show the strong dependence of the operator response on the threshold value. The output-input relation is further derived from solution of Prandtl-Ishlinskii model (2.4), by considering only five play operators, $r = [1.3, 2.6, 3.9, 5.2, 6.5]$, $q=0.5$ and $\Delta t=0.01$, as shown in Figure 2.2(b). The density function of the form $p(r) = 0.1e^{-0.1r}$ is assumed. The example shows symmetric hysteresis loop, attributed to the symmetric output of the play hysteresis operators, shown in Figure 2.2(a). Furthermore, the hysteresis loops of the Prandtl-Ishlinskii model presented in Figure 2.2(b) do not exhibit output saturation due to unbounded play operator. It can be concluded that the Prandtl-Ishlinskii model could adequately describe symmetric hysteresis loops but it cannot characterize asymmetric and saturated major and minor hysteresis properties. However, the Prandtl-Ishlinskii model can characterize symmetric hysteresis loops of piezoceramic actuators.

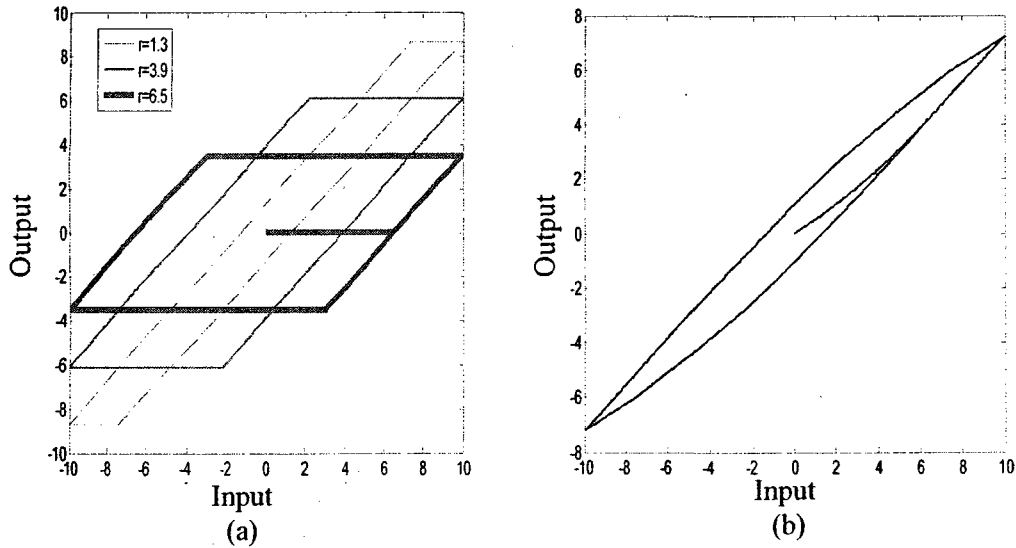


Figure 2.2: Input-output relations of: (a) play operators corresponding to different threshold values, and (b) the Prandtl-Ishlinskii model under $v(t) = 10\sin(2\pi t)$.

Although the Prandtl-Ishlinskii model has been applied for characterizing the hysteresis properties of piezoceramic actuators [30, 53], it exhibits a number of limitations. Some of the primary limitations of the classical Prandtl-Ishlinskii model are summarized below:

- **Output-Input asymmetry:** The Prandtl-Ishlinskii models yield symmetric output-input hysteresis loops, which are attributed to the symmetric nature of the play operator under increasing and decreasing inputs. The model applications have thus reported for the piezoceramic actuators, which generally show symmetric major and minor hysteresis loops.
- **Output saturation:** Owing to the unbounded nature of the play operator, the Prandtl-Ishlinskii model cannot be applied to characterize the output saturation property, which is widely observed in various smart actuators and ferromagnetic materials.
- **Rate-dependent hysteresis:** The smart actuators and various materials invariably exhibit hysteresis that is dependent upon the rate of the applied input. The Prandtl-Ishlinskii model cannot describe the rate dependence of the hysteresis, which is attributed to the rate-independent play operator and density function.

The classical Prandtl-Ishlinskii model, therefore, cannot accurately characterize the hysteresis properties of magnetic materials and smart actuators, which invariably exhibit nonlinear dependence on the rate of input, output saturation and output asymmetry about the input. Kuhnen [29] proposed deadzone operators in addition to the classical play operator of the Prandtl-Ishlinskii model so as to characterize asymmetric hysteresis nonlinearities of the magnetostrictive actuators. This model, however, could not characterize saturated hysteresis properties. Furthermore, the resulting model is considered to be quite complex for control application.

The prediction ability of the Prandtl-Ishlinskii model could be enhanced, particularly in the content of the above sated nonlinearities, by considering alternate play operator and density function. In the subsequent sections, three different Prandtl-Ishlinskii models are formulated in a systematic manner for charactering; (i) rate-independent asymmetric hysteresis with output saturation; (ii) rate-dependent symmetric hysteresis; and (iii) generalized rate-dependent asymmetric hysteresis properties with output saturation. Generalized and rate-dependent play operators are proposed to describe the nonlinear hysteresis properties of different actuators in a generalized manner.

2.3 A Generalized Rate-Independent Prandtl-Ishlinskii Model

Brokate and Sprekels [2] and Visintin [3] have described an alternative play operator with symmetric as well as asymmetric output-input characteristics. Although this operator was proposed nearly 80 years ago, its application to describe hysteresis in conjunction with the Prandtl-Ishlinskii model has not yet been explored. This operator may also describe the output saturation property and is thus termed 'generalized play operator' in the dissertation.

2.3.1 THE GENERALIZED PLAY HYSTERESIS OPERATOR

The generalized play operator is a nonlinear play operator, where an increase and decrease in the input v causes the output w to increase and decrease, respectively, along the curves γ_l and γ_r , as shown in Figure 2.3. The minor loops of the input v and the output w are bounded by the curves γ_l and γ_r ($\gamma_l \leq \gamma_r$) which are continuous envelope functions for the input-output properties [3]. The output of this generalized operator can

exhibit asymmetric loops. The generalized play operator for any input $v(t) \in C_m[0, T]$ is analytically defined as:

$$\begin{aligned}
 S_r[v](0) &= f_r^\gamma(v(0), 0) = z(0) \\
 S_r[v](t) &= s(v(t), S_r[v](t_i)); \text{ for } t_i < t \leq t_{i+1} \text{ and } 0 \leq i \leq N-1 \\
 s(v, z) &= \max(\gamma_l(v) - r, \min(\gamma_r(v) + r, z))
 \end{aligned} \tag{2.6}$$

where $\gamma_l, \gamma_r : \mathfrak{R} \rightarrow \mathfrak{R}$ are strictly increasing and continuous envelope functions.

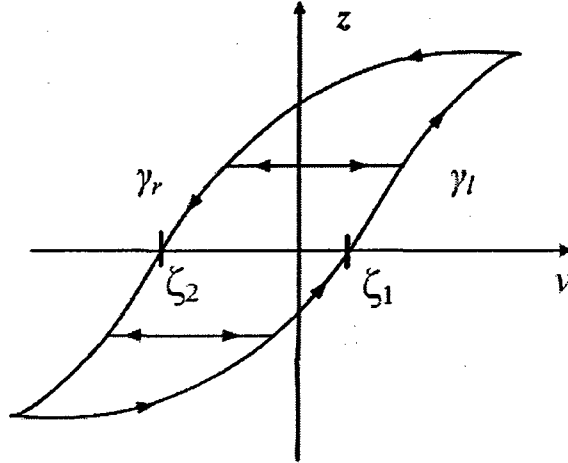


Figure 2.3: Generalized play operator.

In the above formulation, r refers to the threshold value of the classical play operator, which is the magnitude of increasing or decreasing input $v(t)$ corresponding to zero output $w(t)$, as illustrated in Figure 2.1. Unlike the classical play operator, the generalized operator yields zero outputs, $z(t)=0$, at two different values, ζ_1 and ζ_2 , of the increasing and decreasing inputs $v(t)$, as shown in Figure 2.3. The difference in the magnitudes of ζ_1 and ζ_2 allows for describing asymmetric hysteresis loops. These constants corresponding to increasing and decreasing inputs are related to the envelope

functions and the threshold r in the following manner:

$$\begin{aligned}\zeta_1 &= \gamma_l^{-1}(r) \quad \text{for } \dot{v}(t) > 0 \\ \zeta_2 &= \gamma_l^{-1}(-r) \quad \text{for } \dot{v}(t) < 0\end{aligned}\tag{2.7}$$

The above equations can be expressed as:

$$\begin{aligned}\gamma_l(\zeta_1) &= r \quad \text{for } \dot{v}(t) > 0 \\ \gamma_r(\zeta_2) &= -r \quad \text{for } \dot{v}(t) < 0\end{aligned}\tag{2.8}$$

Then Equation (2.8) yields a relationship between the constants ζ_1 , ζ_2 , and the threshold r , as:

$$r = \frac{\gamma_l(\zeta_1) - \gamma_r(\zeta_2)}{2}\tag{2.9}$$

For a given threshold r and envelope functions γ_l and γ_r the generalized play hysteresis operator can be constructed using (2.8) and (2.9).

Some of the key properties of the generalized play operator can be described as follows:

- **Lipschitz-continuity:** For a given input $v(t)$, the Lipschitz-continuity of the generalized play operator can be ensured when the functions γ_l and γ_r are Lipschitz continuous [2, 3].
-
- **Rate-independent:** The generalized play operator S_r is a rate-independent hysteresis operator, provided:

$$S_r[v] \circ G = S_r[v \circ G]\tag{2.10}$$

- **Range:** For a given input $v(t) \in C[0, T]$ and $z(0) = S_r[v](0) = s(v(0), 0)$, then the maximum and the minimum values of the generalized play operator depend on the envelope functions γ_r and γ_l , respectively, such that:

$$\begin{aligned} \max_{t \in [0, T]} S_r[v](t) &= s(\max_{t \in [0, T]} \gamma_r(v(t)), z(0)) \\ \min_{t \in [0, T]} S_r[v](t) &= s(\min_{t \in [0, T]} \gamma_l(v(t)), z(0)) \end{aligned} \tag{2.11}$$

The above stated properties suggest that the generalized play hysteresis operator can exhibit asymmetric output by selecting different envelope functions for increasing and decreasing input. Moreover, by choosing bounded envelope functions, the play hysteresis operator can exhibit saturated output since the maximum and minimum output of operator, as shown in (2.11), depends on the selected envelope functions. The application of the generalized operator to the Prandtl-Ishlinskii model could thus help to characterize asymmetric and saturated hysteresis loops. Moreover, the analytical inversion of the model could also be realized since the functions γ_l and γ_r are Lipschitz continuous. The inverse constructed using invertible envelope functions, could then be employed as a feedforward compensator for the asymmetric and saturated hysteresis effects.

2.3.2 INPUT-OUTPUT RELATIONSHIP OF THE GENERALIZED PRANDTL-ISHLINKSII MODEL

The generalized Prandtl-Ishlinskii model is subsequently formulated upon integrating the generalized play operator S_r and the density function as:

$$\Phi[v](t) = \int_0^R p(r) S_r[v](t) dr \tag{2.12}$$

The above model integrating the play operator with appropriate envelope functions can describe the minor and major hysteresis loops of smart actuators and materials with asymmetry and saturation properties. The model may also be expressed as:

$$\Phi[v](t) = \sum_{i=1}^n p(r_i) S_{r_i}[v](t) \quad (2.13)$$

where n is the number of the generalized play operators.

Remark 2.1: The classical play operator, defined in (2.1), can be shown to be is a special case of the generalized play operator. The generalized play operator (2.6) reduces to the classical operator when identical envelope functions, $\gamma_r(v) = \gamma_l(v) = v$.

Remark 2.2: The classical Prandtl-Ishlinskii model is a special case of the generalized model. By letting $\gamma_r(v) = \gamma_l(v) = v$, the generalized model reduces to the classical Prandtl-Ishlinskii model, described in (2.4).

Remark 2.3: The generalized play hysteresis operator is hysteresis operator with nonlocal-memory effect, where the output of the generalized operator depends on the current value of input as well as the past values of output.

Example 2.2 :The response characteristics of the Prandtl-Ishlinskii models based on asymmetric generalized as well as the classical play operators are illustrated under a complex harmonic input of the form: $v(t)=4.6\sin(\pi t)+3.1\cos(3.4\pi t)$, $t \in [0, 5]$. This input permits for evaluating major as well as minor loops in the play hysteresis operators' outputs. The simulations are performed using different envelope functions to study their influence on the outputs of the generalized play operators. For the illustrative example, hyperbolic-tangent functions are selected as the envelope functions of the generalized play operator, such that: $\gamma_r(v) = 6 \tanh(0.4v)$ and $\gamma_l(v) = 6 \tanh(0.25v)$. A constant density function $p(r)=0.45$ is further chosen for both the classical and the generalized models in order to relax its effect in the responses. A total of 11 play operators are

selected for the simulation with threshold values as: $r = [0, 0.525, 1.05, 1.575, 2.1, 2.625, 3.15, 3.675, 4.2, 4.725, 5.25]$.

Figures 2.4(a) and 2.4(b) show the input-output relations of the classical (CPO) and generalized play operators (GPO), respectively, corresponding to threshold values, $r = 0, 1.575, 3.15, \text{ and } 4.725$, under the selected complex harmonic input. Both the play operators (GPO and CPO) exhibit increasing hysteresis with increasing threshold value. The CPO, however, yields symmetric major and minor hysteresis loops under increasing and decreasing inputs, while the GPO exhibits highly asymmetric input-output curves under the same inputs. Furthermore, unlike the outputs of the CPO, the outputs of the GPO exhibit saturation. Figures 2.5(a) and 2.5(b) show the outputs of the classic and generalized Prandtl-Ishlinskii models incorporating classical and generalized play operators, respectively, for same values of r . The results clearly show that the generalized model yields saturated asymmetric major and minor hysteresis loops, which are attributed to the selected envelope functions. The results further show that the width of the hysteresis loops under negative input is more than that under the positive input, which is also attributed to the selected envelope functions. The model with classical operators, however, exhibits unsaturated and symmetric major and well as minor hysteresis loops. The generalized Prandtl-Ishlinskii model can also yield symmetric hysteresis loops for envelope functions, $\gamma_l(v) = \gamma_r(v)$, as it would be the case for the classical model. The generalized model, however, characterizes the output saturation unlike the classical model, as it is evident from outputs of the operator and the model, shown in Figures 2.6(a) and 2.6(b), respectively. The results thus suggest that the generalized Prandtl-Ishlinskii model comprising the generalized play operator can describe the symmetric as well as asymmetric hysteresis properties with output saturation. The output-input relationships, however, are strongly determined by the envelope functions of the generalized play hysteresis operators.

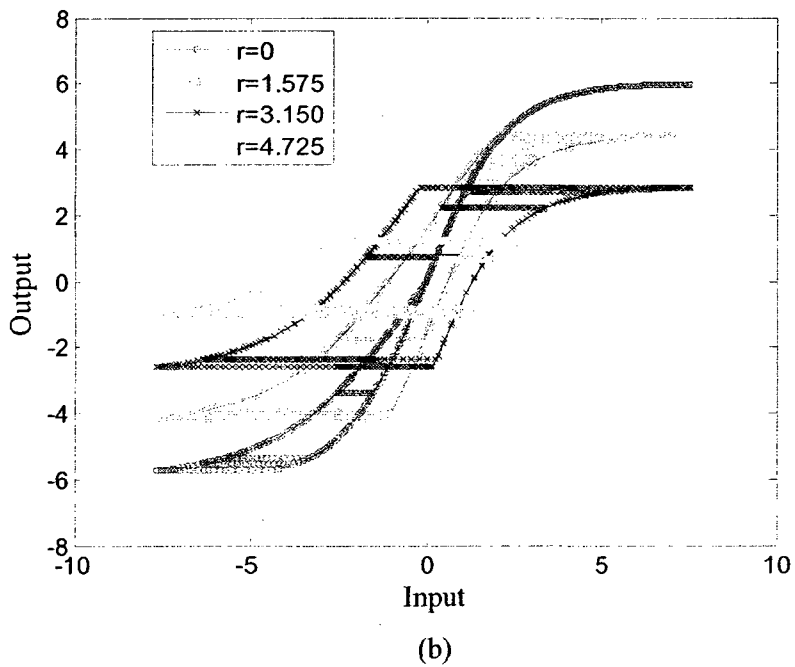
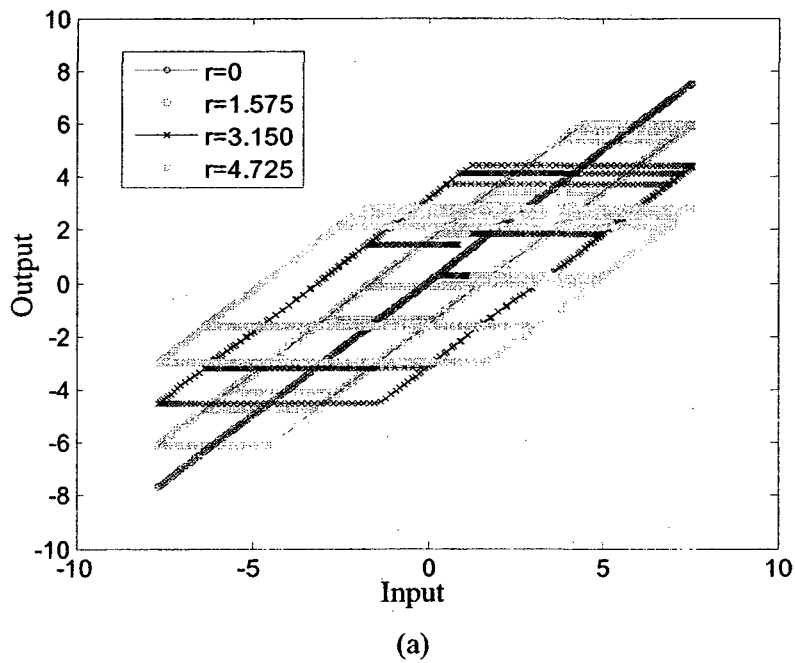
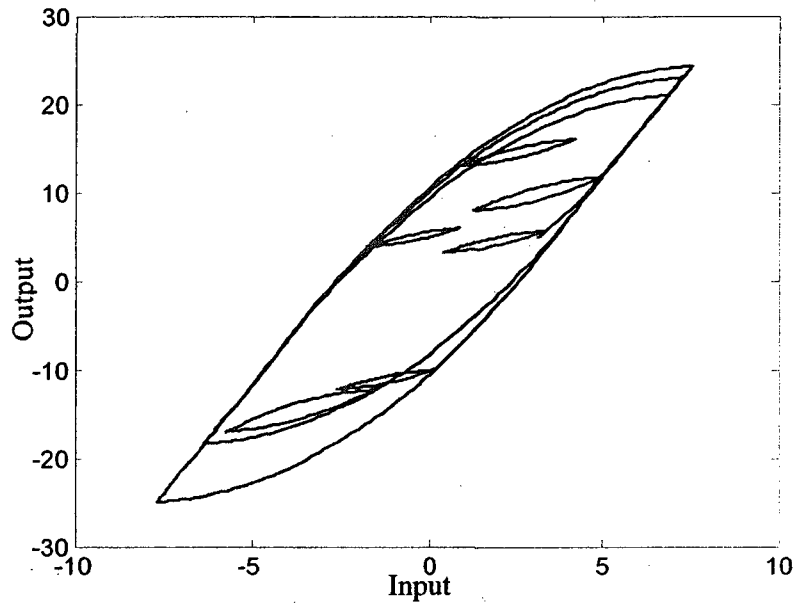
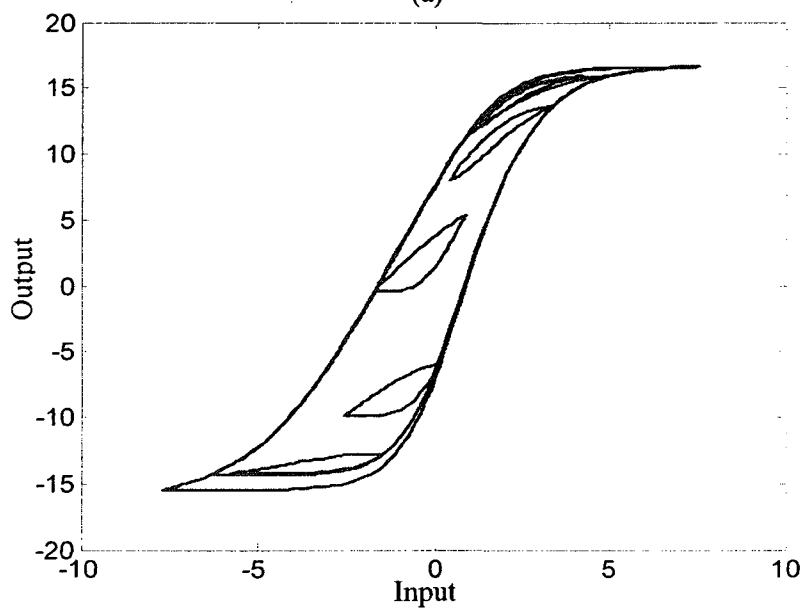


Figure 2.4: Input–output properties of the play hysteresis operators under $v(t) = 4.6\sin(\pi t) + 3.1\cos(3.4\pi t)$: (a) Classic play operator, $\gamma_l(v) = \gamma_r(v) = v$; and (b) Generalized play operator, $\gamma_l(v) = 6 \tanh(0.4v)$ and $\gamma_r(v) = 6 \tanh(0.25v)$.

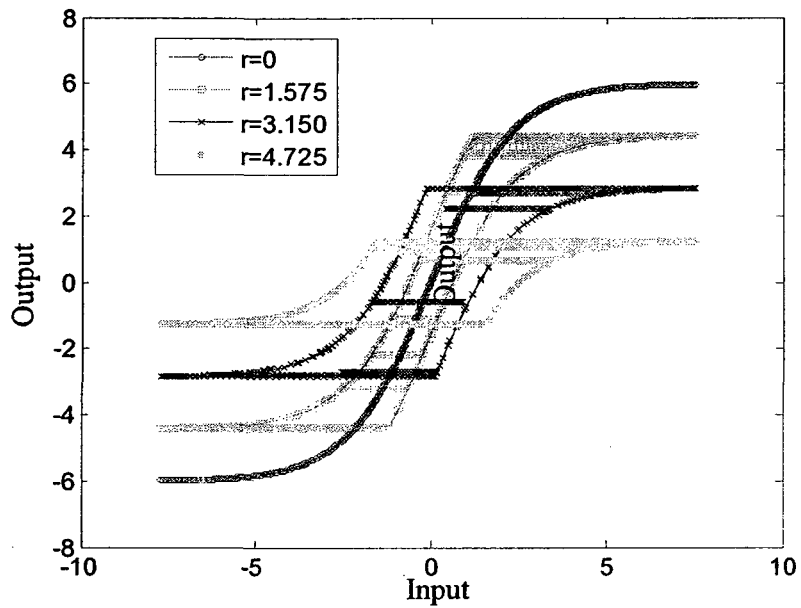


(a)

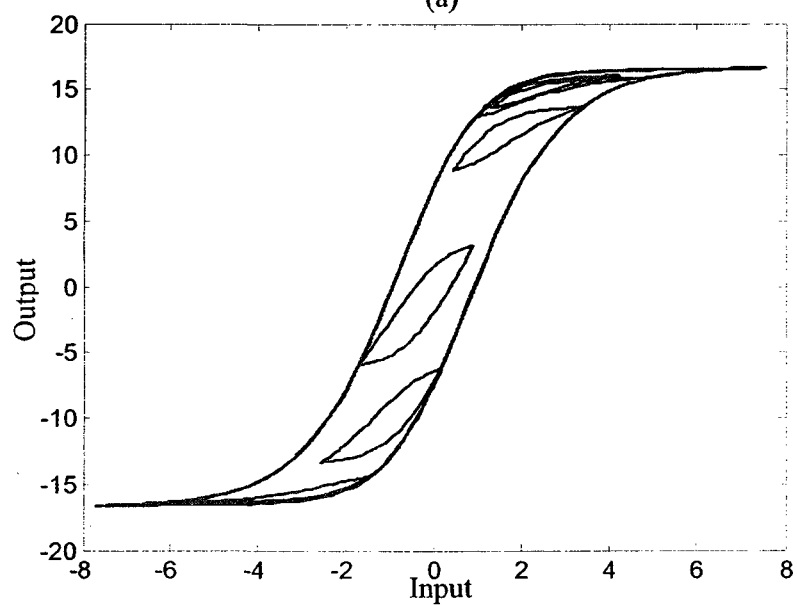


(b)

Figure 2.5: Response characteristics of the Prandtl-Ishlinskii hysteresis models employing: (a) classical play operator; and (b) generalized play operator.



(a)



(b)

Figure 2.6: Input-output relations of: (a) the generalized play operators corresponding to different threshold values; and (b) the generalized Prandtl-Ishlinskii model under $v(t) = 4.6\sin(\pi t) + 3.1\cos(3.4\pi t)$, and $\gamma_l(v) = \gamma_r(v) = 6\tanh(0.4v)$.

2.4 Prandtl-Ishlinskii Model Based Rate-Dependent Play Operator

Both the classical and the generalized Prandtl-Ishlinskii models are considered applicable for characterizing rate-independent hysteresis properties of materials and actuators. This is attributed to the rate-independent classical and generalized play operators. Various materials and actuators, however, exhibit output-input hysteresis that is strongly dependent upon the rate of applied input in a highly nonlinear manner [33, 64, 68]. These studies have invariably shown that the majority of the smart actuators and ferromagnetic materials generally exhibit greater hysteresis with increasing time rate of the input, while the output amplitude decreases.

2.4.1 FORMULATION OF RATE-DEPENDENT PLAY HYSTERESIS OPERATOR

An alternate play operator comprising the rate of the input (dv/dt) is proposed for integration to the Prandtl-Ishlinskii for characterizing rate-dependent hysteresis properties materials and smart actuators. The definition of the play operator, presented in (2.1), suggests that the width of the play hysteresis operator is directly related to the threshold r , which is also evident from Figure 2.2(a). The increase in the hysteresis with increasing the rate of the input may thus be characterized by a relatively larger threshold r . Furthermore, the output of play hysteresis operator depends on either $v - r$ for $\dot{v} > 0$ or $v + r$ for $\dot{v} < 0$, while r is always positive. Unlike the operator used in the Preisach model, where the input is limited to either '-1' or '+1' [1], the outputs of play operator employed in Prandtl-Ishlinskii model are not limited to fixed values. The results in Figure 2.2(a) further show that the peak output of the operator decreases with increasing values of r . Moreover, the width of the hysteresis loops is directly related to the threshold r , which is

illustrated in Figure 2.2, for an input of the form $v(t)=10\sin(2t)$ with initial value $F_{\bar{r}}[v](0)=0$.

The properties of the play hysteresis operator may thus be further exploited for describing the rate-dependent output-input properties of the smart actuators and ferromagnetic materials. The identification of an appropriate threshold value, however, forms the most important task for defining the hysteresis properties. Consequently, a dynamic threshold, $\bar{r} = r(\dot{v})$, is proposed and a relationship among the output of the play operator, the dynamic threshold \bar{r} and the input $v(t)$, is formulated based on the reported and measure output-input properties (presented in Chapter 3) of smart actuators, as:

$$F_{\bar{r}}(v(t)) = f(\bar{r}, v(t)) \quad (2.14)$$

Analytically, let $C_m[0, T]$ represent the space of piecewise monotone continuous functions. For any input, $v(t) \in C_m[0, T]$, let $0 = t_0 < t_1 < \dots < t_N = T$ be a partition within the span $[0, T]$, such that the function v is monotone on each of the sub-intervals $[t_i, t_{i+1}]$. The output of the rate-dependent play operator is then proposed as a function of the dynamic threshold, as:

$$\begin{aligned} F_{\bar{r}}(v(0)) &= f_{\bar{r}}(v(0), 0) = \bar{w}(0) \\ F_{\bar{r}}(v(t)) &= f_{\bar{r}}(v(t), F_{\bar{r}}(v(t_i))); \text{ for } t_i < t \leq t_{i+1} \text{ and } 0 \leq i \leq N-1 \\ f_{\bar{r}}(v, \bar{w}) &= \max(v - \bar{r}, \min(v + \bar{r}, \bar{w})) \end{aligned} \quad (2.15)$$

A dynamic threshold function of the following form is initially proposed on the basis of the observed output-input properties of a piezoceramic actuator:

$$\bar{r} = \alpha \ln(\beta + \lambda |\dot{v}(t)|^\varepsilon) \quad (2.16)$$

where $\alpha > 0$, $\beta \geq 1$, $\lambda > 0$, and $\varepsilon \geq 1$ are positive constants.

Remark 2.4: In the above formulations, the choice of the dynamic threshold \bar{r} is not unique. This would depend upon the nature of hysteresis of a particular material or a device.

The properties of the proposed rate-dependent play hysteresis operator comprising proposed dynamic threshold function (2.16) are evaluated to ensure their general applicability, which are summarized below:

- The output hysteresis of a rate-dependent operator increases monotonically with increase in the time rate of input, $\dot{v}(t)$. This is apparent from (2.16). An increase in the rate of input would yield a higher value of the dynamic threshold, $\bar{r} = r(\dot{v}(t))$. For two inputs of different time rates, such that: $\max[\dot{v}_1(t)] > \max[\dot{v}_2(t)]$ and $\dot{v}_1(0) > \dot{v}_2(0)$, the proposed dynamic threshold function would yield $\max[r(\dot{v}_1(t))] > \max[r(\dot{v}_2(t))]$.
- The hysteresis of the proposed play operator also increases monotonically with increase in the amplitude of input $v(t)$, and thus the magnitude of $\dot{v}(t)$. A higher amplitude would thus yield a higher value of \bar{r} , as it is evident from (2.16).
- The dynamic threshold function \bar{r} yields a nearly constant value when the rate of input is very small or when a low frequency input is applied, which yields $\bar{r} = \alpha \ln(\beta)$. The proposed operator can thus describe the rate-independent hysteresis properties.

2.4.2 RATE-DEPENDENT PRANDTL-ISHLINSKII MODEL

The rate-dependent Prandtl-Ishlinskii model is formulated upon integrating the proposed rate-dependent play operator (2.15). The output of the rate-dependent model $\bar{\Pi}(v(t))$ is then expressed analytically as:

$$\bar{\Pi}(v(t)) = qv(t) + \int_0^R p(\bar{r})F_{\bar{r}}(v(t))d\bar{r} \quad (2.17)$$

The above model may also be expressed as:

$$\bar{\Pi}(v(t)) = qv(t) + \sum_{i=1}^n p(\bar{r}_i)F_{\bar{r}_i}(v(t)) \quad (2.18)$$

The numerical implementation of the generalized rate-dependent Prandtl-Ishlinskii model is realized using discrete input $v(k)$ corresponding to interval k with a step size h ($k=0, 1, 2, \dots, N; N=T/h$) such that:

$$\bar{\Pi}(k) = qv(k) + \sum_{i=1}^n p(\bar{r}_i)F_{\bar{r}_i}(v(k)) \quad (2.19)$$

The time rate of the input is estimated from the discrete inputs, such that:

$$\bar{v}_k = (v(t_k) - v(t_{k-1})) / (t_k - t_{k-1}) \quad (2.20)$$

Example 2.3: The response characteristics of the proposed rate-dependent Prandtl-Ishlinskii hysteresis model, presented in (2.17), is illustrated for a complex harmonic input of the form: $v(t)=6\sin(2\pi ft)+3\sin(3\pi ft)$; where f is the fundamental frequency of the inputs. The simulations are performed under different input fundamental frequencies (10, 50, 100, and 200 Hz) to study the influence of the rate of the input. The input further permits for evaluations of major and minor loops in the operators' outputs. The simulations were performed by arbitrary selecting the constants in dynamic threshold model (2.16) as: $\alpha=1.8$, $\beta=1.0$, $\lambda=0.001$ and $\varepsilon=1$. The simulation parameters were

selected are: $T=4/f$, $N=301$, $\Delta t=0.02/f$, $w(0)=0$ and $q=0.1$. A constant density function, $p(r)=0.005e^{-0.01r}$, is further chosen for the model in order to relax its effect in the output responses. Figure 2.7 shows the output-input relationships attained from the Prandtl-Ishlinskii model using the rate-dependent play hysteresis operator under inputs corresponding to the selected fundamental frequencies. Simulation results show an increase in hysteresis and decrease in output amplitude of the hysteresis loops with increase in the fundamental frequency of the input. The hysteresis of the major loops is considerably larger than those of the minor loops due to varying input amplitudes. The simulation results show that rate-dependent Prandtl-Ishlinskii model based on the dependent play operator, can exhibit rate-dependent hysteresis loops. Furthermore, the simulation results show that the rate-dependent hysteresis effects maintain the wipe-out property and the memory effects in the output.

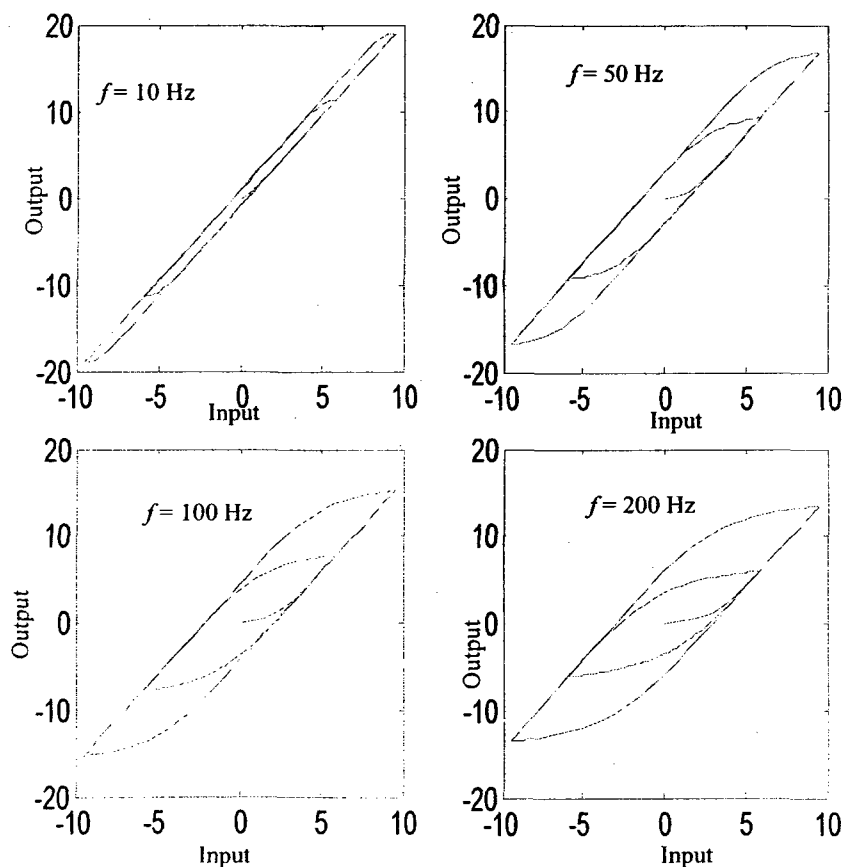


Figure 2.7: The input-output properties of the Prandtl-Ishlinskii model employing the rate-dependent play operator under inputs at different frequencies.

2.4.3 RATE-DEPENDENT PRANDTL-ISHLINSKII MODEL BASED DYNAMIC DENSITY FUNCTION

The rate-dependent Prandtl-Ishlinskii model described in (2.17) can be further enhanced by employing a dynamic density function. Mayergoyz [1] proposed a rate-dependent Preisach model by introducing the speed of the output in the Preisach function. In a similar manner, Ben Mrad and Hu [64] and Yu et al. [34] further proposed a rate-dependent density function to the Preisach model to characterize the rate-dependent hysteresis effects of piezoceramic actuators. A dynamic density function for the Prandtl-Ishlinskii model can also be formulated in a similar manner as a function of the dynamic threshold, apart from input $v(t)$ and its time rate $\dot{v}(t)$. The rate-dependent Prandtl-Ishlinskii model with dynamic density function is thus formulated upon integrating the dynamic density function $p(\bar{r}, v(t), \dot{v}(t))$ and the function $\bar{h}(v(t), \dot{v}(t))$ in the model, such that:

$$\bar{\Pi}(v(t)) = \bar{h}(v(t), \dot{v}(t)) + \int_0^R p(\bar{r}, v(t), \dot{v}(t)) F_{\bar{r}}(v(t)) d\bar{r} \quad (2.21)$$

where $\bar{h}(v(t), \dot{v}(t))$ and $p(\bar{r}, v(t), \dot{v}(t))$ are positive continuous functions. The validity of the proposed rate-dependent model is examined in Chapter 4 under various inputs, including harmonic, complex harmonic and triangular waveforms, using the measured data of different smart actuators in a wide frequency range.

Remark 2.5: The choices of \bar{h} and p are not unique. These would depend upon the nature of rate-dependent hysteresis of a particular material or actuator.

2.5 Prandtl-Ishlinskii Model Based Generalized Rate-Dependent Play Operator

Owing to the symmetric properties of rate-dependent play operator, the rate-dependent Prandtl-Ishlinskii model cannot be applied to characterize the asymmetric rate-dependent hysteresis properties. Alternatively, a generalized rate-dependent play operator, which is constructed using envelope functions, can be proposed to describe asymmetric rate-dependent hysteresis properties as a function of the dynamic threshold as well as generalized rate-independent play hysteresis operator (2.6).

2.5.1 GENERALIZED RATE-DEPENDENT PLAY HYSTERESIS OPERATOR

The rate dependence of the output is characterized by introducing the dynamic threshold \bar{r} in the generalized play operator formulation in a manner similar to that applied to the symmetric play hysteresis operators. The resulting modified generalized play hysteresis operator could describe the rate-dependent asymmetric hysteresis nonlinearities. This operator can be analytically described for input $v(t) \in C_m[0, T]$ as:

$$\begin{aligned}
 S_{\bar{r}}(v(0)) &= s_{\bar{r}}(v(0), 0) = \bar{z}(0) \\
 S_{\bar{r}}(v(t)) &= s_{\bar{r}}(v(t), S_{\bar{r}}(v(t))) ; \text{ for } t_i < t \leq t_{i+1} \text{ and } 0 \leq i \leq N-1 \quad (2.22) \\
 s_{\bar{r}}(v, \bar{z}) &= \max(\gamma_r(v) - \bar{r}, \min(\gamma_r(v) + \bar{r}, \bar{z}))
 \end{aligned}$$

2.5.2 THE GENERALIZED RATE-DEPENDENT PRANDTL-ISHLINSKII MODEL

The generalized rate-dependent Prandtl-Ishlinskii model is formulated upon integrating the above generalized play operator together with the density function $p(\bar{r})$.

This density function is expected to enhance prediction abilities of the generalized model for asymmetric hysteresis nonlinearities. The output of the model $\bar{\Phi}(v(t))$ is then expressed as:

$$\bar{\Phi}(v(t)) = \int_0^R p(\bar{r}) S_{\bar{r}}(v(t)) d\bar{r} \quad (2.23)$$

The model can also be expressed as:

$$\bar{\Phi}(v(t)) = \sum_{j=1}^n p(\bar{r}_j) S_{\bar{r}_j}(v(t)) \quad (2.24)$$

where n is the number of the generalized rate-dependent play operators. The numerical implementation of the generalized Prandtl-Ishlinskii model is formulated using discrete inputs $v(k)$ with a step size of h ($k=0, 1, 2, \dots, N; N=T/h$), such that:

$$\bar{\Phi}(v(k)) = \sum_{j=1}^n p(\bar{r}_j) S_{\bar{r}_j}(v(k)) \quad (2.25)$$

Example 2.4: The response characteristic of the proposed generalized rate-dependent Prandtl-Ishlinskii model is illustrated through simulation parameters in Example 2.3. To relax the symmetric properties in the rate-dependent hysteresis loops is relaxed by selecting following envelope functions:

$$\begin{aligned} \gamma_l(v) &= 1.3v \\ \gamma_r(v) &= 1.0v + 1.50 \end{aligned} \quad (2.26)$$

Figure 2.8 presents the responses of the generalized rate-dependent Prandtl-Ishlinskii model under complex harmonic inputs corresponding to different fundamental frequencies (10, 50, 100, and 200 Hz). The results show that as the fundamental frequency of the input increases, the hysteresis increases and in the amplitude of the major and minor loops decreases. The results further show that the model employing the

generalized rate-dependent play operator yields asymmetric rate-dependent hysteresis loops. It is thus ascertained that the generalized rate-dependent play operator not only relaxes the symmetry of the rate-dependent Prandtl-Ishlinskii model, but it could also yield the rate-dependent hysteresis effects.

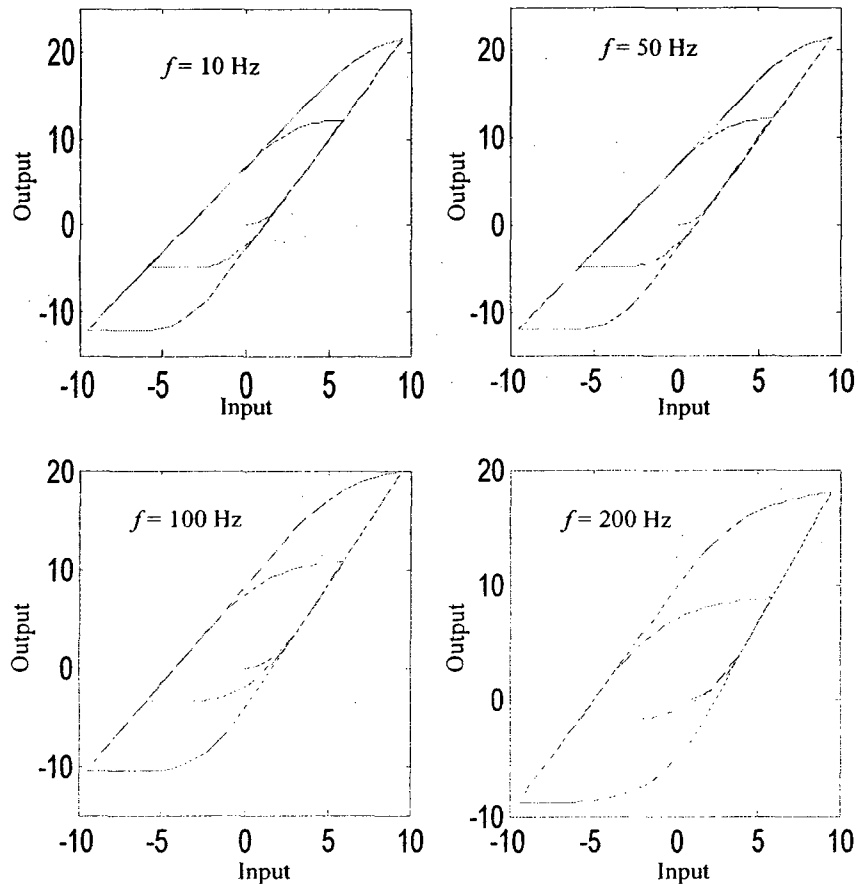


Figure 2.8: Simulation results attained from the Prandtl-Ishlinskii model employing the generalized rate-dependent play operator under a complex harmonic input at different fundamental frequencies.

2.6 Summary

The hysteresis properties of smart actuators exhibit symmetric as well as asymmetric hysteresis loops that are strongly dependent upon the rate of the input.

Furthermore, the outputs of the smart actuators generally exhibit saturation. Three different Prandtl-Ishlinskii models are formulated to characterize these nonlinearities in a systematic manner. A generalized play operator is initially proposed to characterize asymmetric output-input property by selecting different envelope functions. The generalized operator is integrated to the Prandtl-Ishlinskii model to obtain characterization of asymmetric as well as symmetric major and minor hysteresis loops with output saturation. The results show that the integration of the proposed generalized play operator to the classical Prandtl-Ishlinskii model can effectively characterize the asymmetric saturated hysteresis properties of a class of materials and smart actuators.

A rate-dependent play operator is subsequently proposed on the basis of dynamic threshold functions in an attempt to describe the rate dependence of the output-input hysteresis. A rate-dependent Prandtl-Ishlinskii model is then formulated on the basis of the rate-dependent operator and a dynamic density function. The simulation results show that the hysteresis increases considerably with increasing frequency of the input, although the model yields only symmetric hysteresis loops. Finally a generalized rate-dependent Prandtl-Ishlinskii model is proposed by introducing the dynamic threshold within the generalized play operator together with a dynamic density function. The simulation results attained under a complex harmonic input at different frequencies demonstrated that the generalized model describe the symmetric as well as asymmetric rate-dependent hysteresis properties of materials and smart actuators with output saturation. The envelope and dynamic density functions in the model, however, are not unique and must be defined from the hysteresis properties of the particular actuator or material. The nonlinear rate-dependent hysteresis of different actuators is thus thoroughly described in

the following chapter. The model parameters are subsequently identified in Chapter 4 and the model validity is demonstrated under wide ranges of inputs.

Chapter 3: Characterization of Hysteresis Properties of Smart Actuators

3.1 Introduction

The input-output characteristics of smart actuators, such as piezoceramic, magnetostrictive, and SMA actuators, invariably exhibit hysteresis nonlinearities. The presence of hysteresis is known to cause considerable positioning errors in micro/nano-positioning applications. The hysteresis nonlinearities may also lead to instability in the closed-loop operations of smart actuators [31]. The positioning accuracy of such actuators could be significantly enhanced through hysteresis compensation of the closed-loop system. A number of hysteresis models have thus been developed to characterize the hysteresis nonlinearities and to develop control methods for hysteresis compensation [21-36]. Many actuators generally exhibit asymmetric output-input characteristics that are strongly dependent upon the rate of the input. Such extreme nonlinearities present considerable challenges in modeling of hysteresis properties. The reported hysteresis compensation methods, however, generally ignore the effects of input on the hysteresis and yield errors under inputs at higher frequencies.

The hysteresis properties of smart actuators, whether symmetric or asymmetric, could be characterized using the generalized Prandtl-Ishlinskii model formulated in the previous chapter. The development of a reliable model, however, necessitates thorough understanding and characterization of input-output characteristics of smart actuators. Although the hysteresis of smart actuators has been the subject of a vast number of studies [e.g., 20, 21, 27], the characterization of the hysteresis properties of smart actuators subjected to different rates of inputs have been presented in a relatively fewer

studies. Hu and Ben Mrad [64] measured the hysteresis of a piezoceramic actuator and reported that the width of measured voltage–displacement curve was nearly 15% of the peak actuator expansion at very low excitation frequencies. Ge and Jouaneh [22] measured the hysteresis properties of a piezoceramic actuator under sinusoidal excitations at 0.1 and 100 Hz and concluded that the properties were comparable under both excitations, although the response to 100 Hz excitation revealed larger hysteresis. The measurements performed by Yu et al. [34], on the other hand, showed that the hysteresis of a piezoceramic actuator could be considered rate-independent only under excitations at frequencies below 10 Hz. The study also showed larger hysteresis under sinusoidal excitations, when compared to that attained under a triangular input. Tan and Baras [25] measured hysteresis properties of a magnetostrictive actuator under sinusoidal excitations in the 10 - 300 Hz range, and concluded that the hysteresis in the output displacement increased as the excitation frequency of the input current was increased. In a similar manner, Oates et al. [74.] demonstrated the rate-dependent hysteresis in a magnetostrictive actuator through measurements under inputs in the 100-500 Hz range. Gorbet et al. [21] and Hughes and Wen [20] conducted measurements of shape memory alloy (SMA) actuators, which showed saturated major and minor hysteresis nonlinearities between the input temperature and the output displacement.

In this chapter, the input-output characteristics of three different smart actuators, including piezoceramic, SMA, and magnetostrictive actuators, are thoroughly analyzed for charactering their hysteresis properties, particularly the major and minor hysteresis loops and their dependence on the rate of the input. For this purpose, a comprehensive experimental study was undertaken to characterize hysteresis properties of a

piezoceramic actuator under sinusoidal and triangular waveform excitations in a wide frequency range (1 to 500 Hz). The data for two different SMA and magnetostrictive actuators were obtained from the University of Waterloo [21] and the University of Maryland [25] laboratories, respectively. The acquired data were analyzed to illustrate the nonlinear hysteresis properties and their dependence on the rate of input, and to identify target responses for model parameters identifications.

3.2 Experimental Characterization of Hysteresis of a Piezoceramic Actuator

The hysteresis properties of a piezoceramic actuator, P-753.31C, were characterized in the laboratory under a wide range of operating conditions involving frequency, bias and magnitude of the excitation voltage. The actuator provided a maximum displacement of 100 μm from its static equilibrium position, and it integrated a capacitive sensor (sensitivity = $1\mu\text{m}/\text{V}$; resolution $\leq 0.1 \text{ nm}$) for measurement of the actuator displacement response. The natural frequency of this piezoceramic actuator is 2.9 KHz. A voltage amplifier (LVPZT, E-505) with a fixed gain of 10 provided excitation voltage to the actuator in the 0 to 100 V range. The experimental setup is schematically presented in Figure 3.1.

The experiment was designed to study the effects of main factors on the hysteresis properties of the actuator; which included bias, frequency, magnitude and type of excitation voltage. Different values of positive bias were introduced in the input signal to ensure a positive excitation of the piezoceramic actuator. The measurements were performed under two types of excitation voltages; harmonic and triangular. The

experiments under harmonic excitations were conducted with different bias and amplitudes at several discrete frequencies in the 1 to 500 Hz range. The input voltage and output displacement signals were acquired and stored into a multi-channel oscilloscope, which were subsequently expressed by the Lissajous curves. The experiments under triangular input waveforms were conducted to study the hysteresis effects under a constant excitation rate.

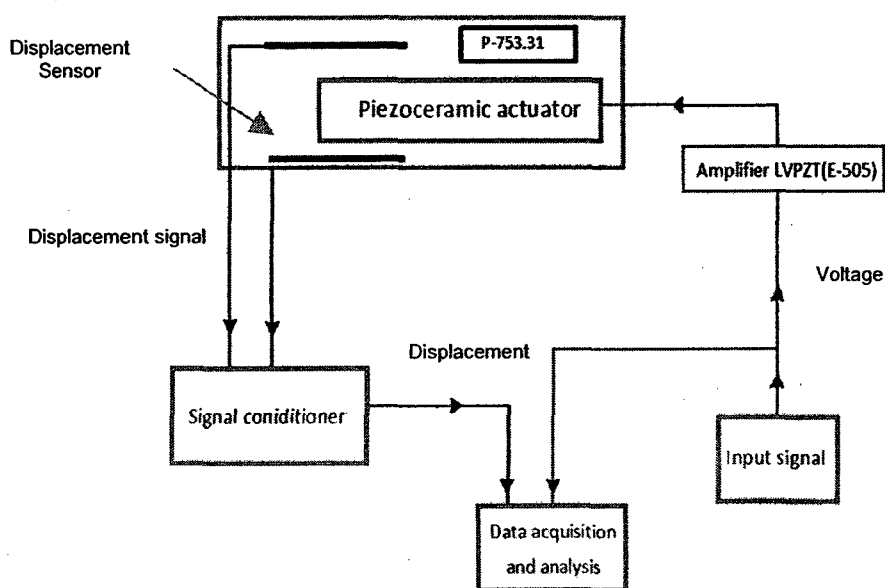


Figure 3.1: A schematic representation of the experimental setup.

The experiments were designed to include three different series with objectives to derive: (i) the effects of input rate on the major hysteresis loops; (ii) the effects of input rate on the minor hysteresis loops; and (iii) the influence of the input waveform. Results attained are used to fully characterize the rate-dependent hysteresis effects, which are discussed in the following sections. Each measurement was repeated 3 times. Although the measurements were invariably repeatable, mean data of the 3 trials were considered for characterizing the hysteresis properties.

3.2.1 MAJOR HYSTERESIS LOOP TESTS

In the first series of experiments, the response characteristics of the actuator were measured to characterize the major hysteresis loops at 12 different excitation frequencies (0.1, 1, 10, 20, 50, 100, 150, 200, 300, 350, 400, and 500 Hz). For this purpose, harmonic excitation signal with bias of 40 V was synthesized to ensure positive voltage input during loading and unloading, while the magnitude was fixed as 40 V. The resulting major loops relating displacement responses to the input voltage are shown in Figure 3.2 for various excitation frequencies. The results clearly show that the hysteresis is strongly dependent upon the rate of input, particularly at frequencies above 10 Hz. An increase in excitation frequency not only yields larger width of the major loop but also reduces the peak displacement output of the actuator, which has also been observed in a few reported studies [34, 64]. The major loop hysteresis is quantified by the peak hysteresis H normalized with respect to peak-to-peak output M , as shown in Figure 3.3. The measured data was further analyzed to quantify hysteresis and displacement attenuation as a function of the excitation frequency. The percent hysteresis of the actuator is illustrated in Figure 3.4 (a) as a function of the input frequency. The results show that percent hysteresis increases nearly exponentially with increasing excitation frequency at frequencies above 10 Hz. Figure 3.4(b) illustrates the considerable attenuation of the peak-to-peak displacement response with increasing frequency, which also tends to be considerable at frequencies above 10 Hz. The results suggest that the rate-independent hysteresis models could be considered valid for describing the actuator hysteresis under excitations below 10 Hz only.

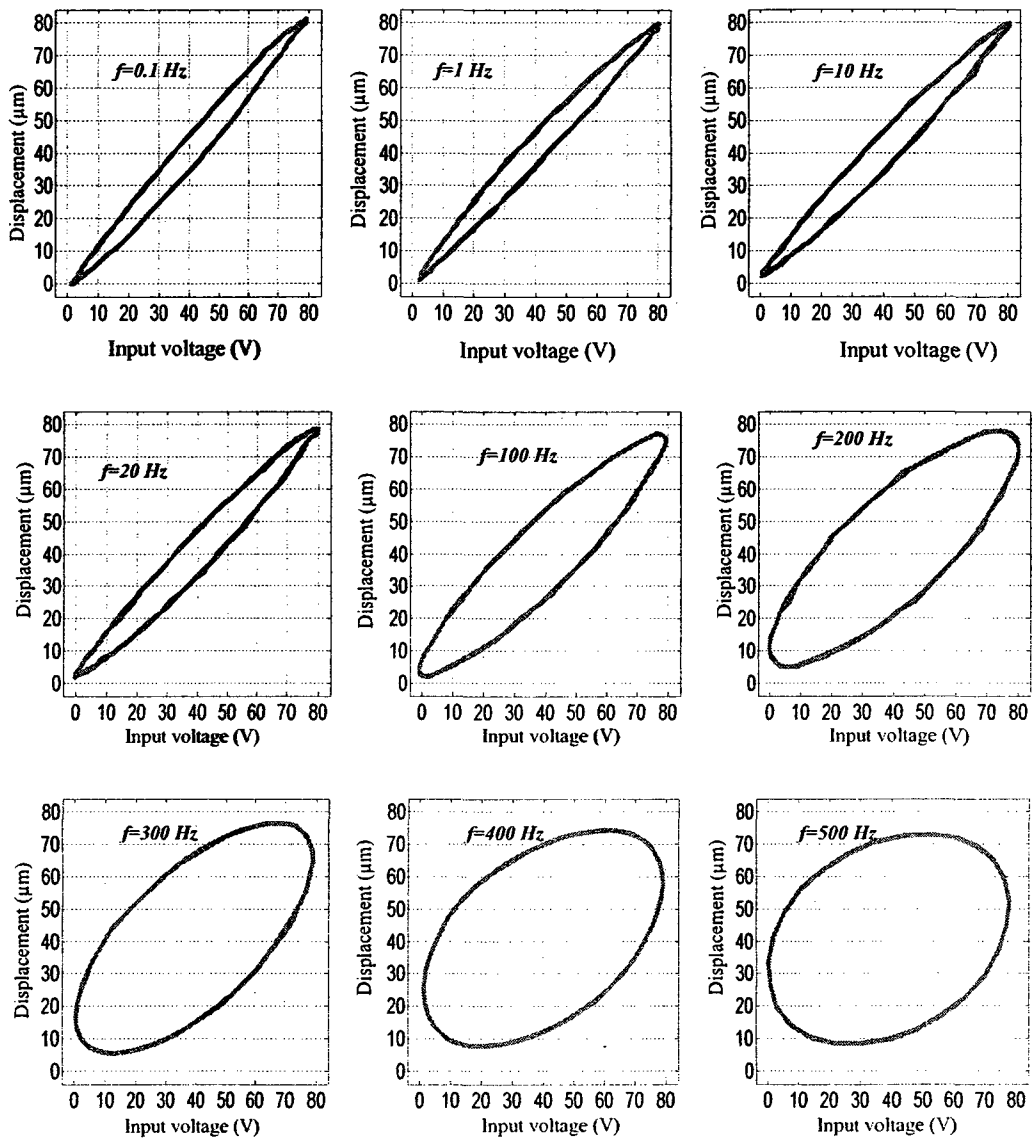


Figure 3.2: Measured major hysteresis loops relating displacement response of a piezoceramic actuator to the applied voltage at different frequencies.

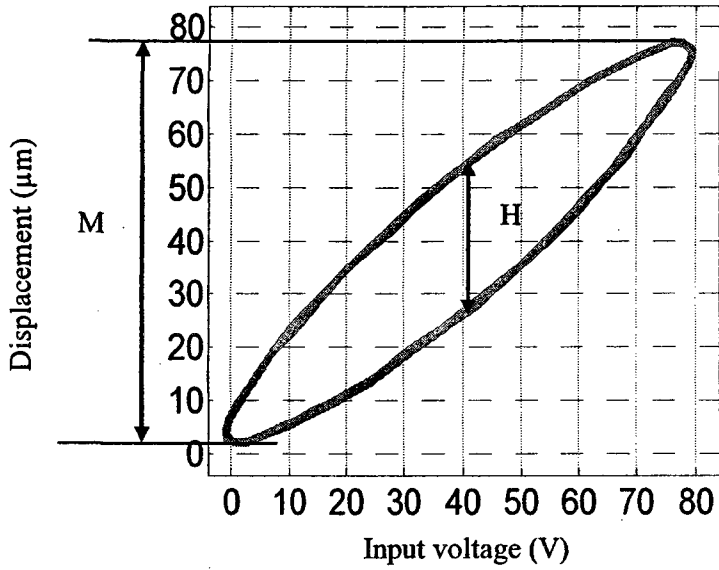
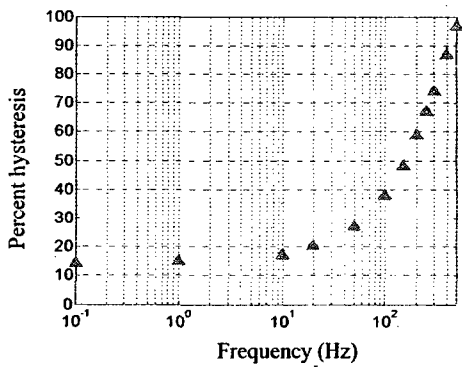
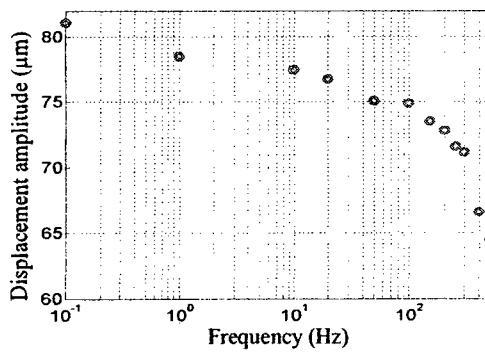


Figure 3.3: Measured major hysteresis loop.



(a)



(b)

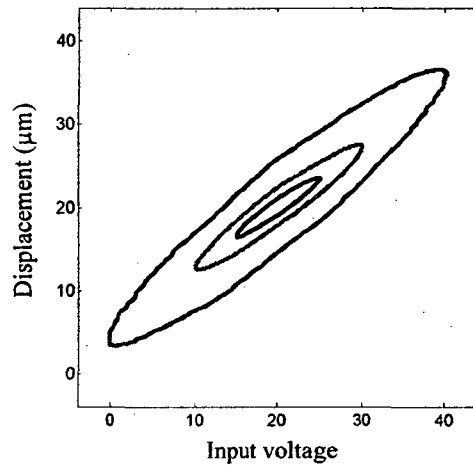
Figure 3.4: (a) Variation in percent hysteresis of major hysteresis loops and, (b) Peak-to-peak displacement response at different excitation frequencies.

3.2.2 MINOR HYSTERESIS LOOPS TEST

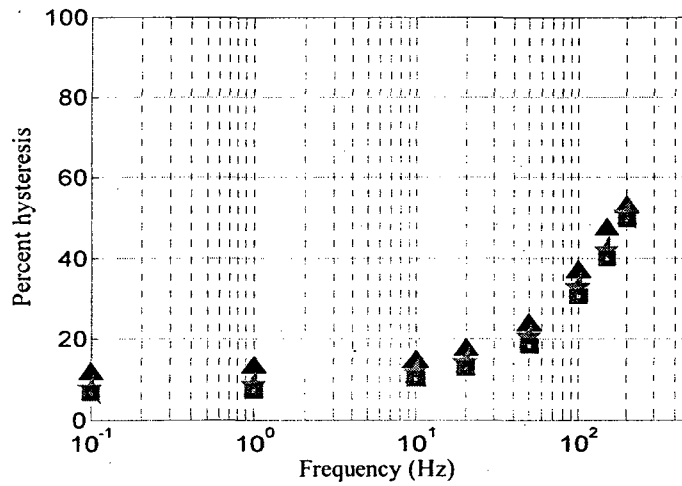
This series attempted to characterize minor hysteresis loops of the actuator under harmonic excitations of various amplitudes and frequencies in the 0.1 to 200 Hz range (0.1, 1, 10, 20, 50, 100, 150, and 200 Hz). The experiments were conducted in two stages, where the first stage involved the study of influence of excitation amplitude on the hysteresis, while the bias was held constant (20 V). For this purpose, three different levels of excitation voltages were considered (5, 10, and 20 V), which resulted in excitation voltages of 20 ± 5 , 20 ± 10 and 20 ± 20 V, respectively. In the second stage, three different bias voltages (30, 60, and 90 V) were considered in conjunction with constant amplitude of 10 V to characterize the effect of bias voltage on the minor hysteresis loops. The variations in the bias voltage resulted in excitation voltages of 30 ± 10 , 60 ± 10 and 90 ± 10 V, respectively.

Figure 3.5 illustrates the minor hysteresis loops under excitation at 100 Hz and percent hysteresis as a function of frequency measured during the first stage of experiments under the three excitations, 20 ± 5 , 20 ± 10 and 20 ± 20 V. Results clearly show significant effect of input magnitude on the percent hysteresis; a higher magnitude of excitation yields slightly larger hysteresis. The change in the output-input curve yields greater attenuation of the actuator output under lower excitation voltages, in addition to that caused by the excitation frequency, as seen in Figure 3.6. Both the percent hysteresis and attenuation of output displacement tend to be considerable at frequencies above 10 Hz. Figure 3.7 shows that the variations in bias voltage caused an insignificant effect on the percent hysteresis. Figure 3.8 illustrates the peak-to-peak displacement responses measured during the second stage of the experiments under bias voltages of 30, 60 and 90

(amplitude = 20 V) as a function of the excitation frequency. These also suggest relatively small effect of bias voltage on the output attenuation.

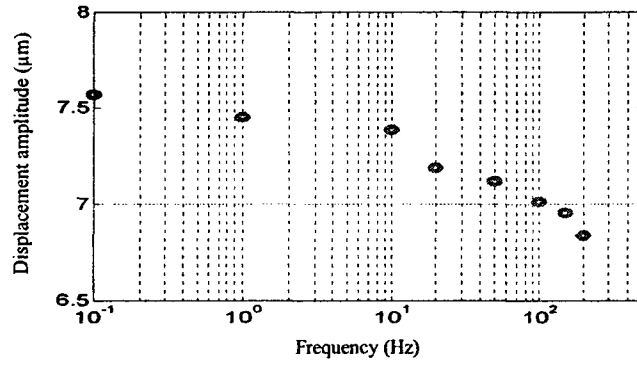


(a)

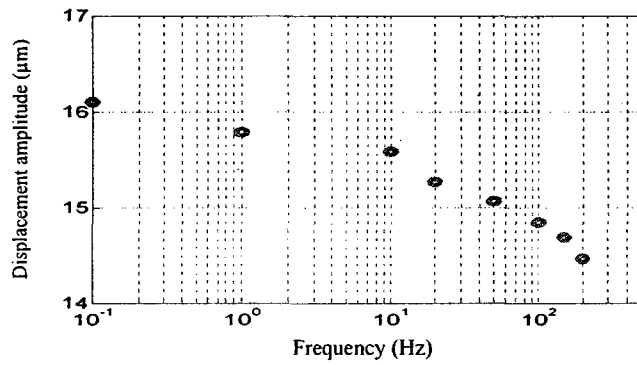


(b)

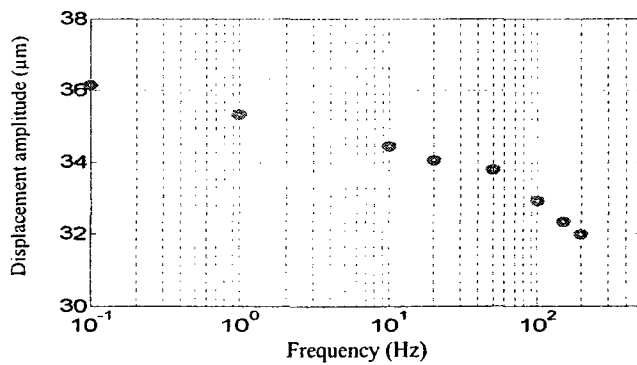
Figure 3.5: (a) Influence of excitation magnitude on the minor hysteresis loops at an excitation frequency of 100 Hz, and (b) Variation in percent hysteresis of the minor loops as a function of excitation frequency (Bias = 20V; Amplitudes: square -5; star-10; and ; triangle -20).



(a)



(b)



(c)

Figure 3.6: Peak-to-peak displacement response of the actuator corresponding to different excitation frequencies and a constant bias input voltage of 20 V: (a) 20±5; (b) 20±10; and (c) 20±20.

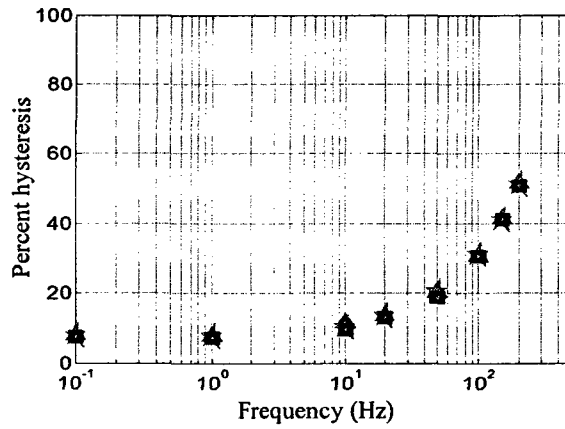


Figure 3.7: Variations in percent hysteresis of the minor loops as a function of frequency and bias voltage (amplitude 10 V; square – 30 ± 10 ; star – 60 ± 10 ; and triangle – 90 ± 10).

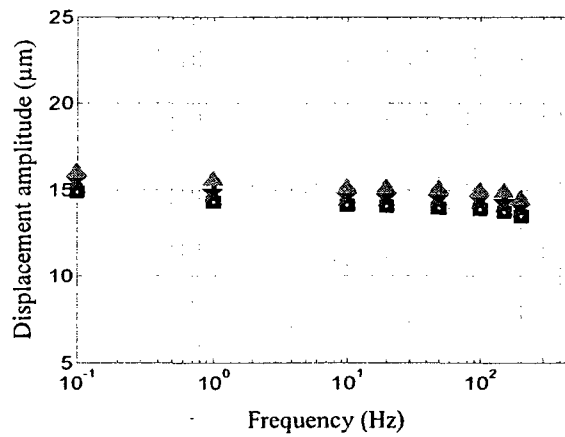


Figure 3.8: Influence of bias voltage on the peak-to-peak displacement response of the piezoceramic actuator under different excitation frequencies (Amplitude=20V; Bias voltage: square – 30 V; star – 60 V; and triangle – 90 V).

3.2.3 INFLUENCE OF THE INPUT WAVEFORM

A few studies have also shown the influence of excitation waveform on the response hysteresis of piezoceramic actuators using harmonic and triangular excitations at low frequencies of 5 Hz [34] and below 20 Hz [69]. It was shown that a triangular waveform yields slightly lower maximum hysteresis nonlinearity H of the mean curve when compared to that under a harmonic excitation. Such differences may be attributed to difference in the time rate of the input waveform. In this study, the hysteresis properties of the actuator are measured under triangular and sinusoidal input waveforms of identical amplitude (40 V) with a bias of 40 V but four different excitation frequencies (1, 10, 100, 200 Hz). The measured data revealed nearly negligible effect of the waveform at frequencies of 1 and 10 Hz, while the waveform effect was apparent at higher frequencies (100 and 200 Hz), as shown in Figure 3.9.

The peak hysteresis loop nonlinearities H tends to be lower under the triangular input compared to that under sinusoidal input, which can be attributed to relatively lower magnitude of rate of change of the triangular input compared to that of the sinusoidal input, as shown in Figure 3.10. The figure compares the input waveforms at selected frequencies and their rate (dv/dt). Moreover, the constant rate of change of the input most likely yields relatively lower slope of the output-input curve under the triangular input. The sharp discontinuity in the triangular also further yields considerably lower peak-to-peak displacement response compared to response to the sinusoidal input, which could be attributed to limited bandwidth of the actuator [69].

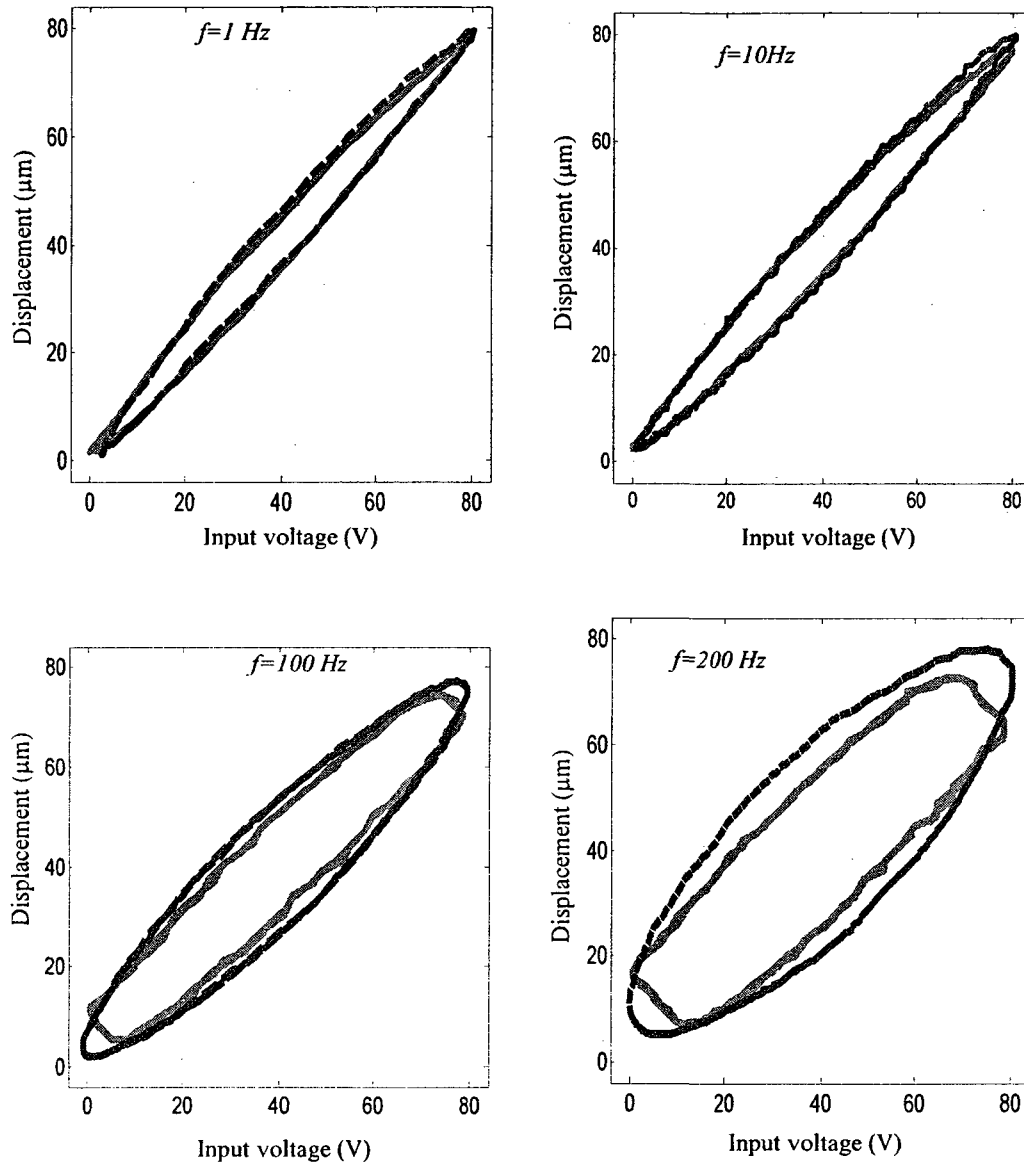


Figure 3.9: Comparisons of major hysteresis loops under sinusoidal and triangular excitations at different frequencies (---, sinusoidal; —, triangular; Amplitude = 40 V; Bias = 40 V).

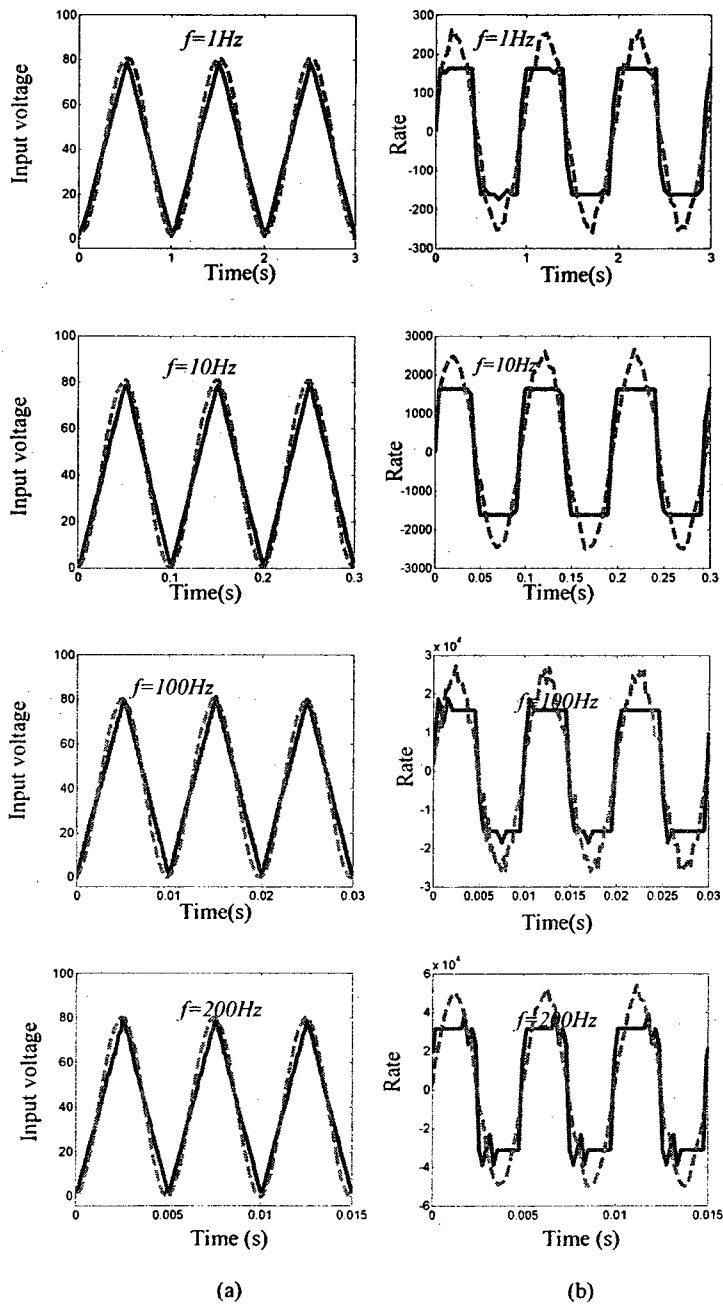


Figure 3.10: Comparisons of the sinusoidal and triangular waveforms and their rates at different excitation frequencies: (a) Waveforms; and (b) Rates (----, sinusoidal; ———, triangular).

3.3 Input-Output Characteristics of Magnetostrictive Actuators

Magnetostriction is the phenomenon of strong coupling between the magnetic and mechanical properties. Some ferromagnetic materials as Terfenol-D show this phenomenon between the output strain and the applied magnetic field. The output strains are produced due to the applied magnetic field which produces changes in magnetization. Magnetostrictive actuators have been widely used in micro-positioning applications and vibration control.

The major and minor hysteresis loop properties of a magnetostrictive actuator have been measured by Xiaobo Tan [25, 33]. The measurements were performed under increasing triangular waveform input currents with amplitude ranging from -0.7 to 1.2 A. The study also measured the hysteresis properties under harmonic excitations at different frequencies in the 10 to 100 Hz (10, 20, 50, and 100 Hz). The magnitude of the input current ranged from -0.7 to 0.9 A. The measured data was acquired and analyzed to study the major and minor hysteresis loops and rate dependence of the actuator hysteresis. Figure 3.11 shows the measured output displacement vs input current relationships for a magnetostrictive actuator acquired under increasing triangular input currents, with amplitude ranging from -0.7 to 1.2 A [25]. The measured data clearly show asymmetric major and minor hysteresis loops as well as output saturation in the output displacement.

Figure 3.12 illustrates hysteresis properties of a magnetostrictive actuator at different excitation frequencies. The results attained under inputs at four frequencies in the 10 to 100 Hz range show considerable variations in the hysteresis loops. Figure 3.13 illustrates the percent hysteresis of the actuator, while Figure 3.14 illustrates variations in percent hysteresis as a function of frequency of the input. The results show that the

hysteresis increases with frequency in a nonlinear manner. This dependence of output magnitude on the excitation frequency, however, would differ with type of actuator or material.

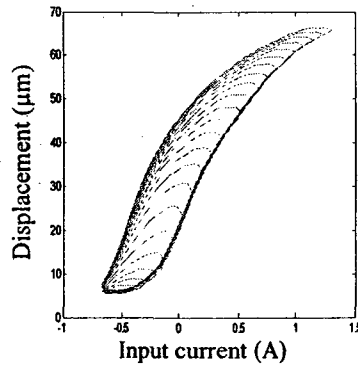


Figure 3.11: Measured output-input responses of a magnetostrictive actuator [25].

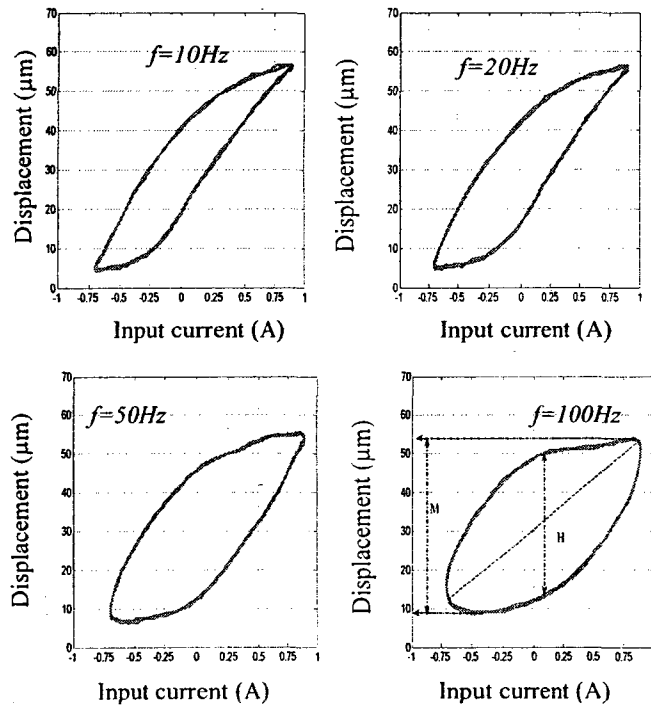


Figure 3.12: Measured hysteresis loops relating displacement response of a magnetostrictive actuator to its applied current at different excitation frequencies [33].

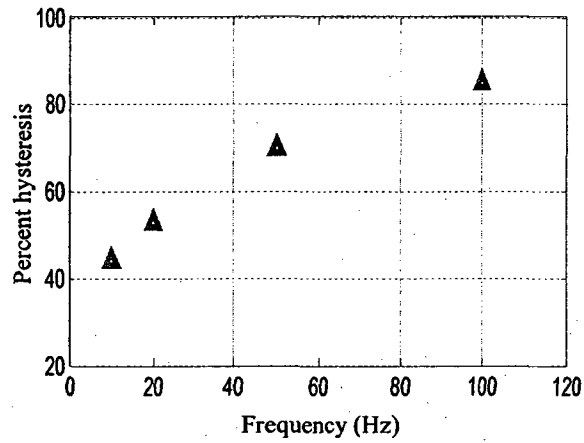


Figure 3.13: Percent hysteresis of the magnetostrictive actuator under excitations at different frequencies (based on data obtained from [33]).

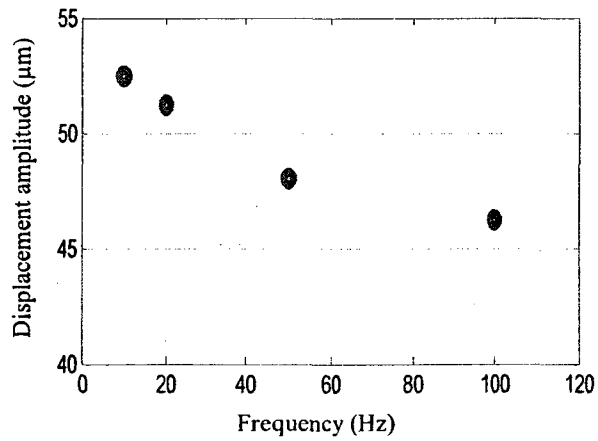


Figure 3.14: Variations in displacement amplitude of a magnetostrictive under excitations at different frequencies (based on data obtained from [33]).

3.4 Input-Output Characteristics of SMA Actuators

The output-input hysteresis properties of two shape memory alloy (SMA) actuators have been measured by Robert Gorbet [21]. The study performed measurements on two SMA actuators, including a one-wire and two-wire actuators. The measurements were performed to establish relationships between the output displacement and the input temperature. The variations in input temperature were realized by applying triangular waveform currents of varying magnitudes. For single-wire SMA actuator, the current was varied from 0 to 1 A, which resulted in input temperature variations from 0 to 175° C. The input current for the two-wire SMA actuator ranged from -1 to 1 A resulting temperature variations from -175 to 175° C.

The input current variations were at a low frequency. The acquired data were analyzed to derive the minor and major hysteresis loops of the two SMA actuators, while the rate dependence of the actuators output and hysteresis could not be established. The output displacement responses of the two actuators are illustrated in Figure 3.15 as a function of variations in the input temperature. The results clearly show highly asymmetric output-input relations of both actuators. The asymmetry is evident in both the major as well as minor hysteresis loops. The results also show notable output saturation. The output displacement of the single-wire actuator tends to saturate most notably at temperatures exceeding 80°C. The two-wire actuator also exhibit similar saturation when the magnitude of the temperature approaches 50°C.

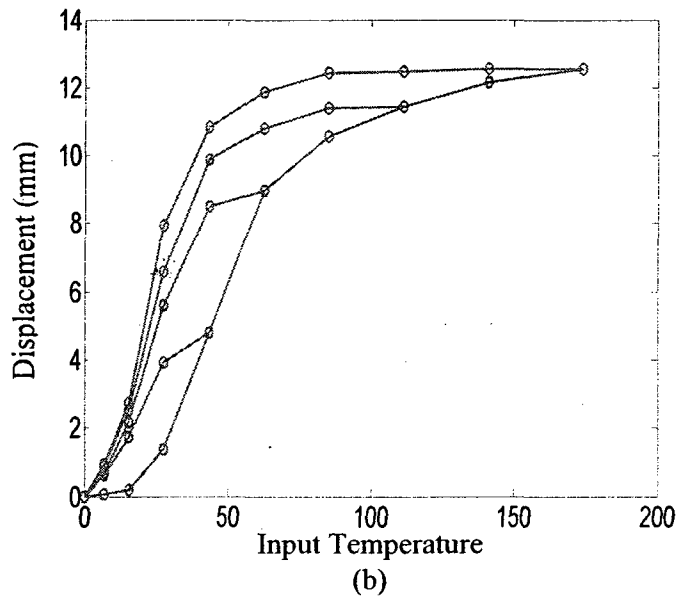
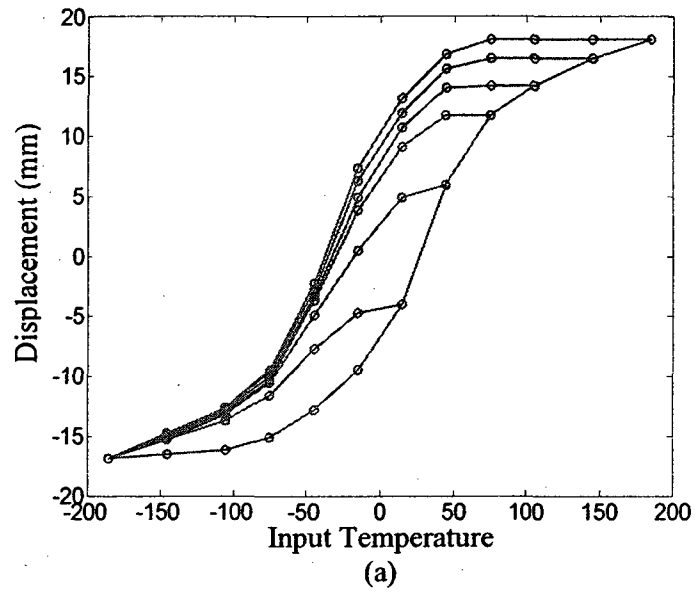


Figure 3.15: Measured output-input responses of two smart actuators: (a) a two-wire SMA actuator; and (b) a one-wire SMA actuator wire [21].

3.5 Discussions

The experimental results of the smart actuators show different hysteresis properties between the input and the output. These hysteresis properties are presented in Table 3.1 for piezoceramic, magnetostrictive and SMA actuators. The piezoceramic actuator show symmetric hysteresis loops without output saturation, while the magnetostrictive and SMA actuators show asymmetric major and minor hysteresis loops as well as output saturation in the output displacement. The piezoceramic actuator show symmetric rate-dependent hysteresis effects between the input voltage and the output displacement, where the hysteresis increases as the excitation frequency of the input voltage increases at frequencies above 10 Hz, while the amplitude of the output displacement decreases. On the other hand, the magnetostrictive actuator exhibits asymmetric rate-dependent hysteresis effects when the frequency of the input current increases.

Table 3.1: Hysteresis properties of smart actuators.

Smart actuator	Rate-independent	Rate-dependent	Symmetric	Asymmetric	Output saturation
Piezoceramic	✓	✓	✓	×	×
Magnetostrictive	✓	✓	×	✓	✓
Shape Memory Alloys	✓	----	✓	✓	✓

The experimental results show that developing a hysteresis model to characterize the hysteresis properties of the smart actuators is a challenge. The required hysteresis model should exhibit the following hysteresis properties:

- Symmetric hysteresis loops to characterize the rate-independent hysteresis properties of the piezoceramic actuators.
- Asymmetric hysteresis loops to characterize the rate-independent hysteresis properties of the magnetostrictive and SMA actuators.
- Output saturation to characterize saturated hysteresis loops of the magnetostrictive and SMA actuators
- Symmetric rate-dependent hysteresis loops to characterize the rate-dependent hysteresis properties of the piezoceramic actuators.
- Asymmetric rate-dependent hysteresis loops to characterize rate-dependent hysteresis properties of the magnetostrictive actuators.

The following Prandtl-Ishlinskii models, presented in Table 3.2, can be applied to characterize symmetric, asymmetric and rate-dependent hysteresis properties. These models are:

- The classic Prandtl-Ishlinskii model, constructed by classic play operator, can be used to characterize rate-independent and symmetric hysteresis loops of the piezoceramic actuators.
- The generalized Prandtl-Ishlinskii model, implemented using the generalized rate-independent play hysteresis operator, can be used to characterize asymmetric and saturated hysteresis loops of the SMA and magnetostrictive actuators.
- The rate-dependent Prandtl-Ishlinskii model based rate-dependent play operator can be applied to characterize rate-dependent hysteresis loops of the piezoceramic actuators.
- The generalized rate-dependent Prandtl-Ishlinskii model based generalized rate-dependent play operator can be used to characterize asymmetric rate-dependent hysteresis loops of the magnetostrictive actuators.

Table 3.2: Hysteresis properties of the Prandtl-Ishlinskii hysteresis models.

Hysteresis model	Rate - independent	Rate-dependent	Symmetric	Asymmetric	Output saturation
Classic PI	✓	×	✓	×	×
Rate-dependent PI	✓	✓	×	✓	×
Generalized PI	✓	×	✓	✓	✓
Generalized rate-dependent PI	✓	✓	✓	✓	✓

3.6 Summary

Hysteresis properties of piezoceramic, magnetostrictive, and SMA actuators are thoroughly characterized under a range of excitation either from reported data or laboratory measurements. Measurements performed on a piezoceramic actuator under different input voltages in the 1 to 500 Hz frequency range revealed strong dependence of the response and the hysteresis on the excitation frequency. The hysteresis nonlinearities of the major as well as minor loops increased considerably with increasing input frequency, while the peak-to-peak displacement amplitude decreased. This dependence was particularly strong at frequencies above 10 Hz. It was thus concluded that the majority of the widely reported hysteresis models would be applicable for under excitations up to 10 Hz only. The experimental results attained under triangular waveform inputs in the 1 to 200 Hz showed that a triangular waveform yields relatively smaller hysteresis nonlinearities compared to that under a sinusoidal input, which is attributed to relatively smaller magnitude of the constant rate of change of the triangular input.

Unlike the piezoceramic actuators, the measured output-input characteristics of the magnetostrictive and SMA actuators showed asymmetric major as well as minor hysteresis loops between the input and the output. These actuators also show output saturation in the major as well as minor hysteresis loops. The magnetostrictive actuators further revealed rate-dependent hysteresis effects similar to the piezoceramic actuators. The results suggested that the asymmetry in the major/minor hysteresis loops, the rate dependence of the hysteresis effects and output saturation must be adequately considered in the hysteresis model. The Prandtl-Ishlinskii models formulated in Chapter 2 can adequately describe these nonlinear hysteresis effects. The classic Prandtl-Ishlinskii model, presented in Section 2.2, can effectively characterize the symmetric rate-independent hysteresis loops such that observed for the piezoceramic actuator at low excitation frequencies. The generalized Prandtl-Ishlinskii model, presented in Section 2.3, can yield asymmetric hysteresis major and minor hysteresis loops with output saturation as observed in the magnetostrictive and SMA actuators. The rate-dependent Prandtl-Ishlinskii models, presented in Sections 2.4 and 2.5, can effectively describe the symmetric as well as asymmetric rate-dependent hysteresis properties. The classic and the generalized Prandtl-Ishlinskii models are subsequently explored in Chapter 4 to characterize the observed hysteresis properties of the smart actuators.

Chapter 4: Modeling Rate-Dependent and Asymmetric Hysteresis Nonlinearities of Smart Actuators

4.1 Introduction

Smart materials based actuators, such as piezoceramic, magnetostrictive and shape memory alloy actuators are widely used in micro-positioning, vibration control and manufacturing applications [32-52]. These actuators, however, exhibit hysteresis phenomenon, which can cause inaccuracy and oscillations in the system response, and could lead to instability of the closed-loop system. A number of models have been proposed to characterize the hysteresis phenomenon in smart actuators. Hughes and Wen [20] proposed Preisach model comprising a second-order polynomial density function and evaluated the fundamental wipe-out and minor-loop congruent properties of piezoceramic and SMA actuators, which were verified experimentally. Ge and Jouaneh [22] characterized the hysteresis in a piezoceramic actuator using modified relay operators with threshold values of 0 and +1, which replaced the threshold values of -1 and +1 of the classical operator. The effectiveness of the FOD (first-order decreasing curves) method in identifying different forms of the Preisach function was demonstrated by Gorbet et al. [21, 60] to characterize the hysteresis properties of two different SMA actuators. Choi et al. [72] proposed a proportional relationship between the major hysteresis loop and FOD curves of a SMA actuator to further simplify the parameters identification of a hysteresis model-based modified operator. Preisach model also has been used to characterize hysteresis properties of magnetostrictive actuators. As an example, Tan and Baras [25] characterized major and minor hysteresis loops of magnetostrictive actuators using Preisach model together with the recursive parameter

identification approach. Another phenomenological operator-based hysteresis model is the Krasnosel'skii-Pokrovskii model which is constructed by integral of a density function and the Krasnosel'skii-Pokrovskii operator. Unlike the relay operator, the Krasnosel'skii-Pokrovskii operator is constructed using two piecewise Lipschitz continuous functions and two threshold values [4]. Banks et al. [28] and Galinaities [27] applied this model to characterize hysteresis effects in smart actuators. These hysteresis models have been mostly applied to describe rate-independent hysteresis effects in ferromagnetic and smart actuators, although the rate-dependent hysteresis nonlinearities of such actuators have been widely demonstrated.

Alternatively, dynamic density functions have been defined to predict rate-dependent hysteresis properties in conjunction with Preisach model [33, 34, 64, 74]. Smith et al. [7] presented a homogenized energy model using Preisach model to characterize the rate-dependent hysteresis in a magnetostrictive actuator over a wide frequency range (1-2 kHz). Ang et al. [68] proposed a dynamic function and dead zone operator for the Prandtl-Ishlinskii model in an attempt to characterize the rate-dependent hysteresis in piezoceramic actuators. The validity of the model was demonstrated for a harmonic input at 10 Hz, and a complex harmonic input comprising 5, 20 and 35 Hz components.

In this chapter, it is shown that the generalized Prandtl-Ishlinskii model based play hysteresis operator can be used to characterize symmetric as well as asymmetric rate-independent hysteresis properties of different smart actuators with output saturation by selecting different envelope functions. The validity of the resulting generalized Prandtl-Ishlinskii model is demonstrated by comparing the model responses in terms of

saturated symmetric and asymmetric major and minor hysteresis loops with the measured input-output characteristics of magnetostrictive, SMA and piezoceramic actuators. The validity of the proposed model is demonstrated using measured data acquired for piezoceramic and magnetostrictive actuators, which show symmetric and asymmetric rate-dependent hysteresis, respectively.

4.2 Classical Prandtl-Ishlinskii model for Characterizing Hysteresis in Smart Actuators

Classic Prandtl-Ishlinskii model (2.5) has been used to characterize rate-independent and symmetric hysteresis properties of piezoceramic actuators [30]. In this section, the properties of the Prandtl-Ishlinskii model are explored and the model is applied to characterize hysteresis properties of piezoceramic, magnetostrictive and SMA actuators. A density function of the following form is selected for the classic Prandtl-Ishlinskii model:

$$p(r) = \rho e^{-\tau r} \quad (4.1)$$

where τ is a constant and ρ is a positive constant. The threshold function of the play operator is chosen as:

$$r_j = cj \quad j = 1, 2, 3, \dots, n. \quad (4.2)$$

where c is a positive constant. The parameters of the classical Prandtl-Ishlinskii model are identified through minimization of an error squared function given by:

$$J(X) = \sum_{i=1}^M (\Pi(v(i)) - y_m(i))^2 \quad (4.3)$$

where $\Pi(v(i))$ is the response of the classical Prandtl-Ishlinskii model, y_m is the measured displacement of an actuator, M is the number of data points considered, J is the error function for the major as well as minor hysteresis loops, and X is the parameters vector given by: $\{X\} = \{\tau, \rho, q, \text{ and } c\}$. The error minimization problem was solved using the MATLAB optimization toolbox, subject to following constraints:

$$\rho, q, c > 0$$

The solutions of the minimization problem were attained for different starting parameter vectors, which converged to very similar solutions. The minimization problem was solved using the data for the piezoceramic actuator under a complex harmonic input, $v(t)=50+10\sin(2\pi t)+ 36\cos(5.1\pi t)$. The resulting model parameters identified using the piezoceramic actuator data are summarized in Table 4.1. The results, shown in Figure 4.1, show that the classic Prandtl-Ishlinskii model can accurately characterize the symmetric major as well as minor hysteresis properties of a piezoceramic actuator.

The application of the classical Prandtl-Ishlinskii model is further attempted to characterize the saturated asymmetric hysteresis properties of SMA and magnetostrictive actuators, described in Sections 3.3 and 3.4, respectively. The resulting model parameters identified using reported measured data for two SMA and a magnetostrictive actuator are summarized in Table 4.2. Figures 4.2 and 4.3 illustrate the comparisons of the measured and the model displacement responses of the two actuators, respectively. From the results, it is apparent that the classical model yields substantial errors in predicting asymmetric hysteresis and output saturation properties of a class of smart actuators. This attributed to the symmetric and unbounded properties of the play hysteresis operator.

Table 4.1: Identified parameters of the classical Prandtl-Ishlinskii model.

Parameter	Value
c	2.243
ρ	0.056
τ	0.041
q	0.631

Table 4.2: Identified parameters of the classical Prandtl-Ishlinskii model using the reported measured data for two SMA and a magnetostrictive actuators.

Parameter	Two-wire SMA actuator	One-wire SMA actuator	Magnetostrictive actuator
c	2.338	4.8735	0.1751
ρ	7.712×10^{-3}	37.442×10^{-3}	2.4944
τ	5.494×10^{-3}	17.120×10^{-3}	0.7502
q	2.882×10^{-7}	0.02681	0.3464

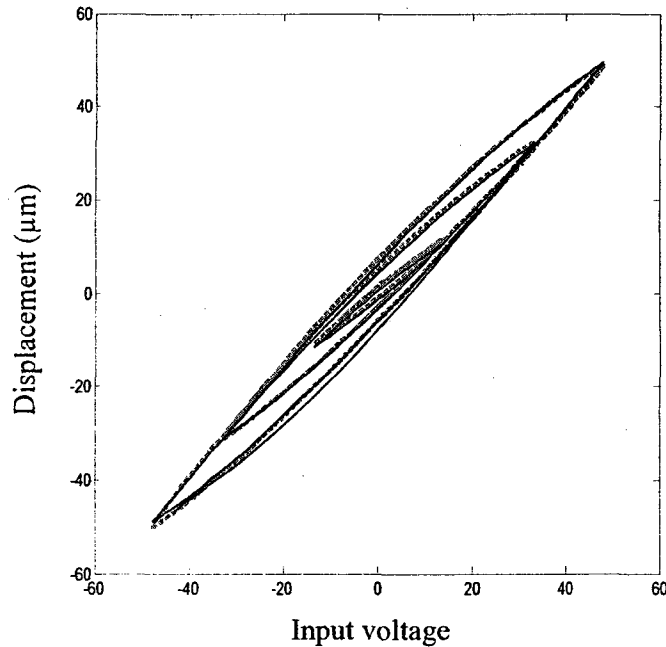


Figure 4.1: Comparisons of displacement responses of the classic Prandtl-Ishlinskii hysteresis model with the measured data of a piezoceramic actuator under complex harmonic input (---, measured; —, model).

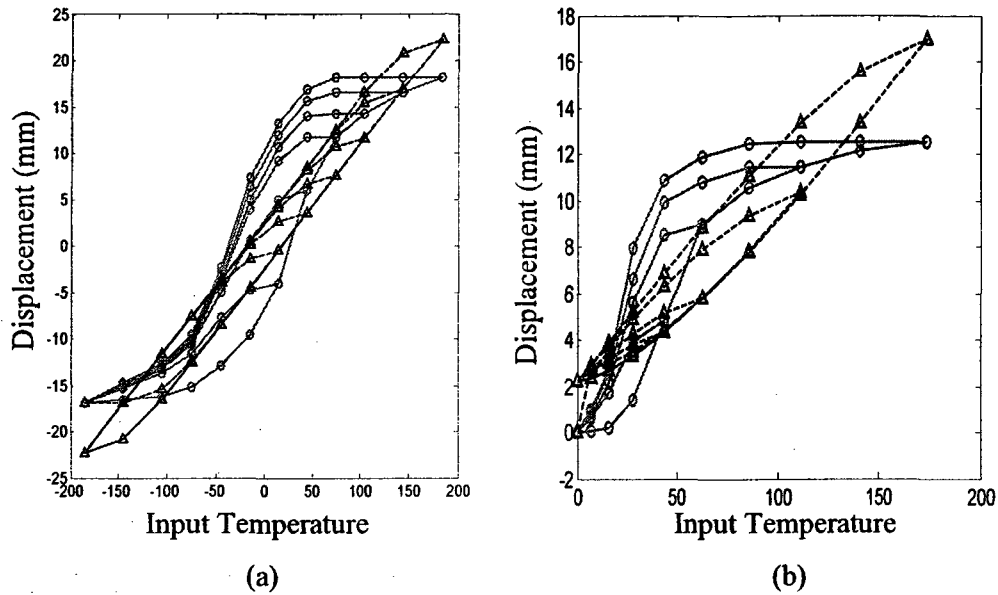


Figure 4.2: Comparisons of displacement responses of the classical Prandtl-Ishlinskii model with the measured data of two SMA actuators: (a) one-wire SMA actuator wire; and (b) two-wire SMA actuator. (—○—, measured; --△--, model).

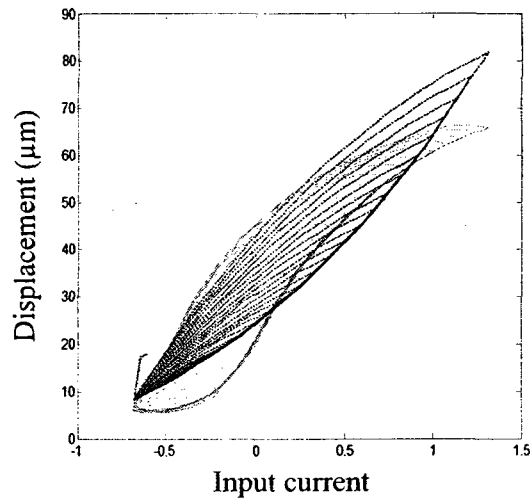


Figure 4.3: Comparisons of displacement responses of the classical Prandtl-Ishlinskii model with the measured responses of the magnetostrictive actuator (——, measured; , model).

4.3 Generalized Rate-Independent Prandtl-Ishlinskii Model for Characterizing Hysteresis in Smart Actuators

In this section, the generalized Prandtl-Ishlinskii model, described in Chapter 2, is applied for characterizing asymmetric hysteresis properties of SMA and magnetostrictive actuators with output saturation. The validity of generalized Prandtl-Ishlinskii model (2.13) is demonstrated by comparing the model responses with the measured major and minor hysteresis loops of the SMA, magnetostrictive and piezoceramic actuators.

4.3.1 FORMULATION OF ENVELOPE FUNCTIONS AND PARAMETERS IDENTIFICATION

The parameters of the generalized play hysteresis operator and the density function need to be defined on the basis of known characteristics of a smart actuator. A hyperbolic tangent function perhaps a better choice for the envelope functions to describe the output of such a function is continuous and invertible. The suggested envelope functions for generalized play operator (2.10) are expressed as:

$$\begin{aligned}\gamma_r(v) &= a_o \tanh(a_1 v + a_2) + a_3 \\ \gamma_l(v) &= b_o \tanh(b_1 v + b_2) + b_3\end{aligned}\tag{4.4}$$

where $a_o > 0$, $a_1 > 0$, a_2 , a_3 , $b_o > 0$, $b_1 > 0$, b_2 , and b_3 are constants to be identified using the experimental data.

The model parameters are identified using the reported measured output-input data, presented in Figure 3.15, for two SMA (single and double wires) and magnetostrictive actuators. The generalized model parameters are identified through minimization of an error sum squared function (4.3). The parameters vector for the

generalized model is given by: $\{X\}=\{a_0, a_1, a_2, a_3, b_0, b_1, b_2, b_3, \tau, \rho, \text{ and } c\}$. The error minimization problem was solved using the MATLAB optimization toolbox, subject to following constraints:

$$a_0, a_1, b_0, b_1, \rho, c > 0$$

The solutions of the minimization problem were attained for different starting parameter vectors, which converged to very similar solutions. The minimization problem was solved using the data for all three actuators and the resulting model parameters are summarized in Table 4.3.

The applicability of the generalized Prandtl-Ishlinskii model for characterizing symmetric hysteresis of piezoceramic actuators was further investigated. The simulations were performed for both the generalized and classical Prandtl-Ishlinskii models employing similar density and threshold functions, described in (4.1) and (4.2), respectively. Linear envelope functions of the following form were used in generalized play operator (2.6):

$$\begin{aligned} \gamma_r(v) &= a_0 v + a_1 \\ \gamma_l(v) &= b_0 v + b_1 \end{aligned} \tag{4.5}$$

where $a_0 > 0$, $a_1, b_0 > 0$, and b_1 are constants.

Parameters identification of the generalized Prandtl-Ishlinskii model was performed also on the output-input characteristics of the piezoceramic actuator. The measured data which is presented in Figure 4.1 were used to solve the error minimization problem defined in (4.3) to identify the model parameters. Table 4.4 summaries the identified parameters of the generalized Prandtl-Ishlinskii model. It can be seen that the

coefficients a_o and b_o of the two envelope functions are quite comparable, which suggests similar envelope functions for nearly symmetric hysteresis properties of the piezoceramic actuator.

Table 4.3: Parameters of the generalized Prandtl-Ishlinskii model identified using the reported measured data for two SMA actuators and a magnetostrictive actuator.

Parameters	Two-wire SMA actuator	One-wire SMA actuator	Magnetostrictive actuator
c	2.3665	0.013	0.857
ρ	0.17533	1.281	1.361
τ	0.0049	0.011	0.214
a_o	21.7265	1.545	15.991
a_1	0.01124	0.019	0.978
a_2	0.0001	0.288	-0.373
a_3	0	-0.923	0
b_o	23.1275	0.672	14.109
b_1	0.01494	0.026	0.973
b_2	1.8176	-0.239	0.648
b_3	0	-0.159	0

Table 4.4: Identified parameters for the generalized Prandtl-Ishlinskii models using the measured output-input characteristics of the piezoceramic actuator.

Parameters	Generalized Prandtl-Ishlinskii model
C	1.194
ρ	0.388
τ	0.081
a_o	0.326
a_1	5.535
b_o	0.396
b_1	-9.982

4.3.2 EXPERIMENTAL VERIFICATIONS

The validity of the generalized Prandtl-Ishlinskii model incorporating the generalized play operator with hyperbolic-tangent envelope functions is investigated by comparing the model responses with the available measured data of the SMA, magnetostrictive and piezoceramic actuators. Figures 4.4 and 4.5 illustrate comparisons of the generalized model responses of the SMA and magnetostrictive actuators, respectively, with the measured data. The results clearly suggest that the model can effectively predict asymmetric hysteresis properties of both types of actuators. Moreover, the model can also characterize output saturation of both the SMA actuators in the proximity of the extreme input temperatures, as seen in the output displacement vs input temperature properties of the one- and two-wire SMA actuators. Figure 4.5, in a similar manner, illustrates comparisons of the major and minor loops in the displacement responses of the model with the corresponding measured data. The results suggest reasonably good agreements between the model and measured displacement responses.

The effectiveness of the generalized model in predicting the asymmetric saturated hysteresis responses of the single-wire SMA and magnetostrictive actuators can also be seen from comparisons of the displacement responses in the time domain, presented in Figures 4.6 and 4.7, respectively. The figures present the comparison of the model responses with the measured data for both actuators. The results show notable prediction error for both the actuator models. The peak errors in the displacement responses of the generalized Prandtl-Ishlinskii model using generalized play operator with the hyperbolic envelope functions of the one-wire SMA and magnetostrictive actuators are 0.66 mm and

2.94 μm , respectively, which are approximately 3% of the maximum outputs for both the actuators.

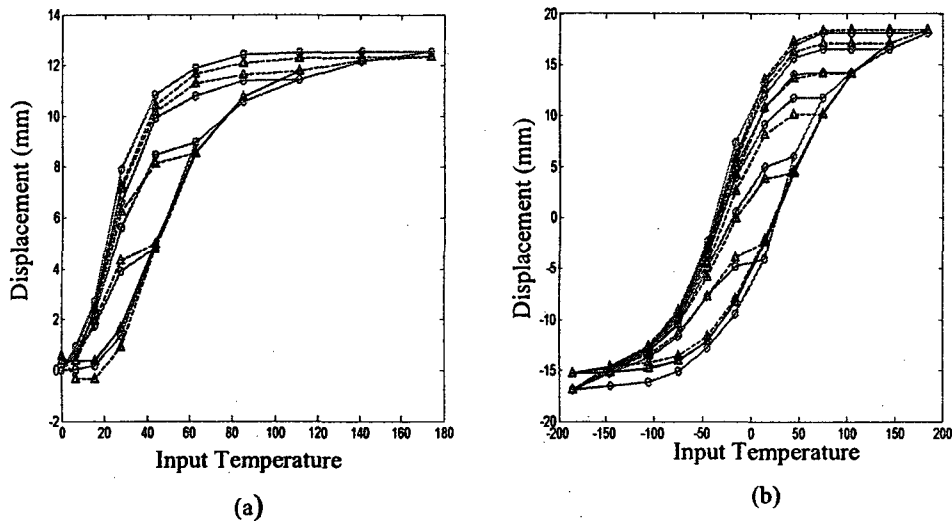


Figure 4.4: Comparisons of displacement responses of the generalized Prandtl-Ishlinskii model with the measured data of two SMA actuators: (a) one-wire SMA actuator wire; and (b) two-wire SMA actuator. (--- Δ ---, model; — \circ —, measured).

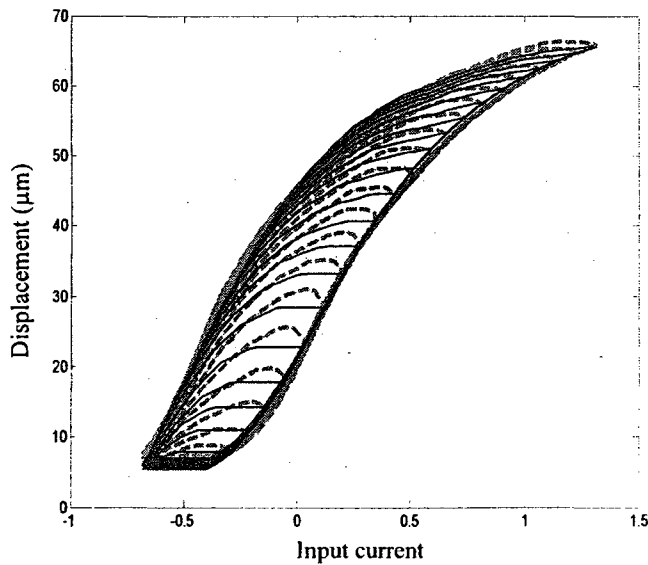


Figure 4.5: Comparisons of displacement responses of the generalized Prandtl-Ishlinskii model with the measured responses of the magnetostrictive actuator (-----, measured; —, model).

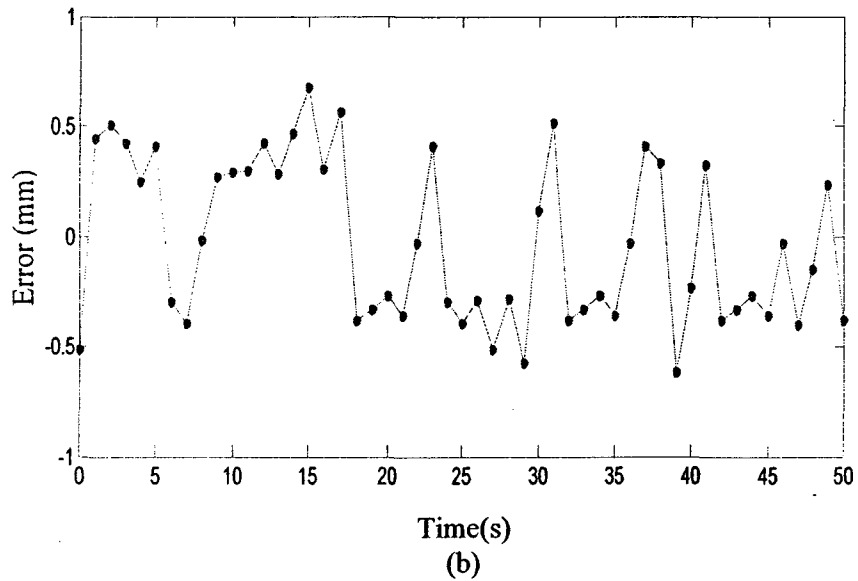
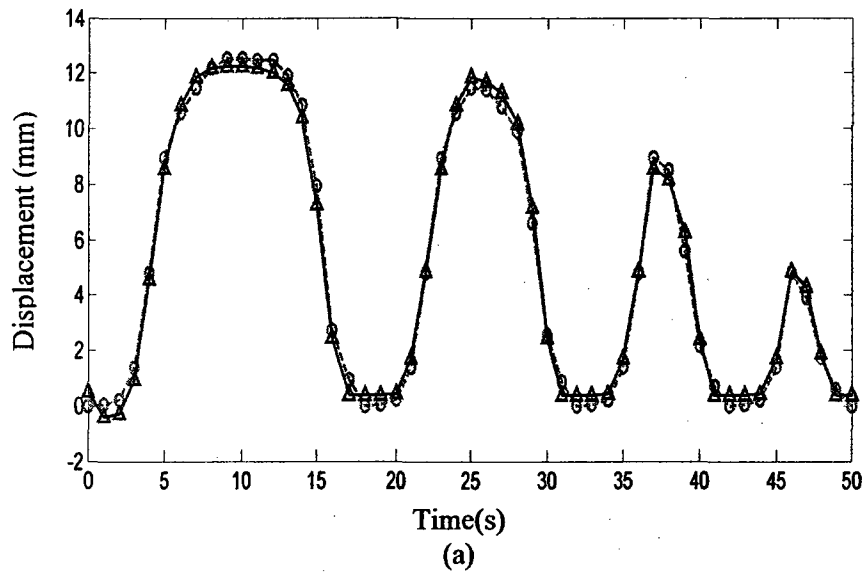
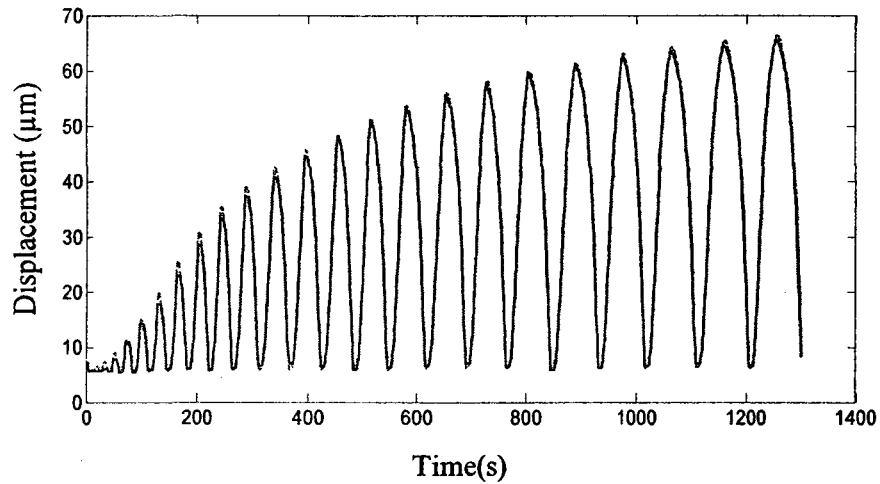
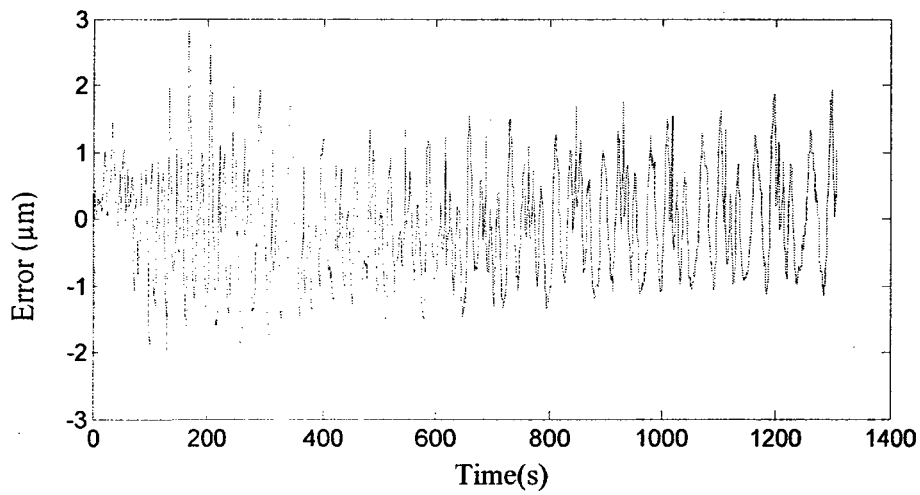


Figure 4.6: (a) Comparisons of time histories of displacement responses of the generalized Prandtl-Ishlinskii model with the measured data of the single-wire SMA actuator (- - Δ - - , measured; — \circ — , model); and (b) variations in the error.



(a)



(b)

Figure 4.7: (a) Comparisons of time histories of displacement responses of the generalized Prandtl-Ishlinskii model with the measured data of the magnetostrictive actuator (---, measured; —, model); and (b) variations in the error magnitude.

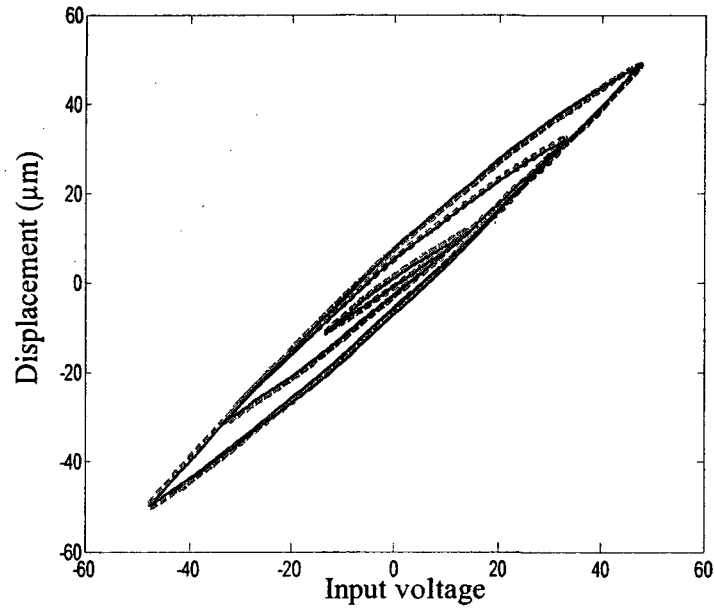


Figure 4.8: Comparisons of displacement responses of the Prandtl-Ishlinskii hysteresis models with the measured data of the piezoceramic actuator under complex harmonic (---, measured; —, model).

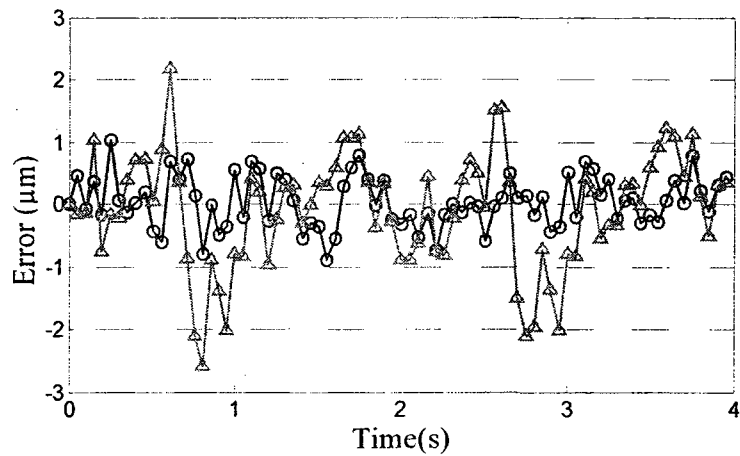


Figure 4.9: Comparisons of differences in output displacements of the generalized and classical Prandtl-Ishlinskii models and the measured data under complex harmonic input, (—△—, classical model; —○—, generalized model).

The output-input responses of the generalized model employing linear envelope functions are also evaluated under complex harmonic input of the form, $v(t) = 10\sin(2\pi t) + 36\cos(5.1\pi t)$ in order to characterize symmetric hysteresis of the piezoceramic actuator. The results are compared with the measured data for the piezoceramic actuator in Figure 4.8. Although the validity of the classical Prandtl-Ishlinskii model in predicting the symmetric hysteresis properties presented in Figure 4.1 has been demonstrated, the generalized model can provide enhanced prediction of the symmetric hysteresis properties. Figure 4.9 presents a comparison of output errors of the two models, classic and generalized Prandtl-Ishlinskii models, in the time domain, with respect to the laboratory-measured data. The peak deviation between the generalized Prandtl-Ishlinskii model responses and the measured data are in the order of $1.02\mu\text{m}$. While classic Prandtl-Ishlinskii model shows $2.59\mu\text{m}$ peak errors under complex harmonic and triangular inputs, respectively. These results suggest that the generalized Prandtl-Ishlinskii model could also characterize symmetric hysteresis properties more accurately, when compared to the classical model.

4.4 Rate-Dependent Prandtl-Ishlinskii Model for Characterizing Rate-Dependent Hysteresis of a Piezoceramic Actuator

The measured output-input characteristics of the piezoceramic actuator, presented in Chapter 3, exhibit hysteresis effects that strongly dependent on the rate of the input. The effect was particularly strong at above 10 Hz. Both the classical and generalized models would yield significant errors under inputs at frequencies above 10 Hz. Furthermore, the measured responses revealed certain dependence on the type of the input. This was evident from the responses attained under triangular waveform inputs in

the 1 to 200 Hz, which revealed relatively smaller width of the hysteresis loops compared to that under a sinusoidal input.

The dependence of the output in the rate of input could be incorporated within the generalized and classical Prandtl-Ishlinskii models through formulation of the rate-dependent play operator and dynamic density function. A rate-dependent Prandtl-Ishlinskii model is thus formulated for charactering the hysteresis responses of smart actuators over a wide range of input frequencies, such that:

$$\bar{\Pi}(v(t)) = \bar{h}(v(t), \dot{v}(t)) + \int_0^R \bar{g}(v(t), \dot{v}(t)) \bar{p}(\bar{r}) F_{\bar{r}}(v(t)) d\bar{r} \quad (4.6)$$

where $\bar{g}(v, \dot{v})$ and $\bar{h}(v, \dot{v})$ are positive continuous functions of the current input $v(t)$ and its time rate $\dot{v}(t)$. The choices of the functions $\bar{h}(v, \dot{v})$ and $\bar{g}(v, \dot{v})$ are not unique, these would depend upon the nature of hysteresis of particular material or device. The functions $\bar{h}(v, \dot{v})$ and $\bar{g}(v, \dot{v})$ of the following forms may be chosen to characterize rate-dependent hysteresis effects:

$$\bar{h}(v(t), \dot{v}(t)) = a_1 e^{-m_1 \dot{v}(t)} e^{m_2 v(t)} \quad (4.7)$$

$$\bar{g}(v(t), \dot{v}(t)) = a_2 e^{-n_1 \dot{v}(t)} e^{n_2 v(t)} \quad (4.8)$$

where a_1, a_2, m_1, m_2, n_1 and n_2 are constants. The dynamic threshold \bar{r} is selected as:

$$\bar{r} = \alpha \prod_{l=1}^{\bar{z}_r} \ln(\beta_l + \lambda_l |\dot{v}(t)|^{\epsilon_l}) \quad (4.9)$$

where λ_l and α are positive constants, $\beta_l \geq 1$ and $\epsilon_l \geq 1$. The order of the rate-dependent threshold is determined by positive integer z_r that decides the order of the dynamic threshold. A higher-order threshold function was found to characterize

hysteresis effects more accurately under high frequency inputs. A second-order dynamic threshold \bar{r} ($z_r = 2$) is formulated in the following manner:

$$\bar{r} = \alpha \ln(\beta_1 + \lambda_1 |\dot{v}(t)|^{\varepsilon_1}) \ln(\beta_2 + \lambda_2 |\dot{v}(t)|^{\varepsilon_2}) \quad (4.10)$$

4.4.1 PARAMETERS IDENTIFICATION

The measured major hysteresis loop under different excitation frequencies of the piezoceramic actuator was applied to identify the parameters of the rate-dependent Prandtl-Ishlinskii model. Dynamic threshold (4.10) and the functions $\bar{h}(v, \dot{v})$ and $\bar{g}(v, \dot{v})$ defined in (4.7) and (4.8), respectively, need to be defined on the basis of known characteristics of a specific actuator. The experimental data obtained for the piezoceramic actuator under harmonic inputs at various frequencies in the 1 to 500 Hz range are applied to identify the model parameters. The parameter vector $X = \{\alpha, \beta_1, \beta_2, \lambda_1, \lambda_2, \varepsilon_1, \varepsilon_2, a_1, a_2, \rho, \tau, m_1, m_2, n_1, n_2\}$, was identified through minimization of an error sum-squared function over a wide frequency range, given by:

$$J(X) = \sum_{j_f=1}^n \sum_{i=1}^M C_{j_f} (\bar{\Pi}(v(i)) - y_m(i))^2 \quad (4.11)$$

subject to:

$$\alpha, \lambda_1, \lambda_2, \varepsilon_1, \varepsilon_2, a_1, a_2, \rho > 0$$

$$\beta_1, \beta_2 \geq 1$$

where $\bar{\Pi}(v(t))$ is the displacement response of the rate-dependent Prandtl-Ishlinskii model corresponding to a particular excitation frequency and y_m is the measured displacement under the same excitation frequency. The error function is constructed

through summation of squared errors over a range of input frequencies. A weighting constant C_{j_f} ($j_f=1, \dots, n$) was introduced to emphasize the error minimization at higher frequencies. The index i ($i=1, \dots, M$) refers to the number of data points considered to compute the error function J for one complete hysteresis loop. A total of 100 data points ($M=100$) were available for each measured hysteresis loop.

The solutions of the minimization problem with various starting vectors resulted in the following solution for the model parameters: $\alpha=1.0$, $\lambda_1=0.00710$, $\lambda_2=0.00128$, $\beta_1=1.0$, $\beta_2=2.3$, $\varepsilon_1=1.0$, $\varepsilon_2=1.0$, $a_1=0.189$, $a_2=0.116$, $m_1=n_1=2.9 \times 10^{-6}$, and $m_2=n_2=0$ were subsequently used to simulate the rate-dependent Prandtl-Ishlinskii model to examine its validity for characterizing major as well as minor hysteresis loops under harmonic inputs in the 1-500 Hz frequency range. The following inputs are applied also to excite the piezoceramic actuator: (i) sinusoidal input voltages of amplitude 40 V at 1, 10, 20, 150, 200, 250, 300, 350, and 500 Hz, (ii) complex harmonic input voltages of the form, $v(t)=50+10\sin(2\pi ft) +36\cos(3.4\pi ft)$, at 1, 10, 50, and 100 Hz, and (iii) triangular input voltages of amplitude 40 V at 1, 10, 150, and 200 Hz.

4.4.2 MAJOR HYSTERESIS LOOP SIMULATION

The simulation results attained under harmonic inputs (amplitude=40V) in the 1 to 500 Hz frequency range are compared with the measured major hysteresis loops data to demonstrate the validity of the rate-dependent Prandtl-Ishlinskii model. Figure 4.10 compares the model responses with the measured data under excitations at different frequencies in the 1 to 500 Hz range. The results suggest good agreements between the model and measured results, while the peak displacement error is below 5 μm ,

irrespective of the rate of the input. In practice, both the measured and model results show increasing hysteresis and decreasing output amplitude with increasing excitation frequency. Figure 4.11 illustrates corresponding outputs of the rate-dependent play operator at different excitation frequencies, where the nonlinearity in the output increases as the excitation frequency of the input voltage increases.

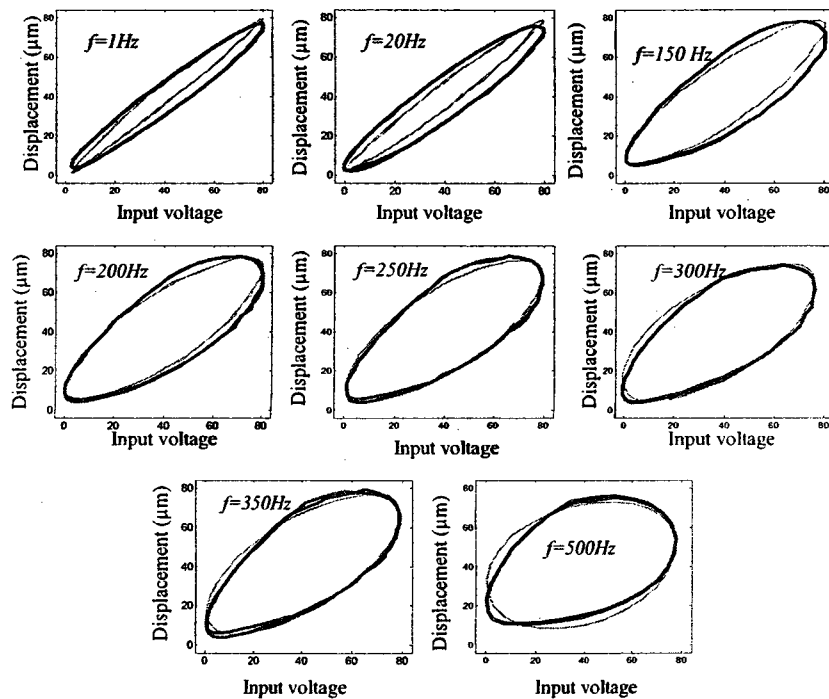


Figure 4.10: Comparisons of measured responses with the results derived from rate-dependent model under inputs at different excitation frequencies (———— , measured; ————— , model).

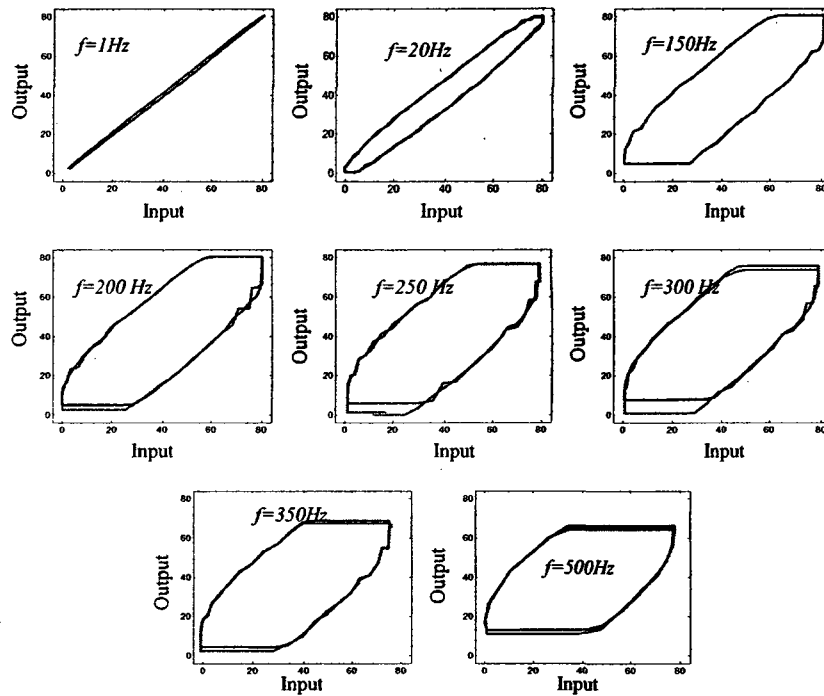


Figure 4.11: Input output relationships of the rate-dependent play operator at different frequencies.

4.4.3 MINOR HYSTERESIS LOOP SIMULATION

The ability of the rate-dependent Prandtl-Ishlinskii model in predicting minor hysteresis loop behavior is further investigated over a wide range of excitation frequencies. For this purpose, the model responses to an input of the form, $v(t)=50+10\sin(2\pi f t)+36\cos(3.4\pi f t)$, are evaluated and compared with the measured data at 1, 10, 50 and 100 Hz fundamental frequencies. The simulation results of the rate-dependent model attained under selected fundamental frequencies are compared with the measured displacement responses in Figure 4.12. The results demonstrate reasonably good agreements in minor loop responses of the model with the measured data, irrespective of the fundamental frequency considered. Time histories of displacement responses of the rate-dependent Prandtl-Ishlinskii model are further compared with the

measured data obtained under the complex harmonic excitations with fundamental frequencies of 1, 10, 50 and 100 Hz in Figure 4.13. The figure also shows the time-histories of error between the model and measured responses. The results suggest very good agreements between the predicted and measured displacement responses, while the peak displacement error is below 5 μm , irrespective of the fundamental frequency. Table 4.5 summarizes the percentage of norm and peak errors of the rate-dependent model at different fundamental frequencies, which tend to be bounded between 5.06-6.50% and 3.57-4.77%, respectively.

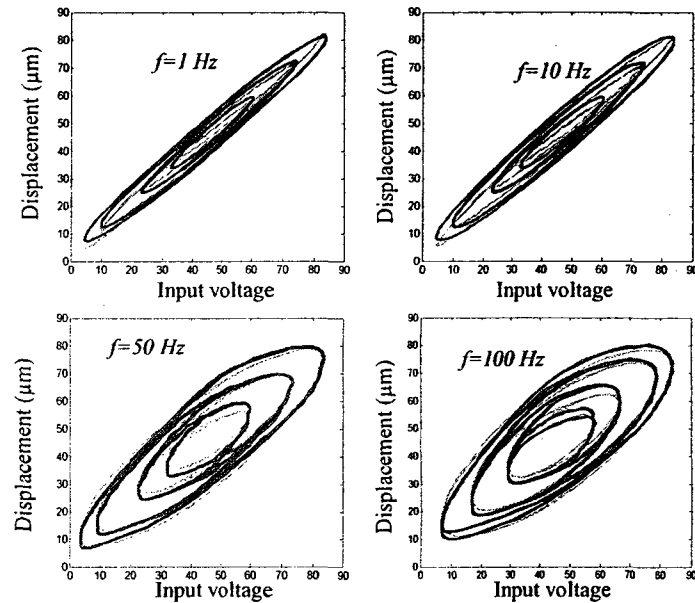
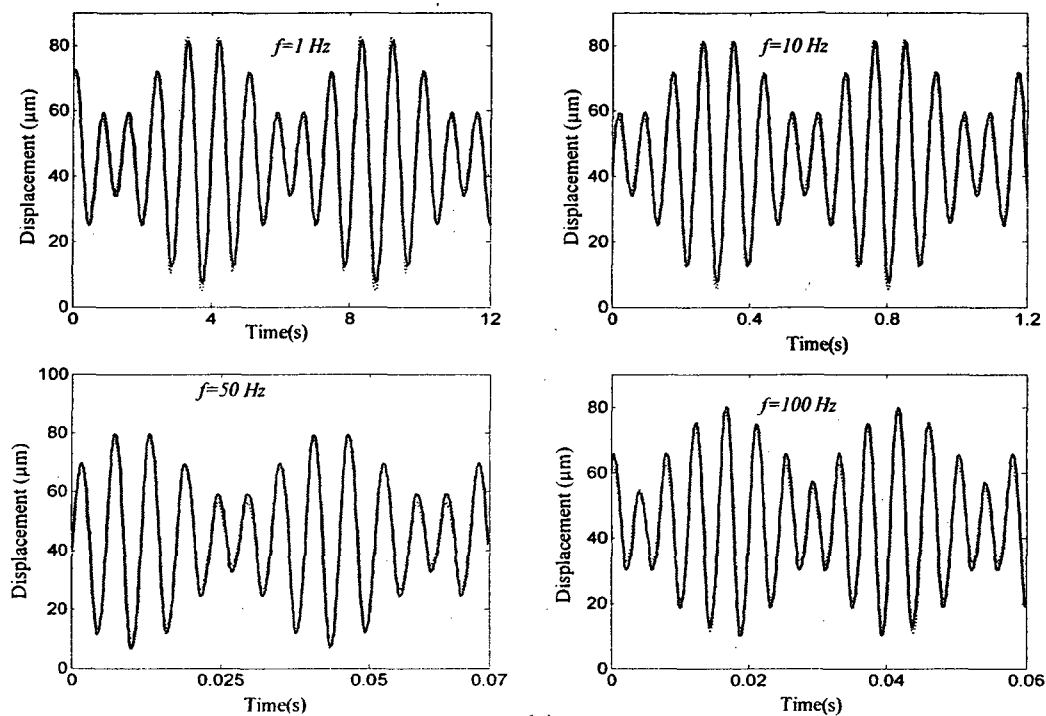


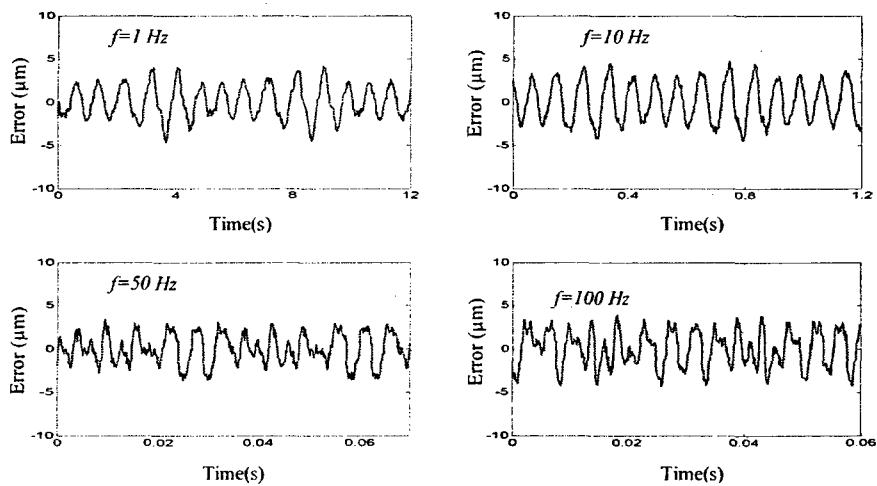
Figure 4.12: Comparisons of measured responses with the results derived from rate-dependent Prandtl-Ishlinskii model under inputs at different fundamental frequencies (——— , measured; - - - - , model).

Table 4.5: Percent errors between the model and measured displacement responses at different excitation frequencies.

Frequency (Hz)	Percentage of norm error %	Percentage of maximum error %
1	6.11	3.85
10	6.18	4.77
150	5.06	3.57
200	6.50	4.30



(a)



(b)

Figure 4.13: (a) Time histories of measured and model displacement responses at different fundamental frequencies (....., measured; —, model). (b) Time histories of error in measured and model displacement responses at different fundamental frequencies.

4.4.4 TRIANGULAR WAVEFORM INPUT

The validity of the model is further explored under a triangular waveform voltage input at four excitation frequencies (1, 10, 100 and 200 Hz). The excitation was defined to yield peak amplitude of 40 V with a bias of 40 V, as it was applied in experiments. The model simulations were performed using the model parameters identified under distinct harmonic inputs to ascertain the general applicability of the model. Figure 4.14 illustrates comparisons of the model results in terms of major hysteresis loops with the corresponding measured data under the selected excitation frequencies. The results show good agreements between the model results and the measured data, although some deviations are evident in both the peak-to-peak displacement response and width of the hysteresis loop. The model results exhibit oscillations in the response corresponding to upper half of the triangular waveform, $v(t) > 40$ V, at higher frequencies, which are also evident in the measured data. These oscillations are caused by discontinuity in $\dot{v}(t)$ of the triangular input. The results further show asymmetric responses under upper and lower halves of the triangular waveform, where the oscillations are absent under the lower half of the waveform. This asymmetry is attributed to opposite signs of higher magnitudes of time rate of input at the extremities ($\dot{v}(t) > 0$ near $v(t) \approx 0$ V; and $\dot{v}(t) < 0$ near $v(t) \approx 80$ V), which cause relatively small and large magnitudes, respectively, of the functions $\bar{h}(v, \dot{v})$ and $\bar{g}(v, \dot{v})$ described in (4.7) and (4.8). Such oscillations tend to diminish at lower frequencies, which can be attributed to relatively smaller magnitudes of $\dot{v}(t)$ and hysteresis.

The time histories of the displacement responses of the rate-dependent model are also compared with the measured data obtained under the triangular excitations at

frequencies of 1, 10, 100 and 200 Hz in Figure 4.15. The figure also shows the error between the model and measured responses. The results clearly show very good agreements between the predicted and measured displacement responses under triangular waveform excitations at all the selected frequencies, as it was observed under harmonic and complex harmonic excitations. The peak displacement error is below $5 \mu\text{m}$ under excitations at 1 and 10 Hz, while the peak error increases to nearly $5.15 \mu\text{m}$ at 200 Hz.

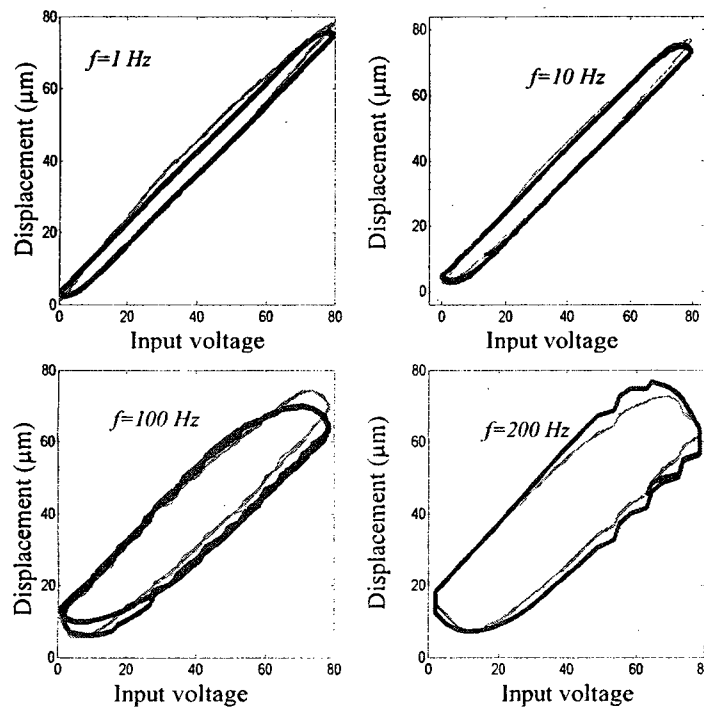


Figure 4.14: Comparisons of measured responses with the results derived from rate-dependent Prandtl-Ishlinskii model under triangular inputs at different frequencies (—, measured; - - -, model).

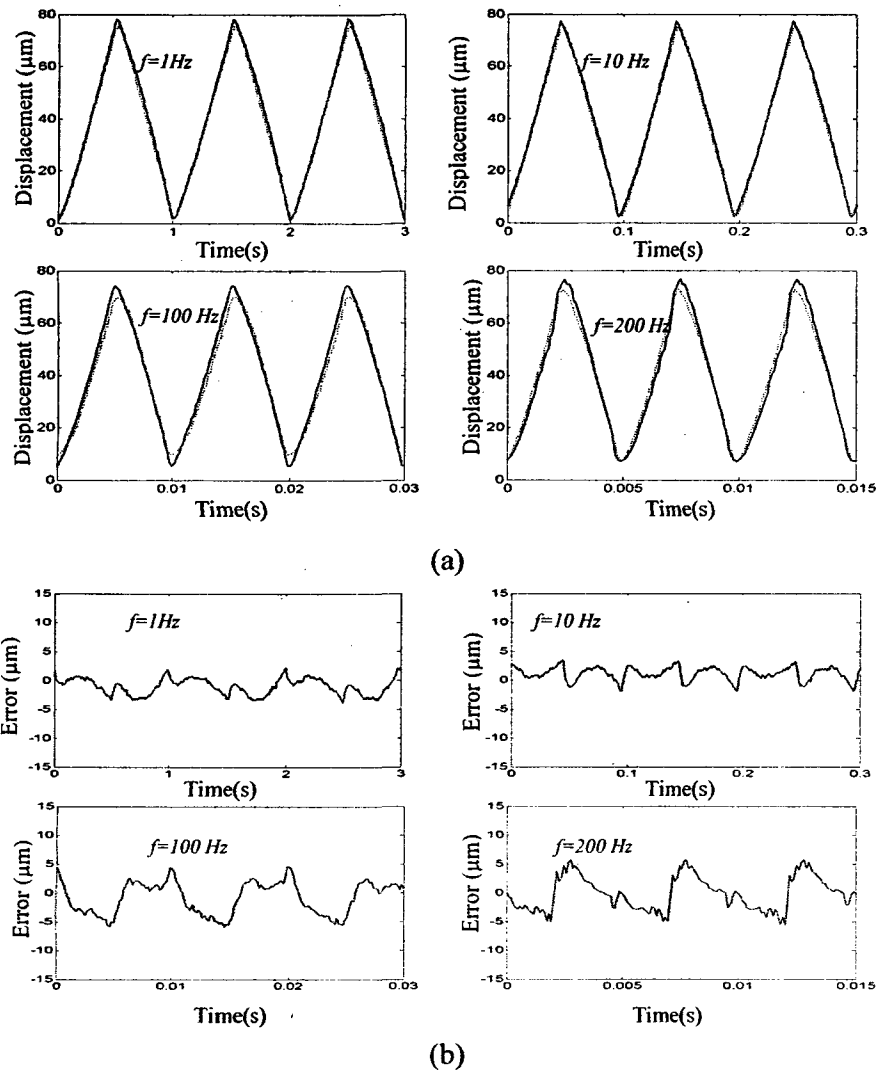


Figure 4.15: (a) Comparisons of measured displacement responses with those of the rate-dependent model under triangular inputs at different excitation frequencies (..... , measured; ——— , model); and (b) Error between the measured and model displacement responses.

4.5 Generalized Rate-Dependent Prandtl-Ishlinskii Model

Smart material actuators invariably exhibit rate-dependent hysteresis that may be either symmetric or asymmetric depending upon the actuation principle. The generalized Prandtl-Ishlinskii model, described in Section 2.5, is further enhanced to describe rate-

dependent symmetric and asymmetric hysteresis. The generalized rate-dependent Prandtl-Ishlinskii model, presented in (2.23), is realized upon integration of a density function and the generalized rate-dependent play operator, capable of generating minor as well as major hysteresis loops with varying slopes of the ascending and descending input-output curves. The dynamic threshold function has been described in (4.10) to enhance the prediction of rate-dependent hysteresis effects. The validity of the resulting generalized rate-dependent model is demonstrated by comparing the displacement responses of the model with the measured symmetric and asymmetric responses obtained for the piezoceramic and magnetostrictive actuators, respectively, under inputs at different frequencies in the 1-200 Hz and 10-100 Hz ranges. The model validity for the SMA actuator was not attempted since the data was not available and the fact that the rates of variations in the input temperature are relatively low.

4.5.1 PARAMETERS IDENTIFICATION

On the basis of the observed hysteresis properties of a magnetostrictive actuator, higher-order polynomial envelope functions are defined to realize asymmetric hysteresis properties of the operator and the model. These envelope functions are expressed as:

$$\begin{aligned}\gamma_r(v) &= \sum_{n=1}^{s_r} a_n v^n + a_o \\ \gamma_l(v) &= \sum_{n=1}^{s_l} b_n v^n + b_o\end{aligned}\tag{4.12}$$

where s_l and s_r are the orders of envelope function $\gamma_l(v)$ and $\gamma_r(v)$, respectively. The constants of the proposed functions can be selected to realize different degree of asymmetry in the hysteresis properties. The generalized rate-dependent Prandtl-Ishlinskii

model is formulated using dynamic threshold \bar{r} (4.9) is selected to characterize the rate-dependent hysteresis. A classical form for the function $\bar{h} = qv$ and density function (4.1) are chosen in order to characterize the rate-dependent asymmetric hysteresis properties. The parameters of the envelope functions, dynamic threshold, and density function need to be defined on the basis of known characteristics of specific smart actuators. Rate-dependent play operators are defined by constructing first ($s_l = s_r = 1$) and third-order ($s_l = s_r = 3$) envelope functions, as described in (4.12), in order to illustrate the influence of the order on the outputs of the rate-dependent Prandtl-Ishlinskii model. The experimental data obtained for the magnetostrictive actuator [33] and the piezoceramic actuator under harmonic inputs at various frequencies in the 10-100 and 1-200 Hz ranges, respectively, were considered for model parameters identification. The parameters identification, however, was limited to the generalized model alone in order to investigate its ability to predict both symmetric and asymmetric hysteresis effects of the respective actuators.

The model parameters vector $X = \{\alpha, \beta_1, \beta_2, \lambda_1, \lambda_2, \rho, \tau, a_0, a_1, a_2, a_3, b_0, b_1, b_2, b_3, q\}$, was identified through minimization of the error sum-squared function the displacement response of the generalized rate-dependent Prandtl-Ishlinskii model and the measured displacement over entire range of excitation frequencies. The error minimization problem was solved under the following constrains:

$$\alpha, \lambda_1, \lambda_2, \epsilon_1, \epsilon_2, \rho, q > 0$$

$$\beta_1, \beta_2 \geq 1$$

The minimization problem for the magnetostrictive actuator, solved considering only one level of input current amplitude of 0.8 A with a bias of 0.1 A ($n_3=1$), since the data was available only under this excitation. Four different excitation frequencies ($n_2=4$),

namely, 10, 20, 50, and 100 Hz, however were considered, with a total of 60 data points ($n_f=60$) for each hysteresis loop. For the piezoceramic actuator, the input voltage amplitude was limited to 40 V ($n_3=1$), while the data corresponding to four different frequencies of 1, 50, 100, and 200 Hz ($n_2=1$) were considered with a total of 50 data points ($n_f=50$) for each hysteresis loop. A weighting constant C_{j_f} ($j_f=1, 2, 3,$ and 4) was introduced corresponding to selected excitation frequencies of 10, 20, 50 and 100 Hz for the magnetostrictive; and 1, 50, 100 and 200 Hz for the piezoceramic actuator, to emphasize the error minimization at higher frequencies. The solutions were obtained for a range of starting vectors and weighting constants. The weighting constants corresponding to minimize weighted sum squared error over the entire frequency range selected, which are summarized in Table 4.6 for both models. Table 4.7 presents the identified parameters of the generalized rate-dependent Prandtl-Ishlinskii models based upon linear and nonlinear envelope functions for the piezoceramic and magnetostrictive actuators.

Table 4.6: Weighting constants C_{j_f} applied in the minimization function for identification of parameters based upon magnetostrictive and piezoceramic actuator data.

Magnetostrictive actuator			Piezoceramic actuator		
Frequency(Hz)	C_{j_f}		Frequency(Hz)	C_{j_f}	
	$s_l=s_r=1$	$s_l=s_r=3$		$s_l=s_r=1$	$s_l=s_r=3$
10	13	11	1	22	14
20	15	29	50	27	12
50	24	12	100	28	22
100	33	14	200	44	32

Table 4.7: Identified parameters of the generalized rate-dependent Prandtl-Ishlinskii model using rate-dependent play operator of linear ($s_l = s_r = 1$) and nonlinear ($s_l = s_r = 3$) envelope functions for the magnetostrictive and piezoceramic actuators.

Parameter	Rate-dependent play operator of linear envelope functions		Rate-dependent play operator of nonlinear envelope functions	
	Magnetostrictive Actuator	Piezoceramic actuator	Magnetostrictive actuator	Piezoceramic actuator
α	3.721	2.795	4.848	1.792
β_1	1.199	2.745	1.090	2.264
β_2	1.199	1.021	1.199	1.101
λ_1	0.063	1.137×10^{-3}	1.7312×10^{-2}	1.642×10^{-6}
λ_2	0.002	1.085×10^{-4}	6.322×10^{-3}	1.658×10^{-5}
ρ	0.005	0.011	0.005	0.020
τ	0.092	0.044	0.092	0.038
a_0	19.908	0.681	-7.737	0.480
a_1	23.268	0.681	30.265	0.239
a_2	----	----	1.629	1.611×10^{-4}
a_3	----	----	2.861	5.609×10^{-5}
b_0	-5.424	-0.199	-3.338	-0.199
b_1	3.190	0.4584	25.276	0.248
b_2	----	----	-9.789	-6.883×10^{-4}
b_3	----	----	9.098	3.785×10^{-5}
q	1.408	0.217	-7.510	0.218

4.5.2 EXPERIMENTAL VERIFICATIONS

The validity of the generalized rate-dependent Prandtl-Ishlinskii models employing the rate-dependent play operators with linear and nonlinear envelope functions is examined by comparing the model responses with the measured data for the both actuators under different excitation frequencies. Figure 4.16 illustrates comparisons of the displacement responses of the generalized model based on asymmetric linear ($s_l = s_r = 1$) and nonlinear envelope functions ($s_l = s_r = 3$) with the measured data of the magnetostrictive actuator corresponding to inputs at different discrete frequencies (10, 20, 50, and 100 Hz). The results clearly suggest that the model can effectively predict the

asymmetric hysteresis properties of the actuator. Both the measured data and the model results exhibit relatively larger displacement amplitude of the actuator under negative current, even though the magnitude of the negative current is smaller (0.7 A) due to the bias current of 0.1 A. The comparisons also show slight deviations in the measured and model responses. The magnitude of the deviation is observed to be relatively large when linear and envelope functions are used to construct the generalized play operator.

The time histories of displacement responses of the models employing linear and nonlinear envelope functions subject to excitations at the selected frequencies are also compared with the measured data in Figure 4.17. The results show reasonably good agreements between the model responses and the measured data corresponding to all the selected excitation frequencies. While the model with linear envelope function yields notable errors in the vicinity of the peak responses, the use of nonlinear envelope function reduces this error. The reason is that the gradient at the turning point changes with frequency and this will not be accounted by varying the threshold value. The time histories of the displacement errors corresponding to different input frequencies are also shown in Figure 4.18. The peak errors in responses of the model employing linear and nonlinear envelope functions vary within the above-stated bounds. The results further show that the model can effectively predict the rate-dependent hysteresis effect with reasonably good accuracy. Table 4.8 summarizes the peak errors between the measured data and outputs of the models employing rate-dependent play operator with linear and nonlinear envelope functions in terms of absolute peak displacement error and the peak percent error based on the measured response.

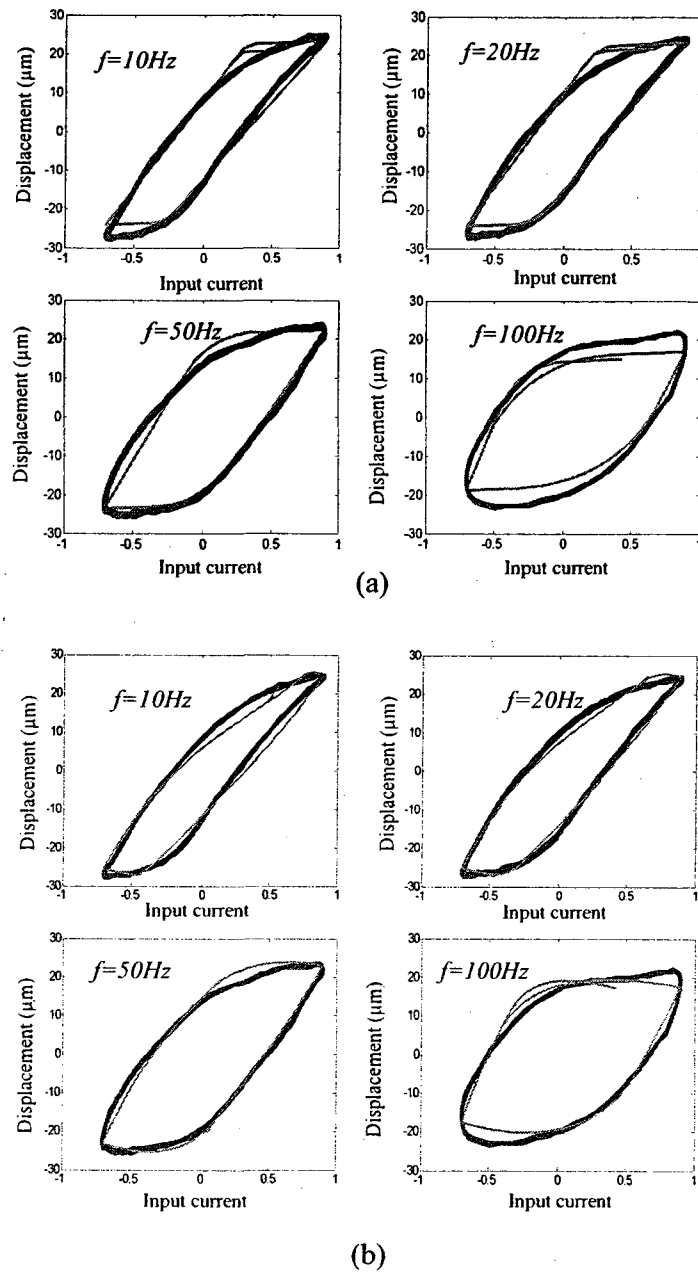


Figure 4.16: Comparisons of displacement responses of the generalized rate-dependent Prandtl-Ishlinskii model with the measured responses of a magnetostrictive actuator under different input frequencies: (a) play operator with linear envelope functions, $s_l = s_r = 1$; and (b) play operator with nonlinear envelope functions, $s_l = s_r = 3$. (———, measured; ———, model).

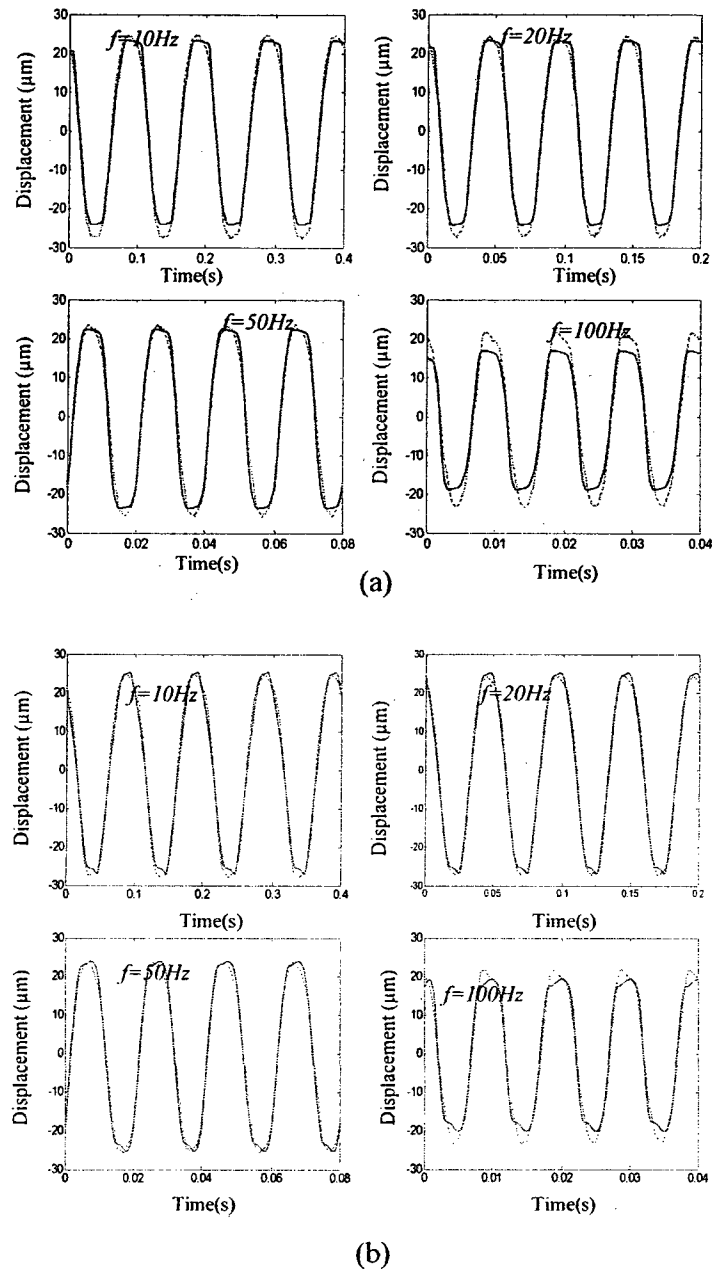


Figure 4.17: Comparisons of time histories of displacement responses of models with the measured data of a magnetostrictive actuator at different input frequencies: (a) play operator with linear envelope function, $s_l = s_r = 1$; and (b) play operator with nonlinear envelope function, $s_l = s_r = 3$, (—, measured; ----, model).

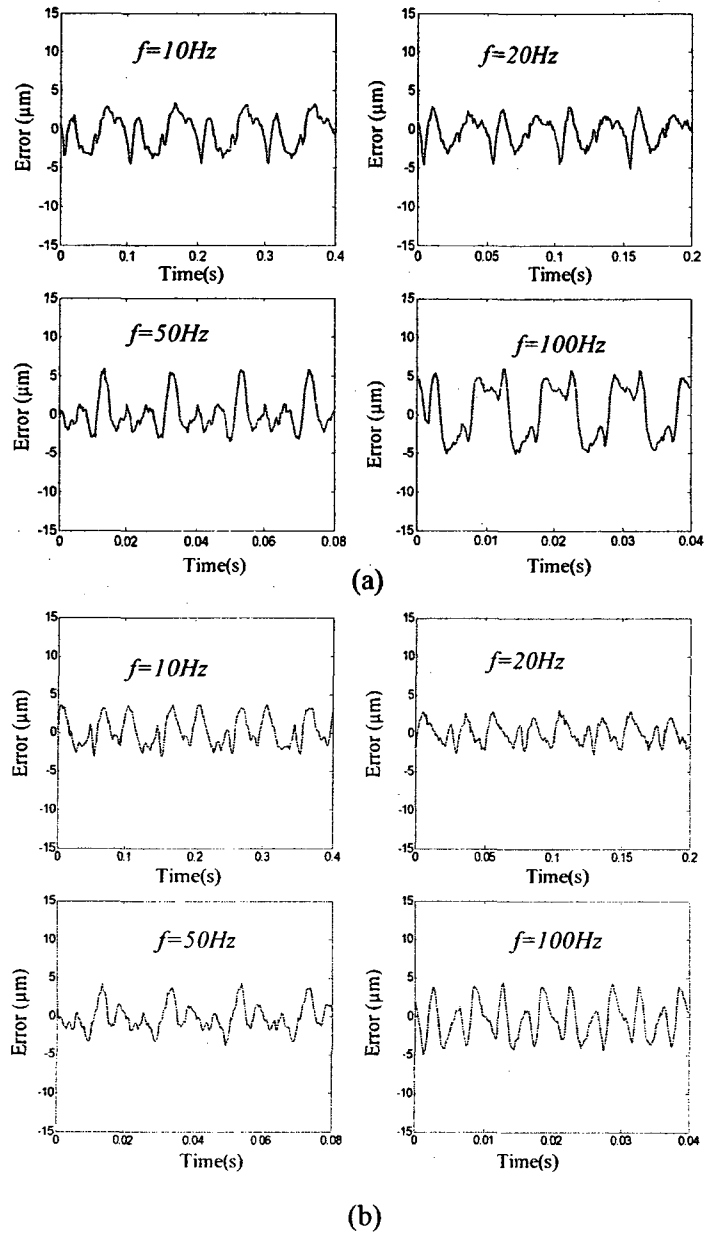


Figure 4.18: Time histories of errors between the model and measured displacement responses of the magnetostrictive actuator at different input frequencies: (a) play operator with linear envelope functions, $s_l = s_r = 1$; and (b) play operator with nonlinear envelope functions, $s_l = s_r = 3$.

As seen in the table, the peak errors of the generalized rate-dependent Prandtl-Ishlinskii model using rate-dependent play operator with linear and nonlinear envelope functions are bounded between 4.50 to 6.01 μm and 3.09 to 5.00 μm , respectively. The corresponding peak percent peak errors are bounded between 8.58% to 13.08% and 5.98% to 10.95%. The results suggest that the use of rate-dependent play operator of nonlinear envelope function ($s_l = s_r = 3$) can help to reduce the prediction error over the range of excitation frequencies considered in the study. Furthermore, the measured and model responses of both the rate-dependent play operators show increasing hysteresis and decreasing output amplitude with increasing excitation frequency of the input current.

Table 4.8: Displacement and percent peak errors between responses of the models based on linear ($s_l = s_r = 1$) and nonlinear ($s_l = s_r = 3$) envelope functions of rate-dependent play operator and the measured data of the magnetostrictive actuator at different excitation frequencies.

Frequency(Hz)	Peak error in μm (percent error)	
	$s_l = s_r = 1$	$s_l = s_r = 3$
10	4.50 (8.58)	3.75 (7.15)
20	5.13 (9.92)	3.09 (5.98)
50	6.01 (12.19)	4.36 (8.78)
100	5.97 (13.08)	5.00 (10.95)

The validity of the generalized rate-dependent Prandtl-Ishlinskii model employing generalized rate-dependent play operators with linear and nonlinear envelope functions is also investigated for predicting symmetric hysteresis properties of the piezoceramic actuator. The generalized model was solved under a sinusoidal voltage input at four different frequencies using the parameters listed in Table 4.7. The resulting displacement

responses of the models are compared with the corresponding measured data in Figure 4.19. Although the results attained from both the models show reasonably good agreements with the measured data, irrespective of the frequency, the model with nonlinear envelope functions yields relatively lower error. Both the model results and the measured data show increasing hysteresis and decreasing output amplitude with increasing frequency of the input voltage.

The time histories of the models responses are further compared with the measured data in Figure 4.20 for the selected excitation frequencies. The results again suggest reasonably good agreements between the predicted and measured displacement responses of both the models, irrespective of the selected input frequency, although deviations in the vicinity of the peak response are also evident, particularly at the higher frequency of 200 Hz. The use of nonlinear envelope functions in the rate-dependent play operator yields slightly better prediction of the response hysteresis as it was observed for the asymmetric hysteresis properties of the magnetostrictive actuator. The model employing the rate-dependent play operator with linear envelope function, however, provides lesser error under input frequencies of 50 and 100 Hz. Figure 4.21 illustrates the errors between the model responses and the measured data of the piezoceramic actuator. The results show that the peak errors, generally, occur in the vicinity of the peak response and remain in the order of 6 μm for the model with linear envelope functions, irrespective of the input frequency. The peak magnitude and percent errors of both the models corresponding to different excitation frequencies are further summarized in Table 4.9.

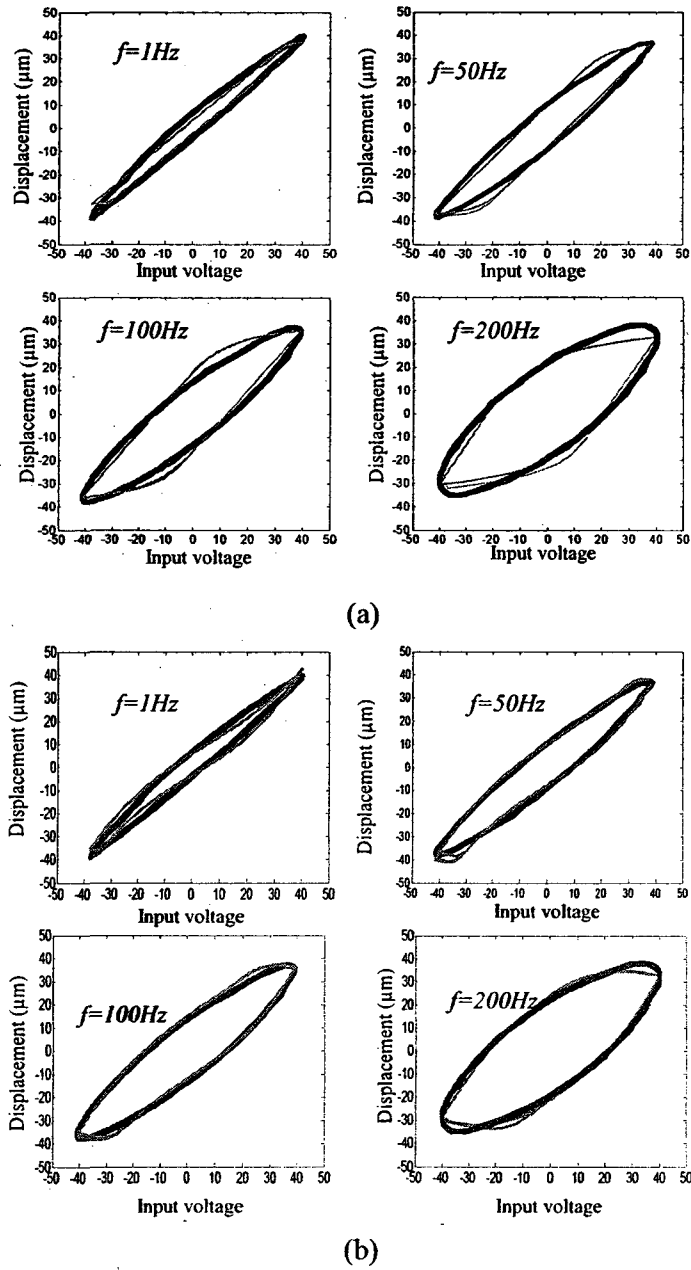


Figure 4.19: Comparisons of displacement responses of the generalized rate-dependent model with the measured data of a piezoceramic actuator under different input frequencies (-----, measured; ———, model): (a) play operator with linear envelope function, $s_l = s_r = 1$; and (b) play operator with nonlinear envelope function, $s_l = s_r = 3$.

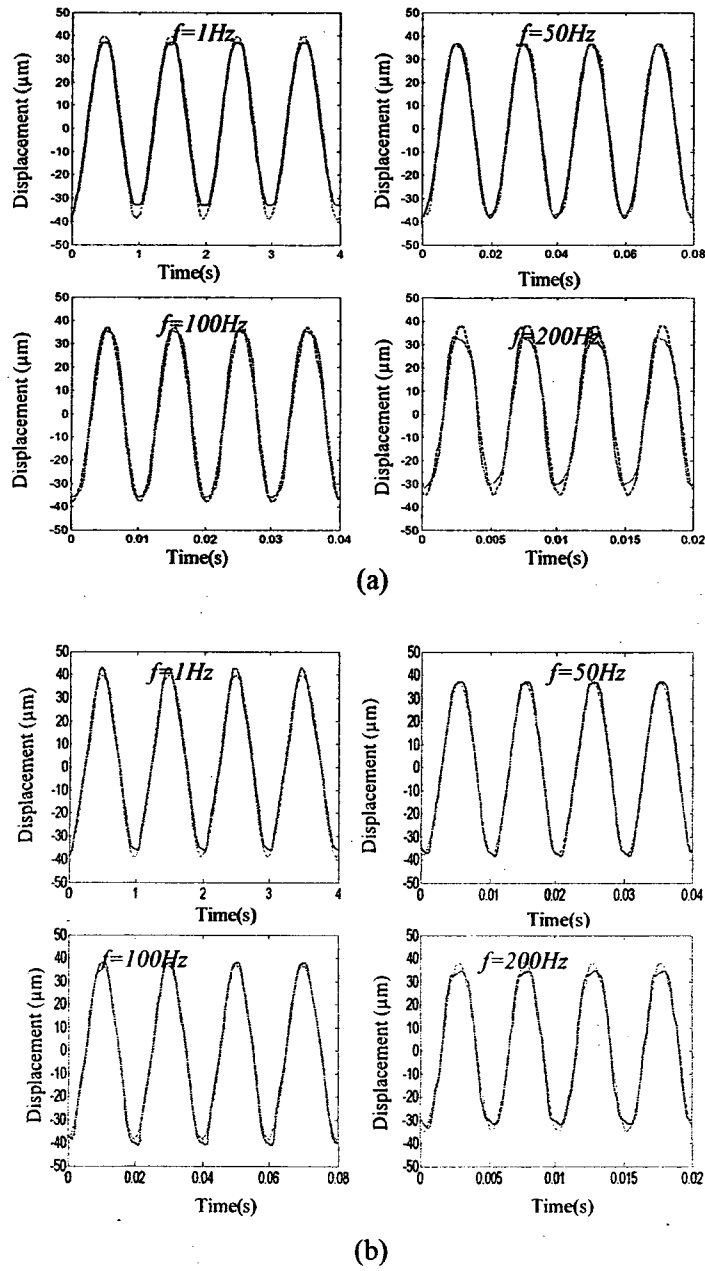


Figure 4.20: Time histories of displacement responses of the model and the piezoceramic actuator at different input frequencies (——— , measured; - - - - - , model) : (a) rate-dependent play operator with linear envelope functions, $s_l = s_r = 1$; and (b) rate-dependent play operator with nonlinear envelope functions, $s_l = s_r = 3$.

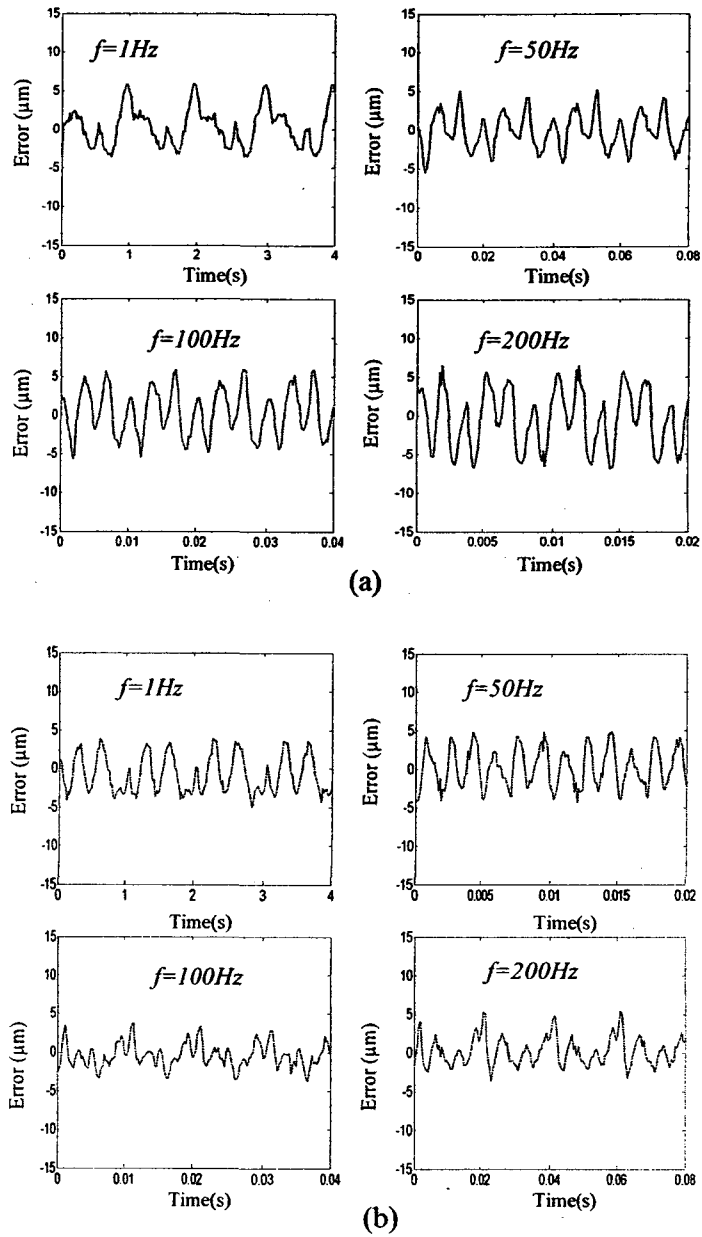


Figure 4.21: Time histories of errors between the model and measured displacement responses of the piezoceramic actuator at different input frequencies: (a) play operator with linear envelope functions, $s_l = s_r = 1$; and (b) play operator with nonlinear envelope functions, $s_l = s_r = 3$.

Table 4.9: Peak displacement and percent peak errors between responses of the models based on linear ($s_l=s_r=1$) and nonlinear ($s_l=s_r=3$) envelope functions of rate-dependent play operator and the measured data of the piezoceramic actuator at different excitation frequencies.

Frequency(Hz)	Peak error in μm (percent error)	
	$s_l=s_r=1$	$s_l=s_r=3$
10	5.87 (7.48)	4.99 (6.36)
50	5.44 (7.24)	5.49 (7.30)
100	6.08 (8.11)	3.81 (5.09)
200	6.84 (9.39)	4.87 (6.68)

4.6 Summary

The validity of the generalized Prandtl-Ishlinskii model in predicting asymmetric and saturated major as well as minor input-output hysteresis loops was demonstrated for two different SMA actuators and a magnetostrictive actuator on the basis of the available measured data. The peak prediction errors for the actuators considered in the study were observed to be within 3% of the maximum output under triangular inputs of varying magnitudes. It is concluded that the Prandtl-Ishlinskii model comprising the generalized play operator can also describe symmetric hysteresis properties of a piezoceramic actuator, when linear envelope functions are employed. Although the classical model can also characterize the symmetric hysteresis properties, the generalized model revealed relatively smaller error for the piezoceramic actuator considered in the study.

The validity of the rate-dependent Prandtl-Ishlinskii model was also examined under harmonic, complex harmonic and triangular waveforms, in a wide frequency range. The effectiveness of the model in characterizing major as well as minor hysteresis loops is particularly demonstrated under inputs at different frequencies. Comparisons of model results with the measured data obtained for the piezoceramic and magnetostrictive

actuators revealed reasonably good agreements between the two in terms of both the major and minor hysteresis loops under harmonic and complex harmonic input voltages, irrespective of the excitation frequency. The simulation results revealed considerable increase in width of the hysteresis loops with increasing frequency of the input voltage, while the corresponding amplitude of output displacement decreased. The model results of the piezoceramic actuator attained under triangular waveform inputs in the 1 to 200 Hz frequency range also revealed very good agreements with the measured data. Both the experimental and model results showed that a triangular waveform yields relatively smaller width of the hysteresis loops compared to that under a sinusoidal input, which is attributed to relatively smaller magnitude of the constant rate of change of the triangular input. The large values of the time rate of change of triangular input near the extremities, however, caused oscillations in the responses at higher frequencies, which were evident from both the measured and model results.

From the results, it can be concluded that the Prandtl-Ishlinskii model comprising the generalized rate-dependent play operator described by nonlinear envelope function can provide better predictions of the symmetric as well as asymmetric hysteresis properties under different rates of inputs. Furthermore, the generalized rate-dependent model can also predict the rate-independent hysteresis characteristics reasonably well, as it is evident from the responses under low frequency inputs. The use of higher order envelope functions of the rate-dependent play operator helps reduce the prediction error of the rate-dependent Prandtl-Ishlinskii model.

The generalized Prandtl-Ishlinskii models are considered to be analytically invertible. This property is extremely desirable for real-time hysteresis compensations

and micro-positioning control. The analytical invertible generalized Prandtl-Ishlinskii models are investigated in the following chapter.

Chapter 5: Formulations of Inverse Prandtl-Ishlinskii Models for Hysteresis Compensation

5.1 Introduction

The exact inverses of the Preisach and Krasnosel'skii-Pokrovskii models are not available, only numerical methods can be used to obtain approximate inversions of these models [22, 24, 26, 40, 53, 54, 58, 61, 69-71]. Ping and Ge [23] applied the inverse Preisach model as a feedforward compensator with PID controller to reduce hysteresis effects of a piezoceramic actuator. Galinaitis [27] proposed the Krasnosel'skii-Pokrovskii operator instead of the used relay operator in the Preisach model and its inverse to characterize and to compensate the hysteresis effects of a piezoceramic actuator. Tan and Baras [25] applied an adaptive control approach to compensate hysteresis effects in a magnetostrictive actuator using the Preisach hysteresis model and its inverse. Nealis and Smith [71] proposed a robust control method for smart material actuators to achieve enhanced tracking performance using the inverse Preisach model. Song et al. [41], in a similar manner, applied the inverse Preisach model in conjunction with a lag-lead controller for compensation of hysteresis effects in a piezoceramic actuator.

Unlike the Preisach and Krasnosel'skii-Pokrovskii models, the Prandtl-Ishlinskii model is analytically invertible, and it can be conveniently implemented as a feedforward compensator for mitigating the hysteresis nonlinearities. The analytically derived inverse offers significant benefits in real-time control applications. This is because the compensation error can be obtained which will make it possible to design robust controller with stability analysis, which is lacking in studies using numerical inverse.

However, the advantage of the Prandtl-Ishlinskii model is limited by the class of hysteresis it can describe, namely the symmetric and rate-independent hysteresis with unbounded output. Krejci and Kuhnen [30] applied the Prandtl-Ishlinskii model to characterize and to compensate hysteresis nonlinearities of a piezoceramic actuator. In this chapter, the analytical inversions of the proposed generalized Prandtl-Ishlinskii model, the rate-dependent Prandtl-Ishlinskii model, and the generalized rate-dependent Prandtl-Ishlinskii model will be discussed for compensation symmetric, asymmetric, saturated, and rate-dependent hysteresis effects. It should be mentioned that the purpose of the analytical inverse is to obtain the analytical error of the inverse compensation. The error analysis of the inverse compensation will be presented for the Prandtl-Ishlinskii model and its inverse in Chapter 6.

5.2 Analytical inversion of the Prandtl-Ishlinskii model

An inverse Prandtl-Ishlinskii model has been obtained analytically in [2]. In order to construct the analytical inverse for the generalized Prandtl-Ishlinskii models, described in Chapter 2, the Prandtl-Ishlinskii model described by the initial loading curve. The inverse of the Prandtl-Ishlinskii model can be applied to compensate symmetric and rate-independent hysteresis effects. In this section, the inverse of the Prandtl-Ishlinskii model is presented using the initial loading curve concept.

5.2.1 CONCEPT OF THE INITIAL LOADING CURVE (SHAPE FUNCTION)

The initial loading curve (shape function) is essential concept to present an alternative description for the Prandtl-Ishlinskii model as well as to derive the analytical

inversion of the generalized Prandtl-Ishlinskii models. Initial loading curve of the Prandtl-Ishlinskii model can be explained, physically, as a stress-strain curve, which is formulated due to increasing the load from zero to some final value [2]. This curve describes the possible hysteresis loops generated by the Prandtl-Ishlinskii model. The initial loading curve is defined when the initial state of the Prandtl-Ishlinskii model is zero and when the input increases monotonically. Figure 5.1 shows the relation between the vertical height g and the length of its projection onto the v -axis, x . The output g can be expressed when the input v increases and decreases by x as [2]:

$$g(x) = x - 2r \quad (5.1)$$

The output g can be also expressed as [2]:

$$g(x) = \text{sgn}(x) \max(|x| - 2r, 0) \quad (5.2)$$

Then, the previous equation can be modified as:

$$g(x) = 2 \text{sgn}(x) \max(|x|/2 - r, 0) \quad (5.3)$$

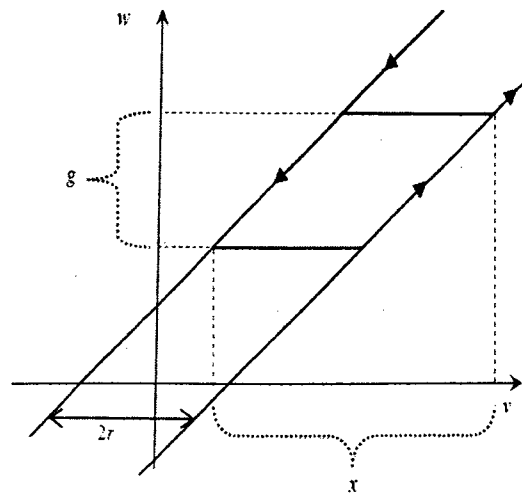


Figure 5.1: the relation between the vertical elevation g and the length of its projection onto the v -axis.

The classical Prandtl-Ishlinskii model is generally expressed analytically as:

$$\Pi[v](t) = qv(t) + \int_0^R p(r)F_r[v](t)dr \quad (5.4)$$

The initial loading curve of Prandtl-Ishlinskii model (5.4) is defined as [2]:

$$\varphi(r) = qr + \int_0^r p(\zeta)g(\zeta)d\zeta \quad (5.5)$$

The derivative of initial loading curve (5.5) with respect to threshold r yields:

$$\varphi'(r) = q + \int_0^r p(\zeta)d\zeta \quad (5.6)$$

The density function of the model is the derivative of Equation (5.6) with respect to the threshold r :

$$\varphi''(r) = p(r) \quad (5.7)$$

Equation (5.7) shows that the second derivative of initial loading curve (5.6) with respect to the threshold r is the density function $p(r)$ of Prandtl-Ishlinskii model (5.4). Also, the constant q of Prandtl-Ishlinskii model can be obtained by substituting zero threshold, $r = 0$, into (5.6) as:

$$\varphi'(0) = q \quad (5.8)$$

Based on Equations (5.7) and (5.8), the alternative description of Prandtl-Ishlinskii model (5.4) using initial loading curve (5.5) can be expressed analytically as [2]:

$$\Pi[v](t) = \varphi'(0)v(t) + \int_0^R F_r[v](t)\varphi''(r)dr \quad (5.9)$$

Remark 5.1: The shape function $\varphi(r)$ of Prandtl-Ishlinskii model is convex and $\varphi''(r) > 0$ [2].

Remark 5.2: For the shape function $\varphi(r) = r$, the Prandtl-Ishlinskii model (5.4) is reduced to $\Pi[v](t) = v(t)$.

Example 5.1: Let's construct the Prandtl-Ishlinskii model using the density function $p(r) = 0.1r$ and $q = 0.17$. The output of the model is expressed analytically as:

$$\Pi[v](t) = 0.17v(t) + \int_0^R 0.1rF_r[v](t)dr \quad (5.10)$$

The output of the model under the harmonic input $v(t) = 7\sin(\pi t)/(1+0.06t)$ for $t \in [0, 13]$ is shown in Figure 5.2.

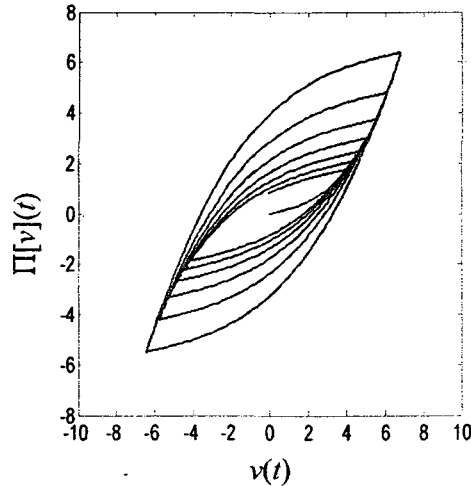


Figure 5.2: Input output relations of Prandtl-Ishlinskii model (5.10).

The initial loading curve of Prandtl-Ishlinskii model (5.10) is defined as:

$$\varphi(r) = 0.17r + \int_0^r 0.1\zeta(r - \zeta)d\zeta \quad (5.11)$$

The input-output relationship for initial loading curve (5.11) is shown in Figure 5.3(a).

Then $\varphi'(r)$ and $\varphi''(r)$ are expressed as:

$$\varphi'(r) = 0.17 + \int_0^r 0.1\zeta d\zeta \quad (5.12)$$

$$\varphi''(r) = 0.1r \quad (5.13)$$

The output of Prandtl-Ishlinskii model (5.9) using initial loading curve (5.11) is presented in Figure 5.3(b). Because the second derivative of the initial loading curve is the density function and the constant $q=0.17$ can be obtained by substituting $r = 0$ in (5.12); the example illustrates that Prandtl-Ishlinskii model indeed can be described analytically using the initial loading curve.

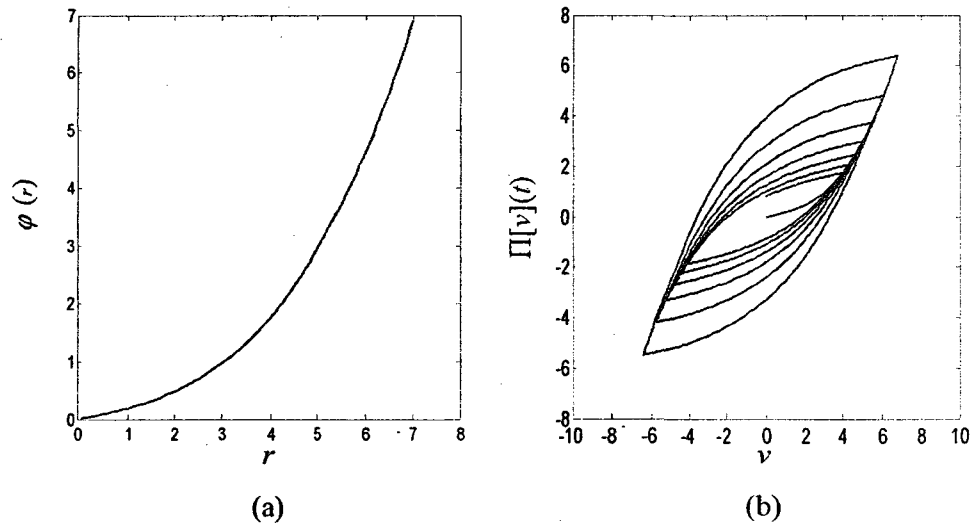


Figure 5.3: Input output relations of: (a) Initial loading curve (5.11); and (b) Prandtl-Ishlinskii model.

5.2.2 INVERSE PRANDTL-ISHLINSKII MODEL

After introducing the Prandtl-Ishlinskii model expressed by the initial loading curve concept, the inverse Prandtl-Ishlinskii model which is also expressed by the initial loading curve can be introduced. This is the key for the development of the general frame of the inverse generalized Prandtl-Ishlinskii model. The inversion of the classical Prandtl-Ishlinskii model is expressed analytically as [30]:

$$\Pi^{-1}[\mathbf{v}](t) = q^{-1}\mathbf{v}(t) + \int_0^{\hat{r}} p(\hat{r})F_{\hat{r}}[\mathbf{v}](t)d\hat{r} \quad (5.14)$$

where \hat{r} is the threshold of the inverse, $F_{\hat{r}}[\mathbf{v}]$ is the play operator of the inverse Prandtl-Ishlinskii model, and the constant q^{-1} is defined as:

$$q^{-1} = \frac{1}{q} \quad (5.15)$$

The threshold \hat{r} of the inverse Prandtl-Ishlinskii model is defined for $l = 0, \dots, n$ and

$\hat{r}_0 < \hat{r}_1 < \dots < \hat{r}_{n+1} = \hat{R} = \infty$ as [30]:

$$\hat{r}_l = \varphi(r_l) \quad (5.16)$$

this yields:

$$\hat{r}_l = \hat{r}_{l-1} + \int_{r_{l-1}}^{r_l} \varphi'(r)dr \quad (5.17)$$

To obtain the analytical inverse of the Prandtl-Ishlinskii model, the output of the composition of the initial loading $\varphi(r)$ and its inverse $\varphi^{-1}(r)$ must yield the threshold r as:

$$\varphi^{-1}(\varphi(r)) = r \quad (5.18)$$

The derivative of Equation (5.18) with respect to the threshold r yields:

$$\varphi'(r)(\varphi^{-1}(\varphi(r)))=1 \quad (5.19)$$

Then, the substitution of (5.16) in (5.19) yields:

$$\varphi'(r)(\varphi^{-1}(\hat{r}))=1 \quad (5.20)$$

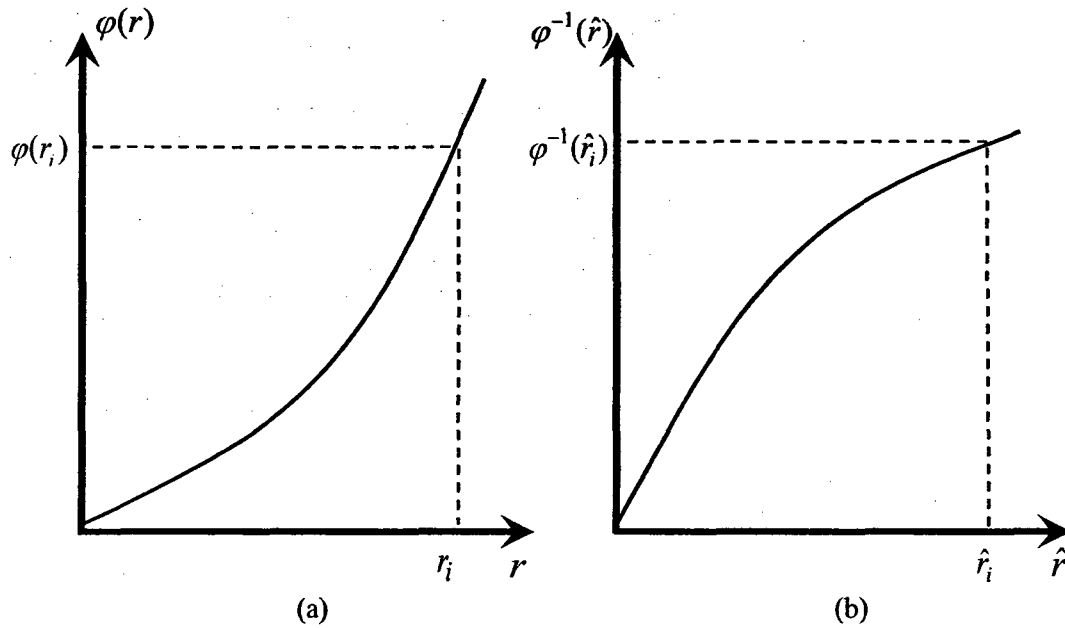


Figure 5.4: Input-output characteristics of: (a) Initial loading curve $\varphi(r)$, and (b) Inverse of initial loading curve $\varphi^{-1}(\hat{r})$.

Figure 5.4 shows the initial loading curve $\varphi(r)$, which is convex, and the inverse of the initial loading curve $\varphi^{-1}(\hat{r})$, which is concave. Because the exact inverse of the initial loading curve $\varphi^{-1}(\hat{r})$ exists, the composition of the initial loading curve and its inverse, as shown in Figure 5.5, yields $\varphi^{-1}(\varphi(r))=r$.

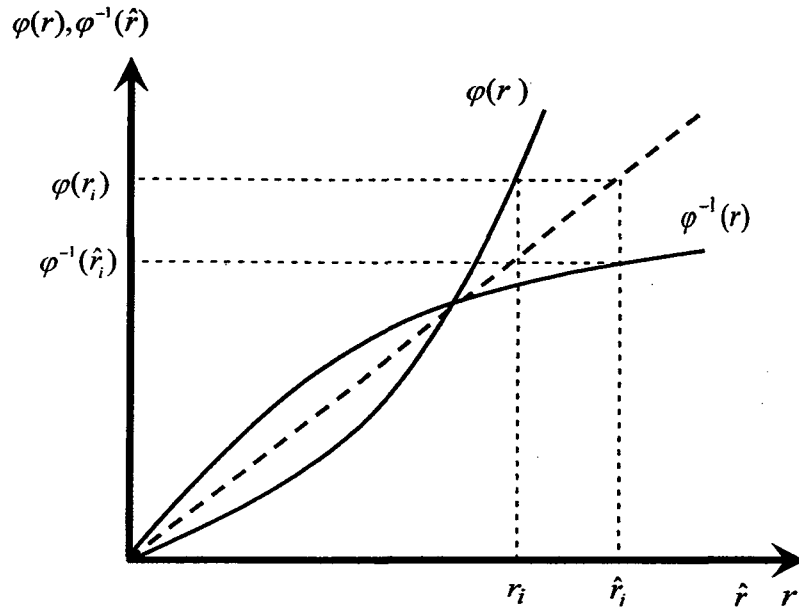


Figure 5.5: Input-output characteristics of composition initial loading curve $\varphi(r)$ and its inverse $\varphi^{-1}(\hat{r})$.

The inverse classical Prandtl-Ishlinskii model based on the initial loading curve can be expressed analytically as [30]:

$$\Pi^{-1}[v](t) = \varphi^{-1}(r)v(t) + \int_0^{\hat{r}} \varphi^{-1''}(\hat{r})F_{\hat{r}}[v](t)d\hat{r} \quad (5.21)$$

In the following the identification of the inverse Prandtl-Ishlinskii model parameters identified using the initial loading curve of the model will be discussed.

The inverse of Prandtl-Ishlinskii model can be also expressed numerically as [30]:

$$\Pi^{-1}[v](t) = q^{-1}v(t) + \sum_{i=1}^n \hat{p}_i F_{\hat{r}_i}[v](t) \quad (5.22)$$

Equation (5.6) can be expressed for $r \in [r_j, r_{j+1})$ $j=0, \dots, n$ as:

$$\varphi'(r) = q + \sum_{i=1}^j p_i, \quad (5.23)$$

Then by substituting (5.23) into (5.17), the threshold \hat{r}_l can be expressed as:

$$\hat{r}_l = \hat{r}_{l-1} + (q + \sum_{i=1}^{l-1} p_i)(r_l - r_{l-1}) \quad (5.24)$$

The summation of Equation (5.24) over l from 1 to j yields [30]:

$$\hat{r}_j = qr_j + \sum_{i=1}^{j-1} p_i(r_j - r_i) \quad (5.25)$$

Equation (5.20) can be expressed as:

$$\varphi^{-1}(\hat{r}_j) = 1/\varphi'(r_j) \quad (5.26)$$

The density function of the inverse model can be computed in each interval $[\hat{r}_j, \hat{r}_{j+1})$

using the following equations:

$$\varphi'(r) = q + \sum_{i=1}^j p_i \quad (5.27)$$

$$(\hat{\varphi}^{-1})'(\hat{r}) = \hat{q}^{-1} + \sum_{i=1}^j \hat{p}_i \quad (5.28)$$

The substitution of (5.27) and (5.28) into (5.26) for each interval $[\hat{r}_j, \hat{r}_{j+1})$ yields:

$$\hat{q}^{-1} + \sum_{i=1}^j \hat{p}_i = \frac{1}{q + \sum_{i=1}^j p_i} \quad (5.29)$$

Then Equation (5.29) can be expressed as:

$$\text{for } j=1: \quad \hat{q}^{-1} + \hat{p}_1 = \frac{1}{q + p_1} \quad (5.30)$$

$$\text{for } j=2: \quad \hat{q}^{-1} + \hat{p}_1 + \hat{p}_2 = \frac{1}{q + p_1 + p_2} \quad (5.31)$$

•
•
•

$$\text{for } j=n: \quad \hat{q}^{-1} + \hat{p}_1 + \hat{p}_2 + \dots + \hat{p}_n = \frac{1}{q + p_1 + p_2 + \dots + p_n} \quad (5.32)$$

The weights of the density function are obtained as:

$$\text{for } j=1: \quad \hat{p}_1 = -\frac{p_1}{q(q + p_1)} \quad (5.33)$$

$$\text{for } j=2: \quad \hat{p}_2 = -\frac{p_2}{(q + p_1 + p_2)(q + p_2)} \quad (5.34)$$

•
•
•

$$\text{for } j=n: \quad \hat{p}_j = -\frac{p_j}{(q + \sum_{i=1}^j p_i)(q + \sum_{i=1}^{j-1} p_i)} \quad (5.35)$$

The parameters of the inverse are identified as [30]:

$$q^{-1} = \frac{1}{q} \quad (5.36)$$

$$\hat{r}_j = qr_j + \sum_{i=1}^{j-1} p_i(r_j - r_i) \quad (5.37)$$

$$\hat{p}_j = \frac{p_j}{(q + \sum_{i=1}^j p_i)(q + \sum_{i=1}^{j-1} p_i)} \quad (5.38)$$

The inverse of the Prandtl-Ishlinskii model is investigated via the following example to compensate the hysteresis effects.

Example 5.2: An input signal of the form: $v(t)=5\sin(2\pi t)+4\cos(6t)$ is considered to evaluate minor as well as major hysteresis loops. The chosen simulation parameters are: $T=20$, $\Delta t=0.01$, $q=0.18$. The following density function is selected as:

$$p(r) = 0.1e^{-0.1r} \quad (5.39)$$

The threshold function is selected as:

$$r_j = 0.24j, \quad j=1, 2, 3, \dots, n=20 \quad (5.40)$$

Figure 5.6 shows the simulation results of the Prandtl-Ishlinskii model and its inverse. Inverse Prandtl-Ishlinskii model is employed to compensate the hysteresis nonlinearities of the Prandtl-Ishlinskii model. Parameters of the inverse Prandtl-Ishlinskii model which are identified by Equations (5.36), (5.37), and (5.38). Figure 5.6 shows the capability of the inverse Prandtl-Ishlinskii model to compensate the hysteresis effects. The results show the exact inverse of Prandtl-Ishlinskii model compensates the symmetric hysteresis nonlinearities. Because the Prandtl-Ishlinskii model can only be applied to characterize symmetric and rate-independent hysteresis properties, the inverse of the model that is presented in this section cannot compensate asymmetric as well as saturated hysteresis properties. In this section, analytical inverse of the generalized Prandtl-Ishlinskii model, which exhibits asymmetric as well as saturated hysteresis loops, is presented analytically.

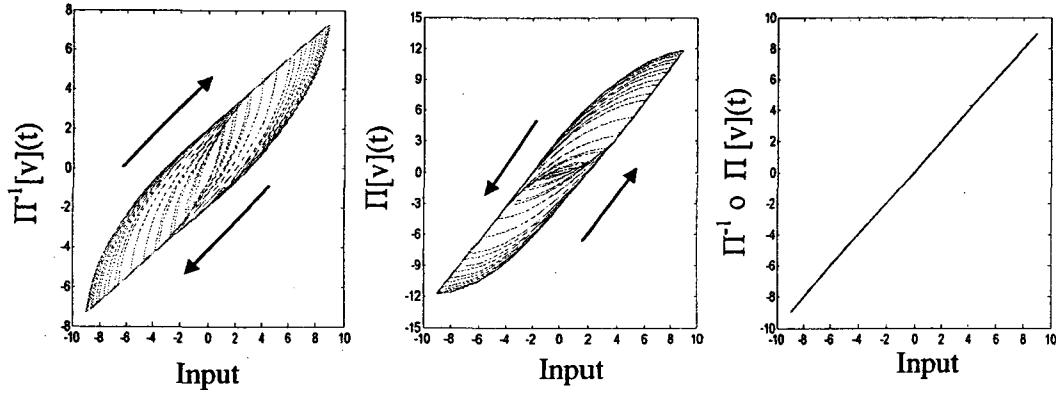


Figure 5.6: Compensation of symmetric hysteresis using inverse Prandtl-Ishlinskii model.

5.2.3 FORMULATION OF INVERSE GENERALIZED PRANDTL-ISHLINSKII MODEL

In this subsection, the inverse of the generalized Prandtl-Ishlinskii model is formulated based on the initial loading curve concept. Generalized Prandtl-Ishlinskii model that is formulated in Chapter 2 using generalized play operator $S_r[v](t)$ to yield output $\Phi[v](t)$ is presented as:

$$\Phi[v](t) = \int_0^R p(r) S_r[v](t) dr \quad (5.41)$$

The output $\Phi[v](t)$ of the generalized Prandtl-Ishlinskii model can be expressed as:

$$\Phi[v](t) = \begin{cases} \Pi^+[\gamma_l(v)](t) & \text{for } \dot{v}(t) \geq 0 \\ \Pi^-[\gamma_r(v)](t) & \text{for } \dot{v}(t) \leq 0 \end{cases} \quad (5.42)$$

where the output of the Prandtl-Ishlinskii model $\Pi^+[v](t)$ and $\Pi^-[v](t)$ for increasing and decreasing input $v(t)$ can be expressed as :

$$\begin{aligned}\Pi^+[v](t) &= \int_0^R p(r)F_r^+[v](t)dr \\ \Pi^-[v](t) &= \int_0^R p(r)F_r^-[v](t)dr\end{aligned}\tag{5.43}$$

Where the outputs of the play operator for increasing and decreasing inputs $v(t)$ are expressed as:

$$\begin{aligned}F_r^+[v](t) &= \max(v(t) - r, w(t)) \\ F_r^-[v](t) &= \min(v(t) + r, w(t))\end{aligned}\tag{5.44}$$

Consequently, Equation (5.41) can be expressed as:

$$\Phi[v](t) = \begin{cases} \Pi^+ \circ \gamma_l(v(t)) & \text{for } \dot{v}(t) \geq 0 \\ \Pi^- \circ \gamma_r(v(t)) & \text{for } \dot{v}(t) \leq 0 \end{cases}\tag{5.45}$$

Then, it can be concluded that Equation (5.41) can be expressed as:

$$\begin{aligned}\Phi^+[v](t) &= \Pi^+[\cdot](t) \circ \gamma_l(v) \\ \Phi^-[v](t) &= \Pi^-[\cdot](t) \circ \gamma_r(v)\end{aligned}\tag{5.46}$$

Equation (5.46) can be further expressed as:

$$\begin{aligned}\Pi^{+^{-1}}[\cdot] \circ \Phi^+[v](t) &= \gamma_l(v) \\ \Pi^{-^{-1}}[\cdot] \circ \Phi^-[v](t) &= \gamma_r(v)\end{aligned}\tag{5.47}$$

Because the envelope functions γ_l and γ_r are invertible, Equation (5.47) can be presented as:

$$\begin{aligned}\gamma_l^{-1} \circ \Pi^{+^{-1}}[\cdot] \circ \Phi^+[v](t) &= v \\ \gamma_r^{-1} \circ \Pi^{-^{-1}}[\cdot] \circ \Phi^-[v](t) &= v\end{aligned}\tag{5.48}$$

It can be concluded from (5.48) that the inverse of the generalized Prandtl-Ishlinskii model can be expressed as:

$$\begin{aligned}\Phi^{+^{-1}}[v](t) &= \gamma_l^{-1} \circ \Pi^{+^{-1}}[v](t) \\ \Phi^{-^{-1}}[v](t) &= \gamma_r^{-1} \circ \Pi^{-^{-1}}[v](t)\end{aligned}\tag{5.49}$$

Using the inverse of the Prandtl-Ishlinskii model $\Pi^{-1}[v](t)$ can be expressed as:

$$\Pi^{-1}[v](t) = \begin{cases} \int_0^R \hat{p}(\hat{r}) F_{\hat{r}}^+[v](t) d\hat{r} & \text{for } \dot{v}(t) \geq 0 \\ 0 \\ \int_0^R \hat{p}(\hat{r}) F_{\hat{r}}^-[v](t) d\hat{r} & \text{for } \dot{v}(t) \leq 0 \end{cases}\tag{5.50}$$

Then, the inverse of the generalized Prandtl-Ishlinskii model can be expressed in terms of density function and play operator as:

$$\Phi^{-1}[v](t) = \begin{cases} \gamma_l^{-1} \circ \int_0^R \hat{p}(\hat{r}) F_{\hat{r}}^+[v](t) d\hat{r} & \text{for } \dot{v}(t) \geq 0 \\ 0 \\ \gamma_r^{-1} \circ \int_0^R \hat{p}(\hat{r}) F_{\hat{r}}^-[v](t) d\hat{r} & \text{for } \dot{v}(t) \leq 0 \end{cases}\tag{5.51}$$

Since Equation (5.51) includes the inverse of the classical Prandtl-Ishlinskii model (5.14) without using the linear term $q^{-1}v$, it is then straight forward to follow the same derivation. The inverse generalized Prandtl-Ishlinskii model can be presented by the initial loading curve concept as:

$$\Phi^{-1}[v](t) = \begin{cases} \gamma_l^{-1} \circ \int_0^R \varphi^{-1}(\hat{r}) F_{\hat{r}}^+[v](t) d\hat{r} & \text{for } \dot{v}(t) \geq 0 \\ 0 \\ \gamma_r^{-1} \circ \int_0^R \varphi^{-1}(\hat{r}) F_{\hat{r}}^-[v](t) d\hat{r} & \text{for } \dot{v}(t) \leq 0 \end{cases}\tag{5.52}$$

The modified initial loading curve for Prandtl-Ishlinskii model (5.43) can be expressed as:

$$\bar{\varphi}(r) = \int_0^r p(\zeta)(\zeta - r)d\zeta \quad (5.53)$$

The density function of the generalized Prandtl-Ishlinskii model can be computed as:

$$\bar{\varphi}''(r) = p(r) \quad (5.54)$$

The generalized Prandtl-Ishlinskii model can be presented as:

$$\Phi[v](t) = \int_0^R \bar{\varphi}''(r) S_r[v](t) dr \quad (5.55)$$

The above equation shows that the generalized Prandtl-Ishlinskii model can be presented by initial loading curve $\bar{\varphi}(r)$. Then the inverse of the generalized Prandtl-Ishlinskii model can be expressed as:

$$\Phi[v](t) = \int_0^R \bar{\varphi}^{-1}(\hat{r}) S_{\hat{r}}[v](t) d\hat{r} \quad (5.56)$$

where \hat{r} is the threshold of the inverse model and $\bar{\varphi}^{-1}$ is the inverse of the modified initial loading curve.

The key properties of the inverse generalized Prandtl-Ishlinskii model are same as these of inverse classical model. Some of these properties are summarized below:

- **Hysteresis operator:** The inverse of the generalized Prandtl-Ishlinskii model is a hysteresis operator since it is formulated by integrating play hysteresis operators and a density function;
- **Clockwise operator:** Since the density function of the inverse generalized model is

negative, the inverse generalized Prandtl-Ishlinskii model yields clockwise input-output curves;

- **Lipschitz-continuity:** For a given input $v(t) \in C [0, T]$, it can be conclude that the inverse generalized Prandtl-Ishlinskii model is Lipschitz continuous;
- **Monotonicity:** For a given input $v(t) \in C [0, T]$, the inverse generalized Prandtl-Ishlinskii model is a monotone operator, since inverse Prandtl-Ishlinskii model is a monotone and the density function $p(r)$ is integrable.

5.2.4 PARAMETERS IDENTIFICATION

In this subsection, the parameters of the inverse generalized Prandtl-Ishlinskii model, the threshold \hat{r} and the density function $\hat{p}(\hat{r})$, are identified. The generalized Prandtl-Ishlinskii model can also be expressed as:

$$\Phi[v](t) = \sum_{i=0}^n p(r_i) S_{r_i}[v](t) \quad (5.57)$$

The inverse of the model (5.57) can be expressed as:

$$\Phi^{-1}[v](t) = \begin{cases} \gamma_l^{-1} \circ \left(\sum_{i=1}^n p(r_i) F_{r_i}^+[v](t) \right) & \text{for } \dot{v}(t) \geq 0 \\ \gamma_r^{-1} \circ \left(\sum_{i=1}^n p(r_i) F_{r_i}^-[v](t) \right) & \text{for } \dot{v}(t) \leq 0 \end{cases} \quad (5.58)$$

Consequently, the inverse of the Prandtl-Ishlinskii model should be reformulated as:

$$\Pi[v](t) = \sum_{i=0}^n p(r_i) F_{r_i}[v](t) \quad (5.59)$$

To obtain the parameters of the inverse model, the composition of the modified initial loading curve and its inverse yields the threshold r as:

$$\bar{\varphi}^{-1}(\bar{\varphi}(r_j)) = r_j \quad (5.60)$$

where $j = 1, 2, \dots, n$. For the threshold $r_0 = 0$, the output of the play operator reduces to the input v as:

$$F_{r=0}[v] = v \quad (5.61)$$

Then, the output of the Prandtl-Ishlinskii model for $j=0$ can be expressed as:

$$\Pi[v](t) = p(0)v \quad (5.62)$$

Consequently, the inverse of the Prandtl-Ishlinskii model for $r_0 = 0$ can be expressed as:

$$\Pi^{-1}[v](t) = (p(0))^{-1}v \quad (5.63)$$

The derivative of the modified initial loading curve with respect to the threshold r can be expressed as:

$$\bar{\varphi}'(r) = p_0 + \sum_{i=1}^j p_i \quad (5.64)$$

where

$$p_0 = p(0) \quad (5.65)$$

In a similar manner the derivative of the modified initial loading curves with respect to the threshold \hat{r} is:

$$(\hat{\varphi}^{-1})'(\hat{r}) = \hat{p}_0 + \sum_{i=1}^j \hat{p}_i \quad (5.66)$$

where

$$\hat{p}_0 = \frac{1}{p_0} \quad (5.67)$$

The thresholds of the inverse are positive and are related to the thresholds r_j of the model as:

$$\hat{r}_j = \sum_{i=0}^j p_i (r_j - r_i) \quad (5.68)$$

Because the derivative of Equation (5.60) with respect to the threshold r can be expressed as:

$$\bar{\varphi}^{-1}(\hat{r}_j) = \frac{1}{\bar{\varphi}'(r_j)} \quad (5.69)$$

Then it can be concluded that the weights of the density function of the inverse generalized Prandtl-Ishlinskii model can be presented as:

$$\hat{p}_j = \frac{p_j}{(p_0 + \sum_{i=1}^j p_i)(p_0 + \sum_{i=1}^{j-1} p_i)} \quad (5.70)$$

5.3 Inverse Rate-Dependent Prandtl-Ishlinskii Models

As shown in Chapter 3, the smart actuators, such as piezoceramic and magnetostrictive actuators show strong rate-dependent hysteresis effects that increases as the excitation frequency of the input increases beyond certain frequency. Inverse of the rate-independent hysteresis models, when employed as feedforward compensators to compensate the rate-dependent hysteresis nonlinearities, can exhibit considerable errors in the output compensation, which may cause inaccuracies and oscillations in the closed-

and open-loop systems responses. Such oscillations, as an example, could be particularly detrimental in applications involving micro/nano-positioning control. In this section, inverse of the rate-dependent Prandtl-Ishlinskii model is presented for the purpose of compensating the rate-dependent hysteresis effects in smart actuators.

5.3.1 INVERSE RATE-DEPENDENT PRANDTL-ISHLINSKII MODEL

Analytical inverse of the rate-dependent Prandtl-Ishlinskii is formulated in this subsection. In other words, exact inverse of this rate-dependent model is reachable, consequently making it more attractive for compensation rate-dependent hysteresis of smart actuators. As shown in Chapter 2, the rate-dependent Prandtl-Ishlinskii model is expressed as:

$$\bar{\Pi}(v(t)) = qv(t) + \int_0^R p(\bar{r})F_{\bar{r}}(v(t))d\bar{r} \quad (5.71)$$

Following the same procedure shown in section 5.2, the inverse rate-dependent Prandtl-Ishlinskii model can be analytically expressed as:

$$\bar{\Pi}^{-1}(v(t)) = q^{-1}v(t) + \int_0^{\hat{r}} \hat{p}(\hat{r})F_{\hat{r}}(v(t))d\hat{r} \quad (5.72)$$

where \hat{r} is the dynamic threshold of the inverse and $\hat{p}(\hat{r}) \leq 0$ defines the dynamic density function of the inverse model. The rate-dependent Prandtl-Ishlinskii model can be also expressed as:

$$\bar{\Pi}(v(t)) = q^{-1}v(t) + \sum_{i=1}^n \bar{p}(\bar{r}_i)F_{\bar{r}_i}(v(t)) \quad (5.73)$$

The inverse of the rate-dependent Prandtl-Ishlinskii model can be presented as:

$$\bar{\Pi}^{-1}(v(t)) = q^{-1}v(t) + \sum_{i=1}^n \hat{p}(\hat{r}_i) F_{\hat{r}_i}(v(t)) \quad (5.74)$$

Based on the pervious description of the rate-dependent Prandtl-Ishlinskii model, the parameters of the inverse are expressed as:

$$q^{-1} = \frac{1}{q} \quad (5.75)$$

$$\hat{r}_j = q\bar{r}_j + \sum_{i=1}^{j-1} \bar{p}_i(\bar{r}_j - \bar{r}_i) \quad (5.76)$$

$$\hat{p}_j = -\frac{\bar{p}_j}{(q + \sum_{i=1}^j \bar{p}_i)(q + \sum_{i=1}^{j-1} \bar{p}_i)} \quad (5.77)$$

Owing to the symmetric properties of the rate-dependent play hysteresis operator, the inverse of the rate-dependent Prandtl-Ishlinskii model can be used only to compensate rate-dependent symmetric hysteresis effects such as piezoceramic actuators. However, the magnetostrictive actuators show asymmetric rate-dependent hysteresis effects. In the following subsection, the inverse of the generalized rate-dependent Prandtl-Ishlinskii model will be presented.

5.3.2 INVERSE GENERALIZED RATE-DEPENDENT PRANDTL-ISHLINSKII MODEL

The generalized rate-dependent Prandtl-Ishlinskii model is formulated upon integrating the generalized rate-dependent play operator together with the density function $p(\hat{r})$. This model exhibits high capability to characterize asymmetric rate-

dependent hysteresis effects. This model successfully characterizes the asymmetric rate-dependent hysteresis effects of magnetostrictive actuator at different excitation frequencies. The model output $\bar{\Phi}(v(t))$ is expressed as:

$$\bar{\Phi}(v(t)) = \int_0^R p(\bar{r}) S_{\bar{r}}(v(t)) d\bar{r} \quad (5.78)$$

Inverse of the generalized rate-dependent Prandtl-Ishlinskii model is presented to compensate the asymmetric rate-dependent hysteresis effects in smart actuators. The inverse of model can be used as a feedforward compensator in the control system. The exact inverse of the generalized rate-dependent Prandtl-Ishlinskii model can be derived if the inverse of the envelope functions γ_l^{-1} and $\gamma_r^{-1} : R \rightarrow R$ exists. Then, the inverse of the generalized rate-dependent Prandtl-Ishlinskii model can be analytically expressed as:

$$\bar{\Phi}^{-1}(v(t)) = \begin{cases} \gamma_l^{-1} \circ (\bar{\Pi}^{*+1}(v(t))) & \text{for } \dot{v}(t) \geq 0 \\ \gamma_r^{-1} \circ (\bar{\Pi}^{*-1}(v(t))) & \text{for } \dot{v}(t) \leq 0 \end{cases} \quad (5.79)$$

where output of the inverse rate-dependent Prandtl-Ishlinskii model can be expressed under increasing and decreasing input as:

$$\begin{aligned} \bar{\Pi}^{*+1}(v(t)) &= \int_0^R \hat{p}(\hat{r}) F_{\hat{r}}^+(v(t)) d\hat{r} \\ \bar{\Pi}^{*-1}(v(t)) &= \int_0^R \hat{p}(\hat{r}) F_{\hat{r}}^-(v(t)) d\hat{r} \end{aligned} \quad (5.80)$$

The generalized Prandtl-Ishlinskii model can also be expressed as:

$$\bar{\Phi}(v(t)) = \sum_{j=1}^n p(\bar{r}_j) S_{\bar{r}}(v(t)) \quad (5.81)$$

where n is the number of the generalized rate-dependent play operators that are used in the implementation. The parameters of the inverse, the density function $\hat{p}(\hat{r})$ and the threshold \hat{r} , are expressed as:

$$\hat{p}_o = \frac{1}{\bar{p}_o} \quad (5.82)$$

$$\hat{p}_j = \frac{\bar{p}_j}{(\bar{p}_o + \sum_{i=0}^j \bar{p}_i)(\bar{p}_o + \sum_{i=0}^{j-1} \bar{p}_i)} \quad (5.83)$$

$$\hat{r}_j = \sum_{i=0}^j \bar{p}(\bar{r}_i)(\bar{r}_j - \bar{r}_i) \quad (5.84)$$

Remark 5.3: The above formulation of inverse generalized Prandtl-Ishlinskii model follows the same presented in section 5.3. The only difference is the dynamic threshold.

5.4 Inverse Generalized Prandtl-Ishlinskii Model for Compensation

In this section, simulation results are carried out to compensate asymmetric and saturated hysteresis of different input/output relationships. Hysteresis is obtained using generalized Prandtl-Ishlinskii. The analytical inverse of the generalized Prandtl-Ishlinskii model is employed as a feedforward compensator to compensate asymmetric as well as saturated hysteresis nonlinearities.

5.4.1 COMPENSATION OF ASYMMETRIC HYSTERESIS LOOPS

The effectiveness of inverse of the generalized Prandtl-Ishlinskii model in compensating asymmetric hysteresis nonlinearities is investigated in this section. An

input signal of the form: $v(t)=5\sin(2\pi t)+4\cos(6t)$ is considered to evaluate minor as well as major hysteresis loops. The following envelope functions are proposed to construct the asymmetric hysteresis loops using the generalized model:

$$\begin{aligned}\gamma_l(v) &= v \\ \gamma_r(v) &= 1.2v + 1.9\end{aligned}\tag{5.85}$$

The chosen simulation parameters are: $T=20$ and $\Delta t=0.01$. The following density function is selected as:

$$p(r) = 0.07e^{-0.1r}\tag{5.86}$$

The thresholds of the generalized play operator are selected as:

$$r_j = 0.24j, \quad j=0, 1, 2, \dots, n = 49\tag{5.87}$$

Figure 5.7 shows the simulation results of the generalized Prandtl-Ishlinskii model. The figure shows the capability of the model to show asymmetric major as well as minor hysteresis loops. Inverse generalized Prandtl-Ishlinskii model is employed to compensate saturated hysteresis nonlinearities of the generalized Prandtl-Ishlinskii model. Parameters of the inverse generalized Prandtl-Ishlinskii model are identified by Equations (5.68) and (5.70). This inverse model is used as feedforward compensator to compensate hysteresis effects of the generalized Prandtl-Ishlinskii model. Figure 5.8 shows the capability of the inverse generalized Prandtl-Ishlinskii model to compensate the asymmetric hysteresis effects. The results show that the exact inverse of generalized Prandtl-Ishlinskii yields linear input-output relationship between the input and the output of the inverse compensation.

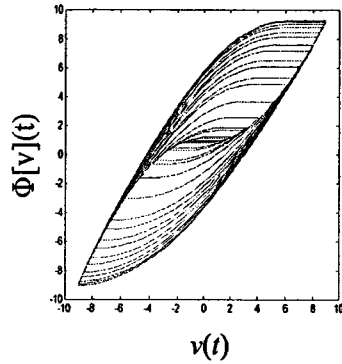


Figure 5.7: Input-output relations of generalized Prandtl-Ishlinskii model of $\gamma_l(v)=1.3v-0.4$ and $\gamma_r(v)=1.7v-1.9$.

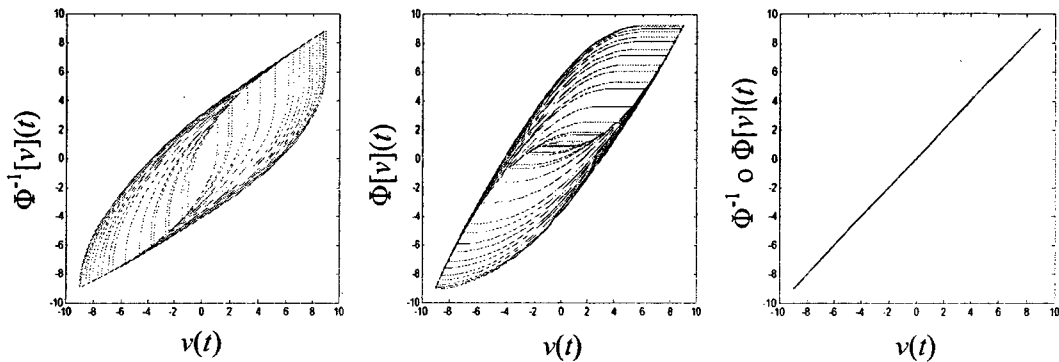


Figure 5.8: Compensation of asymmetric hysteresis loops with inverse generalized Prandtl-Ishlinskii model of $\gamma_l(v)=v$ and $\gamma_r(v)=1.2v+1.9$.

5.4.2 COMPENSATION OF SATURATED HYSTERESIS LOOPS

The effectiveness of the inverse generalized Prandtl-Ishlinskii model in compensating the saturated hysteresis effects is illustrated in this section. Simulation results are carried out to show capability of the inverse generalized Prandtl-Ishlinskii hysteresis model to compensate the saturated hysteresis nonlinearities. The following envelope functions are proposed for the pervious simulation in Section 5.4.1:

$$\begin{aligned}\gamma_i(v) &= 8 \tanh(0.22v - 0.6) \\ \gamma_r(v) &= 7.7 \tanh(0.2v + 0.1) + 0.1\end{aligned}\tag{5.88}$$

Figure 5.9 shows the input-output characteristics of the generalized Prandtl-Ishlinskii model. The figure shows the saturation property in the output of the generalized Prandtl-Ishlinskii model for major as well as minor hysteresis loops. Inverse generalized Prandtl-Ishlinskii model is employed to compensate the saturated hysteresis nonlinearities of the generalized Prandtl-Ishlinskii model. Parameters of the inverse generalized Prandtl-Ishlinskii model which are computed via Equations (5.68) and (5.70). Inverse of the generalized Prandtl-Ishlinskii model is employed as a feedforward compensator to compensate saturated hysteresis effects of the generalized Prandtl-Ishlinskii model. Figure 5.10 shows the capability of the inverse generalized Prandtl-Ishlinskii model to compensate the saturated hysteresis effects. The results show that the inverse generalized Prandtl-Ishlinskii model, which is obtained analytically, can be applied to compensate hysteresis nonlinearities with output saturation.

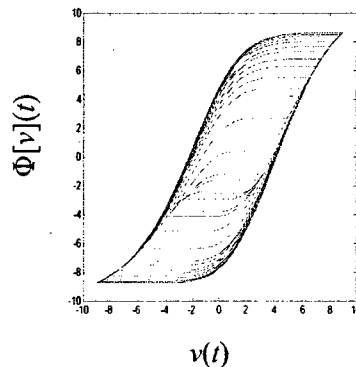


Figure 5.9: Input-output relations of generalized Prandtl-Ishlinskii model of $\gamma_i(v) = 8 \tanh(0.22v - 0.6)$, $\gamma_r(v) = 7.7 \tanh(0.2v + 0.1) + 0.1$.

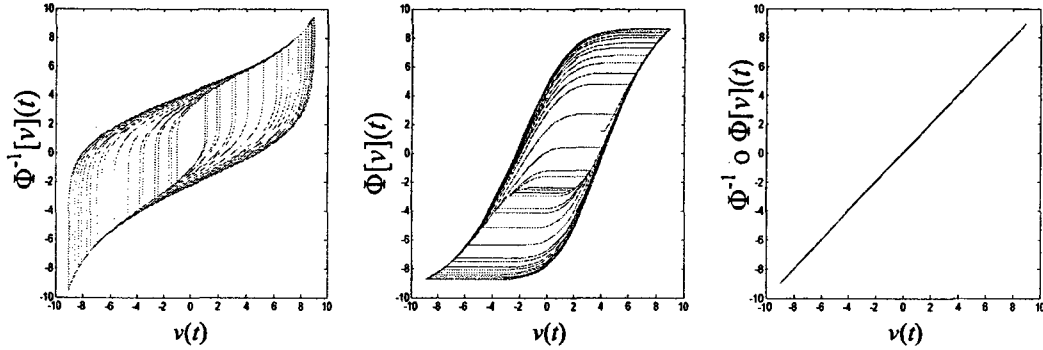


Figure 5.10: Compensation of saturated hysteresis loops with inverse generalized Prandtl-Ishlinskii model $\gamma_l(v) = 8 \tanh(0.22v - 0.6)$, $\gamma_r(v) = 7.7 \tanh(0.2v + 0.1) + 0.1$.

5.5 Inverse Rate-Dependent Prandtl-Ishlinskii Models for Compensation

The simulations were performed to compensate symmetric and asymmetric rate-dependent hysteresis nonlinearities using inverse symmetric and asymmetric rate-dependent Prandtl-Ishlinskii models as feedforward compensators at different excitation frequencies. The rate-dependent model is constructed with rate-dependent play operator, while the generalized rate-dependent Prandtl-Ishlinskii model is constructed using the generalized rate-dependent play hysteresis operator. In this section compensation of the rate-dependent hysteresis nonlinearities presented in Examples 2.3 and 2.4 are carried out.

5.5.1 COMPENSATION OF RATE-DEPENDENT HYSTERESIS

An input signal of the form: $v(t) = 6\sin(2f\pi t) + 3\sin(3f\pi t)$; is considered to evaluate minor as well as major hysteresis loops, while four fundamental frequencies are considered ($f = 10, 50, 100, \text{ and } 200 \text{ Hz}$). The simulation parameters of Example 2.3 were chosen. In this example, the results obtained from the model show an increase in the

hysteresis nonlinearities as the fundamental frequency increases. The inverse of the rate-dependent model is employed to compensate the rate-dependent hysteresis nonlinearities. The parameters of the inverse rate-dependent Prandtl-Ishlinskii model are computed by Equations (5.75), (5.76), and (5.77). As shown in Figure 5.11, the inverse of the rate-dependent model is used as a feedforward compensator to compensate the rate-dependent hysteresis effects at different excitation frequencies. The inverse of the rate-dependent model compensates the hysteresis effects at different fundamental frequencies.

5.5.2 COMPENSATION OF ASYMMETRIC RATE-DEPENDENT HYSTERESIS

Compensation of asymmetric rate-dependent hysteresis nonlinearities are carried out via inverse generalized rate-dependent Prandtl-Ishlinskii model. Simulation parameters of Example 2.4 are used in this subsection. The inverse of the generalized rate-dependent model is applied as a feedforward compensator. The parameters of the inverse model are computed by Equations (5.82), (5.83), and (5.84). The results obtained in Example 2.4 show an increase in the hysteresis, as the fundamental frequency increases. The results further show that the model employing the generalized rate-dependent play operator yields asymmetric rate-dependent hysteresis loops. As shown in Figure 5.12, the inverse generalized rate-dependent Prandtl-Ishlinskii model compensates asymmetric rate-dependent hysteresis nonlinearities. The results show that the inverse generalized rate-dependent Prandtl-Ishlinskii model compensates asymmetric rate-dependent hysteresis nonlinearities.

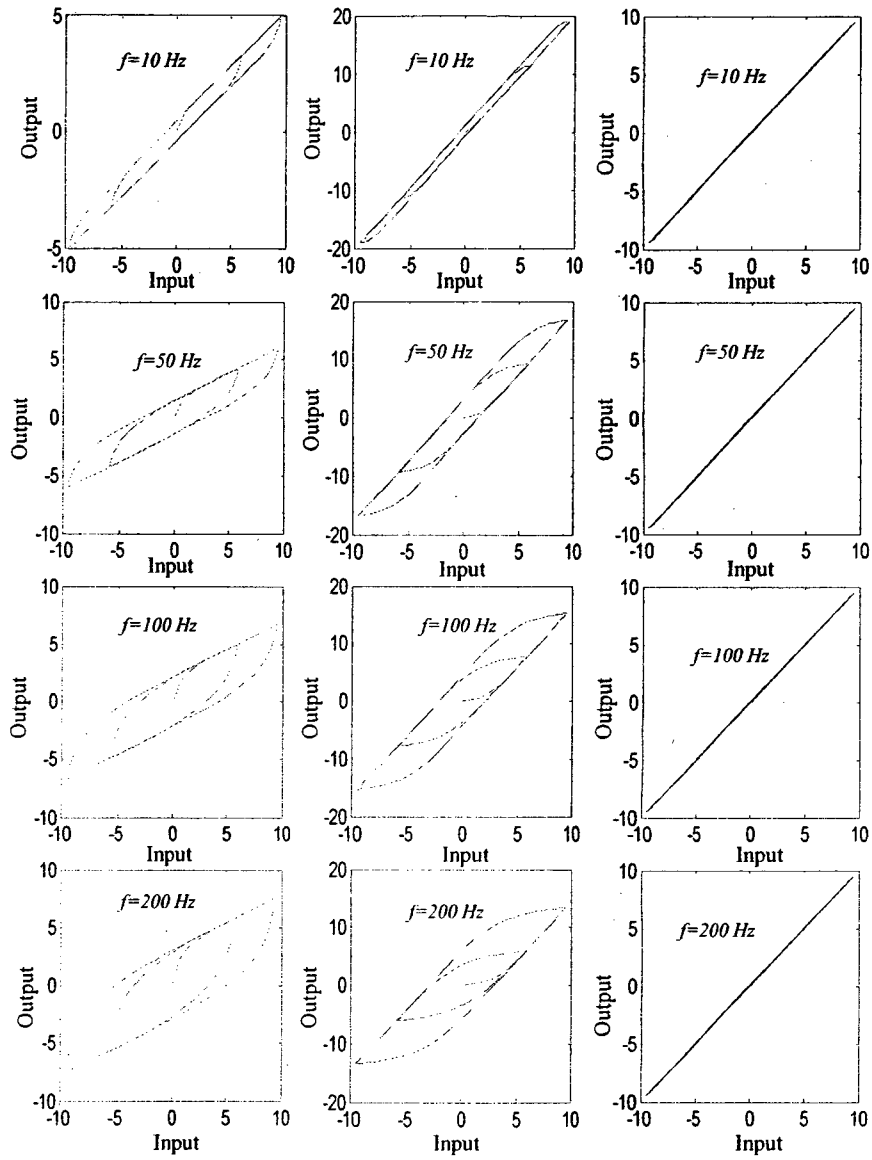


Figure 5.11: Compensation of rate-dependent symmetric hysteresis nonlinearities at different excitation frequencies using inverse rate-dependent Prandtl-Ishlinskii model as a feedforward compensator.

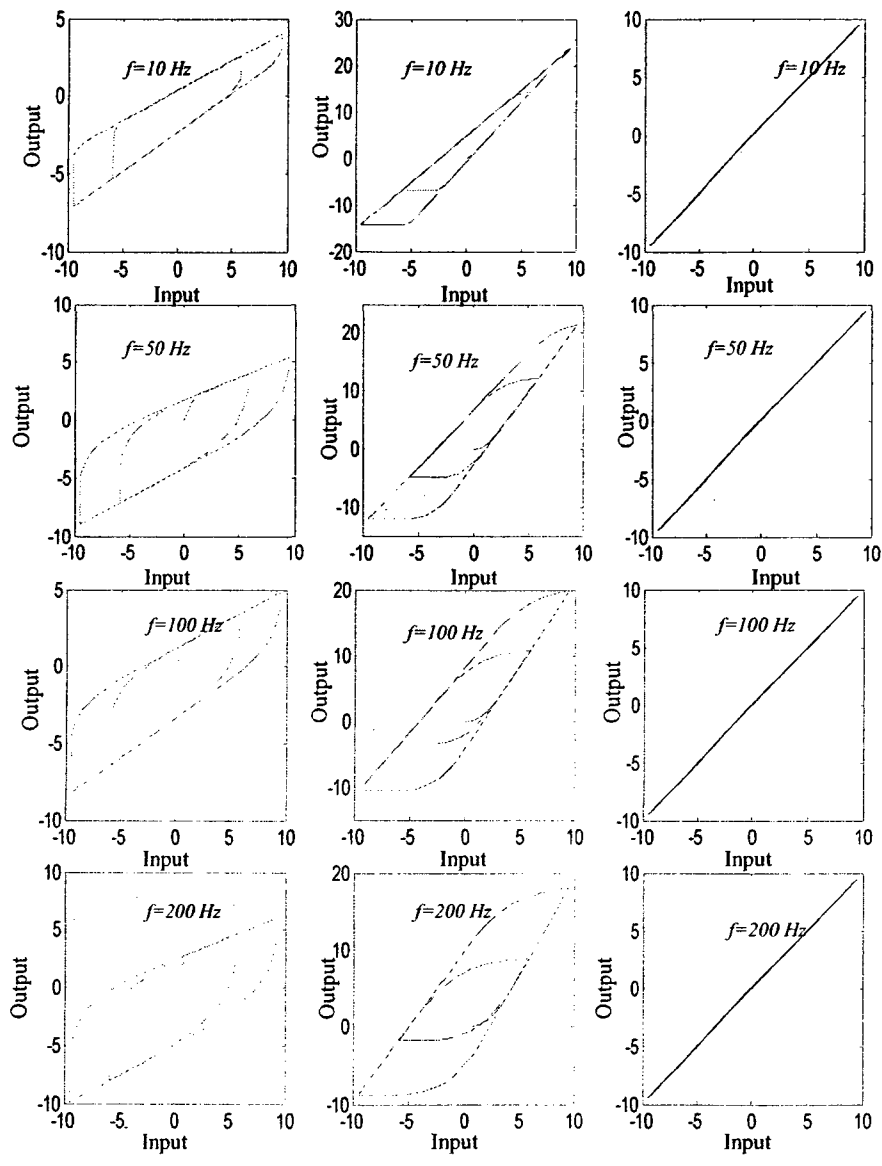


Figure 5.12: Compensations of asymmetric rate-dependent hysteresis nonlinearities at different excitation frequencies using inverse generalized rate-dependent Prandtl-Ishlinskii model as a feedforward compensator.

5.6 Experimental Verification of Hysteresis Compensation

The generalized Prandtl-Ishlinskii model can also describe the symmetric hysteresis properties such as those observed in piezoceramic actuators, by letting $\gamma_i(v) = \gamma_r(v)$, which is still different from the classical Prandtl-Ishlinskii model. The effectiveness of the inverse generalized model in compensating the symmetric hysteresis effects is investigated through simulation and laboratory experiments. The experiments were performed on a piezoceramic actuator (P-753.31C).

5.6.1 PARAMETERS IDENTIFICATION AND MODEL VALIDATION

Two different experiments were performed in the laboratory involving characterization of hysteresis and compensation. The experiments were performed initially to characterize the major and minor hysteresis properties of the piezoceramic actuator. The measured data were used to identify the generalized model parameters. The inverse generalized model was subsequently identified and applied as a feedforward compensator in the ControlDesk platform. The measurements were then performed to measure the compensated displacement response under the same input. Figure 5.13 illustrates a schematic of the experimental setup for both the experiments, where the input in the characterization experiment was directly applied to the actuator. In the compensation experiment, the input was applied to the actuator through the inverse model.

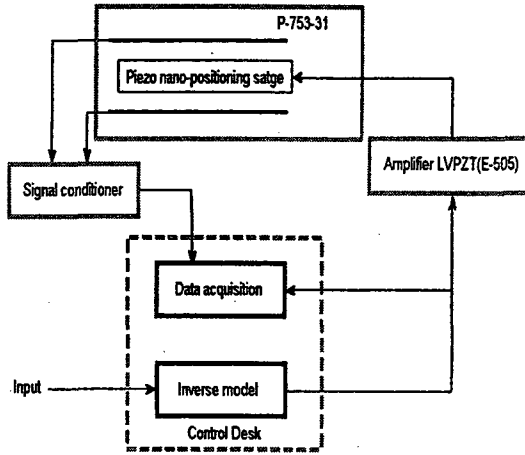


Figure 5.13: Experimental setup for compensation of hysteresis nonlinearities of the piezoceramic actuator using inverse generalized Prandtl-Ishlinskii model as a feed forward compensator.

The measured displacement and input voltage data were used for identifying the parameters of the generalized Prandtl-Ishlinskii model subject to the complex harmonic input used in the experimental study. Considering the nearly symmetric hysteresis properties of the piezoceramic actuator, linear envelope functions were chosen, such that:

$$\gamma_l(v) = \gamma_r(v) = c_o v + c_l \quad (5.89)$$

where c_o is a positive constant. The following density function is proposed for the model:

$$p(r) = \rho e^{-\tau r} \quad (5.90)$$

while the threshold r_j were chosen as:

$$r_j = cj, \quad j = 0, 1, 2, \dots, 9 \quad (5.91)$$

The model parameters (c , ρ , τ , c_o , and c_l) were identified through minimization of the error function defined in (4.3). Solutions were attained for a number of starting values of

the parameter vector, which converged to similar values. The generalized Prandtl-Ishlinskii model parameters were identified as: $c=3.47$, $\rho=0.54$, $\tau=0.16$, $c_o=0.89$, $c_I=0.37$. The validity of the generalized Prandtl-Ishlinskii model employing the generalized play operators was examined by comparing the model displacement responses with the measured data, as shown Figure 5.14. The results clearly suggest that the model can effectively predict the hysteresis properties of the piezoceramic actuator. Furthermore, the output-input properties appear to be symmetric and the generalized model can accurately describe the symmetric hysteresis loops. Figure 5.15(a) presents a comparison of output of the model in the time domain, with respect to the laboratory-measured data. The peak deviation between the generalized Prandtl-Ishlinskii model responses and the measured data is in the order of $2.8 \mu\text{m}$, as shown in Figure 5.15 (b).

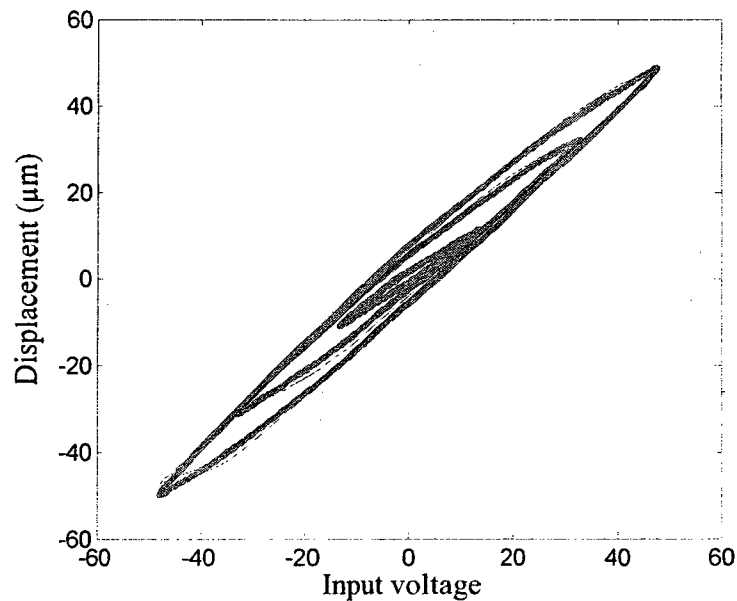


Figure 5.14: Comparisons of output-input responses of the generalized model with the measured responses (—, measured; - - -, model).

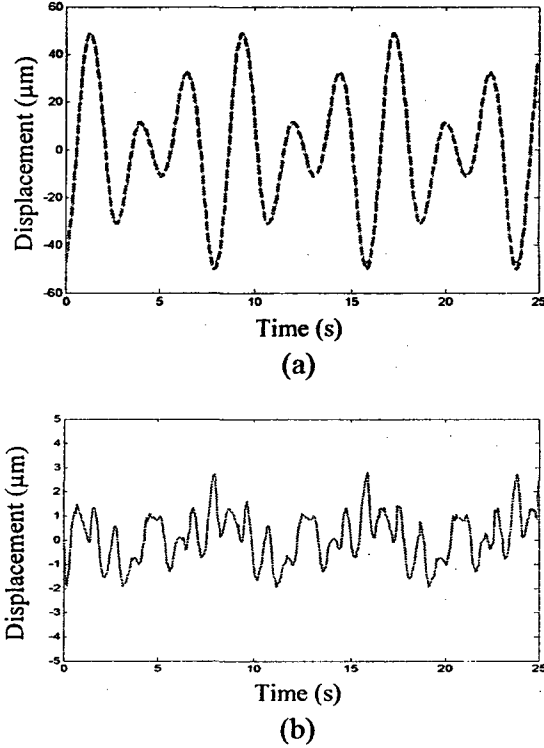


Figure 5.15 Time histories of measured and model displacement responses (- - - - - , measured; ————, model). (b) Time histories of error in measured and model displacement responses.

5.6.2 MOTION TRACKING EXPERIMENT

The inverse of the generalized Prandtl-Ishlinskii hysteresis model was derived and employed as a feedforward controller to compensate the hysteresis nonlinearities of the piezoceramic actuator. The parameters of the inverse model were identified from those of the generalized model together with the relations (5.66), (5.67), and (5.68). The thresholds of the play hysteresis operator of the inverse are: $\{0, 1.86, 4.79, 8.33, 12.22, 16.3161, 20.53, 24.80, 29.12, 33.46\}$, while the density function values were derived as: $\{1.87, -0.68, -0.20, -0.089, -0.044, -0.023, -0.013, -0.007, -0.004, -0.002\}$. The input-output characteristics of the inverse generalized Prandtl-Ishlinskii model are shown in

Figure 5.16 under the complex harmonic input.

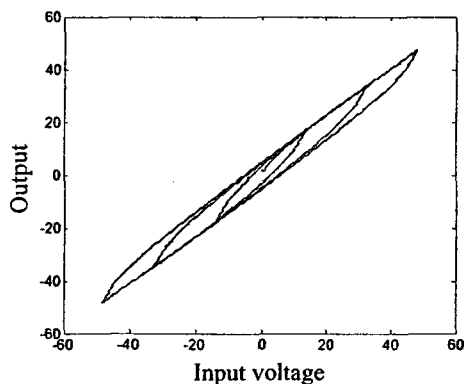


Figure 5.16: Input-output characteristics of the inverse generalized Prandtl-Ishlinskii model.

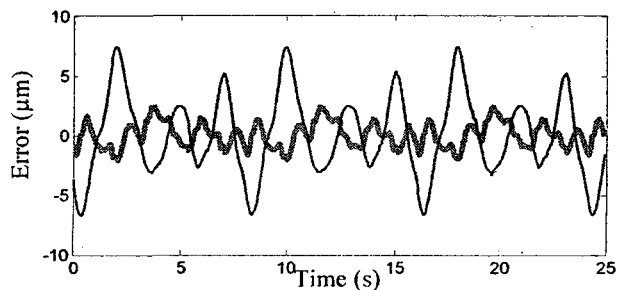
The measured input-output characteristics of the piezoceramic actuator with inverse model feedforward compensator are illustrated in Figure 5.17(b), while the errors with and without the compensator are compared in Figure 5.17(a). The results show that the inverse model feedforward compensator can effectively suppress the hysteresis effect, although some deviations are also evident. These deviations may be attributed to small prediction errors of the model as seen in Figure 5.14.

The compensation effectiveness of the inverse model is further evaluated by comparing the time histories of the measured displacement responses of the piezoceramic actuator with and without the inverse feedforward compensator. For the purpose, the positioning error is computed as the deviation between the measured displacement and the input voltage. It should be noted that the input voltage defines the desired displacement responses since the sensitivity of the capacitive position sensor is $1 \mu\text{m}/\text{V}$.

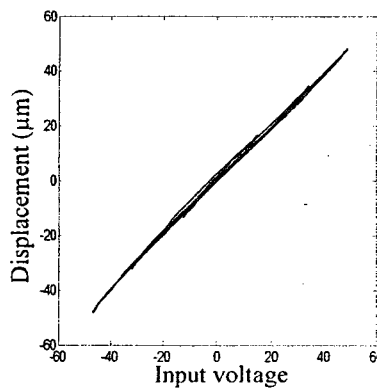
The results clearly show the compensation effectiveness of the inverse model. The peak position error of the piezoceramic actuator is nearly $7.5 \mu\text{m}$ (7.52%), while the peak

error with inverse feedforward controller is only $2.41 \mu\text{m}$ (2.43%). The results suggest that the proposed inverse of the generalized Prandtl-Ishlinskii model could effectively compensate hysteresis effects in real-time application. The exact inverse of the generalized Prandtl-Ishlinskii model can be also conveniently applied in closed-loop control algorithms, which would be most likely enhance compensation the inverse effects.

Remark 5.4: To achieve higher positioning performance, control algorithms in closed-loop systems can be easily developed together with inverse generalized Prandtl-Ishlinskii model to further eliminate the compensation errors as well as unknown disturbance. This is the major motivation for the development of the inverse model.



(a)



(b)

Figure 5.17 (a) Comparison of time-history of error between the output displacement and the input voltage, (———— , without inverse feedforward controller; - - - - - , with inverse feedforward controller). (b) Output-input characteristics of the piezo ceramic stage with Inverse feedforward compensator.

5.6.3 DISCUSSION

As shown in the previous section, the inverse generalized Prandtl-Ishlinskii model shows error in the output of the inverse compensation when the inverse generalized Prandtl-Ishlinskii model is applied as a feedforward compensator. The cause of the compensation error in the output responses is the characterization error of the generalized Prandtl-Ishlinskii model. It is obvious that the error in the output of the inverse compensation will affect the performance of the piezoceramic actuator when it is coupled with a system. Because the inverse Prandtl-Ishlinskii models have been obtained analytically in Chapter 5, the error of the inverse compensation can be derived analytically. To obtain the error of the inverse compensation; the composition expression for the Prandtl-Ishlinskii model and inverse of the estimated Prandtl-Ishlinskii model will be presented and derived, respectively.

5.7 Summary

An analytical inverse of the generalized Prandtl-Ishlinskii model, which is constructed by the generalized play operator, is formulated for the purpose of compensation of the asymmetric and saturated hysteresis nonlinearities. This is carried out by presenting the generalized Prandtl-Ishlinskii model using the initial loading curve, which provides an alternative description for the generalized Prandtl-Ishlinskii model. This inverse can be used as a feedforward compensator to mitigate hysteresis effects. Parameters identification for the inverse generalized Prandtl-Ishlinskii model is discussed using the initial loading curve and envelope functions. Inverse rate-dependent and generalized Prandtl-Ishlinskii models, constructed by rate-dependent and generalized

rate-dependent play operators, consequently, are also obtained analytically. The analytically derived inverse Prandtl-Ishlinskii hysteresis models offer significant benefits in real-time control applications, because the compensation error of the inverse Prandtl-Ishlinskii model can be obtained which will make it possible to design robust controller with stability analysis, which will be presented in Chapter 7. Simulation results show the capability of the inverse generalized Prandtl-Ishlinskii model (inverse feedforward compensator) to compensate asymmetric and saturated hysteresis nonlinearities. On the other hand, rate-dependent and generalized rate-dependent Prandtl-Ishlinskii models have also been used to compensate rate-dependent symmetric as well as asymmetric hysteresis effects.

Modeling and compensation of the hysteresis nonlinearities in a piezoceramic actuator using the generalized Prandtl-Ishlinskii model and its inverse are carried out experimentally. The compensator, which is the inverse of the generalized Prandtl-Ishlinskii model, reduces the hysteresis effects in the output displacement of the piezoceramic actuator. Because of the characterization error between the model and measured output responses of the actuator, the error of the inverse compensation was not zero. The output of the inverse compensation shows slight nonlinear effects between the input voltage and the measured displacement.

Chapter 6: Analytical Error of Inverse Compensation with Prandtl-Ishlinskii Model

6.1 Introduction

To characterize hysteresis in smart actuators using the Prandtl-Ishlinskii model, the density function and the thresholds of the model have to be determined. This is carried out generally by estimation of the density function and the thresholds based on the measured data. However, as shown in Chapter 4 that the characterization errors of the Prandtl-Ishlinskii models are not zero. Using the Prandtl-Ishlinskii model with estimated density and threshold functions to construct the inverse model and to utilize this inverse model for the compensation, as shown in Figure 6.2, will generate the compensation error. Because this error has not been identified in the literature, the stability analysis for the closed-loop control system with inverse compensation has not been presented.

The analytical error of the inverse compensation is presented for a hysteresis with Prandtl-Ishlinskii model presentation. Owing to the analytical inverse of the Prandtl-Ishlinskii model, the error of the inverse compensation is obtained analytically. To derive the error of the inverse compensation analytically, the initial loading curve of the Prandtl-Ishlinskii model and composition of the initial loading curve of the Prandtl-Ishlinskii model are presented. Then, the inverse of the estimated Prandtl-Ishlinskii model is derived and presented based on the initial loading curve and its inverse, respectively. Simulation results for the error of the inverse compensation are demonstrated in details for the inverse of the estimated Prandtl-Ishlinskii model.

6.2 Problem Statement

Figure 6.1 shows when v is applied as an input signal to the hysteretic actuator, the output of the hysteretic actuator $v^*(t)$ can be analytically presented as:

$$v^*(t) = P[u](t) \quad (6.1)$$

where P represents the hysteresis model for the hysteretic actuator. If the inverse of the hysteresis model P^{-1} can be obtained, it can be employed as a feedforward compensator to compensate the hysteresis nonlinearities as shown in Figure 6.2. The inverse operator P^{-1} takes v as input and outputs a signal $P^{-1}[v](t)$, such that the output $P[v](t)$ is v^* , such as:

$$\begin{aligned} v^*(t) &= P \circ P^{-1}[v](t) \\ &= P [P^{-1}[v]](t) \end{aligned} \quad (6.2)$$

where “o” denotes the composition operator.

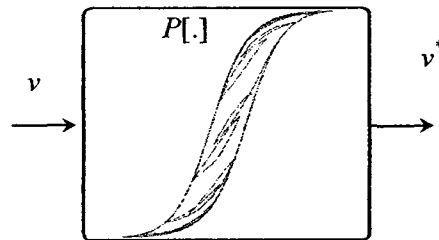


Figure 6.1: Hysteretic actuator.

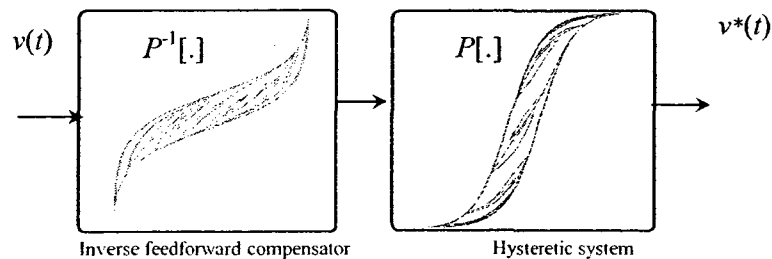


Figure 6.2: Open-loop control with inverse compensation.

The error of the compensated output can be expressed as:

$$e(t) = v(t) - v^*(t) \quad (6.3)$$

However, as shown in Chapter 5, the exact inverse of the Prandtl-Ishlinskii model is achievable and can be obtained analytically. Then the output of the inverse compensation can be presented as:

$$v^*(t) = \Pi \circ \Pi^{-1}[v](t) \quad (6.4)$$

If the exact inverse of the Prandtl-Ishlinskii model can be applied, the error of the inverse compensation should be zero and $v^*(t) = v(t)$. However, as shown in Chapter 4 that the characterization errors of the Prandtl-Ishlinskii models which are used to characterize different hysteresis effects in smart actuators are not zero. Consequently, when the inverse of these hysteresis models, formulated in Chapter 5, are applied to compensate for the hysteresis nonlinearities, the error of the inverse compensation will not be zero and the output of the inverse compensation will not show linear input-output relationship. In this chapter, analytical expression for the error $e(t)$ of the inverse compensation will be derived using the inverse of the estimated Prandtl-Ishlinskii model.

6.3 Analytical Expression of the Composition of the Prandtl-Ishlinskii Model

In this section analytical expression of the composition for the Prandtl-Ishlinskii model will be briefly presented. The expression, which is presented in [77], is essential to obtain the error of the inverse compensation. The Prandtl-Ishlinskii model Π which integrates the play operator F_r and the density function $p(r)$ to characterize the hysteresis

nonlinearities is expressed as:

$$\Pi[v](t) = qv(t) + \int_0^R p(r)F_r[v](t)dr \quad (6.5)$$

Figure 6.3 illustrates the concept of composition of the Prandtl-Ishlinskii model. The figure shows when the output of the Prandtl-Ishlinskii model $\Pi_{\varphi(r)}[v](t)$, constructed with initial loading curve $\varphi(r)$, is applied as an input to another Prandtl-Ishlinskii model $\Pi_{\psi(r)}$ with initial loading curve $\psi(r)$, the composition $\Pi_{\psi(r)}[\Pi_{\varphi(r)}](t)$ can be characterized by Prandtl-Ishlinskii model $\Pi_{\eta(r)}[v](t)$ with initial loading curve $\eta(r)$.

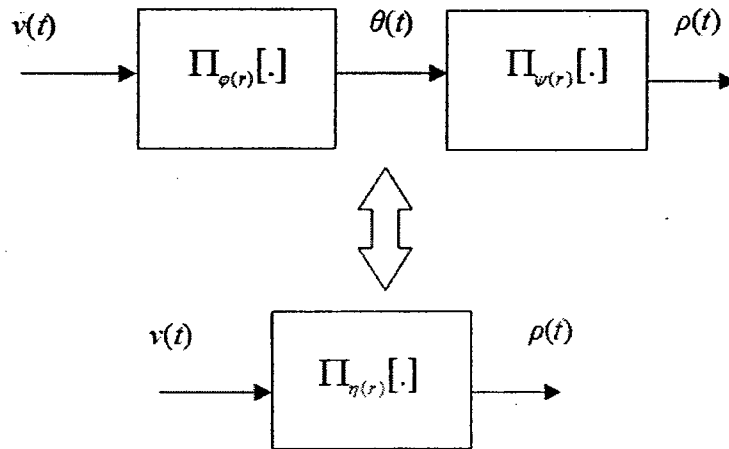


Figure 6.3: Composition of the Prandtl-Ishlinskii model.

Analytically, for two different initial loading curves $\varphi(r)$ and $\psi(r)$, the output of the Prandtl-Ishlinskii models are expressed as :

$$\Pi_{\varphi(r)}[v](t) = \varphi'(0)v(t) + \int_0^R F_r[v](t)\varphi''(r)dr \quad (6.6)$$

$$\Pi_{\psi(r)}[v](t) = \psi'(0)v(t) + \int_0^R F_r[v](t)\psi''(r)dr \quad (6.7)$$

The outputs of the above Prandtl-Ishlinskii models can be denoted as :

$$\theta(t) = \Pi_{\varphi(r)}[v](t) \quad (6.8)$$

$$\rho(t) = \Pi_{\psi(r)}[v](t) \quad (6.9)$$

The composition of the two Prandtl-Ishlinskii model is defined as [77]:

$$\Pi_{\varphi(r)} \circ \Pi_{\psi(r)} [v](t) = \Pi_{\eta(r)}[v](t) \quad (6.10)$$

where

$$\eta(r) = \varphi \circ \psi(r) \quad (6.11)$$

Equation (6.10) can be written as:

$$\Pi_{\varphi \circ \psi(r)}[v](t) = \Pi_{\eta(r)}[v](t) \quad (6.12)$$

The Prandtl-Ishlinskii model of the initial loading curve $\eta(r)$ can be expressed as:

$$\Pi_{\eta(r)}[v](t) = \eta'(0)v(t) + \int_0^R F_r[v](t)\eta''(r)dr \quad (6.13)$$

where $\eta''(r)$ is a density function and $\eta'(0)$ is a positive constant. Equation (6.13) shows that the composition of the Prandtl-Ishlinskii model with initial loading curves φ and ψ is a Prandtl-Ishlinskii model with initial loading curves $\eta(r)$.

6.3.1 ILLUSTRATIVE EXAMPLE

Consider an input of the form $v(t) = 7 \sin(\pi t)/(1 + 0.06t)$ and $t \in [0, 13]$ for Prandtl-Ishlinskii model presented in (6.5). The Prandtl-Ishlinskii models constructed with $\varphi''(r) = 0.1r$, $\psi''(r) = 0.12r$, $\varphi'(0) = 0.17$, and $\psi'(0) = 0.2$ are expressed as:

$$\Pi_{\varphi(r)}[v](t) = 0.17v(t) + \int_0^R F_r[v](t)(0.1r)dr \quad (6.14)$$

$$\Pi_{\psi(r)}[v](t) = 0.2v(t) + \int_0^R F_r[v](t)(0.12r)dr \quad (6.15)$$

The chosen simulation parameters are: $\Delta t=0.005$, $r \in [0, 7]$, and $\Delta r=0.01$. Outputs of models (6.14) and (6.15) are shown in Figures 6.4(a) and 6.4(b), respectively. The output of Prandtl-Ishlinskii model $\Pi_{\varphi(r)}[v](t)$, which is also denoted as $\theta(t)$, is applied as an input signal to Prandtl-Ishlinskii model $\Pi_{\psi(r)}$ (6.15). Then obtain the output of the Prandtl-Ishlinskii model $\rho(t)$ constructed by the initial loading curve $\psi(r)$:

$$\rho(t) = 0.2\theta(t) + \int_0^R F_r[\theta](t)(0.12r)dr \quad (6.16)$$

The input-output characteristics of the composition between the outputs $\theta(t)$ and $\rho(t)$ is shown in Figure 6.4(c). The initial loading curves of Prandtl-Ishlinskii models (6.14) and (6.15) are expressed as:

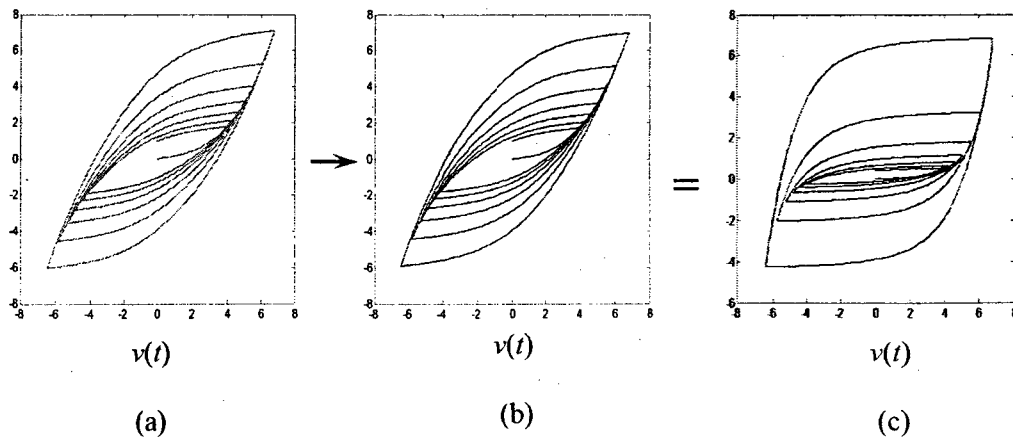


Figure 6.4: Input-output characteristics of Prandtl-Ishlinskii models: (a) $\Pi_{\psi(r)}[v]$, (b) $\Pi_{\varphi(r)}[v]$, and (c) $\Pi_{\eta(r)}[v]$.

$$\varphi(r) = 0.1r + \frac{1}{50}r^3 \quad (6.17)$$

$$\psi(r) = 0.17r + \frac{1}{60}r^3 \quad (6.18)$$

Then the initial loading curve $\eta(r)$ is expressed as:

$$\eta(r) = \frac{17r}{1000} + \frac{r^3}{1000} + \frac{3r^5}{5000} + \frac{3r^7}{12500} + \frac{r^9}{125000} \quad (6.19)$$

The outputs of Initial loading curves (6.17), (6.18), and (6.19) are shown in Figure 6.5.

Prandtl-Ishlinskii model that is constructed using initial loading curve $\eta(r)$ is defined as:

$$\Pi_{\eta(r)}[v](t) = \eta'(0)v(t) + \int_0^R F_r[v](t)\eta''(r)dr \quad (6.20)$$

where the density function is expressed as :

$$\eta''(r) = \frac{6r}{1000} + \frac{60r^3}{5000} + \frac{126r^5}{12500} + \frac{72r^7}{12500} \quad (6.21)$$

and,

$$\eta'(0) = \frac{17}{1000} \quad (6.22)$$

Figure 6.6 illustrates comparison between the output of Prandtl-Ishlinskii models (6.20) and (6.16). The Figure shows perfect matching between the outputs of the models.

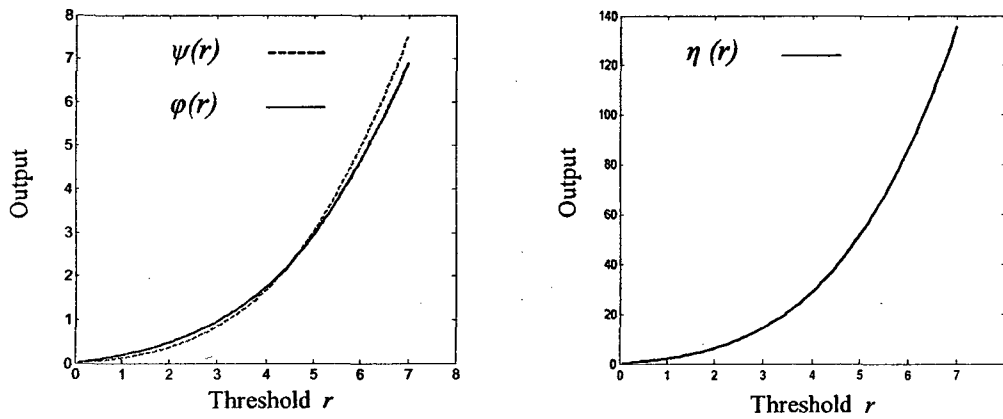


Figure 6.5: Input-output characteristics of initial loading curves given by (6.17), (6.18), and (6.19).

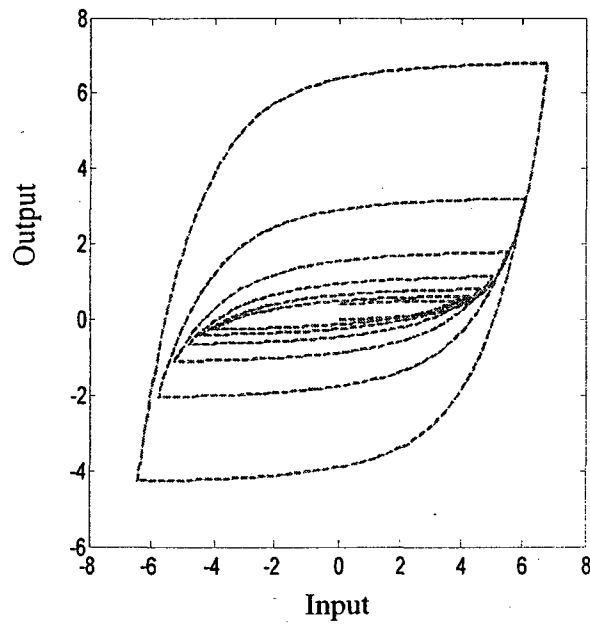


Figure 6.6: Comparison between outputs of Prandtl-Ishlinskii models (6.16) (-----) and (6.20) (—————).

6.4 Inverse of the Estimated Prandtl-Ishlinskii Model

After introducing the composition of the Prandtl-Ishlinskii model, the expression for the inverse of estimated Prandtl-Ishlinskii model is also required. Owing to the characterization error between the measured data and the outputs of the hysteresis models, the error of the inverse compensation cannot be zero. In this section, the inverse of the estimated Prandtl-Ishlinskii model is derived. This inverse will be employed to derive the error of the inverse compensation.

As shown in Section 5.2 that the Prandtl-Ishlinskii model is identified by the initial loading curve. In a similar manner, the inverse of the Prandtl-Ishlinskii model is presented by the inverse of the initial loading curve. Consequently, the inverse of the estimated Prandtl-Ishlinskii model is identified using the inverse of the estimated initial loading curve. Let the initial loading curve of the Prandtl-Ishlinskii model is φ , the inverse of the estimated initial loading curve is $\psi = \hat{\varphi}^{-1}$, and the estimated density function of the inverse Prandtl-Ishlinskii model is $\hat{p}^*(\hat{r}) = \psi''(r) \leq 0$. Then, the analytical inverse of the estimated Prandtl-Ishlinskii model is expressed as:

$$\Pi_{\psi(r)}[v](t) = \hat{q}^{-1}v(t) + \int_0^{\hat{r}} \hat{p}^*(\hat{r}) F_{\hat{r}}[v](t) d\hat{r} \quad (6.23)$$

where \hat{r} is the threshold of the inverse model. This threshold can be expressed for $l = 0, 1, 2, \dots, n$ as:

$$\hat{r}_l = \hat{r}_{l-1} + \int_{\hat{r}_{l-1}}^{\hat{r}_l} \hat{\varphi}'(r) dr \quad (6.24)$$

As shown in (6.23), the inverse of the Prandtl-Ishlinskii model is a Prandtl-Ishlinskii model. It can be concluded that the inverse of the estimated Prandtl-Ishlinskii model is Lipschitz continuous and maps $C [0, T]$ to $C [0, T]$. The inverse of estimated Prandtl-Ishlinskii model can be also numerically expressed as:

$$\Pi_{\psi(r)}[v](t) = \hat{q}^{-1}v(t) + \sum_{i=1}^n \hat{p}_i^* F_{\hat{r}_i}[v](t) \Delta \hat{r}_i \quad (6.25)$$

To compute the threshold of the inverse, the following steps are carried out for $r \in [r_j, r_{j+1})$, where $j=0, 1, 2, \dots, n$:

$$\varphi'(r) = q + \sum_{i=1}^j \hat{p}_i^* \Delta r_i \quad (6.26)$$

Then the threshold \hat{r} :

$$\hat{r}_l = \hat{r}_{l-1} + (q + \sum_{i=1}^{l-1} p_i)(r_l - r_{l-1}) \quad (6.27)$$

for $l=0, 1, 2, \dots, n$, the summation of equation (6.27) from 1 to j :

$$\hat{r}_j = qr_j + \sum_{i=1}^{j-1} p_i (r_j - r_i) \Delta r_i \quad (6.28)$$

To compute the weights of the density function of the inverse model in each interval $[\hat{r}_j, \hat{r}_{j+1})$ for $j=0, 1, 2, \dots, n$:

$$(\hat{\varphi}^{-1})'(\hat{r}) = 1/\varphi'(r) \quad (6.29)$$

Then,

$$\varphi'(r) = q + \sum_{i=1}^j p_i \Delta r_i \quad (6.30)$$

$$(\hat{\varphi}^{-1})'(\hat{r}) = q^{-1} + \sum_{i=1}^j \hat{p}_i^* \Delta \hat{r}_i \quad (6.31)$$

The following equation can be obtained by substituting (6.30) and (6.31) in (6.29):

$$q^{-1} + \sum_{i=1}^j \hat{p}_i^* \Delta \hat{r}_i = \frac{1}{q + \sum_{i=1}^j p_i \Delta r_i} \quad (6.32)$$

Equation (6.32) can be expressed as:

$$\text{for } j=1: \quad \hat{q}^{-1} + \hat{p}_1^* \Delta \hat{r}_1 = \frac{1}{q + p_1 \Delta r_1} \quad (6.33)$$

$$\text{for } j=2: \quad \hat{q}^{-1} + \hat{p}_1^* \Delta \hat{r}_1 + \hat{p}_2^* \Delta \hat{r}_2 = \frac{1}{q + p_1 \Delta r_1 + p_2 \Delta r_2} \quad (6.34)$$

⋮

$$\text{for } j=n: \quad \hat{q}^{-1} + \hat{p}_1^* \Delta \hat{r}_1 + \hat{p}_2^* \Delta \hat{r}_2 + \dots + \hat{p}_n^* \Delta \hat{r}_n = \frac{1}{q + p_1 \Delta r_1 + p_2 \Delta r_2 + \dots + p_n \Delta r_n} \quad (6.35)$$

Then, the density function of inverse of Prandtl-Ishlinskii model (6.25) on each interval can be expressed as:

$$\text{for } j=1: \quad \hat{p}_1^* = -\frac{p_1 \Delta r_1}{q(q + p_1 \Delta r_1) \Delta \hat{r}_1} \quad (6.36)$$

$$\text{for } j=2: \quad \hat{p}_2^* = -\frac{p_2 \Delta r_2}{(q + p_1 \Delta r_1 + p_2 \Delta r_2)(q + p_2 \Delta r_2) \Delta \hat{r}_2} \quad (6.37)$$

$$\text{for } j=n: \quad \hat{p}_j^* = \frac{p_j \Delta r_i}{(q + \sum_{i=1}^j \hat{p}_i \Delta r_i)(q + \sum_{i=1}^{j-1} \hat{p}_i \Delta r_i) \Delta r_i} \quad (6.38)$$

6.5 Analytical Error of the inverse Compensation of the Prandtl-Ishlinskii Model

For the first time in the literature, the error of the inverse compensation is formulated analytically for the Prandtl-Ishlinskii model using the inverse of the estimated Prandtl-Ishlinskii model. This analytical formulation shows that the error of the inverse compensation of the Prandtl-Ishlinskii model is still a Prandtl-Ishlinskii model.

Theorem 6.1: When the inverse of the estimated Prandtl-Ishlinskii model $\Pi_{\hat{\varphi}^{-1}(r)}$ is applied as a feedforward compensator to mitigate the hysteresis nonlinearities of the Prandtl-Ishlinskii model $\Pi_{\varphi(r)}$, as shown in Figure 6.7, the error of the inverse compensation for the input $v(t) \in C[0, T]$ can be expressed as:

$$e(t) = (1 - \eta_r'(0))v(t) - \int_0^R F_r[v](t)\eta''(r)dr \quad (6.39)$$

where $\eta(r) = \varphi(\hat{\varphi}^{-1}(r))$ is initial loading curve, $\eta_r'(0)$ is a positive constant, and $\eta_r''(r)$ is the density function.

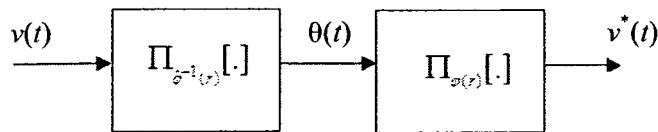


Figure 6.7: Illustration of inverse compensation of the Prandtl-Ishlinskii model.

Proof:

The error of the inverse compensation can be expressed as:

$$e(t) = v(t) - v^*(t) \quad (6.40)$$

The output of compensation $v^*(t)$ can be expressed using initial loading curves φ and $\hat{\varphi}^{-1}$ as:

$$v^*(t) = \Pi_{\varphi(r)} \circ \Pi_{\hat{\varphi}^{-1}(r)}[v](t) \quad (6.41)$$

where $\Pi_{\hat{\varphi}^{-1}}$ is the inverse of the estimated Prandtl-Ishlinskii model, which is presented in Section 6.4. Using the composition expression for the Prandtl-Ishlinskii model that is presented in Section 6.3, the output of the inverse compensation that is presented in (6.41) can be expressed as:

$$v^*(t) = \Pi_{\varphi \circ \hat{\varphi}^{-1}(r)}[v](t) \quad (6.42)$$

Then, by substituting (6.41) in (6.40), the error of the output compensation is expressed as:

$$e(t) = v(t) - \Pi_{\varphi \circ \hat{\varphi}^{-1}(r)}[v](t) \quad (6.43)$$

The initial loading curve of the Prandtl-Ishlinskii model and its inverse can be expressed as:

$$\eta(r) = \varphi(r) \circ \hat{\varphi}^{-1}(r) \quad (6.44)$$

Using Equation (6.44), the error can be then defined as:

$$e(t) = v(t) - \Pi_{\eta(r)}[v](t) \quad (6.45)$$

Then, the output of the Prandtl-Ishlinskii model with the inverse of the estimated Prandtl-Ishlinskii model can be presented as:

$$\Pi_{\eta(r)}[v](t) = \eta'(0)v(t) + \int_0^R F_r[v](t)\eta''(r)dr \quad (6.46)$$

then, error of the inverse compensation (6.45) can be expressed as:

$$e(t) = (1 - \eta_r'(0))v(t) - \int_0^R F_r[v](t)\eta''(r)dr \quad (6.47)$$

■

Remark 6.1: For the Prandtl-Ishlinskii model of initial loading curve $\varphi(r)$, if the exact inverse of the Prandtl-Ishlinskii model is constructed with $\varphi^{-1}(r)$, then the initial loading curve in (6.39) is simplified as:

$$\eta(r) = r \quad (6.48)$$

and

$$\eta'(0) = 1 \quad (6.49)$$

then, the error of the inverse compensation (6.47) is reduced to:

$$e(t) = 0 \quad (6.50)$$

and the compensated output is reduced to :

$$v^*(t) = v(t) \quad (6.51)$$

6.6 Simulation Results

In this section, simulations are carried out for the error of the inverse compensation of the Prandtl-Ishlinskii model. The parameters of the inverse of the estimated Prandtl-Ishlinskii model are computed by Equations (6.28) and (6.38). A harmonic input of the form, $v(t) = 7 \sin(\pi t) / (1 + 0.06t)$, $t \in [0, 13]$ is used as a desired input signal. The following initial loading curve is applied to formulate the Prandtl-Ishlinskii model:

$$\varphi(r) = 0.17r + \int_0^r 0.1\zeta(r-\zeta)d\zeta \quad (6.52)$$

In this subsection, the exact inverse of Prandtl-Ishlinskii hysteresis model is constructed by using the inverse of initial loading curve (6.52). The simulation results for the model and its inverse are presented in Figures 6.8(a) and 6.8(b), respectively. The inverse of the Prandtl-Ishlinskii model, constructed by the initial loading curve $\varphi^{-1}(r)$, is applied as a feedforward compensator to compensate the hysteresis nonlinearities of the Prandtl-Ishlinskii model that is constructed by the initial loading curve $\varphi(r)$. The compensated output, presented in Figure 6.8(c), shows linear relationship between the desired input and the compensated output. The figure shows that the inverse feedforward compensator mitigates the hysteresis nonlinearities.

The compensation output, which is also computed by (6.46), is presented in Figure 6.9(a). This Figure shows linear relationship between the input signal and the output of the compensation. The error of the inverse compensation that is obtained from Theorem 6.1 is presented in Figure 6.9 (b). The figure shows that the error of the inverse compensation is zero, $e(t)=0$.

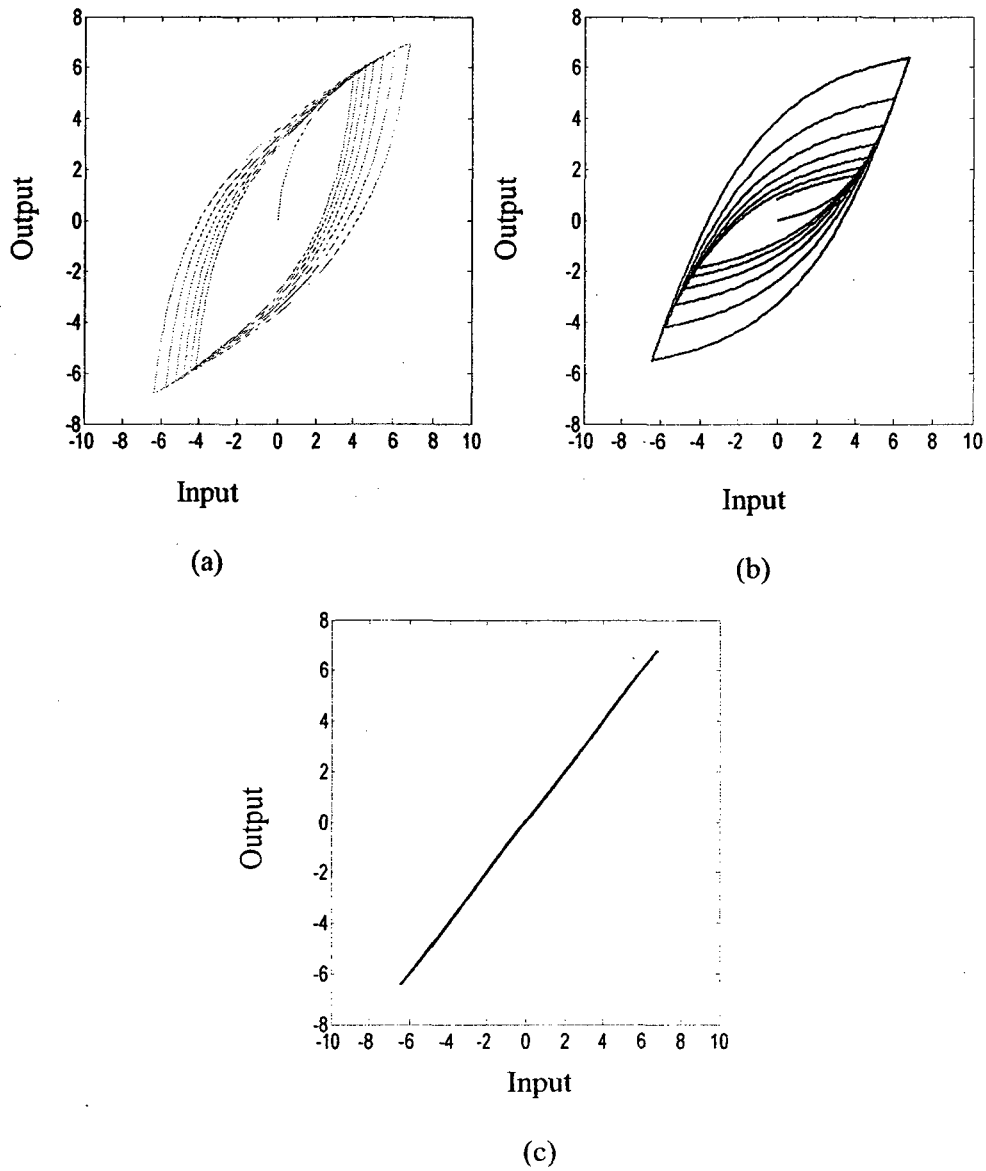


Figure 6.8: Input-output characteristics of: (a) Inverse of Prandtl-Ishlinskii model, (b) Prandtl-Ishlinskii model, and (c) Compensation with the inverse Prandtl-Ishlinskii model.

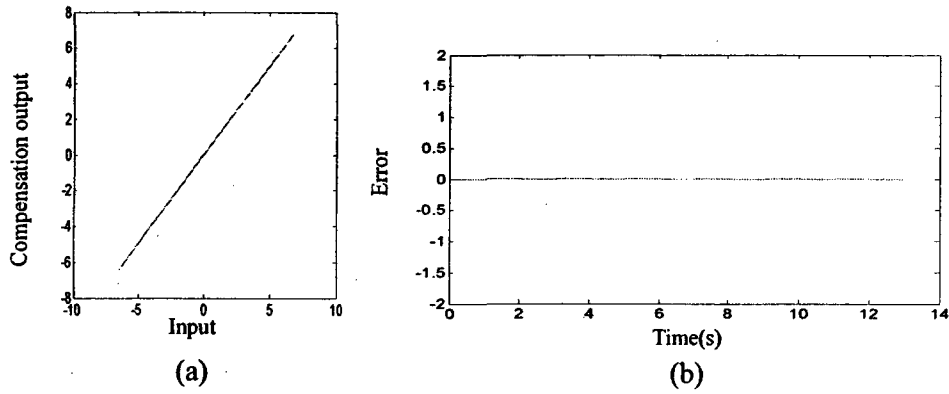


Figure 6.9: (a) The input-output characteristics of the inverse compensation (b) Time histories of the error of the inverse compensation.

The following estimated initial loading curve is employed to construct the inverse Prandtl-Ishlinskii model:

$$\hat{\varphi}(r) = 0.2r + \int_0^r 0.2\zeta(r-\zeta)d\zeta \quad (6.53)$$

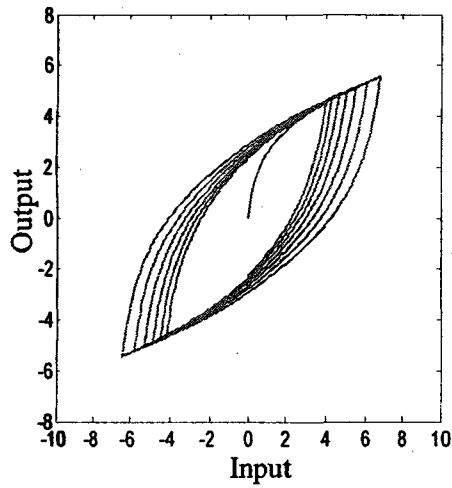
As shown in Figure 6.10, the inverse of the estimated Prandtl-Ishlinskii model, which is constructed by the inverse of the estimated initial loading curve $\hat{\varphi}^{-1}(r)$, is applied as a feedforward compensator to compensate the hysteresis nonlinearities of the Prandtl-Ishlinskii model that is obtained using initial loading curve (6.52). The input-output characteristic of the inverse of the estimated Prandtl-Ishlinskii model is shown in Figure 6.10(a). The output of the inverse compensation that is presented in Figure 6.10(c) shows hysteresis nonlinearities.

Using Theorem 6.1, the output of the inverse compensation, obtained via Equation (6.46), is presented in Figure 6.11(a) and the input-output characteristic of the error of the inverse compensation is shown in Figure 6.11(b). While, the time history of the error is presented Figure 6.11(c). The simulation results show the capability of Theorem 6.1 to

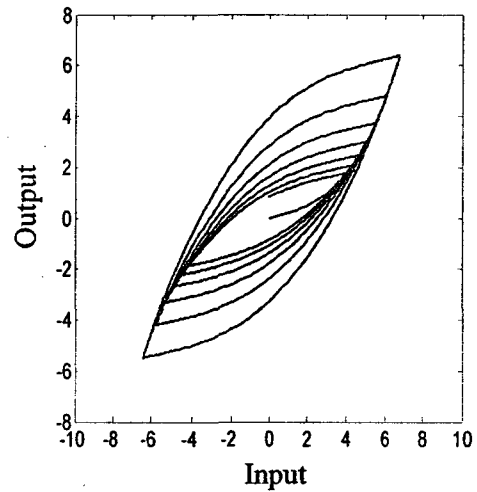
compute the error of the inverse compensation for the Prandtl-Ishlinskii model. The results demonstrate that the error of the inverse compensation shows hysteresis nonlinearities between the desired input and the output of the inverse compensation. Consequently, it can be concluded that the error of the compensation may cause undesirable inaccuracies or oscillations and even instability.

6.7 Summary

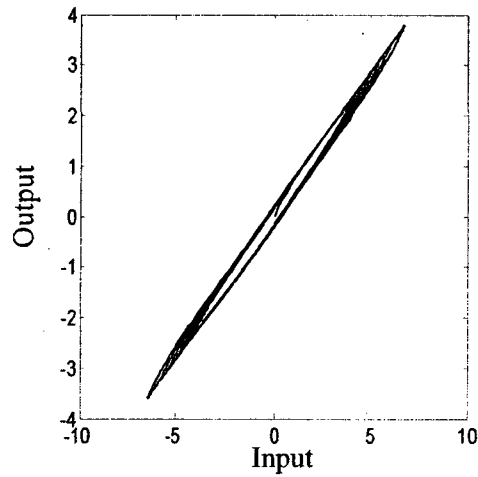
Stability analysis generally cannot be constructed for inverse-based control methods when the compensated output of the hysteretic actuator is coupled to a system because the error of inverse compensation has not been identified in the literature. For the first time in the literature, analytical error of the inverse compensation of Prandtl-Ishlinskii hysteresis model has been presented. The inverse of the estimated Prandtl-Ishlinskii, which is applied as a feedforward compensator, is employed to derive the error of the inverse compensation. The analytical error of the inverse compensation is presented in Theorem 6.1. This error shows hysteresis nonlinearities between the desired input and the compensated output, which can be easily understood physically. The analytical inverse of the hysteresis is a hysteresis; therefore their compensation should still be a hysteresis. This explanation coincides with analytical analysis. It can be concluded that the error of the compensation may cause undesirable inaccuracies or oscillations and even instability. Simulation results show the capability of Theorem 6.1 to compute the error of the inverse compensation. The error of the inverse compensation is used in Chapter 7 to design controller for a nonlinear plant proceeded by the hysteretic system with inverse compensation in a closed-loop system.



(a)

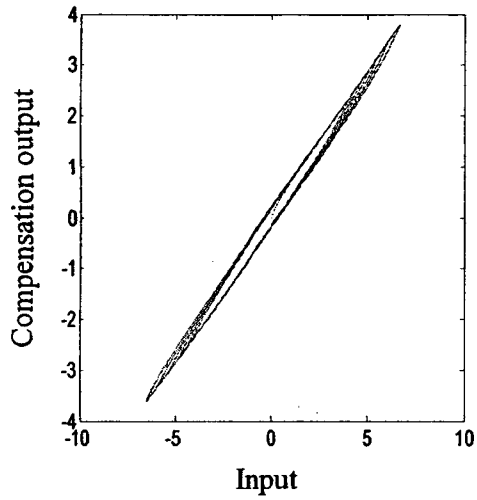


(a)

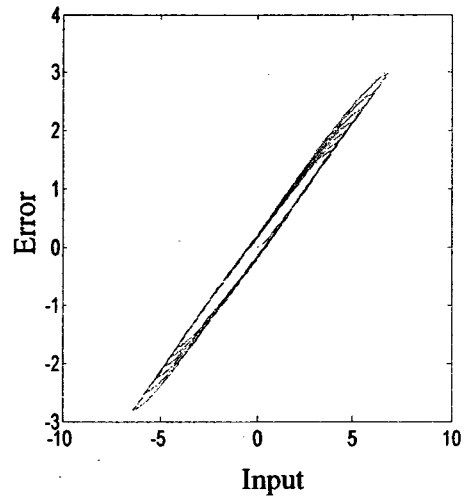


(c)

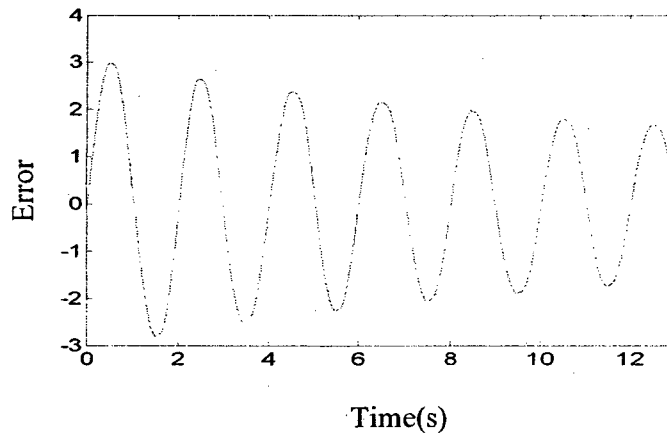
Figure 6.10: Input-output characteristics of: (a) Inverse of Prandtl-Ishlinskii model, (b) Prandtl-Ishlinskii model, and (c) Compensation with the inverse of the estimated Prandtl-Ishlinskii model.



(a)



(b)



(c)

Figure 6.11: (a) The output of the inverse compensation (b) Input-output characteristics of the error of the compensation (c) Time history of the error.

Chapter 7: An Adaptive Controller Design for Inverse Compensation Error

7.1 Introduction

The previous chapter presents the analytical error of the inverse compensation for the Prandtl-Ishlinskii model. The results show that the error of the inverse compensation can be also presented by a Prandtl-Ishlinskii model. Obviously, the error of the inverse compensation will cause undesirable inaccuracies or oscillations and even instability. Owing to the analytical error expression of the inverse compensation, controller design as well as corresponding stability analysis for a controlled plant actuated with inverse compensation that proceeded with the output of the inverse compensation is presented in this chapter.

Su et al. [55] proposed an adaptive robust controller to control a system preceded with hysteresis nonlinearities of the Prandtl-Ishlinskii model without using inverse compensation. Because the error after the inverse compensation is a Prandtl-Ishlinskii model, therefore, the control design presented in [55] can be used to control a plant that preceded with inverse compensation of the Prandtl-Ishlinskii model. It should be mentioned that the purpose of this chapter is:

- i. To couple the output of the inverse compensation into a controlled plant in a closed-loop system.
- ii. To perform the stability analysis for a closed-loop system when the inverse compensation is applied to compensate the hysteresis nonlinearities.
- iii. To study the effects of the inverse compensation and its error on the tracking error performance of the closed-loop system.

7.2 Problem Statement

Figure 7.1 presents a controlled system consisting of a plant (dynamic system) preceded by a hysteretic actuator with its inverse compensation. In this figure, the hysteretic actuator is characterized by the Prandtl-Ishlinskii model $\Pi_{\varphi(r)}$ and the inverse of the estimated Prandtl-Ishlinskii $\Pi_{\hat{\varphi}^{-1}(r)}$ is applied as a feedforward compensator to compensate the hysteresis nonlinearities of the hysteretic actuator. The output of the inverse compensation $\Pi_{\varphi \circ \hat{\varphi}^{-1}(r)}$ is applied as an input signal to a controlled plant, generally characterized as a dynamic system. The controller shown in Figure 7.1 is applied to compensate the error generated by the inverse compensation. This error has been derived in Chapter 6. The dynamic system is described in the following canonical form:

$$x^n(t) + \sum_{i=1}^k a_i Y_i(x(t), \dot{x}(t), \dots, x^{n-1}(t)) = b \Pi_{\varphi \circ \hat{\varphi}^{-1}(r)}[u](t) \quad (7.1)$$

where Y_i presents the known continuous linear or nonlinear functions. The parameters a_i and control gain b are constants. The output of the inverse compensation is expressed analytically as:

$$\Pi_{\varphi \circ \hat{\varphi}^{-1}}[u](t) = \eta_r'(0)u(t) + \int_0^R F_r[u](t)\eta''(r)dr \quad (7.2)$$

It is a common assumption that the sign of b is known. Without loss of generality, assume that b is a positive constant, $b > 0$. System (7.1) can be represented with as:

$$x^n(t) + \sum_{i=1}^k a_i Y_i(x(t), \dot{x}(t), \dots, x^{n-1}(t)) = b \eta_r'(0) u(t) + b \int_0^R F_r[u](t) \eta''(r) dr \quad (7.3)$$

The above equation yields a linear relation of the input signal, $b \eta_r'(0) u(t)$, and a nonlinear term, $b \int_0^R F_r[u](t) \eta''(r) dr$.

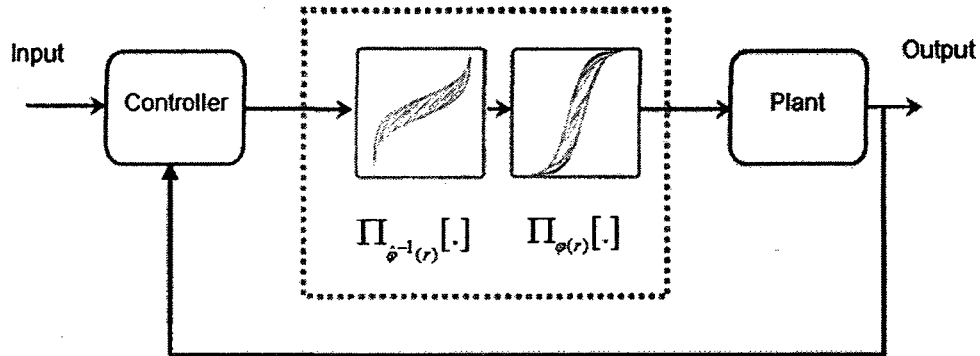


Figure 7.1: Closed-loop control system with inverse compensation.

Remark 7.1: It is clear that the first term on the right-hand side of (7.3) is a linear function of the signal $u(t)$. In this case, it is possible to combine the currently available controller design techniques with the error of the inverse compensation of Prandtl-Ishlinskii model. This was the primary motivation behind derivation of the analytical inverse as well as the error of the inverse compensation.

Remark 7.2: If the hysteresis in the system is known, that is, $p(r)$ and $F_r[u](t)$ are given or can be accurately estimated, for any continuous input function $u(t)$ at a time instant t , the inverse mitigates the nonlinear effects, and the error $e(t)$ is zero. Then, system (7.3) can be expressed as:

$$x^n(t) + \sum_{i=1}^k a_i Y_i(x(t), \dot{x}(t), \dots, x^{n-1}(t)) = bu(t) \quad (7.4)$$

7.3 Control Design

In this section, an adaptive variable structure controller is applied to control plant (7.1) that preceded by the inverse compensation where the inverse is constructed by the Prandtl-Ishlinskii model. The controller is designed by the error of the inverse compensation will guarantee the global stability and yield tracking within a desired precision. Assume that the reference signal $x_d(t)$ is a smooth bounded signal and its time derivatives $x_d^{(i)}$ ($1 \leq i \leq n$) are bounded. The control objective is to design a control law $u(t)$ to force state vector $x = [x, \dot{x}, \dots, x^{(n-1)}]^T$ to follow a desired trajectory $x_d = [x_d, \dot{x}_d, \dots, x_d^{(n-1)}]^T$, i.e. $x \rightarrow x_d$ as $t \rightarrow \infty$. In this chapter, the back-stepping design method is used in the design of the robust controller. Using the back-stepping approach, system (7.3) can be expressed as:

$$\begin{aligned} \dot{x}_1(t) &= x_2(t) \\ &\cdot \\ &\cdot \\ &\cdot \\ \dot{x}_{n-1}(t) &= x_n(t) \end{aligned} \tag{7.5}$$

$$\dot{x}_n(t) = -\sum_{i=1}^k a_i Y_i(x(t)) + b(1 - \eta_r'(0))u(t) - b \int_0^{\infty} F_r[u](t) \eta''(r) dr$$

Define new variables for $i = 2, 3, \dots, n$, as:

$$\begin{aligned} z_1(t) &= x_1 - x_d(t) \\ z_i(t) &= x_i - x_d^{i-1} - \alpha_{i-1} \end{aligned} \tag{7.6}$$

where α_i which is the virtual control at the i th step is defined as:

$$\begin{aligned}\alpha_1(t) &= -c_1 z_1(t) \\ \alpha_i(t) &= -c_i z_i(t) - z_{i-1}(t) + \dot{\alpha}_{i-1}(x_1, \dots, x_{i-1}, x_d, \dots, x_d^{i-1})\end{aligned}\quad (7.7)$$

According to the analysis in Chapter 6, it is easily deduced that $\eta_r'(0) = \varphi(\hat{\varphi}^{-1})'(0)$ is a positive constant, then $b_\eta = b\eta_r'(0)$ is an unknown positive parameter. To avoid chattering, as in [75, 76], a smooth function $sg(z)$ is adopted:

$$sg_i(z_i) = \begin{cases} \frac{z_i}{|z_i|} & , |z_i| \geq \delta_i \\ \frac{z_i}{(\delta_i^2 - z_i^2)^{n-i+2} + |z_i|} & , |z_i| < \delta_i \end{cases}\quad (7.8)$$

where δ_i are positive design parameters. A function $f_i(z_i)$ is also used as:

$$f_i(z_i) = \begin{cases} 1 & , |z_i| \geq \delta_i \\ 0 & , |z_i| < \delta_i \end{cases}\quad (7.9)$$

Then,

$$sg_i(z_i)f_i(z_i) = \begin{cases} 1 & , z_i \geq \delta_i \\ 0 & , |z_i| < \delta_i \\ -1 & , |z_i| \leq -\delta_i \end{cases}\quad (7.10)$$

To ensure the resultant functions are differentiable, similarly, z_i^2 are replaced by $(|z_i| - \delta_i)^{n-i+2} f_i$ in the Lyapunov function and z_i are replaced by $(|z_i| - \delta_i)^{n-i+2} sg_i$ in the design procedure.

Step 1: Choose the design virtual control law α_1 as:

$$\alpha_1 = -(c_1 + \frac{1}{4})(|z_1| - \delta_1)^n sg_1(z_1) - (\delta_2 + 1)sg_1(z_1)\quad (7.11)$$

where c_1 is a positive design parameter. Consider the following Lyapunov function V_1 , defined in [75], as:

$$V_1 = \frac{1}{n+1} (|z_1| - \delta_1)^{n+1} f_1 \quad (7.12)$$

then, the derivative of V_1 yields:

$$\dot{V}_1 = (|z_1| - \delta_1)^n f_1 s_{g_1}(z_1) \dot{z}_1 \quad (7.13)$$

Considering $\dot{z}_1 = z_2 + \alpha_1$, the following inequality can be obtained:

$$\begin{aligned} \dot{V}_1 &= (|z_1| - \delta_1)^n f_1 s_{g_1}(z_1) (z_2 + \alpha_1) \\ &\leq -(c_1 + \frac{1}{4})(|z_1| - \delta_1)^{2n} f_1 + (|z_1| - \delta_1)^n (|z_2| - \delta_2 - 1) f_1 \end{aligned} \quad (7.14)$$

Step i ($i = 2, \dots, n-1$) choose:

$$\alpha_i = -(c_i + \frac{5}{4})(|z_i| - \delta_i)^{n-i+1} s_{g_i}(z_i) + \dot{\alpha}_{i-1} - (\delta_{i+1} + 1) s_{g_i}(z_i) \quad (7.15)$$

The corresponding Lyapunov function is also adopted as [75]:

$$V_i = \frac{1}{n-i+2} (|z_i| - \delta_i)^{n-i+2} f_i + V_{i-1} \quad (7.16)$$

The derivative \dot{V}_i is given by:

$$\begin{aligned} \dot{V}_i &= (|z_i| - \delta_i)^{n-i+1} s_{g_i}(z_i) \dot{z}_i + \dot{V}_{i-1} \\ &= -\sum_{k=1}^i c_k (|z_k| - \delta_k)^{2(n-k+1)} f_k + (|z_i| - \delta_i)^{n-i+1} f_i (|z_{i+1}| - \delta_{i+1} - 1) \\ &\quad - \frac{1}{4} (|z_i| - \delta_i)^{2(n-i+1)} f_i + M_i \end{aligned} \quad (7.17)$$

where M_i is expressed as:

$$\begin{aligned}
M_i &= (|z_i| - \delta_i)^{2(n-i+1)} f_i - \frac{1}{4} (|z_{i-1}| - \delta_{i-1})^{2(n-i+1)} f_{i-1} \\
&\quad + (|z_{i-1}| - \delta_{i-1})^{n-i+1} (|z_i| - \delta_i - 1) f_{i-1}
\end{aligned} \tag{7.18}$$

Since $M_i \leq 0$ [75], it can be concluded that:

$$\begin{aligned}
\dot{V}_i &\leq -\sum c_k (|z_k| - \delta_k)^{2(n-k+1)} f_k + \\
&\quad (|z_i| - \delta_i)^{n-i+1} f_i (|z_{i+1}| - \delta_{i+1} - 1) - \frac{1}{4} (|z_i| - \delta_i)^{2(n-i+1)} f_i
\end{aligned} \tag{7.19}$$

Step n : In the last step, the compensation error of Prandtl-Ishlinskii model and its inverse are considered. The following definitions are given:

$$\tilde{a} = \hat{a} - a \tag{7.20}$$

$$\tilde{\beta} = \hat{\beta} - \beta \tag{7.21}$$

$$\tilde{\eta}_b''(t, r) = \hat{\eta}_b''(t, r) - \eta_b''(r) \tag{7.22}$$

where \hat{a} , $\hat{\beta}$, and $\hat{\eta}_b''(t, r)$ are estimate of a , β , and $\eta_b''(r)$, respectively. Define $B_o(t)$

as:

$$B_o(t) \triangleq \int_0^R \eta_b''(r) |F_r[u](t)| dr \tag{7.23}$$

Then the estimated $\hat{B}_o(t)$ is defined as:

$$\hat{B}_o(t) \triangleq \int_0^R \hat{\eta}_b''(t, r) |F_r[u](t)| dr \tag{7.24}$$

Choose the Lyapunov function V_n as:

$$V_n = \sum_{i=1}^n \frac{1}{n-i+2} (|z_i| - \delta_i)^{n-i+2} f_i + \frac{1}{2} \tilde{a}^T \bar{\Gamma} \tilde{a} + \frac{b_n}{2\gamma} \tilde{\beta}^2 + \frac{1}{2\bar{q}} \int_0^R (\eta_b)''(t, r) dr \quad (7.25)$$

Then \dot{V}_n can be expressed as:

$$\begin{aligned} \dot{V}_n = & \dot{V}_{n-1} + (|z_n| - \delta_n) f_n s g_n(z_n) \dot{z}_n + \tilde{a}^T \bar{\Gamma} \dot{\tilde{a}} + \frac{b_n}{\gamma} \tilde{\beta} \dot{\tilde{\beta}} + \\ & \frac{1}{2\bar{q}} \int_0^R \tilde{\eta}_b(t, r) \frac{\partial}{\partial t} \tilde{\eta}_b''(t, r) dr \end{aligned} \quad (7.26)$$

In the last step, the control law is designed as follows:

$$u = \hat{\beta} \bar{u} \quad (7.27)$$

$$\bar{u} = -(c_n + 1)(|z_n| - \delta_n) s g_n(z_n) - \hat{a}^T Y + u_n + x_d^{(n)} + \dot{\alpha}_{n-1} \quad (7.28)$$

$$u_n = -s g_n(z_n) \hat{B}_o(t) \quad (7.29)$$

The adaptation laws are expressed as:

$$\dot{\hat{\beta}} = -\gamma \bar{u} (|z_n| - \delta_n) f_n s g_n(z_n) \quad (7.30)$$

$$\dot{\hat{a}} = (|z_n| - \delta_n) f_n s g_n(z_n) \bar{\Gamma} Y \quad (7.31)$$

$$\frac{\partial}{\partial t} \tilde{\eta}_r''(t, r) = \bar{q} (|z_n| - \delta_n) f_n |F_r[u](t)| \quad (7.32)$$

where γ , \bar{q} , and $\bar{\Gamma}$ are adaptation gains. According to the definition in (7.6), it can be obtained that:

$$\begin{aligned} \dot{z}_n = & \dot{x}_n - x_d^{(n)} - \dot{\alpha}_{n-1} \\ = & a^T Y + b_n u(t) + \int_0^R F_r[u](t) \eta_b''(r) dr - x_d^{(n)} - \dot{\alpha}_{n-1} \end{aligned} \quad (7.33)$$

Considering the results in (7.19) and (7.33), Equation (7.26) can be expressed as:

$$\begin{aligned}
\dot{V}_n = & -\sum_{i=1}^{n-1} c_i (|z_i| - \delta_i)^{2(n-i+1)} f_i + (|z_{n-1}| - \delta_{n-1})^2 (|z_n| - \delta_n - 1) f_{n-1} - \\
& \frac{1}{4} (|z_{n-1}| - \delta_{n-1})^4 f_i + (|z_n| - \delta_n) f_n s g_n(z_n) \\
& (a^T Y + b_\eta u(t) + \int_0^R F_r[u](t) \eta_b''(r) dr - x_d^{(n)} - \dot{\alpha}_{n-1}) \\
& + \tilde{a} \bar{\Gamma}^{-1} \dot{\tilde{a}} + \frac{b_\eta}{\gamma} \tilde{\beta} \dot{\tilde{\beta}} + \frac{1}{\bar{q}} \int_0^R \tilde{\eta}_b''(t, r) \frac{\partial}{\partial t} \tilde{\eta}_b''(t, r) dr
\end{aligned} \tag{7.34}$$

By using the control law in (7.27) and definition (7.21), which can be expressed as

$\hat{\beta} = \tilde{\beta} + \beta$, Equation (7.34) can be presented as:

$$\begin{aligned}
\dot{V}_n \leq & -\sum_{i=1}^{n-1} c_i (|z_i| - \delta_i)^{2(n-i+1)} f_i + M_n - (|z_n| - \delta_n) f_n s g_n(z_n) \tilde{a}^T Y \\
& + (|z_n| - \delta_n) f_n s g_n(z_n) b_\eta \tilde{\beta}(\bar{u}) + (|z_n| - \delta_n) f_n s g_n(z_n) \int_0^R F_r[u](t) \eta_b''(r) dr \\
& + \tilde{a} \bar{\Gamma}^{-1} \dot{\tilde{a}} + \frac{b_\eta}{\gamma} \tilde{\beta} \dot{\tilde{\beta}} + \frac{1}{\bar{q}} \int_0^R \tilde{\eta}_b''(t, r) \frac{\partial}{\partial t} \tilde{\eta}_b''(t, r) dr
\end{aligned} \tag{7.35}$$

where M_n is expressed as:

$$M_n = (|z_{n-1}| - \delta_{n-1})(|z_n| - \delta_n - 1) f_{n-1} - (|z_n| - \delta_n)^2 f_n \tag{7.36}$$

Then inequality (7.35) is expressed as:

$$\begin{aligned}
\dot{V}_n \leq & -\sum_{i=1}^{n-1} c_i (|z_i| - \delta_i)^{2(n-i+1)} f_i + M_n + \tilde{a} \left(-(|z_n| - \delta_n) f_n s g_n(z_n) Y + \bar{\Gamma}^{-1} \dot{\tilde{a}} \right) \\
& + b_\eta \tilde{\beta} \left(\frac{1}{\gamma} \dot{\tilde{\beta}} + (|z_n| - \delta_n) f_n s g_n(z_n) \bar{u} \right) + (|z_n| - \delta_n) f_n s g_n(z_n) u_h \\
& + (|z_n| - \delta_n) f_n s g_n(z_n) \int_0^R F_r[u](t) \eta_b''(r) dr + \frac{1}{\bar{q}} \int_0^R \tilde{\eta}_b''(t, r) \frac{\partial}{\partial t} \tilde{\eta}_b''(t, r) dr
\end{aligned} \tag{7.37}$$

By adopting the adaptive laws defined in (7.30), (7.31), and (7.32), the following inequality can be obtained:

$$\dot{V}_n \leq -\sum_{i=1}^n c_i (|z_i| - \delta_i)^{2(n-i+1)} f_i \quad (7.38)$$

From (7.29), it is obvious that V_n is non-increasing function, and by Barbalat's Lemma, it concludes that $(|z_i| - \delta_i) \rightarrow 0$ as $t \rightarrow \infty$. Thus, it is obtained that:

$$\lim_{t \rightarrow \infty} |x(t) - x_d(t)| = \delta_1 \quad (7.39)$$

The above suggests that the inverse compensation error of the closed-loop system can be reduced to desired precision. Proposed adaptive controller design (7.27) together with the update laws in (7.30), (7.31) and (7.32) can guarantee the global boundedness of the closed-loop system.

Remark 7.3: It is important to note that the dynamic system (7.1) is only used as an illustration to determine how the controller can be designed with the error of the inverse compensation. However, it can be extended for a general class of systems. It should be mentioned that the goal of this chapter is to show the controller design strategy in a simple setting that reveals its essential features.

7.4 Simulation Results

In this section, the methodology of employing the error of the inverse compensation with the robust controller presented in the previous section is illustrated using the following nonlinear system:

$$\dot{x}(t) = a \frac{1 - e^{-x(t)}}{1 + e^{x(t)}} + \Pi_{\phi^{-1} \circ \phi(r)}[v](t) \quad (7.40)$$

where $\Pi_{\hat{\varphi}^{-1} \circ \varphi(r)}[v](t)$ is the output of the inverse compensation when the inverse of the estimated Prandtl-Ishlinskii is applied as a feedforward compensator to compensate for the hysteresis nonlinearities. The initial loading curve $\varphi(r)$ that is applied to characterize the hysteretic actuator is described by:

$$\varphi(r) = 0.17r + \int_0^R 0.11\xi(r - \xi)dr \quad (7.41)$$

The estimated initial loading curve employed to construct the inverse Prandtl-Ishlinskii model as a feedforward compensator to compensate the hysteresis nonlinearities in closed-loop control system is assumed as:

$$\hat{\varphi}(r) = 0.2r + \int_0^R 0.2\xi(r - \xi)dr \quad (7.42)$$

In order to demonstrate the significance of considering the hysteresis nonlinearities in control design, the simulation is carried out considering the nonlinear term of the Prandtl-Ishlinskii model ($u_N \neq 0$) and without considering the nonlinear term ($u_N = 0$). The initial states for the simulation parameters are selected as: $R=40$, $N = 4000$, $\hat{\alpha}(0) = 0.13$, $\hat{\beta}(0) = 0.431$, and $x(0) = 1.05$, while a harmonic signal of the form $x_d(t) = 12.5\sin(2.3t)$, is applied as the desired trajectory. Owing to the lack of an analytical approach for selecting the control constants, an iterative simulation is carried out to select these constants. For this purpose, an adaptive structure control law is used together with the adaptation laws. The parameters of the robust adaptive controller are selected as: $\delta_l = 0.150$, $\bar{q} = 0.001$, $c_l = 10$, $\gamma = 0.09$, and $\bar{\Gamma} = 0.09$. Estimated initial loading curve (7.42) is applied to construct the inverse of the estimated Prandtl-Ishlinskii model.

Simulation results are shown in Figure 7.2, where the results involving the nonlinear term ($u_N \neq 0$) are indicated by solid line, while those excluding the nonlinear term ($u_N = 0$) are shown by dotted line. As shown in Figure 7.2(a), the output of the inverse compensation shows hysteresis effects between the desired input and the compensated output. The control signal with and without considering the nonlinear part is shown in Figure 7.2(b). The output of the inverse compensation with and without considering the nonlinear term of the model is presented in Figure 7.2(c). The time history for the desired trajectory and the system output $x(t)$ are shown in Figure 7.2(d). In Figure 7.2(e), the time history of the tracking errors of the state $x(t)$ with and without considering the nonlinear part of the model are presented.

The controller constructed based on the error of the inverse compensation clearly demonstrates excellent tracking performance as evident from the results. The controller can thus effectively overcome the error of the inverse compensation. The results also show the necessity to consider the compensation error which is generally ignored by the vast of majority publications using the inverse approach.

To show the significant of the derived error of the inverse compensation in closed-loop control system, the simulations were performed: (i) without considering the inverse of the Prandtl-Ishlinskii model, where the estimated initial loading curve is $\hat{\phi}(r) = r$; and (ii) with considering the exact inverse of the Prandtl-Ishlinskii model, where estimated initial loading curve (7.41) is applied. The time histories without using the inverse and with using the exact inverse are shown in Figures 7.3(a) and 7.3(b), respectively. The results show higher tracking error when the simulation is carried out without considering the inverse of the Prandtl-Ishlinskii model in the closed-loop control

system. On the other hand, better tracking performance can be obtained when the exact inverse is considered instead of the inverse of the estimated Prandtl-Ishlinskii model. It can be concluded that better tracking performance can be achieved in the control design by considering the inverse Prandtl-Ishlinskii model as well as the error of the inverse compensation.

7.5 Summary

The error of the inverse compensation is applied to design a robust controller to control a system that it is preceded by a hysteretic actuator in a closed-loop control system. The primary purpose is to consider the derived error of the inverse compensation with the adaptive controller to achieve high tracking performance. The control law ensures global stability of the entire system and achieves both stabilization and tracking within a desired precision. Simulations that performed on a nonlinear system with the error of the inverse compensation illustrate the effectiveness of considering the error of the inverse. The results demonstrate better tracking performance when the compensation error of the estimated Prandtl-Ishlinskii model is considered in the closed-loop control system.

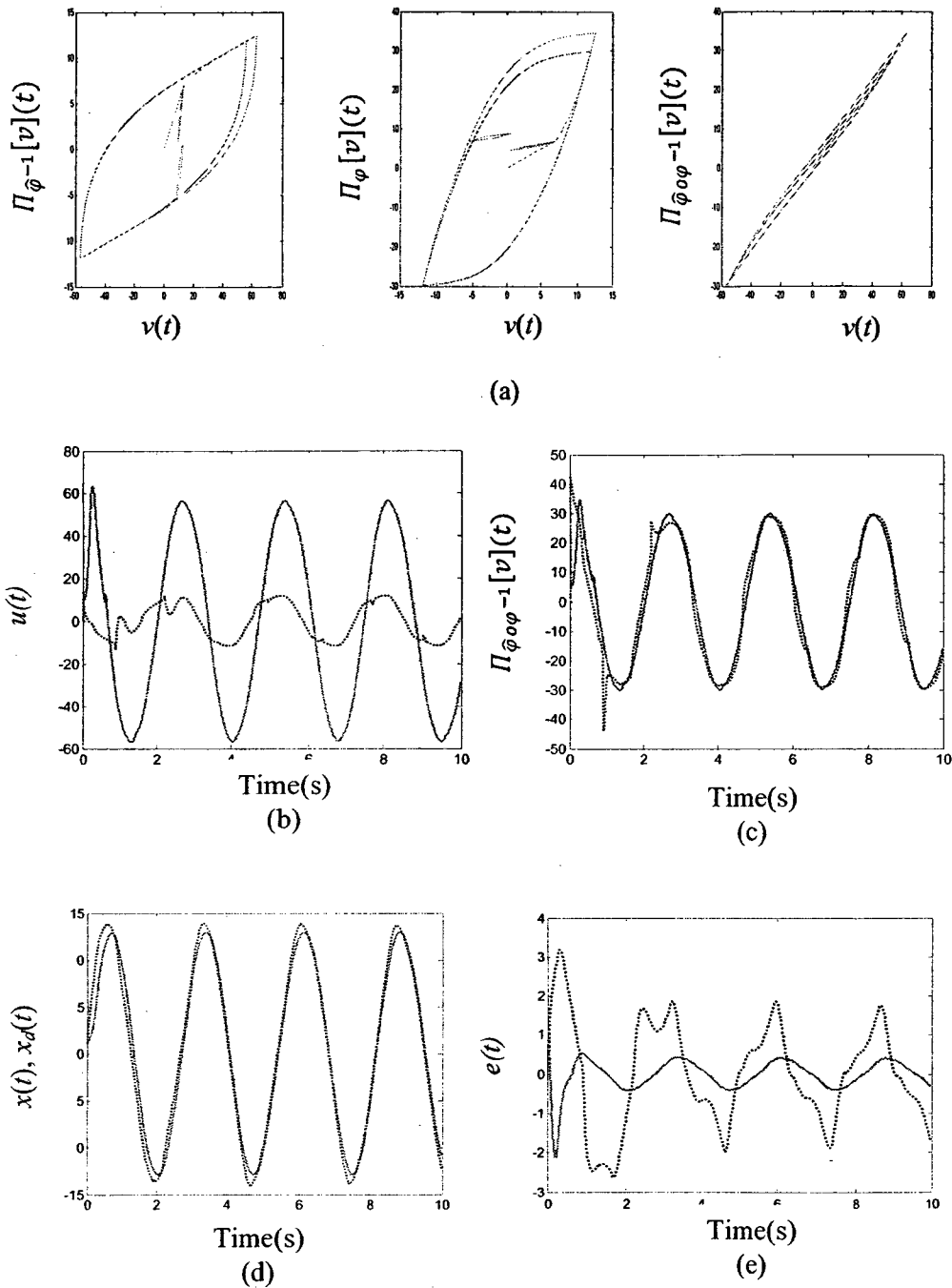
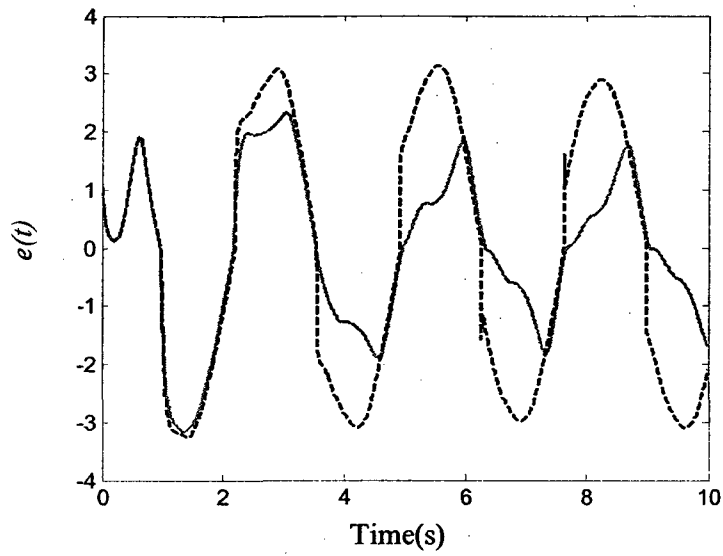
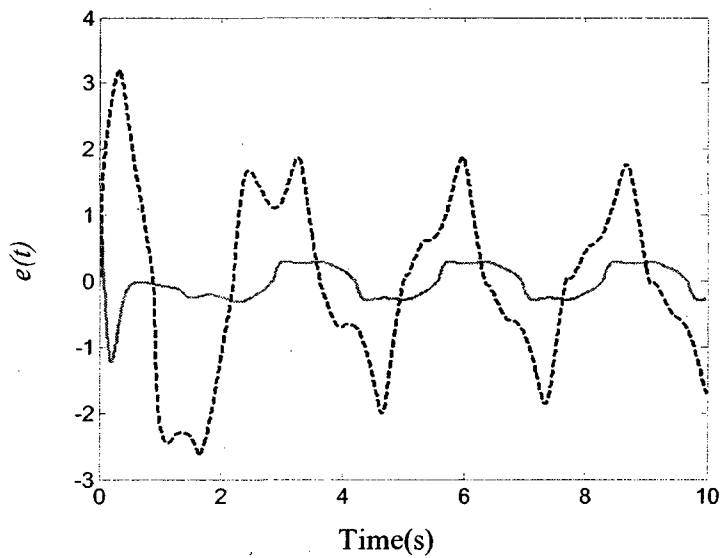


Figure 7.2: (a) Inverse compensation based on the estimated initial loading curve, (b) Control signal with $u_h \neq 0$ and $u_h = 0$, (c) Output of the inverse compensation with $u_h \neq 0$ and $u_h = 0$ (d) Desired trajectory $x_d(t)=12.5\sin(2.3t)$ and the system output $x(t)$, (e) Tracking errors with $u_h \neq 0$ and $u_h = 0$. (—, $u_h \neq 0$; ·····, $u_h = 0$).



(a)



(b)

Figure 7.3: Tracking errors of the output with $u_h \neq 0$ and $u_h = 0$, (a) without considering the inverse, (b) considering the exact inverse. (———, $u_h \neq 0$; ······, $u_h = 0$)

Chapter 8: Conclusions and Recommendations for Future Studies

8.1 Major Contributions

The hysteresis phenomenon, invariably, occurs in smart actuators, such as piezoceramics, magnetostrictive and shape memory alloys actuators. When a plant is preceded by such hysteresis nonlinearity, the system usually exhibits undesirable inaccuracies or oscillations and even instability due to the hysteresis effects. The dissertation research has proposed controller design for compensation of hysteresis nonlinearities on the basis of proposed generalized Prandtl-Ishlinskii models and their inversions. The major contributions of the dissertation research are summarized below:

- (i) A generalized Prandtl-Ishlinskii model is proposed on the basis of generalized play operator, with different loading and unloading envelope functions, to describe the symmetric as well as asymmetric major and minor hysteresis loops with output saturation.
- (ii) Dynamic density and threshold functions are proposed to formulate a generalized rate-dependent Prandtl-Ishlinskii model for describing the symmetric as well as asymmetric and rate-dependent hysteresis effects together with output saturation.
- (iii) The validity of the proposed generalized models are thoroughly demonstrated for different smart actuators, namely, piezoceramic, SMA and magnetostrictive, for a wide range of inputs involving harmonic and triangular waveforms of different magnitudes and frequencies.
- (iv) Relationships between the parameters of the generalized play operator and classic play operator are proposed to facilitate identification of the generalized operator.
- (v) Inversions of the proposed generalized models are formulated analytically using the initial loading curve with an objective to develop inverse-model based compensation method. The applicability of the inverse models is

demonstrated for compensation of saturated symmetric and asymmetric hysteresis of smart actuators over a wide range of input frequencies. Furthermore, the initial loading curve is explored to facilitate compensation of the hysteresis effects.

- (vi) An analytical method is developed for estimation of the compensation error on the basis of the proposed models and their inverse.
- (vii) An adaptive controller design is used together with essential control laws to achieve compensation of the hysteresis effects of a smart actuator that coupled with a plant. Stability analysis of the closed-loop systems is presented.

8.2 Major conclusions

The dissertation research on compensation of hysteresis nonlinearities involved five sequential major developments, namely: developments in generalized models for describing hysteresis nonlinearities of smart actuators; develops in exact analytical inversions of the generalized models; compensation of hysteresis effects using the model inverse; compensation error analysis; and controller design. The major conclusions drawn from each task are summarized below:

8.2.1 DEVELOPMENTS IN GENERALIZED HYSTERESIS MODELS

- The smart actuators, invariably, exhibit symmetric or asymmetric major and minor hysteresis loops with output saturation.
- The hysteresis effects are strongly influenced by the rate of input; an increase in the input frequency yields higher hysteresis but lower peak output.
- The classic Prandtl-Ishlinskii model cannot describe saturated asymmetric and rate-dependent hysteresis effects of smart actuators but can yield an exact analytical inverse for real-time compensation of the hysteresis effects.

- The use of dynamic threshold and density functions in the rate of input in the Prandtl-Ishlinskii model can provide reasonably good prediction of the rate-dependent hysteresis of the smart actuators. The peak prediction error was below 5% for the piezoceramic and magnetostrictive actuators under inputs up to 500 Hz.
- A generalized play operator with different loading and unloading envelope functions can be effectively applied in the Prandtl-Ishlinskii model to describe asymmetric hysteresis loops with output saturation. The resulting generalized Prandtl-Ishlinskii model revealed peak prediction error in order of 3% for SMA and magnetostrictive actuators.
- The threshold values of the generalized play operator can be directly estimated from those of the classic play operator.
- The generalized Prandtl-Ishlinskii model comprising the generalized play operator with dissimilar envelope functions also yields better estimation of the nearly symmetric hysteresis loops, as observed in the piezoceramic actuators.

8.2.2 DEVELOPMENTS IN INVERSE HYSTERESIS MODELS

- Since the generalized Prandtl-Ishlinskii model is a mere extension of the classic Prandtl-Ishlinskii model, the inverse of the generalized Prandtl-Ishlinskii model can be defined analytically.
- Unlike the numerically-derived inverse hysteresis, the proposed inverse of the generalized Prandtl-Ishlinskii model is unique.
- An analytical inverse of the generalized Prandtl-Ishlinskii model is insured if the envelope functions are continuous and invertible.
- It is proven that the inverse of the generalized Prandtl-Ishlinskii model is a generalized Prandtl-Ishlinskii model.
- While the Prandtl-Ishlinskii model is based upon its initial loading curve, the inverse Prandtl-Ishlinskii model is based on the inverse initial loading curve. The inverse generalized Prandtl-Ishlinskii model further necessitates the inverse of the envelope functions of the generalized play operator.

- The shape function of the initial loading curve of the Prandtl-Ishlinskii model is convex, while that of the inverse is concave. The composition of the initial loading curve and its inverse yields a linear function in threshold.
- The inverse generalized Prandtl-Ishlinskii model yields clockwise input-output curves due to negative density function.

8.2.3 COMPENSTION OF HYSTERESIS EFFECTS USING INVERSE MODEL

- The exact analytical inverse of the generalized hysteresis model can be conveniently applied as a feedforward compensator to achieve hysteresis compensation in real-time applications.
- The compositions of the inverse generalized models and generalized models yield total compensation of the hysteresis error, irrespective of the output saturation, asymmetric nature of the hysteresis loop or magnitude and the rate of the input.
- The experimental investigations in compensation of hysteresis effects in a piezoceramic actuator using the model inversion resulted in peak compensation error in the order of 2.4%, while it was nearly 7.5% in the absence of the feedforward compensator. The compensation error of the feedforward compensator was attributed to the characterization error, which was found to be in the order of 2.8%.

8.2.4 ERROR ANALYSIS

- The exact analytical inverse of the Prandtl-Ishlinskii model permits determination of error of the inverse compensation analytically, which has not yet been presented in the reported studies.
- It is analytically proven that the input-output characteristics of the error show hysteresis effects between the desired input and the compensated output. The proposed analytical expression of the error of the inverse compensation is thus a Prandtl-Ishlinskii model.
- The compensation error can be suppressed to zero when the exact initial loading curve is known.

- The compensation error resulting from the inverse Prandtl-Ishlinskii model is unbounded due to unbounded nature of the classical play operator. Additional control algorithms are thus vital for error compensation.
- The error of the inverse compensation is a linear relationship between the input and the compensated output and a nonlinear disturbance that may arise from characterization errors.

8.2.5 AN ADAPTIVE CONTROL DESIGN FOR HYSTERESIS COMPENSATION

- The knowledge of exact analytical inverse of the hysteresis model and the error greatly simplifies the task of controller design for hysteresis compensation of a plant preceded by a smart actuator.
- The proposed adaptive control design together with the defined updated adaptive laws guarantees the global boundedness of the closed-loop system and thus the output tracking with greater precision.
- The knowledge of exact error of the inverse compensator permits the real-time applications to plants in a highly efficient manner.
- The control laws ensure global stability of the closed-loop system, which is proven.
- The application of the proposed controller and inverse compensator to a nonlinear plant demonstrated that the controller provides stabilization .

8.3 Recommendation for the Future Studies

The dissertation research represents the use of the Prandtl-Ishlinskii model to model and to compensate hysteresis nonlinearities inherent in smart actuators for micro-positioning applications. The proposed models not only provided reasonably good prediction of the saturated symmetric and asymmetric rate-dependent hysteresis effects but also serve the essential basis for realizing effective compensation of hysteresis in

real-time applications. Following are some suggested further studies that should be undertaken to enhance the hysteresis compensation in varying studies:

- The applicability of the proposed generalized models and their inversions should be explored for compensation of (i) rate-dependent hysteresis in piezoceramic actuators; and (ii) saturated asymmetric rate-dependent hysteresis in magnetostrictive actuators.
- The design of controllers is desirable for compensation of hysteresis effects of the above stated actuators.
- Analysis of the error of the inverse compensation of the rate-dependent Prandtl-Ishlinskii model is desirable for design of an adaptive robust control employing the error of the inverse compensation.
- Further efforts are desirable in extending the proposed methodologies for modelling rate-dependent hysteresis nonlinearities of ferromagnetic materials using the generalized rate-independent and the generalized rate-dependent Prandtl-Ishlinskii models.
- Further efforts are also desirable for compensation of asymmetric and saturated hysteresis nonlinearities of the shape memory alloy actuators using the inverse generalized Prandtl-Ishlinskii model as a feedforward compensator.
- The proposed Prandtl-Ishlinskii models and their inversions may be investigated to model and compensate the hysteresis nonlinearities in ultrasonic motors, which show rate-dependent hysteresis effects.

PUBLICATIONS

Several papers reporting results of this thesis have been published/submitted in journals and well-known international conferences as listed below. These papers were written under guidance of my supervisors, Professor Subhash Rakheja and Professor Chun-Yi Su.

- Mohammad Al Janaideh, Chun-Yi Su and Subhash Rakheja, Development of the rate-dependent Prandtl-Ishlinskii model for smart actuators, *Smart Materials and Structures*, vol. 17, no. 3, pp.1-11, 2008.
- Mohammad Al Janaideh, Subhash Rakheja and Chun-Yi Su, Experimental characterization and modeling of rate-dependent hysteresis of a piezoceramic actuator, *Mechatronics*, vol. 17, no.5, pp. 656-670, 2009.
- Mohammad Al Janaideh, Subhash Rakheja and Chun-Yi Su, A generalized Prandtl-Ishlinskii model for characterizing hysteresis nonlinearities of smart actuators, *Smart Materials and Structures*, vol. 18, no 4, pp. 1-9, 2009.
- Mohammad Al Janaideh, Chun-Yi Su and Subhash Rakheja, Modeling rate-dependent symmetric and asymmetric hysteresis loops of smart actuators, *International Journal of Advanced Mechatronic Systems*, vol. 1, no. 1, pp. 32 – 43, 2008.
- Mohammad Al Janaideh, Chun-Yi Su and Subhash Rakheja, “An analytical generalized Prandtl-Ishlinskii model inversion for hysteresis compensation in micro-positioning control”, submitted for publication in *IEEE/ASME Transactions on Mechatronic systems*.
- Mohammad Al Janaideh, Chun-Yi Su and Subhash Rakheja, “Inverse generalized asymmetric Prandtl-Ishlinskii model for compensation of hysteresis nonlinearities in smart actuators”, in *proceedings of the 2009 IEEE International Conference on Networking, Sensing and Control*, Okayama, Japan, pp. 834 – 839, 2009.
- Mohammad Al Janaideh, Chun-Yi Su and Subhash Rakheja, “Generalized Prandtl-Ishlinskii hysteresis model: hysteresis modeling and inverse construction for compensation in smart actuators”, in *proceedings of 47th IEEE Conference on Decision and Control (CDC)*, Cancun, Mexico, pp. 5182 – 5187, 2008.
- Mohammad Al Janaideh, Subhash Rakheja and Chun-Yi Su, Compensation of hysteresis nonlinearities in smart actuators”, in *proceedings of 2008 ASME Conference on Smart Materials, Adaptive Structures and Intelligent Systems*, Eliicott City (MD), 2008.

- Mohammad Al Janaideh, Subhash Rakheja and Chun-Yi Su, A generalized rate-dependent play operator for characterizing asymmetric and symmetric hysteresis nonlinearities, *in the proceedings of the 2008 American Control Conference*, Seattle (WA), pp. 1911–1916, 2008.
- Mohammad Al Janaideh, Chun-Yi Su and Subhash Rakheja, Development of rate-independent Prandtl-Ishlinskii model for characterizing asymmetric hysteresis nonlinearities of SMA actuators”, *in proceedings of the 2008 IEEE/ASME Advanced Intelligent Mechatronics Conference*, Xi’an, China, pp. 477– 481, 2008.
- Mohammad Al Janaideh, Subhash Rakheja and Chun-Yi Su, A generalized asymmetric Prandtl-Ishlinskii model for characterizing hysteresis nonlinearities, *in proceedings of the 2008 Earth & Space Conference-Intelligent Sensors and Actuators Symposium*, LongBeach (CA), pp. 312–320, 2008.
- Mohammad Al Janaideh, Subhash Rakheja and Chun-Yi Su, A generalized Prandtl-Ishlinskii model for characterizing rate-dependent hysteresis, *in proceedings of the 22nd IEEE International Conference on Control Applications(CCA)*, Singapore, pp. 343–348, 2007.
- Mohammad Al Janaideh, Subhash Rakheja and Chun-Yi Su, Characterization of rate-dependent hysteresis of piezoceramic actuators, *in proceedings of the IEEE International Conference on Mechatronics and Automation*, Harbin, China, pp. 550–555, 2007.
- Mohammad Al Janaideh, Subhash Rakheja and Chun-Yi Su, Characterization of rate-dependent hysteresis, *in proceedings of the 2006 IEEE International Conference on Advances in Dynamics, Instrumentation and Control*, Queretaro, Mexico, pp. 66–77, 2006.
- Mohammad Al Janaideh, Subhash Rakheja and Chun-Yi Su, Inverse rate-dependent Prandtl-Ishlinskii model for hysteresis nonlinearities compensation, accepted for publication in proceedings of IEEE International Conference on Automation and Logistics, Shenyang, China, 2009.

REFERENCES

1. I. Mayergoyz, *Mathematical Models of Hysteresis*, Elsevier, New York, 2003.
2. M. Brokate and J. Sprekels, *Hysteresis and Phase Transitions*, New York, Springer, 1996.
3. A. Visintian, *Differential Models of Hysteresis*, Springer, Berlin, 1994.
4. M. Krasnoselskii and A. Pokrovskii, *Systems with Hysteresis*, Springer, Moscow 1989.
5. F. Preisach, Uber die magnetische nachwirkung, *Zeitschrift fur Physik*, vol. 94, pp. 277–302, 1935.
6. K. Ikuta, M. Tsukamoto and S. Hirose, *Mathematical model and experimental verification of shape memory alloy for designing micro actuator*, In proceedings of IEEE International Conference on Micro-Electro-Mechanical Systems, pp. 103–111, 1991.
7. R. Smith, *Smart Material System: Model Development*, Society for Industrial and Applied Mathematics, 2005.
8. R. Smith, S. Seelecke, Z. Ounaies and J. Simth, *A free energy model for hysteresis in ferroelectric materials*, *Journal of Intelligent Materials Systems and Structures*, vol. 14, no.11, pp. 719–739, 2003.
9. R. Smith and Z. Ounaies, *A domain wall model for hysteresis in piezoelectric materials*, *Journal of Intelligent Material Systems and Structures*, vol. 11, no.1, pp. 62–79, 2000.
10. P. Papadopoulos, Y. Jung and R. Ritchie, *Constitutive modeling and numerical simulation of multivariant phase transformation in superelastic shape memory alloys*, *International Journal for Numerical Methods in Engineering*, vol. 60, no. 2, pp. 429-460, 1997.
11. P. Popov and D. Lagoudas, *A 3d constitutive model for shape memory alloys incorporating pseudoelasticity and detwinning of self-accommodated martensite*, *International Journal of Plasticity*, vol. 23, no.2, 1679-1720, 2007.
12. O. Heintze and S. Seelecke, *A coupled thermomechanical model for shape memory alloys—from single crystal to polycrystal*, *Materials Science and Engineering: A*, vol. 481/482, pp.389-394, 2008
13. B. Chang, J. Shaw and M. Iadicola, *Thermodynamics of shape memory alloy wire: modeling, experiments and application*, *Continuum Mechanics and*

Thermodynamics, vol. 18, no.1-2, pp.83-118, 2006.

14. J. Shaw and C. Churchill, A reduced-order thermomechanical model and analytical solution for uniaxial shape memory alloy wire actuators, *Smart materials and structures*, vol. 18, no. 6, pp.1-21, 2009.
15. D. Jiles and D. Atherton, Theory of ferromagnetic hysteresis, *Journal of Magnetism and Magnetic Materials*, vol. 61, no. 1-2, pp.48-60, 1986.
16. R. Bouc, A mathematical model for hysteresis, *Acustica*, vol. 24, pp.16-25, 1971.
17. Y. Wen, Method for random vibration of hysteretic systems, *Journal of the Engineering Mechanics Division*, vol. 102, no. 2, 1976, pp. 249-263.
18. C. Alhan and H. Gavin, A parametric study of linear and nonlinear, *Engineering structures*, vol. 26, no. 4, 2004, pp. 485-497.
19. X. Ma, S. Rakheja and C-Y. Su, Development and relative assessments of models for characterizing the current dependent hysteresis properties of magnetorheological fluid dampers, *Journal of Intelligent Material Systems and Structures*, vol. 18, no. 5, pp. 487-502, 2007.
20. D. Hughes and J. Wen, Preisach modelling of piezoceramic and shape memory alloy hysteresis, *Smart Materials and Structures*, vol. 6, pp.287-300, 1997.
21. R. Gorbet, D. Wang and K. Morris, Preisach model identification of a two wire SMA actuator, In proceedings of IEEE International Conference on Robotics and Automation, Leuven, Belgium, pp. 2161-2168, 1998.
22. P. Ge and M. Jouaneh, Modeling hysteresis in piezoceramic actuators, *Precision Engineering*, vol. 17, no. 3, pp. 211-221, 1995.
23. P. Ge and M. Jouaneh, Tracking control of a piezoceramic actuator, *IEEE Transaction on Control Systems Technology*, vol. 4, no.3, pp.209 - 216, 1996.
24. X. Tan and H. Khalil, Control Unknown Dynamic hysteretic systems using slow adaption: preliminary results, In proceedings of American Control Conference, NewYork, NewYork, pp. 3294-3299, 2007.
25. X. Tan and J.S. Baras, Adaptive identification and control of hysteresis in smart materials, *IEEE Transactions on Automatic Control*, vol. 50, no. 6. pp. 827 - 839, 2005.
26. R. Iyer, X. Tan and P. Krishnaprasad, Approximate inversion of the Preisach hysteresis operator with application to control of smart actuators, *IEEE Transactions on Automatic Control* , vol. 50, no. 6, pp.798-810, 2005.
27. W. Galinaities, Two methods for modeling scalar hysteresis and their use in

controlling actuators with hysteresis, PhD. dissertation, Department of Mathematics, Blacksburg, Virginia, 1999.

28. H. Banks, A. Kurdila and G. Webb, Identification of hysteretic control influence operators representing smart actuators, *Mathematical Problems in Engineering*, vol. 3, no. 4, pp. 287–328, 1997.
29. K. Kuhnen, Modeling, identification and compensation of complex hysteretic nonlinearities, *European Journal of Control*, vol. 9, no.4, pp. 407–418, 2003.
30. P. Krejci and K. Kuhnen, Inverse control of systems with hysteresis and creep, *IEE Proc Control Theory Application*, vol. 148, no.3, pp. 185-192, 2001.
31. G. Tao and P. Kokotovic, Adaptive control of plants with unknown hysteresis, *IEEE Transactions On Automatic Control*, vol. 40, no.2, pp.200-212, 1995.
32. W. G. Cady, *Piezoelectricity*, McGraw-Hill, New York, 1946.
33. X. Tan and J. Baras, Modeling and control of hysteresis in Magnetostrictive actuators, *Automatica*, vol. 40, no. 9, pp.1469-1480, 2004.
34. Y. Yu, Z. Xiao, N. Naganathan and R. Dukkipati, Dynamic Preisach modeling of hysteresis for the piezoceramic actuator system, *Mechanism and Machine Theory*, vol. 37, no. 1, pp.75-89, 2002.
35. J. Kim and S. Nam, Development of a micro-depth control system for an ultra-precision lathe using a piezo-electric actuator, *International Journal of Machine Tools and Manufacture*, vol. 37, no. 4, pp.495-509, 1997.
36. C. Natale, F. Velardi and C. Visone, Modelling and compensation of hysteresis for magnetostrictive actuators, In proceedings of International conference on Advanced Intelligent Mechatronics, Como, Italy, pp. 774-780,2001
37. B. Choi and M. Han, Vibration control of a rotating cantilevered beam using piezoactuators: experimental work, *Journal of Sound and Vibration*, vol. 277, no. 1-2, pp.436-442, 2004.
38. H. Shin and S. Choi, Position control of a two-link flexible manipulator featuring piezoelectric actuators and sensors, *Mechatronics*, vol. 11, no. 6, pp. 707-729, 2001.
39. B. Agrawal, M. Elshafei and G. Song, Adaptive antenna shape control using piezoelectric actuators, *Acta Astronaut*, vol. 40, no. 11, pp.821–826, 1997.
40. J. Park, K. Yoshida and S. Yokoto, Resonantly driven piezoelectric micropump – fabrication of a micropump having high power density, *Mechatronics*, vol. 9, no. 7, pp. 687–702, 1999.

41. G. Song, J. Zhao, X. Zhou and J. Abreu-Garcia, Tracking control of a piezoceramic actuator with hysteresis compensation using inverse Preisach model, *IEEE Transactions on Mechatronics*, vol. 10, no. 2, pp. 198-209, 2005.
42. J. Kim and S. Nam, Development of a micro-positioning grinding table using piezoelectric voltage feedback, *Institution of Mechanical Engineers, Proceedings of the Part B—Journal of Engineering Manufacture*, vol. 209, no. 6, pp. 469–474, 1995.
43. J. Rasmussen, T. Tsao, R. Hanson and S. Kapoor, A piezoelectric tool servo system for variable depth of cut machining, *Precision Machining: Technology and Machine Development and Improvement*, vol. 58, pp. 119–130, 1992.
44. K. Tan, T. Lee and H. Zhou, Micro-positioning of linear-piezoelectric motors based on a learning nonlinear PID controller, *IEEE Transactions on Mechatronics*, vol. 6, no.4, pp. 428–436, 2001.
45. Y. Li and R. Horowitz, Design and testing of track-following controllers for dual-stage servo systems with PZT actuated suspension, *Microsystems Technologies*, vol. 8, pp. 194–205, 2002.
46. R. Brinkerhoff and S. Devasia, Output tracking for actuator deficient/redundant systems: multiple piezoactuator example, *Journal of Guidance of Control and Dynamics*, vol. 23, no. 2, pp. 370–373, 1999.
47. J. Dewey, K. Leang and S. Devasia, Experimental and theoretical results in output-trajectory redesign for flexible structures, *Journal of Dynamic Systems, Measurement and Control*, vol. 120, pp. 456–461, 1998.
48. D. Croft, D. McAllister and S. Devasia, High-speed scanning of piezo-probes for nano-fabrication, *Journal of Manufacturing Science and Engineering*, vol. 120, no. 3, pp. 617–622, 1998.
49. Y. Kim, H. Nam, S. Cho, D. Kim and J. Bu, A self-actuating PZT cantilever integrated with piezoresistor sensor for AFM with high speed parallel operation, *In proceedings of IEEE International Conference on Micro-Electro-Mechanical Systems*, pp. 689–692, 2002.
50. R. Smith, M. Salapaka, A. Hatch, J. Smith and T. De, Model development and inverse compensator design for high speed nanopositioning, *In proceedings of 41st IEEE Conference on Decision and Control*, Las Vegas, Nevada, pp. 3652–3657, 2002.
51. S. Choi, J. Yoo, M. Cho and Y. Lee, Position control of a cylinder system using a piezoactuator-driven pump, *Mechatronics*, vol. 15, no. 2, pp.239-249, 2005.
52. W. Zhu, B. Martin and Y. Altintas, A fast tool servo design for precision turning

of shafts on conventional CNC lathes, *International Journal of Machine Tools and Manufacture*, vol. 41, no. 7, pp. 953-965, 2001.

53. H. Janocha and K. Kuhnen, Real-time compensation of hysteresis and creep in piezoelectric actuators, *Sensors and Actuators A: Physical*, vol. 79, no. 2, pp.83-89, 2000.
54. J. Tzen, S. Jeng and W. Chieng, Modeling of piezoelectric actuator for compensation and controller design, *Precision Engineering*, vol. 27, no.1, pp. 70-86, 2003.
55. C-Y. Su, Q. Wang, X. Chen and S. Rakheja, Adaptive variable structure control of a class of nonlinear systems with unknown Prandtl-Ishlinskii hysteresis, *IEEE Transactions on Automatic Control*, vol. 50, no. 12, pp. 2069 – 2074, 2005.
56. R. Gorbet, Control of hysteresis systems with Preisach representations, Ph.D. dissertation, University of Waterloo, Ontario, 1997.
57. J. Cruz-Hernandez and V. Hayward, Phase control approach to hysteresis reduction, *IEEE Transactions on Control Systems Technology*, vol. 9, no. 1, pp.17– 26, 2001.
58. J. Schafer and H. Janocha, Compensation of hysteresis in solid-state actuators, *Sensors and Actuators A*, vol. 49, no. 1-2, pp. 97–102, 1995.
59. Q. Wang and C-Y. Su, Robust adaptive control of a class of nonlinear systems including actuator hysteresis with Prandtl–Ishlinskii presentations, *Automatica*, vol. 42, no. 5, pp.859-867, 2006.
60. R. Gorbet, K. Morris and D. Wang, Passivity-Based Stability and Control of Hysteresis in Smart actuators, *IEEE Transactions on Control Systems Technology*, vol. 9, no. 1, 2001.
61. H. Hu and R. Ben Mrad, On the classical Preisach model for hysteresis in piezoceramic actuators, *Mechatronics*, vol. 13, no. 2, pp. 85-94, 2002.
62. G. Song, V. Chaudhry and C. Batur, A Neural Network Inverse Model for a Shape Memory Alloy Wire Actuator, *Journal of Intelligent Material Systems and Structures*, vol. 14, no. 6, pp. 371-377, 2003.
63. G. Song and D. Quinn, Experimental study of the robust tracking control of a shape memory alloy wire actuator, *Journal of Dynamic Systems, Measurement, and Control*, vol. 126, no. 3, pp. 674-677, 2004.
64. R. Ben Mrad and H. Hu, A model for voltage-to-displacement dynamics in piezoceramic actuators subject to dynamic-voltage excitations, *IEEE Transactions on Mechatronics*, vol. 7, no. 4, pp. 479 – 489, 2002.

65. D. Jiles and D. Atherton, Theory of ferromagnetic hysteresis, *Journal of Applied Physics*, vol. 55, no. 6, pp. 2115-2120, 1984.
66. G. Bertotti, Dynamic generalization of the scalar Preisach model of hysteresis, *IEEE Transactions on Magnetics*, vol. 28, no. 5, pp. 2599 – 2601, 1992.
67. C-Y. Su, Y. Stepanenko, J. Svoboda and T. Leung, Robust adaptive control of a class of nonlinear systems with unknown backlash-like hysteresis, *IEEE Transactions on Automatic Control*, vol. 45, no.12, pp. 2427-2432, 2000.
68. W. Ang, F. Garmon, P. Khosla and C. Riviere, Modeling rate-dependent hysteresis in piezoelectric actuators, in proceedings of International Conference of Intelligent Robots and Systems, Lasvegas, Nevada, pp. 1975–1980, 2003.
69. A. Holman, P. Scholte, W. Heerens and F. Tuinstra, Analysis of piezo actuators in translation constructions, *Review of Scientific Instruments*, vol. 66, no. 5, pp. 3208-3215, 1995.
70. R. Smith and R. Zrostilk, Inverse compensation for ferromagnetic hysteresis, In proceedings IEEE Conference on Decision and Control, Phoenix, Arizona, pp. 2875-2880, 1999.
71. J. Nealis and R. Smith, Model-Based Robust Control Design for Magnetostrictive Transducers Operating in Hysteretic and Nonlinear Regimes, *IEEE Transactions on Control Systems Technology*, vol. 15, no. 1, pp. 22-39, 2007.
72. B. Choi, Y. Lee and B. Choi, Fast Preisach modeling method for shape memory Alloy actuators using major hysteresis loops, *Smart Materials and Structures*, vol. 13, no. 5, pp. 1069–1080, 2004.
73. I. Mayergoyz, Dynamic Preisach models of hysteresis, *IEEE Transactions on Magnetics*, vol. 24, no. 6, pp. 2925 – 2927, 1988.
74. W. Oates, P. Evans, R. Smith and M. Dapino, Experimental implementation of a nonlinear control method for magnetostrictive transducers, In proceedings of American Control Conference, New York, NY, pp.4309-4315, 2007.
75. J. Zhou, C. Wen and Y. Zhang, Adaptive backstepping control of a class of uncertain nonlinear systems with unknown backlash-like hysteresis, *IEEE Transactions on Automatic Control*, vol. 49, no. 10, pp. 1751-1757, 2004.
76. J. Zhou, C. Zhang and C. Wen, Robust adaptive output control of uncertain nonlinear plants with unknown backlash nonlinearities, *IEEE Trans. Automatic Control*, vol. no. 3, pp. 503-509, 2007.
77. P. Krejci, Hysteresis, Convexity and Dissipation in Hyperbolic Equation.

78. G. Foliente, Hysteresis modeling of wood joints and structural systems, ASCE Journal of Structural Engineering, vol. 121, no.6, pp. 1013–1022, 1995.
79. M. Battaini and F. Casciati, Chaotic behaviour of hysteretic oscillators, Journal of Structural Control, vol. 3, no.1-2 pp. 7-19, 1996.
80. B. Nguyen and A. Kyoungkwan, Feedforward control of shape memory alloy actuators using fuzzy-based inverse Preisach model, IEEE Transactions on Control Systems Technology, vol.17, no.2, pp. 434-44, 2009.
81. H. Liaw, B. Shirinzadeh and J. Smith, Sliding-mode enhanced adaptive motion tracking control of piezoelectric actuation systems for micro/nano-manipulation, IEEE Transactions on Control Systems Technology, vol. 16, no. 4, pp. 826-833, 2008.
82. R. Iyer and X. Tan, Control of hysteretic systems through inverse, compensation : inversion algorithms, adaptation, and embedded implementation, IEEE Control Systems Magazine, vol. 29, no. 1, pp. 83-99, 2009